

ABSTRACT

Title of Document: CATECHOLS AS MEMBRANE ANION
TRANSPORTERS

Sofya Berezin, Doctor of Philosophy, 2009

Directed By: Professor, Jeffery T. Davis, Department of
Chemistry and Biochemistry

Synthetic anion transporters have potential as antimicrobials, extractants, sensors, etc. Anionophores may also help us understand how natural systems move ions across hydrophobic barriers. While bacterial siderophores and synthetic analogues use catecholates for Fe^{3+} uptake, this work reports of catechols facilitating biomembrane transport of anions. We demonstrate that simple bis-catechol **III-25** is an anion transporter whose activity depends on catechol's substitution and amphiphilicity. We also describe liposomal assays and devised quantitative descriptions that allow one to study facilitated anion transport. These assays indicate that selectivity of **III-25** follows the Hofmeister bias: anions which are easier to dehydrate are made more permeable to the membrane by this bis-catechol. We believe that our description of the ion

selectivity and mechanism for **III-25** opens an outstanding opportunity for those interested in determining the selectivity and mechanism for other synthetic and natural biomembrane ion transporters.

In the beginning of this project we investigated number of simple amides and phenols to evaluate their relative affinity and stoichiometry of interaction with Cl^- anion. ESI-MS and ^1H NMR analysis showed that a dimer, $\text{catechol}_2 \cdot \text{Cl}^-$, was the major complex formed when $\text{TBA}^+ \text{Cl}^-$ was mixed with excess catechol. Based on this finding we attached two catechols to a TREN scaffold. A hydrophobic alkyl amide groups were linked to TREN's third position. Surprisingly, this simple design led to the active analogs **III-23** - **III-26**. A medium-length, **III-25**, was the most active compound, indicating that ion transport ability depends on the ability to partition into the biomembrane.

Finally, we noticed that the experimentally observed weak dependence of the transport rates on the anion's hydration energy, namely, k_{Anion} decreasing in the order $\text{ClO}_4^- > \text{I}^- > \text{NO}_3^- > \text{Br}^- > \text{Cl}^-$, is also seen for some of Nature's anion transporters. Thus, anion permeation into the CFTR chloride channel shows a similar trend. We also observed a nonlinear dependence of k_{Anion} on the concentration of bis-catechol. These findings led us to believe that self-association of **III-25** provides transient pores that allow permeation without requiring complete dehydration of the inorganic anions. Future efforts will include incorporating selectivity filters into these bis-catechols to help overcome the Hofmeister bias.

CATECHOLS AS MEMBRANE ANION TRANSPORTERS

By

Sofya Berezin

Dissertation submitted to the Faculty of the Graduate School of the
University of Maryland, College Park, in partial fulfillment
of the requirements for the degree of
Doctor of Philosophy
2009

Advisory Committee:
Professor Jeffery T. Davis, Chair
Professor Marco Colombini
Professor Bryan Eichhorn
Professor Daniel E. Falvey
Professor Andrei N. Vedernikov

© Copyright by
Sofya Berezin
2009

Dedicated to the Davis' Group

Acknowledgements

I thank my advisor Prof. Jeffery T. Davis for his guidance and support and for inspiring me to pursue this research. I also thank my lab colleagues whose hard work and sacrifices were everyday reminders that earning a Ph.D. in Organic Chemistry requires both a strong interest in creating new compounds and love for learning and teaching.

I thank the faculty and staff of the Chemistry and Biochemistry department for providing me with ample educational, teaching, and research opportunities. I acknowledge your outstanding efforts and achievements towards advancing innovation in the field of natural science. I thank Department of Energy for supporting my graduate research.

I thank my loving family who never doubt that my research efforts lead to the Doctor of Philosophy degree, and foremost, my wonderful husband who made these last seven and half years truly the happiest of my life.

Table of Contents

Dedication.....	ii
Acknowledgements.....	iii
Table of Contents.....	iv
List of Tables.....	vii
List of Figures.....	viii

Chapter 1: Ion Transport from Nature to Material Science as Viewed Through the Lens of an Organic Chemist.....1

1.1. Introduction.....	1
1.2. Ion Transport across Phospholipid Bilayer: Selected General Considerations and Quantitative Descriptions.....	4
1.2.1. Ion passage across the bilayer membrane.....	4
1.2.2. “Unassisted” permeation of ions across phospholipid bilayer.....	7
1.2.3. Permeation of ions mediated by the prokaryotic K ⁺ ion channel found in Nature.....	10
1.2.4. Ion transport mediated by the natural and synthetic ionophores.....	12
1.3. Synthetic and Natural Ion Channels and Transporters at Present.....	18
1.3.1. Introduction.....	18
1.3.2. Synthetic ion channels.....	19
1.3.3. Ion selectivity: K ⁺ ion channel and Cystic Fibrosis Transmembrane Conductance Regulator (CFTR) versus synthetic ion channels.....	24
1.3.4. Synthetic anionophores today: goals and challenges.....	27
1.3.5. General picture of the HPTS-based liposomal assay.....	31
1.3.6. Properties of HPTS.....	35
1.3.7. A broad and complex definition of the ion selectivity.....	37
1.3.8. Liposomes as a tool to obtain structural information about the membrane-active ion-conducting complex.....	46
1.4. Amphiphilic Catechols as Potential Anion Receptors and Membrane Transporters.....	50

Chapter 2: Complexity of Interaction Between Catechol and (Bu)₄N⁺Cl⁻.....60

2.1. Introduction.....	60
2.2. Abstract and Summary of Key Findings in this Chapter.....	64
2.3. Results and Discussion.....	67
2.3.1. ¹ H NMR study.....	67
2.3.1.1. Relative affinity of the receptors II-1 – II-6 toward Cl ⁻ anion in CHCl ₃ solution.....	67
2.3.1.2. Signals of the salt (Bu) ₄ N ⁺ Cl ⁻ shift upfield in presence of H-bond donors. Is there an equilibrium between (Bu) ₄ N ⁺ cation and aggregates ((Bu) ₄ N ⁺ Cl ⁻) _n ?.....	70
2.3.1.3. Multiple binding of H-bond donors to Cl ⁻ anion.....	72

2.3.1.4. Dilution experiment: the combined ^1H NMR data for the salt and receptors provides evidence of ion-paired intermediates $(\text{Bu})_4\text{N}^+\text{Cl}^-\cdots\text{R}$ in solution.....	76
2.3.1.5. ^1H NMR of the salt supports stepwise interaction mechanism.....	78
2.3.1.6. Why are these results important?.....	83
2.3.2. Electronic structure calculations.....	88
2.3.3. ESI-MS study.....	92
2.3.3.1. ESI mass spectra indicate formation of the dimers $\text{R}_2\cdots\text{Cl}^-$ and $\text{R}'\cdots\text{Cl}^-\cdots\text{R}$ in the presence of an excess of H-bond donors.....	92
2.3.3.2. ESI mass spectra indicate presence of the ion-paired intermediates $(\text{Bu})_4\text{N}^+\text{Cl}^-\cdots\text{R}$ when the concentrations of H-bond donors and the salt are comparable in solution.....	94
2.3.3.3. Relative distribution of the clusters in the negative-ion MS is determined by the salt to receptor ratio. Competition for binding to Cl^- anion.....	96
2.3.3.4. Based on the ESI-MS data the following can be concluded.....	98
2.4. Supporting Information for Chapter 2.....	101
2.4.1. Self-association of the receptors II-1, II-3, and II-6 in CHCl_3 solution.....	101
2.4.2. Chemical shift of $(\text{Bu})_4\text{N}^+\text{Cl}^-$ in CHCl_3 is independent on concentration.....	104
2.4.3. Job Plots A and B for receptors II-2, II-4, and II-5.....	105
2.4.4. ESI MS of the salt $(\text{Bu})_4\text{N}^+\text{Cl}^-$ in CHCl_3	107
2.4.5. Dependence of the negative-ion MS on the ratio salt : receptor for H- bond donors II-3 and II-6.....	109
Chapter 3: Anion Binding and Self-Assembly. Bis-Catechols and Methylated Analog.....	113
3.1. Introduction.....	113
3.1.1. New bis-catechol based anion receptors and their structural analogs.....	113
3.2. Results and discussion.....	118
3.2.1. Synthesis.	118
3.2.2. ^1H NMR spectra 2,3-bis-catechols in DMSO-d_6 versus TRENbAlaCAM and enterobactin.....	120
3.2.3. Anion binding study. Relative affinities of bis-catechols and methylated precursors toward Cl^- anion in DMSO-d_6 solution.....	123
3.2.4. Self-assembly of methylated analogs in organic solution and crystalline state.....	133
3.2.4.1. Introduction.....	133
3.2.4.2. Physical properties of methylated precursors.....	135
3.2.4.3. Properties of the compound III-22 as an organogelator.	136
3.2.4.4. ^1H NMR study of dimethoxy compounds in CHCl_3 solution.....	137
3.2.4.5. Conformational control of gelation. Structure of the organogel.....	141
3.2.4.6. Crystal structures of the compounds III-29 and III-30.....	142
3.2.4.7. Conclusion.....	145
3.3. Supporting Information for Chapter 3.....	146
3.3.1. The pKa values of the TRENCAM analog and some other relevant compounds.....	146
3.3.2. Anion binding study.....	147
3.3.3. Modeling of anion binding.....	149

3.3.4. Self-aggregation of the compound III-30 in CDCl ₃	156
Chapter 4: Bis-Catechols as Anion Transporters.....	157
4.1. Results of the Transport Experiments and Discussion.....	157
4.1.1. Relative activity of the bis-catechols and methylated analogs in liposomal assay.....	157
4.1.2. Study of the anion selectivity.....	162
4.2. Modeling of the Ion Transport Kinetics.....	168
4.2.1. Modeling of ion transport in the N ₃ ⁻ -based assay.....	168
4.2.2. Modeling of the ion transport. The assay with intravesicular ClO ₄ ⁻ anion....	171
4.3. Molecular Models of the Anion Transport.....	175
4.3.1. Dependence of the anion transport rate on concentration of the bis-catechol.	175
4.3.2. Mechanism of transport from the point of view of an anion. Energy profile for the bis-catechol assisted anion permeation.....	178
4.4. Conclusion.....	186
4.5. Why are these Results Important? Future Directions.....	189
4.6. Supporting Information for Chapter 4.....	194
4.6.1. Dependence of the HPTS response on pH.....	194
4.6.2. Extraction of the anion transport parameters from the experimental data....	196
4.6.3. Concentration dependence study.....	199
5. Experimental Section.....	201
5.1. Experimental section for Chapter 2.....	201
5.1.1. ¹ H NMR.....	201
5.1.2. <i>Ab initio</i> .calculations.....	201
5.1.3. ESI-MS.....	202
5.2. Experimental section for Chapter 3.....	204
5.2.1. General experimental.....	204
5.2.2. Synthesis of bis-catechol amphiphiles.....	204
5.2.3. ¹ H NMR spectra of compounds	215
5.3. Experimental section for Chapter 4.....	224
5.3.1. General experimental.....	224
5.3.2. Preparation of liposomes.....	224
5.2.3. Ion transport assays.....	225

List of Tables

Table 1.1. Permeabilities of inorganic ions across fluid PC bilayers.....	7
Table 2.1 Values of $K_{a\ 1:1}$, M^{-1} for II-1 – II-6 and Cl^{-} in $CDCl_3$	68
Table 2.2. Dependence of the association constant, $K_{a\ 1:1}$, M^{-1} , and dissociation constant of the salt K_d , M on concentration in $CDCl_3$ solution.....	79
Table S2.1. Chemical shift of α - CH_2 in $(Bu)_4N^{+}Cl^{-}$ as function of the solvent and concentration.....	104
Table 3.1. Relative affinities (K_{a1} , M^{-1}) toward Cl^{-} anion in DMSO- d_6 for bis-catechols III-26, III-28 and HCl salts of their methylated analogs, III-18 and III-22, evaluated using signals of the different acidic protons as indicated below and in Figure 3.8.....	124
Table 3.2. Physical properties of dimethoxy compounds III-12 – III-22, III-29, and III-30.....	135
Table S3.1. Single-step model. The following parameters K_a , M^{-1} , $\Delta\delta = \delta_{max} - \delta_0$, ppm, and R^2 were obtained from the best fit of experimental data sets for compounds III-26 and III-28. The cases, when the single step model could not adequately describe the experimental data sets ($R^2 < 0.99$), are marked bold.....	153
Table S3.2. Two-steps model. The following parameters K_{a1} , K_{a2} , $\Delta\delta_1 = \delta_{max\ 1} - \delta_0$, $\Delta\delta_2 = \delta_{max\ 2} - \delta_{max\ 1}$ and R^2 were obtained from the best fit of experimental data for compounds III-26 and III-28 using data sets which could not be described adequately by a single step model.....	154
Table S3.3. Single-step model. The following parameters K_a and $\Delta\delta = \delta_{max} - \delta_0$ were obtained from the best fit of experimental data for compounds III-18 and III-22.....	155
Table S3.4. Two-steps model. The following parameters K_{a1} , K_{a2} , $\Delta\delta_1 = \delta_{max\ 1} - \delta_0$ and $\Delta\delta_2 = \delta_{max\ 2} - \delta_{max\ 1}$ and R^2 were obtained from the best fit of the experimental data for compounds III-18 and III-22.....	155
Table 4.1. Anion transport rates, k_{Anion} , s^{-1} , turnover numbers per single liposome, n , s^{-1} , and permeability coefficients, P , $cm\ s^{-1}$	167
Table 4.2. Energetics of the anion transport in the presence of the compound III-25 in comparison with the transport “through” and “into” a pore of CFTR Cl^{-} channel.....	180
Table E1.1. Geometric parameters for urea and 1:1 Cl^{-} : urea complex.....	201

List of Figures

Figure 1.1. Schematic representation of the flux of solute A into the liposome.....	6
Figure 1.2. Phospholipid phosphatidylcholine (PC).....	9
Figure 1.3. Liposomes are self-assembled molecular containers composed of phospholipids. A. Electron microphotograph of the liposomes averaging 120 - 300 nm in diameter. The bilayer thickness is 3.0 nm. B. Schematic drawing of the transporter-mediated anion influx into the liposome.....	14
Figure 1.4. Schematic diagram of a voltage-clamp system.....	15
Figure 1.5. <i>p-tret</i> -butylcalix[n]arene esters I-2 that do not exhibit a channel-like behavior in the voltage clamp experiment and thought to act as cation-selective carriers.....	17
Figure 1.6. First synthetic ion channels that demonstrated Na ⁺ transport: multi-macrocyclic channel (I-3), and tri-macrocyclic “hydraphile” (I-4); bis-macrocyclic bola-amphiphile (I-6) and acyclic bola-amphiphile (I-7) reported by Fyles; “hydraphile” (I-5) and simple bola-amphiphile – <i>aplosspan</i> (I-8) reported by Gokel. <i>P</i> – permeability and <i>g</i> – conductance determined from the single channel measurements.....	20
Figure 1.7. Cyclodextrin-based channel (I-9) designed by Mary S. Gin and investigated using liposomal assays. The ion transport rates (<i>k</i> , s ⁻¹) were determined using HPTS-based assay and ²³ Na NMR. A transmembrane nanopores from porphyrin supramolecules (I-10) studied by Koubuke in planar bilayer (no classical open-close transitions were recorded).....	23
Figure 1.8. Crystal structure of the KscA K ⁺ channel protein.....	25
Figure 1.9. Examples of the synthetic Cl ⁻ anion transporters. Isophtalamide (I-9) was investigated in liposomes by Gale, Quesada, and our group in collaboration. The activity of “membrane-anchored” amphiphilic heptapeptide (I-10) was studied by Gokel in liposomes, planar bilayer, and in epithelia cells. Synthetic aminosterol (I-11), mimicking the natural product squalamine, was investigated by Regen using liposomes and bacteria cells.....	28
Figure 1.10. Electron micrograph of the Cyclopore membrane with latex beads on the surface.....	32
Figure 1.11. A Schematic representation of the content in the cuvette used for the fluorescence measurements. B Typical ion transport assays: base pulse assay (green) and no base pulse (blue).....	33
Figure 1.12. 1-hydroxypyrene-3,6,8-trisulphonate (HPTS).....	36

Figure 1.13. Absorption (pH 1, 7.64, and 13) and emission spectra (pH = 7) of HPTS in water.....	36
Figure 1.14. Structures of valinomycin (I-12) and calcimycin (I-13).....	40
Figure 1.15. Structures of SO_4^{2-} selective receptor I-14 and fragment of the crystal structure. Selectivity of I-14 was determined by means of competitive crystallization in the aqueous solution. Structures of Cl^- selective receptors I-15 and I-9; selectivity was determined by ^1H NMR titration and/or ITC in CD_3CN using $(\text{Bu})_4\text{N}^+ \text{X}^-$ ($\text{X}^- = \text{Cl}^-$, Br^- , I^-) as a source of anions.....	42
Figure 1.16. Structures of the compounds I-16 and I-17. Selectivity was determined spectroscopically using $(\text{Alk})_4\text{N}^+ \text{X}^-$ salts ($\text{X}^- = \text{Cl}^-$, Br^- , I^-) as a source of anions by fluorescence measurements (fluorescence of I-16 is quenched upon interaction with the anions) and by ^1H NMR titration (I-16 and I-17).....	44
Figure 1.17. Proposed structure of catechol - Cl^- anion complex I-18 $\cdots\text{Cl}^-$. General structure of bis-catechol-based anion receptors reported by Winstanley and Smith (I-19).....	50
Figure 1.18. Fragment of the crystal structure $(\text{Bu})_4\text{N}^+\text{Cl}^- \cdots \text{I-18}$	51
Figure 1.19. Structures of chlorocatechols (I-20), octylgallate (I-21), and 3,4-dihydroxy alkyl benzoates (I-22).....	52
Figure 1.20. Classical examples of urushiols (I-20) and resorcinolic lipids (I-21).	54
Figure 1.21. Structures of TRENAM (I-22), enterobactin (I-23), synthetic amphiphilic catecholates (I-24, I-25).....	57
Figure 1.22. Hypothetical catechol-based anion receptors A, B, and C.....	59
Figure 2.1. Catechol (II-1), N-methylbenzamide (II-2), acetanilide (II-3), 2-acetamidophenol (II-4), N-methylsalicylamide (II-5), and N1-[-(acetylamino)phenyl]acetamide (II-6).....	61
Figure 2.2. Dependence of the chemical shift for $\alpha\text{-CH}_2$ of $[(\text{Bu})_4\text{N}^+]$ on the fraction of receptors II-1 – II-6 in CDCl_3 solution. Total concentration in the solution is constant: $[\text{R}] + [(\text{Bu})_4\text{N}^+\text{Cl}^-] = 100 \text{ mM}$	71
Figure 2.3. Job Plots. Horizontal axes (x) are fractions of the receptors II-1, II-3, II-6 in the solution, while total concentration is constant $[(\text{Bu})_4\text{N}^+\text{Cl}^-] + [\text{R}] = 100 \text{ M}$. (A) Classical approach. Blue squares \blacksquare : dependence of δx , ppm on x, where δ is chemical shift of the acidic protons as indicated. Pink circles \bullet : dependence of $10\delta x$, ppm on x, where δ is chemical shift of $\alpha\text{-CH}_2$ of the salt $(\text{Bu})_4\text{N}^+\text{Cl}^-$. (B) Dependence of concentration of the complexed form of the receptors II-1, II-3, II-6 (blue rhombs \blacklozenge), obtained from the chemical shifts of the receptors' acidic protons as indicated, on x. Dependence of concentration of the complexed Cl^-	

anions (pink triangles \blacktriangle) in solution, obtained from the chemical shift of the salt, α -CH₂, on x. Solid lines indicate total concentration of the salt (pink ---) and receptors (blue ---) in solution.....74

Figure 2.4. Dilution experiment. The three samples that were diluted contained equimolar concentrations of the salt (Bu)₄N⁺Cl⁻ and receptors II-1, II-3, and II-6 in CDCl₃. Concentration of [R]_{complexed} was calculated from the chemical shift of the acidic protons. The concentration of Cl⁻ anion complexed by the receptor ([Cl⁻]_{complexed}) was calculated from the changes in chemical shift of α -CH₂ in the salt assuming [Cl⁻]_{complexed} = [(Bu)₄N⁺]_{free}.....76

Figure 2.5. Dilution experiment. The samples that were diluted did not contain the equal concentrations of the receptor and the salt but an excess of the receptor: [II-2] = 6*[(Bu)₄N⁺Cl⁻], M and [II-5] = 3*[(Bu)₄N⁺Cl⁻], M.....78

Figure 2.6. The ln K_d as a function of ionic strength $f(I) = 1/(1+d*\beta*I^{0.5})$, where I = [(Bu)₄N⁺]_{free} - ionic strength; $\beta = 1.33 \text{ M}^{-1/2} \text{ \AA}^{-1}$ - the Debye length; A d = 6.86 \AA - distance between ions in the ion pair (Bu)₄N⁺, Cl⁻; B d = 10 \AA - estimated distance between ions in the ion pair (Bu)₄N⁺, Cl⁻...II-1. The following solutions were diluted: II-1 - [II-1] = 2*[(Bu)₄N⁺Cl⁻] = 100 mM, II-2 - [II-2] = 6*[(Bu)₄N⁺Cl⁻] = 600 mM, II-3a - [II-3] = [(Bu)₄N⁺Cl⁻] = 600 mM, II-3b - [II-3] = 3*[(Bu)₄N⁺Cl⁻] = 600 mM, II-4 - [II-4] = 0.92*[(Bu)₄N⁺Cl⁻] = 128 mM, II-5 - [II-5] = 3*[(Bu)₄N⁺Cl⁻] = 105 mM, II-6 - [II-6] = [(Bu)₄N⁺Cl⁻] = 100 mM.....80

Figure 2.7. Anion binding by cyclic ∞ - shaped receptor in apolar media such as CDCl₃.....84

Figure 2.8. Examples of polyanionic guests and polycationic hosts studied in aqueous solution by Anslyn and colleagues.....85

Figure 2.9. A. Classical approach B. New approach developed by Gibson and co-workers. Figure B is taken from the abstract in the original publication.....86

Figure 2.10. Optimized lowest energy conformations for the free receptors II-1 – II-6 and corresponding complexes with Cl⁻ anion. Calculations were carried out using *ab initio* method, 6-31G* basis set, and HyperChem software.....89

Figure 2.11. Correlation between: ln K_{a 1:1} and ΔE_{elec} (a), ln K_{a 1:1} and pK_a (b).....90

Figure 2.12. Negative ion (A) and positive ion (B) mass spectra of CHCl₃ solution containing 5 mM of the salt (Bu)₄N⁺Cl⁻, 15 mM of catechol (II-1), 15 mM of acetanilide (II-3), and 15 mM of receptor II-6.....93

Figure 2.13. Negative-ion mass spectra of the solution containing 20 mM of the salt (Bu)₄N⁺Cl⁻ and 20 mM of H-bond donors II-1, II-3, and II-6.....95

- Figure 2.14.** Negative-ion clusters in CHCl_3 solution of $(\text{Bu})_4\text{N}^+\text{Cl}^-$ and catechol (II-1). Total concentration is $[(\text{Bu})_4\text{N}^+\text{Cl}^-] + [\text{R}] = 40 \text{ mM}$. The ratio salt : receptor changes from 7:1 to 1:7.....97
- Figure 2.15.** Schematic representation of interaction between $(\text{Bu})_4\text{N}^+\text{Cl}^-$ and H-donor in CHCl_3 . X is electronegative oxygen (O) or amide (N-COR group). Ion-paired aggregate formed on the first step dissociates when the second H-bonding unit coordinates to the Cl^- anion.....99
- Figure S2.1.** Dependence of chemical shifts, δ , ppm, of the receptor's acidic protons on concentration of the receptors II-1, II-3, and II-6 in CHCl_3 solution. Values of the chemical shifts of the free receptor (δ_0 , ppm), chemical shift of the dimer (δ_{max} , ppm), and association constants for the process of dimerization (K_a , M^{-1}), shown in the box, are derived from the experimental data points using curve fitting method as described. The generated best fit is indicated as a red solid curve.....102
- Figure S2.2.** Intramolecular H-bonds in the crystal structure of the receptor II-6.....103
- Figure S2.3.** Job Plots. Horizontal axes (x) are fractions of the II-2, II-4, and II-5, the total concentration in solution is constant $[(\text{Bu})_4\text{N}^+\text{Cl}^-] + [\text{R}] = 100 \text{ mM}$. (A) Classic approach. Blue squares \blacksquare : dependence of δx , ppm on x, where δ is chemical shift of the acidic protons as indicated. Pink circles \bullet : dependence of $10\delta x$, ppm on x, where δ is chemical shift of $\alpha\text{-CH}_2$ of the salt $(\text{Bu})_4\text{N}^+\text{Cl}^-$. (B) Dependence of concentration of the complexed form of receptors II-2, II-4, and II-5 (blue rhombs \blacklozenge) and concentration of complexed Cl^- anions (pink triangles \blacktriangle) in solution on x. Solid lines indicate total concentration of the salt (pink ---) and receptors (blue ---) in solution.....105
- Figure S2.4.** Positive- (A) and negative-ion (B and C) mass spectra of the CHCl_3 solution containing 40 mM $(\text{Bu})_4\text{N}^+\text{Cl}^-$. The flow rate of the nebulizing gas N_2 was lower in C than in B.....108
- Figure S2.5.** Negative-ion clusters in CHCl_3 solution of $(\text{Bu})_4\text{N}^+\text{Cl}^-$ and acetanilide (II-3). Total concentration is $[(\text{Bu})_4\text{N}^+\text{Cl}^-] + [\text{R}] = 40 \text{ mM}$. The ratio salt : receptor changes from 7:1 to 1:7.....110
- Figure S2.6.** Negative-ion clusters in CHCl_3 solution of $(\text{Bu})_4\text{N}^+\text{Cl}^-$ and receptor (II-6). Total concentration is $[(\text{Bu})_4\text{N}^+\text{Cl}^-] + [\text{R}] = 40 \text{ mM}$. The ratio salt : receptor changes from 7:1 to 1:3.....112
- Figure 3.1.** A – proposed anion binding mode; B - amphiphilic anion receptor and membrane transporter.....113
- Figure 3.2.** TRENAM (III-1); bis-catechol (III-2) obtained by Winstanley and Smith and proposed anion binding mode (III-2 $\cdots\text{Cl}^-$); catechol (III-3). K_a – anion binding constant obtained using ^1H NMR titration in CD_3CN using $(\text{Bu})_4\text{N}^+\text{Cl}^-$ as an anion source.....115

Figure 3.3. TREN based anion receptor III-4 reported by Smith <i>et al.</i> 1:1 complex with Cl ⁻ anion (III-5) formed in CD ₃ CN/DMSO mixture. Hypothesized 1:2 complex (III-6) formed upon interaction with two HCl molecules in the same solvent mixture.....	116
Figure 3.4. Syntheses of bis-catechols and methylated analogs.....	119
Figure 3.5. The downfield region of the ¹ H NMR spectra of the bis-catechol III-26. The assignment of the signal is based on the analogy to known compounds: natural product enterobactin (III-34) and its synthetic analog TRENbAlaCAM (III-33).....	120
Figure 3.6. TRENbAlaCAM (III-33) and reported assignment of the signals in the downfield region of the ¹ H NMR spectra recorded in DMSO-d ₆	121
Figure 3.7. Enterobactin (III-34) and the downfield region of the ¹ H NMR spectra recorded in DMSO-d ₆ . The spectrum is taken from the original publication....	121
Figure 3.8. Compounds employed to study relative affinity toward Cl ⁻ anion in DMSO-d ₆ . The signals, whose changes upon addition of the salt (Bu) ₄ N ⁺ Cl ⁻ were monitored to obtain the binding constants, are indicated as stars.....	123
Figure 3.9. Five sample spectra of ¹ H NMR titration of the compound III-26 in DMSO-d ₆ using (Bu) ₄ N ⁺ Cl ⁻ as a source of Cl ⁻ anions, [III-26] = 2.5 mM, [(Bu) ₄ N ⁺ Cl ⁻] = 0.023 to 1 M.....	125
Figure 3.10. Sample spectra of ¹ H NMR titration of III-28 in DMSO-d ₆ using (Bu) ₄ N ⁺ Cl ⁻ as a source of Cl ⁻ anions, [III-28] = 2.5 mM, [(Bu) ₄ N ⁺ Cl ⁻] = 0.016 to 1000 mM.....	126
Figure 3.11. Examples of the data sets from the ¹ H NMR titration (black squares) and the best curve fits of the experimental data (red lines) for compound III-26. 2-OH (✿) signal: two-step (A) vs single-step (B); N ⁺ H (✿) signal: two-step (C) versus single-step (D).....	129
Figure 3.12. Examples of the data sets from the ¹ H NMR titration (black squares) and the best curve fits of the experimental data (red lines) for compound III-26. Single-step (dd)CH (✿) and (1)NH (✿) signals; (2)NH (✿) signal: two-step (G) vs single-step (H); (d)CH (✿) signal: two-step (I) vs single-step (J).....	130
Figure 3.13. Schematic representation of the conformers optimized using AM1 method and HyperChem 7.0 software.....	132
Figure 3.14. Methylated analogs, III-18, III-22, III-29, and III-30, whose property to self-assemble has been evaluated in organic solution and in the crystalline state.....	134
Figure 3.15. Reversible formation of the organogel in CD ₃ CN in the presence of 5 mass % of III-22.....	136

Figure 3.16. ^1H NMR of receptor III-22 in CDCl_3 solution at concentrations: a) 250 mM and b) 4mM. Signals of the -NH- groups shift downfield in concentrated solution.....	138
Figure 3.17. ^1H NMR of III-18 in CDCl_3 at concentrations a) 250 mM and b) 4mM. Signals of the -NH- groups are shifted downfield in diluted as well as concentrated solutions.....	139
Figure 3.18. Dependence of the chemical shifts of the two amide signals in ^1H NMR of III-22 on concentration in CDCl_3 solution. The red curve is the best fit obtained using Origin 7.0 program and equation (S2.1) to model the dimerization.....	140
Figure 3.19. a) Intramolecular interactions in the receptors III-18, III-22, III-29, and III-30. b) One of the possible conformations of III-22 optimized by AM1 method using HyperChem software. c) The cross-section of hypothetical fiber formed by the assembly of III-22 in organic media.....	141
Figure 3.20. Fragment of the crystal lattice of compounds III-30. H-bonds are indicated by the dotted lines. Amide groups -NHCO- which are not involved in H-bonding interactions are marked yellow.....	143
Figure 3.21. One of the two unequivalent molecules in the crystal structure III-29. H-bonds are indicated by the dotted lines. CO and NH groups involved in intermolecular interactions are marked yellow.....	144
Figure 3.22. One of the two unequivalent molecules in the crystal structure III-29 which does not form intermolecular interactions. Intramolecular H-bonds are indicated by the dotted lines	144
Figure S3.1. Example of the experimental data set from the ^1H NMR titration experiment (blue squares) and best curve fits (red line) of the receptor III-26: d(CH) (✿) signal single step, 3-OH (✿) signal single step.....	147
Figure S3.2. Compound III-28.....	147
Figure S3.3. Examples of experimental data sets from the ^1H NMR titration experiment (black squares) and best curve fits (red line) for compound III-28. N^+H (✿) signal: two-step (A) vs single-step (B); (d)CH (✿) signal: two-step (C) vs single-step (D); two OH (✿) signals: single step (E, F).....	148
Figure S3.4. Dependence of the chemical shifts of the amide signals (NH) in compound III-30 on concentration in CDCl_3 solution. Red curve is the best fit obtained using Origin 7.0 program and equations (S2.1) to model the dimerization.....	156
Figure 4.1. Amphiphilic anion transporter III-25, analogs with different alkyl chain length (III-23 - III-26) and inactive structural analogs III-15 and III-27.....	158

Figure 4.2. Schematic representation of the anion transport assay (a). Intravesicular 100 mM NaNO ₃ , 10 mM phosphate pH = 6.4, extravesicular 75 mM Na ₂ SO ₄ , 10 mM phosphate pH = 7.5 [§] (b), pH = 6.3 (c and d). Solutions of the amphiphiles in MeOH were injected at $t = 25$ s (or just MeOH was injected in the case of blank), ratio PC : amphiphile = 10 : 1. Aqueous 10% Triton-X was injected at $t = 450$ or 500 s. [§] The extravesicular pH had to be basic to avoid precipitation and ensure solubility of the long-chain analog III-26.....	159
Figure 4.3. Anion transport assays. Extravesicular 100 mM Na ⁺ Anion ⁻ (Anion ⁻ = Cl ⁻ , Br ⁻ , NO ₃ ⁻ , I ⁻ , ClO ₄ ⁻) or 75 mM Na ₂ SO ₄ , 10 mM phosphate pH = 7.15. Intravesicular 10 mM phosphate pH = 5.5, a) 100 mM NaBr, b) 100 mM NaNO ₃ , c) 100 mM NaClO ₄ . Solution of III-25 in MeOH (or MeOH in the case of blank) was injected at $t = 25$ s, ratio PC : III-25 = 10 : 1. Aqueous 10% Triton-X was injected at $t = 1400$ s.....	162
Figure 4.4. Anion transport assay with intravesicular ClO ₄ ⁻ and set of electric circuit diagrams to represent mechanistics of the transport process.....	163
Figure 4.5. Anion transport assay. Extravesicular 100 mM Na ⁺ Anion ⁻ (Anion ⁻ = N ₃ ⁻ , Cl ⁻ , Br ⁻ , NO ₃ ⁻ , I ⁻ , ClO ₄ ⁻) or 75 mM Na ₂ SO ₄ , 10 mM phosphate pH = 7.15. Intravesicular 100 mM NaN ₃ , 10 mM phosphate pH = 6.4. Solution of III-25 in MeOH (or MeOH in the case of blank) was injected at $t = 25$ s, ratio PC : III-25 = 10 : 1; aqueous 10% Triton-X was injected at $t = 1400$ s. Electric circuit diagrams illustrating mechanistics of the ion transport process. 1 – extravesicular NaN ₃ ($t = 0 - 25$ s); 2a, 2b - extravesicular NaX (X ≠ N ₃) ($t = 0 - 25$ s); 3 – process following the injection of III-25 in MeOH at $t = 25$ s; 4 – endpoint of the ion transport: intra and extravesicular solutions are identical. There are two alternatives to consider: H ⁺ transport across phospholipid bilayer is rapid even in the absence of the amphiphile (2a) or there is no H ⁺ /charge transport/electric potential across phospholipid bilayer until III-25 is introduced into solution (2b).....	165
Figure 4.6. Mechanism of anion exchange in the N ₃ ⁻ -based assay.....	168
Figure 4.7. Influence of the electrical field on the anion transport rate in and out of the liposomes, $k_{Anion In}$ and $k_{Anion Out}$	169
Figure 4.8. Schematic representation of the Anion flux.....	169
Figure 4.9. Kinetic profile for a chemical reaction “A” → “C” proceeding through the formation of an intermediate “B”.....	171

Figure 4.10. Kinetic profile of anion exchange in the perchlorate – filled liposomes. $[\text{ClO}_4^-]_{In}$ – concentration of perchlorate anion in the liposomes. $[\text{Anion}]_{In}$ – concentration of the Anion ⁻ in the liposomes. $[\text{Anion}]_{Out} = 0.1 \text{ M} = \text{constant}$. $X(t) = 0.1 - [\text{ClO}_4^-]_{In} - [\text{Anion}]_{In}$	172
Figure 4.11. a) NO_3^- anion transport assay. Intravesicular 100 mM NaN_3 , 10 mM phosphate pH = 6.4. Extravesicular 100 mM Na_2SO_4 , 10 mM phosphate pH = 6.4. The combined data sets for two independent experiments. $[\text{PC}] = 0.585 \text{ mM}$. A solution of the amphiphile III-25 in MeOH was injected at $t = 25 \text{ s}$ (just MeOH (20 μl) was injected in the case of blank). Aqueous 10% Triton-X was injected at $t = 800 \text{ s}$. b) Dependence of NO_3^- anion transport rate on concentration of the amphiphile III-25.....	175
Figure 4.12. Schematic representation of the anion conducting aggregates and the processes that might take place in the solution.....	177
Figure 4.13. Permeation across phospholipid bilayer from the point of view of an anion: 1. Dehydration 2. Translocation.....	178
Figure 4.14. Energetics of permeation through CFTR ion channel Cl^- vs SCN^- , adapted from the reference 30	179
Figure 4.15. Schematic representation of the relations between thermodynamic parameters. Dashed colored arrows represent the hydration energy, ΔG_{Hydr} , for the anions Cl^- , Br^- , I^- . Dashed black arrows indicate the change in the hydration energy, $\Delta\Delta G_{Hydr}$, for a given pair of anions. Solid colored arrows represent “apparent hydration energies”, which are equal to the activation energy of the transport process, ΔG^\ddagger . Solid black arrows represent the change in activation energy for a given pair of anions, $\Delta\Delta G^\ddagger$. Solid red arrows represent “apparent change in hydration energy” - the difference between the hydration energy, ΔG_{Hydr} , and activation energy of transport (“apparent hydration energy”), ΔG^\ddagger , for a given anion.....	183
Figure 4.16. Energetics of the amphiphile-assisted anion transport Cl^- vs I^-	184
Figure 4.17. Synthetic targets: a, b, c.....	190
Figure 4.18. Cyclosteroidal receptors III-35 investigated by A. P. Davis. Compound III-36 as cyclic analog of the bis-catechol III-25.....	191
Figure 4.19. Hydrophobic siderophores.....	192
Figure 4.20. Biologically active quaternary ammonium compounds.....	193

Figure S4.1. Dependence of the Ratio and log Ratio on pH. Ratio refers to the ratio of HPTS fluorescence emissions at 510 nm (I_0/I_1), where I_0 is excitation at 460 nm (basic form of HPTS) and I_1 is excitation at 403 nm (acidic form of HPTS).....	194
Figure S4.2. pH as function of the emission intensities ratio x . Calibration data set (black squares) and best curve fit (red line) generated using Origin 7.0 program.....	195
Figure S4.3. Raw data of the Ratio on time dependence and obtained ion transport rates k_{Anion} , s^{-1} , turnover numbers and permeability coefficients.....	196
Figure S4.4. Curve fitting of the experimental data sets with the equation: $y = P1 - (P2 - P1) * (\exp(P3 * x) - 1) / \exp(P3 * x)$ (S4.2) where $x = t$ - independent variable, $y = \text{Ratio}$ - dependent variable, $P1 = \text{Ratio}_0$, $P2 = \text{Ratio}_\infty$, $P3 = k_{Anion}$ - parameters to obtain. Red line is the best fit obtained using Origin 7.0 program.....	197
Figure S4.5. Examples of the curve fitting of the experimental data sets using equation (S4.2) where x - independent variable, y - dependent variable, $P1$, $P2$, $P3$ - parameters to obtain. Red line is the best fit obtained using Origin 7.0 program.....	199
Figure S4.6. Dependence of the NO_3^- anion transport rate $k_{\text{NO}_3^-} = P3 - k_0$, s^{-1} on Concentration of the bis-catechol III-25. Two independent experiments a and b . ($k_0 = 0.00009 \text{ s}^{-1}$ - blank leakage at $[\text{III-25}] = 0 \text{ mM}$).....	200
Figure E1.1. Principle of the ion source (<i>picture taken from the instrument manual</i>).....	203

Chapter 1: Ion Transport from Nature to Material Science as Viewed Through the Lens of an Organic Chemist.

1.1. Introduction.

Ions are essential for life. Inorganic ions are the most simple and the most abundant in the natural world. They are known to form crystalline and amorphous solids and to exist as hydrated species in the aqueous solution, and as active intermediates in the atmosphere.

“It is generally thought that the first cellular organisms were formed by the enclosure of certain components of the “primeval soup” within a membrane that had to be impervious to macromolecules such as proteins and nucleic acids. Since the ionic composition of these first cells was, by definition, similar to that of the surrounding medium, the permeability of the membrane to ions was initially of little consequence. The adaptation of cells to survival in a variable environment with the accompanying need to regulate osmolarity meant that ionic concentration within the cells had to be maintained independently of external conditions. This required a membrane that formed a barrier to passive ion movement but contained specific mechanisms for the uptake or extrusion of the particular ionic species.”¹

During the course of evolution Nature developed ion channel proteins that function in biomembranes as regulated gates to allow selective passage of ions such as Na^+ , K^+ , Ca^{2+} , and Cl^- with the rates close to the diffusion limit. These ions exist in the aqueous media in abundance in their “free” form. In contrast, other physiologically important ions such as Fe^{3+} form a variety of minerals but are very rarely found in solutions due to their strong tendency to undergo hydrolysis as well as the low solubility of the salts and hydroxides. In the biologically relevant environment they are “never free” but always complexed. To initiate effective Fe^{3+} uptake, for instance, bacteria cells devised siderophores, low molecular weight water-soluble iron chelators that efficiently compete with the chelators found in the environment and even remove iron from the minerals.² In both cases (Fe^{3+} and K^+) selective recognition and binding within the channel membrane protein or by the low molecular weight ionophore/chelator in the aqueous media is the first step in the membrane transport event.

Being charged species, ions, by definition, strongly interact with each other. These interactions, however, are physical in nature and analytical solutions adequately describing the interactions between, for instance, K^+ and Cl^- ions in the aqueous media, as well as in the solid state, can be found. In contrast, selective ion recognition and binding by the natural or synthetic receptor/ionophore is a complex phenomenon. For instance, natural antibiotic valinomycin binds K^+ ion thousand(s) fold more strongly than Na^+ ions “simply because the oxygen cage is perfectly positioned for octahedral coordination of K^+ ion ($r = 1.33 \text{ \AA}$) but cannot collapse a little further to pack against a Na^+ ion ($r = 0.95 \text{ \AA}$)” due to a variety of electrical and

sterical constraints within the macrocycle.^{3,4} Therefore, such a rather “little task” as recognition of size and shape appears as a complex problem, which due to a lack of a simple analytical solution is described/understood using an empirical approach, inductive reasoning, analogy etc.⁵ In contrast to alkali and alkaline earth cations, biologically relevant inorganic anions such as NO_3^- , Cl^- , I^- , HCO_3^- , HSO_4^- , NO_2^- , HPO_4^{2-} , and etc. are far more diversified, coming in a variety of shapes and expressing different affinities towards protons/electrons and nucleophiles/electrophiles. Similar to anions, Fe^{3+} and cations of other transition metals are not just charged “featureless spheres” but have a unique structure of the valent electronic shell to be recognized by the selective ion receptor or membrane transporter. Again, the ion recognition is only the very first step leading to the even more complex event of selective transmembrane transport.

The goal of the first chapter is to introduce the selected key concepts of ion recognition and biomembrane transport, emphasizing the complexity of phenomena. It also includes a discussion of recent advances in the field of selective ion transport by the synthetic biomembrane active compounds. In the last part hydrophobic catechols are described as potential Cl^- anion transporter. The chapter does not aim to provide a comprehensive review of the subject matter, but rather focuses on the facts, concepts, and experiments that are most pertinent to this thesis. The views herein reflect only the opinions of the author.

1.2. Ion Transport across Phospholipid Bilayer: Selected General Considerations and Quantitative Descriptions.

1.2.1. **Ion passage across the bilayer membrane.** Regardless of the mechanism, the basic relation for uncharged solute permeation across phospholipid bilayer is the following⁶:

$$J = P \cdot \Delta C \quad (1.1)$$

where J , $\text{mol} \cdot \text{cm}^{-2} \cdot \text{s}^{-1}$ – transmembrane flux, P , $\text{cm} \cdot \text{s}^{-1}$ – permeability coefficient, ΔC , $\text{mol} \cdot \text{cm}^{-3}$ – concentration gradient across the membrane,

or in alternative form

$$dc/dt = k \cdot \Delta C \quad (1.2)$$

$$\tau = 1/k \quad (1.3)$$

where dc/dt , $M \cdot \text{s}^{-1}$ – rate, k , s^{-1} – rate constant and ΔC , M – concentration gradient across the membrane, τ , s – time constant.

In addition to the rate constant, k , s^{-1} , and permeability coefficient, P , $\text{cm} \cdot \text{s}^{-1}$, one can also define a turnover number, n , s^{-1} , as number of particles translocated across the bilayer per second.

In the case of the charged species, the rate and direction of the ion flows depends not only on the difference in solute concentration on both sides of the membrane but also on the charge difference across the membrane. The driving force for the diffusion of ions consists of two terms: chemical and electrical transmembrane potentials:

chemical *electrical*

$$\Delta G = RT \ln([C_{in}]/[C_{out}]) + zF\Psi \quad (1.4)$$

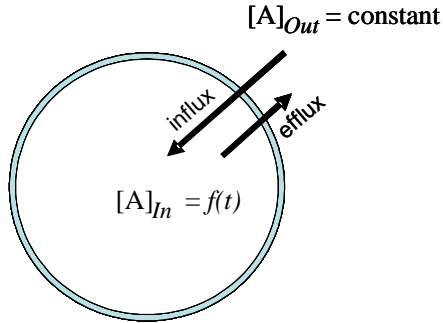
where ΔG – electrochemical potential, C_{in} and C_{out} – concentrations of the ion on two sides of the bilayer, z – ionic charge, T – temperature, R – gas constant, F – Faraday constant, Ψ – electrical membrane potential.

It is straightforward that an externally imposed electric field would change the position of the equilibrium. The fact that this electric field should also influence the kinetics (apparent rate constant) may not be as obvious.

Therefore, if the electrical component in the equation (1.4) is zero, kinetics can be simply described by the equation (1.1). Electrically-silent experiments, conducted in the absence of chemical gradients, can be designed by employing NMR shift reagents or radioactive isotopes. In turn, preestablished transmembrane electrical potential (Ψ) might either speed up ionic fluxes or slow them down depending on the charge of permeating species and direction of the ion flow. For instance, the “concentrative uptake assay”, discussed below, offers an example of transport driven by the electrical potential.⁷ This technique was developed to investigate activity of ion channels found in Nature.

It is useful to describe the kinetics of transport using an example to illustrate the relation between different parameters and meaning of the time constant (τ , s). For instance, let us consider permeation of an uncharged solute A into a small spherical container cell size (or smaller) (Figure 1.1). P_A , $cm*s^{-1}$ – is the membrane permeability of the solute A across the membrane. Initially, there is no A in the

container. In turn, concentration of A outside is a constant. Due to the fast diffusion rates and rather slow permeation of A, the solution inside of the container can be considered an ideal mixture at any given time. The dependence of the intravesicular concentration, $[A]_{In}$, on time, t , can be obtained as follows:



$$J_A = P_A * ([A]_{Out} - [A]_{In})$$

$$P_A = k_A * Volume / Surface Area$$

$$d[A]_{In} / dt = k_A * ([A]_{Out} - [A]_{In})$$

$$d[A]_{In} / ([A]_{Out} - [A]_{In}) = k_A * dt$$

Figure 1.1. Schematic representation of the flux of solute A into the liposome.

Integrating the left side of the equation from $[A]_{In} = 0$ to $[A]_{In} = [A]_t$ and the right side from $t = 0$ to $t = t$, the following expression for $f(t)$ is obtained:

$$[A]_t = f(t) = [A]_{Out} * (\exp(k_A * t) - 1) / \exp(k_A * t)$$

The time constant, τ , s for this process is defined as following: $\tau = t = 1/k_A$

$$[A]_t = f(\tau) = [A]_{Out} * (\exp(k_A * 1/k_A) - 1) / \exp(k_A * 1/k_A) = [A]_{Out} (e - 1)/e = [A]_{Out}$$

$$(2.72 - 1) / 2.72 = 0.63 * [A]_{Out}$$

Therefore, when $t = \tau$ concentration of A inside of the container is 63% of the outside concentration.

1.2.2. **“Unassisted” permeation of ions across phospholipid bilayer.** The present section is a short summary of the discussion on this subject published in the “Phospholipids handbook” edited by G. Cevc.⁶

At a glance, to get through the bilayer, ions must partition from the aqueous solution ($D_s = 78$) into the unpolar ($D_s = 2$) hydrocarbon core. By so doing, ions give up at least some of their waters of hydration. The high cost of dehydration is thought to be a primary determinant of the low permeability of ions and the ion selectivity of phospholipid bilayer. The experimental relative permeability of the alkali cations follows the expected trend $\text{Cs}^+ > \text{Rb}^+ > \text{K}^+ > \text{Na}^+$ (Table 1.1).

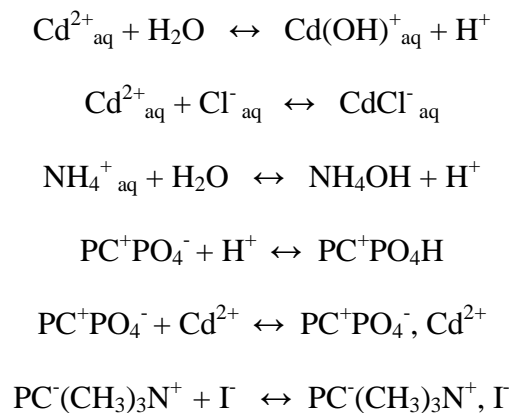
Table 1.1. Permeabilities of inorganic ions across fluid PC bilayers.

Cation	H^+	Na^+	K^+	Rb^+	Tl^+	Cd^{2+}
$P \cdot 10^9, \text{ cm s}^{-1}$	0.005 – 3	0.001	0.003	0.0033	0.004	0.003
Anion	Cl^-	Br^-	I^-	SCN^-	NO_3^-	
$P \cdot 10^9, \text{ cm s}^{-1}$	0.007	0.018	0.030	0.010	0.050	
“Silent”	H_2O	H^+/OH^-	HCl	TlCl	CdCl_2	HgCl_2
$P \cdot 10^9, \text{ cm s}^{-1}$	$4 \cdot 10^6$	1^\S $10^5 - 10^{6\S}$	0.015^\S 70^\S	110	4	10^7

[§] Two values differing by several orders of magnitude, for instance, H^+/OH^- , indicate that the experimentally observed permeability process is biphasic. The table is reproduced with slight changes from reference 1.

One could expect this trend to continue: Alkali Metal⁺ >> Ca²⁺ > Mg²⁺ >> Al³⁺. However, this is not the case. Measured permeability coefficients for divalent and trivalent ions are remarkably high and do not follow the trend than one might anticipate from the dependence on ion charge and size. For instance, Cd²⁺ is as permeable as K⁺ (Table 1.1).

The following events dramatically influence the ion permeabilities observed experimentally. First, the cations associate with negatively charged phospholipid head groups and this “lipid-ion complexation” follows an opposite selectivity sequence (multiply charged ions interact and bind stronger than singly charged). These “lipid-ion aggregates” increase the relative permeability of the bilayer toward multiply charged cations. Second, multiply charged cations can cross the bilayer in the form of electroneutral molecular complexes (or only singly charged aggregates) due to hydrolysis and increased affinity toward ions of opposite charge.⁶ One might consider the following equilibria as an illustration of the above-mentioned points:



where PC⁺PO₄⁻ and PC⁻(CH₃)₃N⁺ are two different schematic representations of phospholipid phosphatidylcholine (PC) (Figure 1.2).

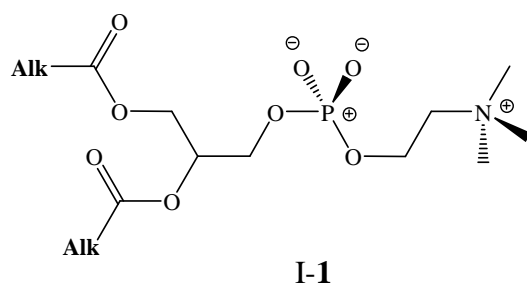


Figure 1.2. Phospholipid phosphatidylcholine (PC).

To determine permeability coefficients one can either measure loss of the ion of interest from liposomes or accumulation of permeating species inside of phospholipid vesicles. Radioactive tracers, NMR detectable isotopes, NMR shift reagents, ion-selective electrodes and fluorophores have been used for these studies. Conductivity measurements in planar phospholipid bilayer have been employed as an alternative to liposome-based methods.⁶

The most recent studies of the mechanism of ion permeation across phospholipid bilayer were conducted by Deamer, Volkov, Paula and their colleagues.⁸ The permeation of ions through phospholipid bilayer has been described using two alternative theories: transient pore and solubility-diffusion mechanisms. The first approach considers the ion transport as passage through the hydrated pores formed due to thermal fluctuation. The second describes permeation as partitioning into the hydrophobic core of the bilayer followed by the fast diffusion across the biomembrane. Two mechanisms/theories (solubility-diffusion versus pores) predict different dependence of the permeability coefficient on bilayer thickness: moderate

versus exponential.⁸ It is also consequential that the transient pore mechanism should better explain the transport phenomena for the “impermeable” solute, whereas the solubility-diffusion mechanism better describes permeation of the more hydrophobic species.⁸

Are the values in Table 1.1 unambiguously determined? Probably not. Thus, for instance, a study by Deamer *et al.* suggests that permeability coefficient for the proton is $P(\text{H}^+/\text{OH}^-) = 10^{-4} \text{ cm s}^{-1}$,^{8d} which is much higher than the values reported in Table 1.1.

1.2.3. Permeation of ions mediated by the prokaryotic K^+ ion channel found in Nature.^{3,7,9} Historically, two membrane systems have been used to study ion channels: planar bilayer and liposomes. Permeation of ions mediated by the natural proteins such as prokaryotic K^+ channel is close to the diffusion rates.⁹ Therefore, activity of a single channel protein can be recorded using electrical measurements. In turn, it becomes increasingly difficult to access the kinetics using liposomes and manual techniques. Due to extremely high turnovers, up to $n = 10^7$ ions per second, it takes milliseconds to equilibrate the intra and extravesicular solutions in a liposome containing a single functionally reconstituted membrane protein.⁹ Rapid-flux techniques with ms time resolution have been developed in an attempt to overcome this problem.⁹ Even in this case the time resolution may not be sufficient enough to measure flux of the most permeable ion of interest. The fluxes of rather “poorly” permeating ions, however, which are difficult or impossible to measure by the electrical methods, can be easily accessed using these techniques.⁹

An alternative, concentrative uptake assay described below offers a convenient time scale: minutes to hours.⁷ For instance, flux measurements under these conditions allow one to evaluate the function of the prokaryotic K⁺ ion channel reconstituted into liposomes using manual techniques.⁷ The experimental setup is the following: the liposomes loaded with concentrated KCl solution are diluted in low-KCl medium containing trace amount of ⁸⁶Rb⁺. (Permeabilities of K⁺ and the biologically irrelevant Rb⁺ through the K⁺ ion channel are almost identical.) Due to the imposed chemical gradients and high permeability of the proteoliposomes towards K⁺ ion, an interior negative electrical potential is set up across bilayer. The isotope tends to equilibrate with this potential and, therefore, accumulates in the liposomes at concentrations much higher than in an external medium. Since K⁺ and Rb⁺ are the only permeant ions, at equilibrium ⁸⁶Rb⁺ concentration ratio should be identical to that of K⁺:

$$[{}^{86}\text{Rb}^+]_{\text{in}}/[{}^{86}\text{Rb}^+]_{\text{out}} = \exp(-F\Psi/RT) = [\text{K}^+]_{\text{in}}/[\text{K}^+]_{\text{out}} \quad (1.5)$$

According to the literature, assuming simple ionic diffusion and constancy of external ⁸⁶Rb⁺ concentrations, the time constant, τ , for influx into a liposome of radius r , containing a single ion channel can be expressed as following:

$$\tau = 4\pi r^3 N_A [\text{K}^+]_{\text{in}} / 3k_{\text{Rb}^+} [\text{K}^+]_{\text{out}} = 4\pi r^3 N_A \exp(-F\Psi/RT) / 3k_{\text{Rb}^+} \quad (1.6)$$

where k_{Rb^+} , s⁻¹M⁻¹ – second-order rate constant,

$$\text{or } \tau = 4\pi r^3 N_A [{}^{86}\text{Rb}^+]_{\text{out}} \exp(-F\Psi/RT) / 3n_{\text{Rb}^+} \quad (1.7)$$

In this case the Rb^+ transport process happens on the time scale of several minutes to several hours, so that it becomes accessible to manual techniques. In the absence of the electrical potential, it would take several milliseconds to equilibrate concentration of the Rb^+ ion in the intra and extravesicular solutions. There are two reasons for the apparent low activity of K^+ channel in this assay. First, since $^{86}\text{Rb}^+$ concentration is extremely low, only $5\ \mu\text{M}$, the association of the channel with this ion and, therefore, turnover number, n_{Rb^+} , dramatically decrease: permeability of $^{86}\text{Rb}^+$ does not change but conductance of this ion vanishes ($n_{\text{Rb}^+} \ll 10^7$). Second, the electrical potential (Ψ) imposes the exponential factor ($\exp(-F\Psi/RT) = [\text{K}^+]_{\text{in}}/[\text{K}^+]_{\text{out}} \gg 1$) that also diminishes the rate/increases time constant.

Keeping in mind the key principle described above, different experiments can be carried out to assay the selectivity and blockage of the natural ion channels in liposomes using this concentrative uptake assay. The examples and experimental details can be found in the literature research articles published by C. Miller.⁷

1.2.4. Ion transport mediated by the natural and synthetic ionophores.^{10,11}

According to the definition given by Pressman: “Ionophores are compounds of moderate molecular weight (200 - 2000) that form lipid-soluble complexes with polar cations, which of K^+ , Na^+ , Mg^{2+} , Ca^{2+} and the biogenic amines are the most significant biologically”.¹¹ Interest in the determination of permeability and selectivity by ion flux measurements in the bilayer membranes dates back to the middle of the twentieth century and was largely driven by the discovery of natural and synthetic cationophores.¹⁰ These low molecular weight, easy-accessible

compounds were instantaneously recognized as unique biological tools. The systems utilized for these studies were the liposomes, red blood cells and cellular organelles such as chloroplasts and mitochondria.^{10,11}

Ion transport mediated by these “low-turnover” transporters (not as active as prokaryotic K^+ channel) have been studied in liposomes using manual techniques. In practice, one might expect to see the following picture. In the presence of a chemical gradient, initial movement of the relatively fast-permeating charged species should slow down in time due to the formation of the opposed transmembrane electrical potential, and subsequently become limited by the permeation rate of counterion (co-transport) or ion of the same charge (ion exchange). Therefore, one unavoidably encounters the problem of creating a stable ionic flux that is rate-limited by the translocation of the ion of interest.¹¹

At this point, it might be worth reviewing the basic features of the liposomes and flux assays. Liposomes are spherical vesicles with a membrane composed of a lipid bilayer that can be easily prepared and filled with the solutions of different compositions (Figure 1.3). Consider an ionophore-mediated uptake/release process in/out of the liposome with the time constant of minutes (translocation of the hydrated ion across the hydrophobic barrier is rate-determining). Due to the high rates of diffusion and small size of the vesicles, the intravesicular solution can be considered an ideal mixture during these transport events. It may be also useful to point out that, if equations (1.2) and (1.3) were used to describe this transport phenomenon, the extracted rate/time constants would be dependent on the size of the liposome. In

contrast, the flux equation (1.1) and permeability coefficient would be the same for the liposome of any size.

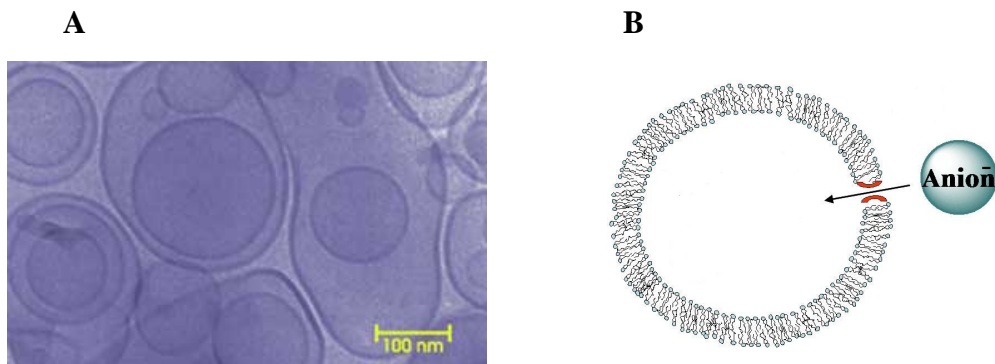


Figure 1.3. Liposomes are self-assembled molecular containers composed of phospholipids. **A.** Electron microphotograph of the liposomes averaging 120 - 300 nm in diameter. The bilayer thickness is 3.0 nm. (This image is reproduced from the web-source, reference^{12a}.) **B.** Schematic drawing of the transporter-mediated anion influx into the liposome.

A planar bilayer offers an attractive alternative for the kinetic measurements of the ionic flux. In this case we observe the electric current fluctuations resulting from the ionophore-mediated translocation of charged species across the bilayer, whereas the concentration of ions does not change during the recording process. The basic features of the voltage clamp experiment are briefly described below. As shown in Figure 1.4, there are two chambers connected through a 0.2 mm window of a planar bilayer. A solution of the ion transporter can be added into one of the

chambers, after formation of the bilayer. Alternatively, the “bilayer window” can be formed using a lipid-ionophore mixture. There are also two ways to access the relative permeability and selectivity data. One can either measure the relative conductance/current in the presence of the given ionophore and ionic compositions in the chambers or use the values of the reverse potential at zero current (or do both). The experimental and theoretical details, as well as many examples, can be found in the literature.^{4,10,11,13}

It is interesting to point out that by using estimates one can show that the surface area of the planar bilayer window that is 0.2 mm in diameter corresponds to the surface area of about four million (4,000,000) phospholipid spherules (liposomes) that are 0.1 μm in diameter, much smaller than the living cell.

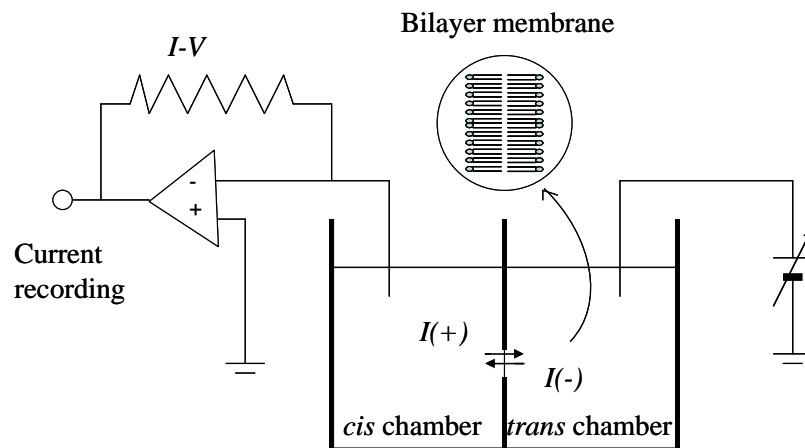


Figure 1.4. Schematic diagram of a voltage-clamp system, adapted from the reference 13a.

In addition, the voltage clamp experiment promised an opportunity to get insight into the mechanism of ion transport.¹¹ This technique was originally developed to study membrane proteins found in Nature. Due to its extreme sensitivity, the voltage clamp experiment allows recording of the pA current arising from the activity, for instance, of a single prokaryotic K⁺ channel ($n_{K^+} = 10^7 \text{ s}^{-1}$) reconstituted into the planar lipid bilayer. The “reading” of the K⁺ ion flow appears to be “rectangular”. Generally speaking, the channel functions in an all-or-none fashion: there is an electric current, when the channel is open, and there is no current when the channel is closed (unless there are more than one conducting states). Therefore, using this technique one can observe a diffusion-controlled permeation through a single membrane-spanning pore. To the first approximation, the diameter of the pore should be wide enough to allow passage of a “single ion flow”, with the rates close to diffusion limit and the life-time of the pore long enough to allow for a recording.¹⁴

In contrast to the K⁺ channel, other type of membrane proteins, such as the prokaryotic Cl⁻ channel-transporter, ClC-ec1, do not have a well-defined pore and do not show the opening-closing events either.^{15,16} The low turnover ($n_{Cl^-} = 4,000 \text{ s}^{-1}$ for ClC-ec1) presents a technical barrier preventing electrophysiological recording of a single membrane protein but “the macroscopic current arising from hundreds to thousands of ClC-ec1 may readily be observed”.¹⁶ Similarly, one might expect to be able to see the macroscopic current arising from a large number of prokaryotic K⁺ channels transporting “poorly” permeating ions, which are conducted with rates that are thousand times lower than the K⁺ ion.

Analogous to the natural transporters, the voltage clamp is used to access the activity of ionophores at low concentrations. The appearance of the electric current in all-or-none fashion was a criteria by which some researchers, at least initially, had distinguished the pore-forming compounds, such as gramicidin, from the classical natural or synthetic ionophores-carriers, such as valinomycin.¹¹ For instance, the *p-tert*-butyl calix[n]arene esters (I-2) are thought to act as cation selective carriers since no single-channel fluctuations occurred, but only the diminishing current level was detected in the voltage clamp experiment (Figure 1.5).^{13a} The permeability of Na⁺ ion by *p-tert*-butylcalix[4]arene ester (I-2) is more than 20 times that of any other alkali metal. This compound is offered by Aldrich as a Na⁺-selective ionophore.

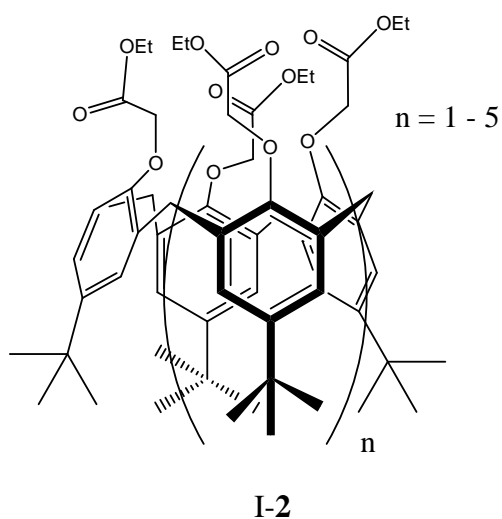


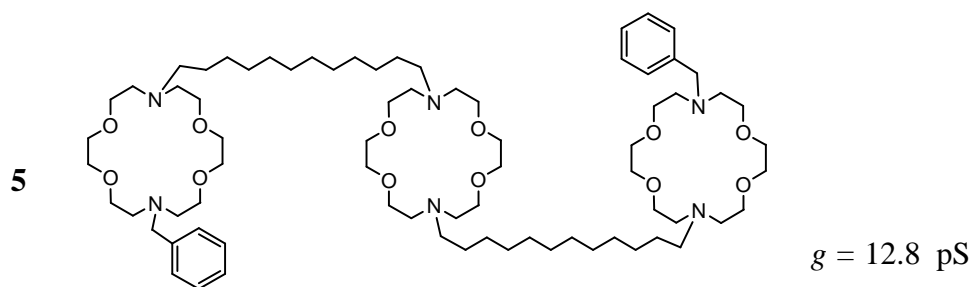
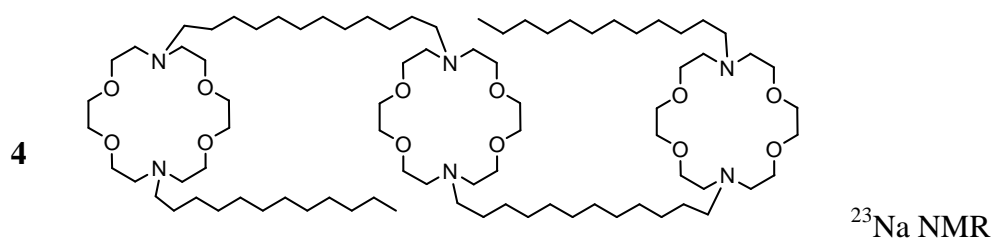
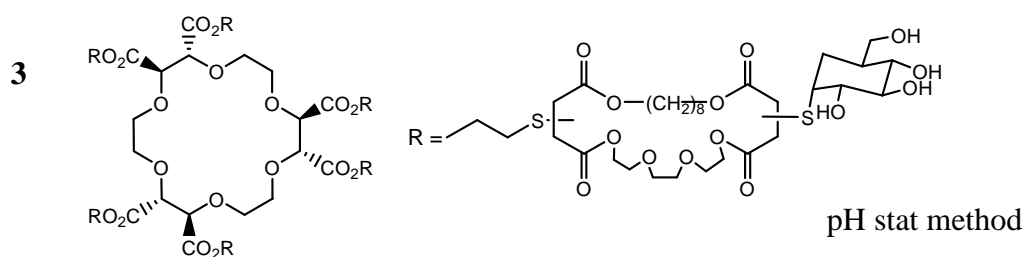
Figure 1.5. *p-tert*-butylcalix[n]arene esters I-2 that do not exhibit a channel-like behavior in the voltage clamp experiment and are thought to act as cation-selective carriers.

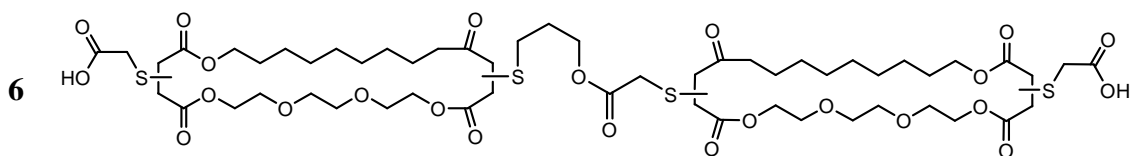
1.3. Synthetic and Natural Ion Channels and Transporters at Present.

1.3.1. **Introduction.** During the last several decades, interest towards biomembrane-active compounds has shifted from the classical cation-selective ionophores towards anion-selective transporters and the creation of synthetic ion channels. The 1998 Science paper by MacKinnon, where the crystal structure of K^+ channel was reported, probably became one of the most cited papers by supramolecular chemists.¹⁷ Extensive efforts were undertaken in organic labs to “mimic” structure and function of an ion channel in biomembranes, giving credit to the structural diversity and complexity of synthetic ion channels that have been reported in the literature. Among other reasons behind this scientific search is that in the long term, the non-natural systems are supposed to provide useful insights into the function of the ion channels and transporters found in Nature.

In turn, synthetic anion membrane transporters are of particular interest since there are no natural “anionophores” known to date that would fit the Pressman’s definition cited above. First of all, synthetic low molecular weight biomembrane transporters selective for anion(s) are envisioned to find application as potential antibiotics, medicines to treat anion channel disorders, such as cystic fibrosis, and novel tools in biomedical research of cellular transport. To this list one must add the classical areas for application of cationophores, which do not require speed as much as specificity, such as: active elements in anion sensors; extractants for environmentally important anions; phase transfer catalysts, etc.¹⁸

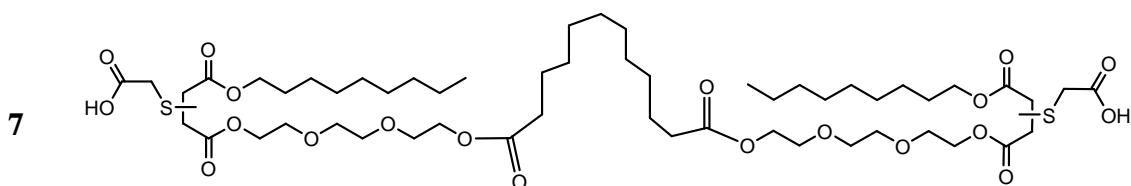
1.3.2. **Synthetic ion channels.** “First synthetic ion channels that demonstrated Na^+ transport were reported months apart by Fyles *et al.*¹⁹ (1989) and by Gokel *et al.*²⁰ (1990).”^{18f} Both structures, a rather complex multi-macrocyclic channel obtained by Fyles (I-3) and Gokel’s tri-macrocyclic “hydraphile” (I-4), were designed to “span” the bilayer (approximately 30 Å in length) and to be cation-selective (Figure 1.6). Although first reports did not contain the voltage clamp recordings, the following studies established that number of “hydraphiles”, such as (I-5), and bis-macrocyclic bola-amphiphile (I-6), a simplified analog of the original channel (I-3), indeed, exhibited a channel-like behavior in planar bilayer membranes: namely, the opening and closing states in all-or-none fashion: Fyles *et al.*²¹ (1996) and Gokel *et al.*²² (1997).



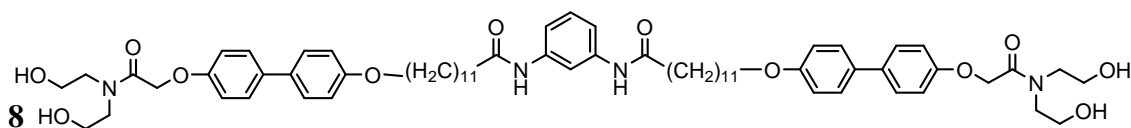


$$g(\text{KCl}) = 15.0 \text{ pS} \quad g(\text{CsCl}) = 29.3 \text{ pS} \quad g(\text{NaCl}) = 9.9 \text{ pS}$$

$$P(\text{K}^+)/P(\text{Cl}^-) = 25 \quad P(\text{Cs}^+)/P(\text{Na}^+) = 8.3 \quad P(\text{Cs}^+)/P(\text{K}^+) = 3.1$$



$$g = 13.7 \text{ pS}$$



$$g = 13 \text{ pS} \quad P(\text{K}^+)/P(\text{Cl}^-) = 2.3$$

Figure 1.6. First synthetic ion channels that demonstrated Na^+ transport: multi-macrocytic channel (I-3), and tri-macrocytic “hydraphile” (I-4); bis-macrocytic bola-amphiphile (I-6) and acyclic bola-amphiphile (I-7) reported by Fyles; “hydraphile” (I-5) and simple bola-amphiphile - *aplosspan* (I-8) reported by Gokel. P – permeability and g – conductance determined from the single channel measurements.

Biological studies revealed that “hydraphiles” are active against *E. coli* and the level of response depends on the structural modifications such as the length and the type of the linkers. In 2001 Fyles reported that channel-like behavior observed in the voltage clamp setup does not necessary require a macrocyclic ring: acyclic bola-amphiphile (I-7) retained the channel-like activity in the planar bilayer.²³

In the most recent report (2009) Gokel has shown that novel rather simple bola-amphiphiles (I-8) can form ion channels in the bilayer with the same level of conductance (13 pS) as the original “hydraphiles” (12.8 pS). He concluded that crown ether groups, while potentially beneficial, may not be necessary for (pS) transport function and suggested a new name *aplosspan* for this simple membrane-spanning structure that mediates ion fluxes across the phospholipid bilayer.²⁴

It was a remarkable observation that these newly designed compounds exhibited a channel-like behavior in the voltage clamp experiments, released cations from the liposomes and were cation-selective ion channels by rational design. These facts made them the first true synthetic analogs of the ion channels found in Nature. Notably, the crystal structure of the first K⁺ ion channel remained unknown until 1998. Although different compounds interact differently with the phospholipid bilayer, the detailed characterization and establishment of the structure-activity relationship are thought to be challenging and laborious to obtain.^{18d,18b,18f}

In turn, the ability of some “small” molecules to form channels with pS conductance and large pores with nS conductance due to self-assembly in the bilayer is intriguing. The structure-activity relations between size^{18g,18h, 25} and lifetime²⁵ of the pore and the structure of the assembly in the bilayer can be derived. These

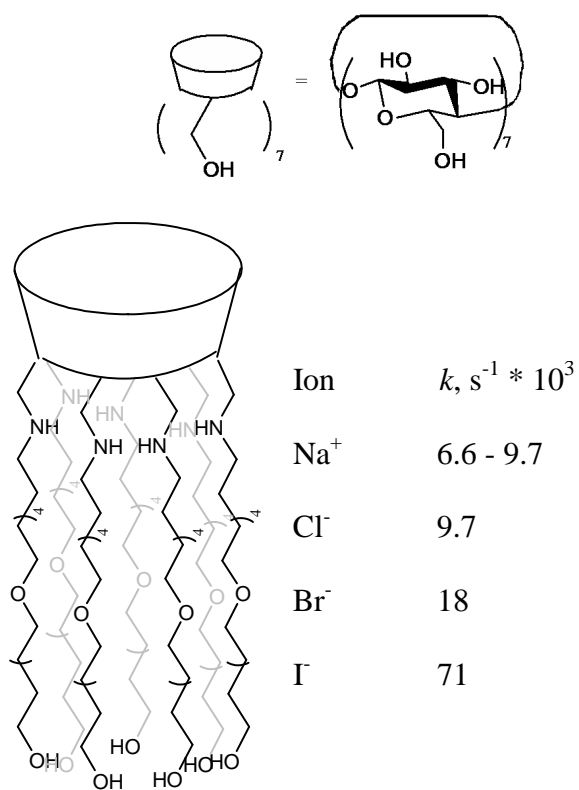
compounds contrast with *p-tert*-butylcalix[n]arene esters I-2, described as carriers, as well as the “bilayer-length” first synthetic ion channels depicted in Figure 1.6.

According to the definition given Fyles and Gokel, the bilayer voltage clamp “is the sole method to unequivocally establish the presence of channel activity”.²⁴ The broader definition of the synthetic ion channels was given by Matile: “...synthetic ion channels and pores are compounds with abiotic scaffold that act in the bilayer”.²⁶

Thus, the compounds which were not tested (or do not exhibit classical “open-close transitions”) in the voltage clamp but interact (do some interesting chemistry) with the phospholipid bilayer also fall under this definition. Synthetic ion channels investigated by Mary S. Gin in liposomes (I-9) and large nanopores studied by Kobuke in the planar bilayer (I-10) could be examples (Figure 1.7).^{27,28}

As an argument to support his definition of the ion channels Matile implies the fact that under the appropriate conditions the classical carrier valinomycin and certain detergents like Triton-X exhibit channel-like behavior, classical “open-close” transitions.^{18g,18h} However, the article, which Matile is referring to, is entitled “Valinomycin acts as a channel in ultrathin lipid membranes” and does not describe the case of the phospholipid bilayer but the monolayer composed of macrocyclic “ultrathin” bipolar lipid.^{13b} Probably, in this case rather large molecules of valinomycin exhibit a detergent like action due to very thin hydrophobic layer.

I-9



I-10

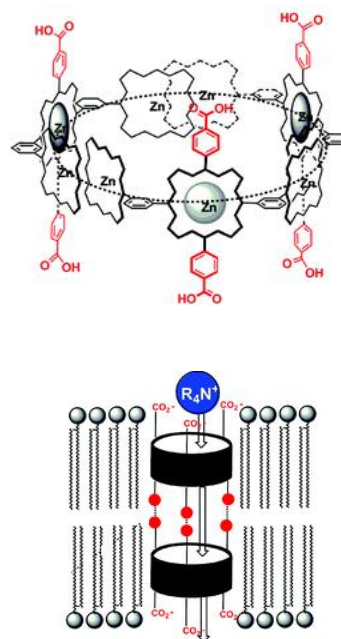


Figure 1.7. Cyclodextrin-based channel (I-9) designed by Mary S. Gin and investigated using liposomal assays. The ion transport rates (k, s^{-1}) were determined using HPTS-based assay and ^{23}Na NMR. A transmembrane nanopores from porphyrin supramolecules (I-10) studied by Kobuke in planar bilayer (no classical open-close transitions were recorded). (Image of the compound I-10 is reprinted from the original publications 28 with permission from the ACS)

1.3.3. Ion selectivity: K⁺ ion channel and Cystic Fibrosis Transmembrane Conductance Regulator (CFTR) versus synthetic ion channels. As mentioned earlier, the 1998 Science paper by MacKinnon, where the crystal structure of KscA K⁺ channel from *Streptomyces lividans* was reported,¹⁷ is often cited by organic chemists working in the field of synthetic ion channels. Therefore, it might be useful to highlight the unique transport property of this particular protein (Figure 1.8).

There is a well established principle that one must sacrifice speed to achieve specificity. Consider a conformationally flexible macrocycle that binds alkali cations in an aqueous solution at rates close to the diffusion limit and exhibits 10³ fold selectivity for K⁺ over Na⁺ upon binding. This selectivity gain is unavoidably transferred into the rate of ion release. This macrocycle would release K⁺ ion with the rate at least 10³ fold below the diffusion limit.^{3,18b}

Doing exactly otherwise, the KscA K⁺ channel lets K⁺ ions flow through the phospholipid bilayer with the speed of diffusion while excluding a smaller Na⁺ ion by a factor of 10³ - 10⁴: “By placing several ions close together inside the pore, the protein manages to lower the effective affinities of these ions via mutual destabilization. Thus, a K⁺ ion entering the pore binds with an affinity of ~ 3 μM when no other K⁺ ions are present inside the channel, but with affinity of ~ 0.1 M when other K⁺ ions already reside there”.³

Therefore, under physiological conditions, when both sites are readily occupied by the K⁺ ions (selectivity is preserved), a dramatic acceleration of the ion release from the pore is observed due to strong negative cooperativity of K⁺ binding.³ The third binding site in KscA K⁺ is not selective and can be occupied by both K⁺ and

Na^+ ions. In the cell this channel (current) is blocked by Na^+ ions from the cytoplasmic side.³

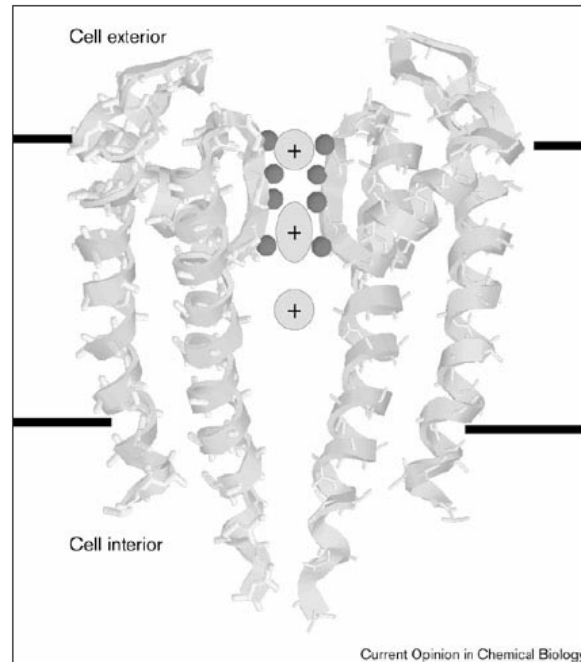


Figure 1.8. Crystal structure of the KscA K⁺ channel protein (This picture is reprinted from the original review 3 with the permission from Elsevier Ltd.)

Therefore, the strong binding of K⁺ ion by the channel and strong negative cooperativity of binding in two adjacent binding sites are the two reasons why K⁺ ions are selectively conducted through such a narrow pore (diameter of the selectivity filter is equivalent of diameter of bare, not hydrated, K⁺ ion) with the diffusion rates. From a different point of view, however, this protein is an excellent Na⁺ membrane transporter: single molecule of KscA K⁺ mediates Na⁺ flux with about the same rate

as the natural antibiotic valinomycin carrier mediates K^+ permeation ($n_K^+ = 10,000 s^{-1}$ for valinomycin¹¹).

Synthetic ion channels reported so far are not so particularly selective (see reference 22a and references in it). For instance, Fyles conducted extensive investigations using voltage clamp experiment and concluded that both conductance and reversal potential data indicate only modest discrimination between the ions in the following order $Cs^+ > K^+ > Na^+ > Cl^-$.^{22a} Notably, $Cs^+ > K^+ > Na^+$ order corresponds to the decreasing crystallographic ionic radii but increasing hydration energy. Maybe, one exception is the recent paper by Cragg whose synthetic ion channel conducts Na^+ in an “all-or-none fashion” while being inactive in the presence of K^+ in the voltage clamp.²⁹ With respect to selectivity, the pores, formed in the presence of the synthetic ion transporters, are more like the pore in CFTR than in KscA K^+ . At some approximation, this membrane protein forms an opening that is about 5 Å wide (wide enough to allow passage of the largely hydrated ions) and 50 Å long that result in conductance: 6 pS, experimental, or 14 pS, theoretical (obtained using Hill equation and given dimensions of the pore).³⁰ Anion channels are known to discriminate imperfectly between cations and anions. Making no exception, CFTR shows only 10-fold difference between Cl^- and Na^+ . Moreover, CFTR does not particularly discriminate among different anions either.³⁰ More details on conductance and permeability in the CFTR ion channel can be found in Chapter 4. It might also be worth noting that some natural anion-selective channels are known to become cation-selective mutants once the positively-charged arginines near the

cytoplasmic and extracellular ends are replaced with the negative-charged glutamic acids.³⁰

The modest discrimination but “reversed” selectivity pattern $\text{Li}^+ \gg \text{Na}^+ > \text{K}^+ > \text{Cs}^+$ for the cation-selective ($\text{K}^+ > \text{Cl}^-$) MOF-based synthetic ion channel (MOF - metal-organic framework) has been recently reported. The selectivity was determined using the reversal potential measurements.³¹ The detailed investigation that would explain this experimental observation is reported to be in progress. The relative permeability selectivity determined from the reversal potential measurements do not necessary correlate with the relative conductance.³¹ If it was shown that this channel conducts the cations across the bilayer in the same sequence by measuring the relative conductances, this would be a truly remarkable observation. Regarding the size of the channel pore authors implied the following “The corrected Hille diameter $d_{\text{Hille}} = 5.4 \text{ \AA}$ was obtained from the estimated conductance at 100 mM KCl, which is larger than the size of the triangular windows (3.8 Å) but smaller than that of the square windows (6.6 Å). This result seems to suggest that... (MOF-based synthetic ion channel) utilizes both windows as ion passages.”³¹

1.3.4. Synthetic anionophores today: goals and challenges. As G. W. Gokel defined in a recent review: “The goal of the organic, biological, or supramolecular chemist, thus, is to understand binding strength, binding dynamics, binding selectivity, transport selectivity and dynamics of chloride transporters”.^{18b} There is a list of synthetic compounds shown to facilitate anion passage across phospholipid bilayer. Particularly, recent efforts by the Matile, Regen, Gokel, A. P.

Davis, Gale, Sessler, Yang, B. Smith, and our groups should be highlighted. There are a number of excellent reviews on this subject that describe the most recent progress: new synthetic compounds as well as techniques/methods employed in this search.¹⁸

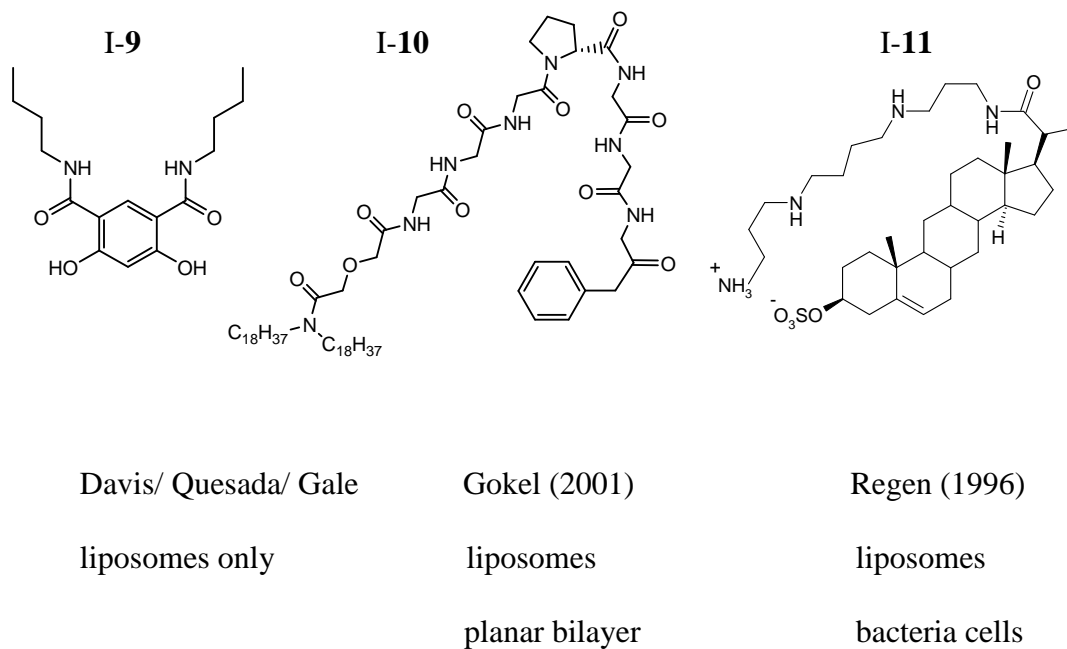


Figure 1.9. Examples of the synthetic Cl⁻ anion transporters. Isophthalamide (I-9) was investigated in liposomes by Gale, Quesada, and our group in collaboration.³² The activity of “membrane-anchored” amphiphilic heptapeptide (I-10) was studied by Gokel in liposomes, planar bilayer, and in epithelia cells.³⁴ Synthetic aminosterol (I-11), mimicking the natural product squalamine, was investigated by Regen using liposomes and bacteria cells.³³

At a glance, the anion transporters can be divided as following: 1) compounds shown to form anion-selective channels in the planar bilayer (classical “open-close” transitions); 2) compounds shown to transport Cl⁻ anion in liposomes; 3) compounds shown to do both; 4) compounds tested in the live cell cultures (Figure 1.9).¹⁸

In the voltage clamp experiment, probably, the best result was reported by Gokel in 2001 for the “membrane-anchored” amphiphilic heptapeptide (I-10) $P(\text{Cl}^-)/P(\text{K}^+) > 10$ (reversed potential measurements for the 1.3 nS single channel).^{34a,35} This compound was also shown to release Cl⁻ anion from the liposomes. It was implied that the time dependence of Cl⁻ anion release reflects the kinetics of the pore-activation (or channel formation) and that Cl⁻ anion efflux in liposomes happens rapidly.

In liposomes, determination of the ion selectivity is not as straightforward as in a planar bilayer. The direct measurement of the ion flux offers some advantages over the indirect measurements such as a pH-stat technique.²¹ Presumably, the ion transporter is considered to be Cl⁻ selective if it releases Cl⁻ anion from the liposomes (for example, by means of an anion exchange) and, if assayed, there is no Na⁺ release to be detected (using NMR or ion-selective electrodes). If it does both, one can say that the transporter is ion-selective for Na⁺ and Cl⁻ ions. In the recent review Gokel implied that the absence of the anion transport data for some synthetic ion transporters, such as “hydrophiles”, simply means that it was not assayed.^{18b,36}

In the recent paper Gokel (2008) suggested that the time dependences for the Na⁺ and Cl⁻ ion release (%) from the liposomes, obtained using ion selective electrodes, can be compared to make a conclusion regarding apparent selectivity.³⁶

He reported an observation that “the ionophore I-3, which has been intensively studied as a cation transporter, conducts Cl^- as well as it does Na^+ ”.³⁶ The structural modification (replacement of the central crown-based unit with the amide-based linker) alters the apparent rates of ion release and the apparent selectivity (Cl^- versus Na^+) observed in the liposomal assay. In the conclusion Gokel implies that interaction of the Cl^- and Na^+ ions with the transporter molecule(s) determines the selectivity of Cl^- and Na^+ release observed in the liposomal assay.³⁶ Regarding the mechanism of transport Gokel noted the following: “... once a conductance pore is formed, ion release occurs nearly instantly. Thus, we presume that the curves ... reflect a combination of insertion dynamic and conformational adjustment required to establish an appropriate conductance pathway.”

In 1996 the following explanation for the ion dependence of the transport rates observed in the liposomal assay in the case of bis-macrocyclic bolaamphiphiles (I-3) and its structural analogs was proposed by Fyles: “... the pH-stat experiment does not directly probe the ion translocation process. It simply probes the cation dependence of the initiation of a transport process that rapidly equilibrates each vesicle within a time of a single opening”.^{21a}

The efforts of Matile’s group to determine and compare the ion selectivity obtained from the liposomal assays using the pH sensitive dye HPTS and the ion selectivity obtained using voltage clamp are of particular interest.^{37,38} For a number of compounds studied Matile has established the following correlation: cation selective ion channels in the planar bilayer are cation-selective transporters in the liposomes, while anion-selective transporters are anion-selective channels.³⁸ The ion selectivity

in the planar bilayer was determined from the single-channel current or macroscopic current observed as a sum of single-channels with pS conductance.^{38b,38c}

Matile also made an attempt to compare the selectivity sequences obtained for the ions of the same charge and, indeed, correlations have also been established. "... permeability ratios ... confirm that the determination of anion selectivity under these conditions gives empirically correct sequence..."³⁸ The recent independent report also confirms the agreement between the data obtained using these two techniques for the MOF-based synthetic ion channel with pS conductance (MOF - metal-organic framework).³¹ These correlations, however, are based on a purely empirical observation and lack physical basis; therefore, they have to be accepted cautiously.

Therefore, in addition, to the fact that, at the present time, synthetic anion receptors are not as selective/specific as, for example, the crown ethers one must add another problem. Creation of the anion-selective or specific for certain anion transmembrane transporter meets another challenge with definition and experimental determination of selectivity in the membrane transport studies.

1.3.5. General picture of the HPTS-based liposomal assay. Although some researchers might disagree,^{39,18b} and say that "preparation of the liposomes is something of an art",^{18b} our experience tells us that liposomes are stable and very easy to prepare, once you learn how to do it, and there is no problem with reproducibility of the results. The liposomal assays, which employ a pH-sensitive dye HPTS, were applied as an alternative to the pH-stat technique that employs the pH-stat titrimeter.²¹ A general picture of the HPTS-based assay, used to evaluate the ion

transport activity and selectivity of synthetic transporters in liposomes, is discussed below.

Egg-yolk phosphatidylcholine (EYPC) is used to prepare large unilamellar vesicles 100 μm in diameter. This crude estimate of the “average” size is based on the diameter of the pores in the Cyclopore membrane used for the extrusion procedure (Figure 1.10).

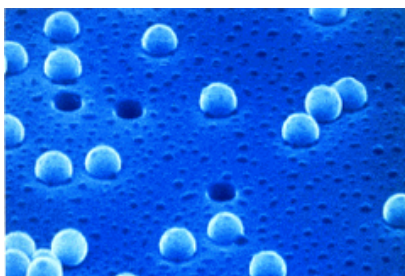


Figure 1.10. Electron micrograph of the Cyclopore membrane with latex beads on the surface. (This image is reprinted from the manufacturer web-site, reference 12b.)

A pH-sensitive dye, HPTS, can be incorporated into the liposomes. Extravesicular dye can be removed by means of the size-exclusion chromatography. The stock solution of liposomes contains 10 mM phosphate buffer and 100 mM salt MX (in and out of the vesicles). A very small aliquot of this solution is added into a cuvette containing 2 ml of 100 mM salt M_1X_1 in 10 mM phosphate buffer as it is schematically shown in Figure 1.11 A. Right after mixing, the cuvette is placed into a fluorimeter on the stirring mode. The fluorescence response due to encapsulated HPTS can be instantaneously recorded. This reading contains the following useful information: 1) the intravesicular pH (ratio) and the concentration of phospholipid

(intensity) are exactly what they were expected to be (or not); 2) the liposomes are “good” (not leaky in the presence of pH gradient).

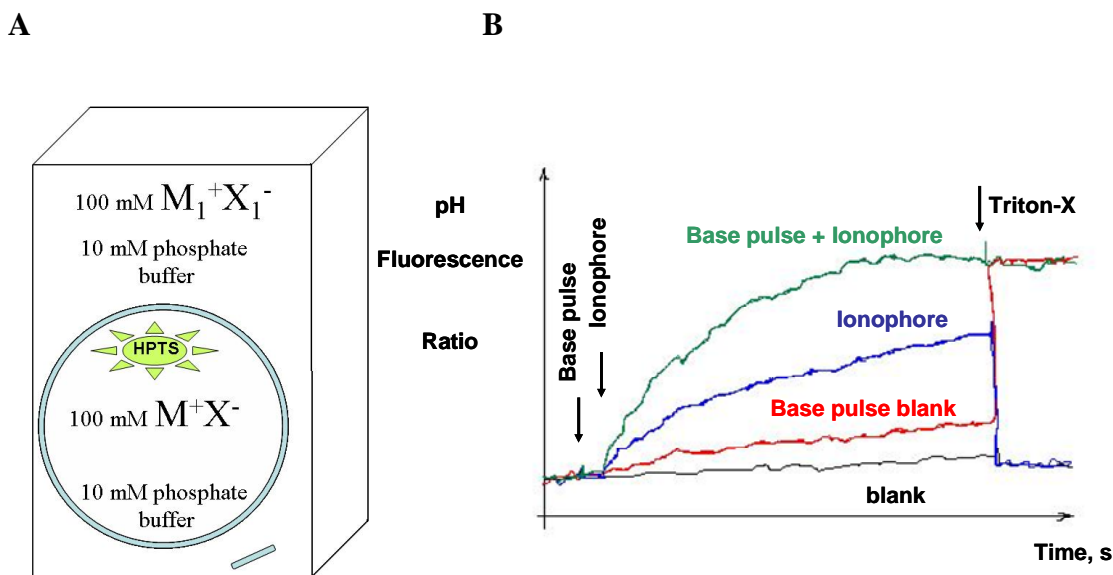


Figure 1.11. **A** Schematic representation of the content in the cuvette used for the fluorescence measurements. **B** Typical ion transport assays: base pulse assay (green) and no base pulse (blue).

Within the first 100 s after mixing a solution of the ionophore is added through the injection port (Figure 1.11 **B**). The “blank” experiment means that only the solvent was injected. The dependence of the HPTS fluorescence on time is recorded. At the end of the experiment, 10% aqueous Triton-X is added to lyse all the liposomes. As it is shown in Figure 1.11 **A**, there is an easy access to pH and electrolyte composition of the extravesicular solution. To change intravesicular content one would have to make new liposomes.

In the literature the most suggested way to evaluate ion selectivity is to do a base pulse assay.^{21,38,39,40} Upon addition of the base into the cuvette, the pH inside of the liposomes does not change instantaneously but instead slowly on the experimental time scale. The following injection of the ion transporter results in the rate increase. Depending on the electrolyte in the extravesicular solution the response/rate may be different. First of all, to qualitatively determine the ion selectivity sequences, an interpretation of the observed response has to be devised (for original interpretations of the base pulse assay see the following references: Matile³⁸, Regen^{33,40}, Fyles^{21,39}).

For instance, using multistep organic synthesis and advanced separation technique, Matile obtained families of compounds known as rigid rods, push-pull rodes, π -slides, π -stacks, artificial β -sheets.³⁸ To explain the dependence of the response on the nature of the extravesicular electrolyte in the base pulse assay for these ion transporters Matile implied the following “... results suggest that focus on antiport ($\text{Anion}^-/\text{OH}^-$ and $\text{H}^+/\text{Cation}^+$) without consideration of the osmotically disfavored symport ($\text{Anion}^-/\text{H}^+$ and $\text{OH}^-/\text{Cation}^+$) should be reasonable in most cases.”^{37,38a}

Several more recent reports from our group (2002, 2005, 2006, 2009)⁴¹ and from Matile (2007, 2008)^{42,43} indicate that to observe the pH change and give an original interpretation of the response one does not necessarily need to do a base pulse. The pH change might be driven only by the anion gradients when $X \neq X_1$ (where X and X_1 are intra and extravesicular anions as indicated in the Figure 1.11. **A**).

Technically, a very different HPTS-based experiment was carried out by Mary S. Gin (2005).²⁷ In this case the liposomes, as well as the extravesicular solutions contained the buffer (HEPES) and no electrolyte, while solutions of the different salts NaX were added through the injection port. The original qualitative and quantitative measures of the ion transport and selectivity in the presence of (I-7) were devised (Figure 1.7.) The rate of Na⁺ transport obtained from this HPTS-based assay was consistent with the rate determined by ²³Na NMR. More details of these experiments can be found in the original publication.²⁷ In a 2007 review Matile *et al.* gave the following summary of the findings: "...a ring of ammonium cations was positioned next to the cyclodextrin portal to select for anions. Despite these cations a highly facilitated Na⁺ flux ...was observed... However, a pH-sensitive dye assay was modified to show that (I-7) exhibited anion selectivity regarding transport rates across vesicle membranes (I⁻ > Br⁻ > Cl⁻). Cl⁻ and Na⁺ ions were transported at a similar rate".⁴⁴ It is unfortunate that since this original report no membrane active compounds have been evaluated using this original and promising approach devised by Mary S. Gin and her colleagues.

1.3.6. Properties of HPTS.⁴⁵ 1-hydroxypyrene-3,6,8-trisulfonate (HPTS) is a pH-sensitive fluorophore (Figure 1.12.) The protonated form of HPTS (absorbance max around 403 nm) and the conjugate base (absorbance max around 460 nm) have different absorption but exhibit one and the same emission spectra (Figure 1.13.). This is because the protonated form "may not have a chance to emit the light". HPTS is a photoacid: the pKa of the phenolic group decreases from 7.3 in the ground state

to 1.4 in the excited state and the proton is likely to be lost before the light is emitted. Thus, in both cases (excitation at 403 nm and 460 nm) emission of the same species, the phenolate, is observed.

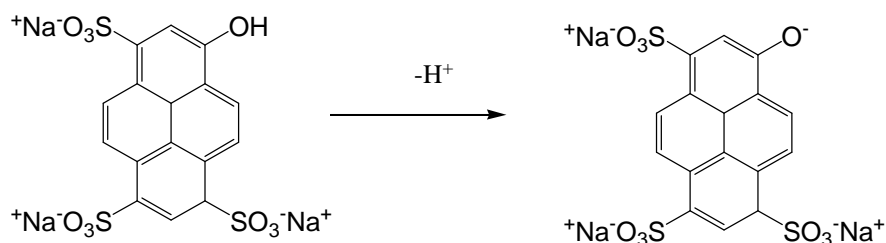


Figure 1.12. 1-hydroxypyrene-3,6,8-trisulfonate (HPTS).

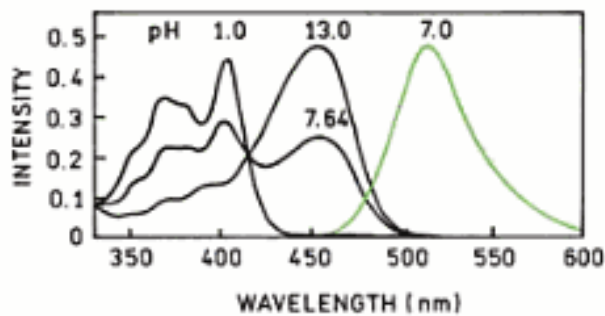


Figure 1.13. Absorption (pH 1, 7.64, and 13) and emission spectra (pH = 7) of HPTS in water. This image is reprinted from the on-line book preview, reference 45.

According to the standard procedure, the fluorescence of intravesicular HPTS is monitored by excitation at both 403 nm and 460 nm and recording the emission at 510 nm. The logarithm of the ratio of two emission intensities (log ratio) should have

a linear dependence on pH. The spectrum (Figure 1.13) might provide an explanation why the experimental dependence of pH on log ratio may not be a linear function at high pH. Apparently, this is due to the fact that the absorption spectra of the protonated form and the conjugate base are overlapping. Excitation at 403 nm in very basic solution (when the protonated form is no longer present) would unavoidably excite some electronic levels of the conjugate base with the maximum in absorbance around 460 nm.

“...phenol and tyrosine each show two emissions, the long-wavelength emission being favored by a high concentration of proton acceptors. The pK_a of the phenolic hydroxyl group decreases from 11 in the ground state to 4 in the excited state. Following excitation, the phenolic proton is lost to proton acceptors in the solution. Depending upon concentration of these acceptors, either the phenol or the phenolate emission may dominate the emission spectra... It seems any excited-state process will be dependent on the details of the local probe environment. Under most conditions excited-state ionization of HPTS is complete prior to emission, so that only the phenolate emission is observed.”⁴⁵ At high pH we also observed a slight dependence of the ratio on the nature of electrolyte in aqueous solution (100 mM NaNO_3 versus 75 mM Na_2SO_4). It is not clear, however, if the observation was due to the different “reading” of pH-sensitive electrode or if there is an electrolyte-dependent change in the emission spectra.

1.3.7. A broad and complex definition of the ion selectivity. At a glance, the ion-selective receptor is a small organic molecule (or aggregate of molecules) that

discriminates between ions. To study ion selectivity one needs to measure a difference in response generated upon interaction of the receptor with different ions. This response/selectivity depends on the technique that is employed and the type of interaction that is studied; for instance, binding or fluorescence properties or membrane transport. At a glance, the anion selective membrane transporter could be a lipophilic compound that selectively and reversibly binds the anion. The ion selectivity, however, is not an intrinsic property of the ionophore but can change upon interaction with the environment as illustrated by the examples below.

The interaction of crown ethers and natural ionophore valinomycin (**I-12**) with alkali metals is a classic example of selective binding. In addition, valinomycin has evolved to selectively and efficiently transport K^+ ion across biological membranes. Furthermore, this natural product has been successfully employed as a carrier in the ion selective electrode (ISE). In the latter case the ionophore is dissolved in the polymer supported liquid membrane and the response/selectivity is generated when the equilibrium is established between organic and aqueous phases. Notably, selected crown ethers are a better match for this purpose: the devices based on synthetic compounds discriminate better between K^+ and Na^+ ions than the one based on the natural product.⁴⁶ In this case the kinetics of the ion exchange between organic and aqueous phases should be fast enough to generate a stable (not kinetic) response but it does not necessarily have to be “as fast as possible.”

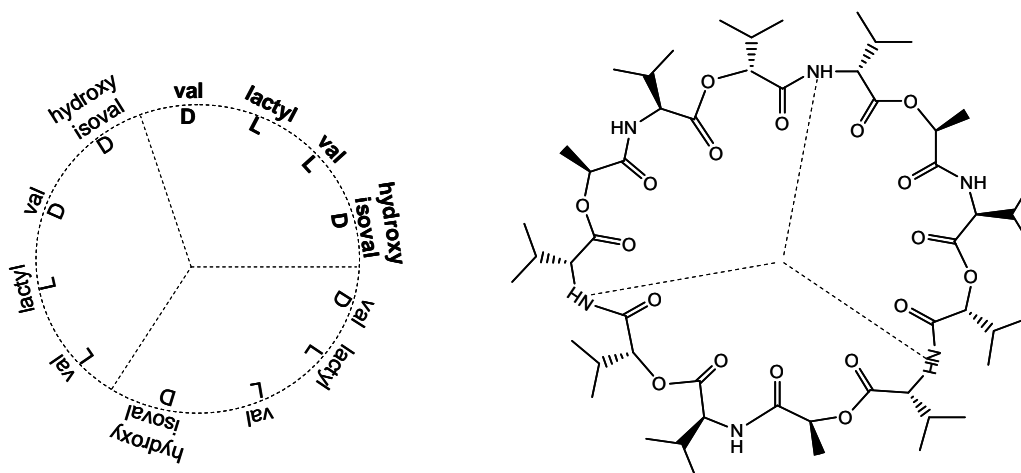
Another natural antibiotic, calcimycin (A23187) (**I-13**), transports alkaline earth cations but not the alkali cations across biological membranes. This ionophore contains a carboxylic group which is deprotonated upon formation of a dimeric

electroneutral complex which has been crystallized with Ca^{2+} , Mg^{2+} , Fe^{2+} and other dications. The relative complex stabilities determined by the organic phase extraction technique are $\text{Mn}^{2+} \gg \text{Ca}^{2+} \approx \text{Mg}^{2+} \gg \text{Sr}^{2+} > \text{Ba}^{2+}$.⁴⁷ Once incorporated as a carrier into the ISE, the reported selectivity, however, was found to be in the contrasting order: $\text{Ba}^{2+} > \text{Sr}^{2+} > \text{Ca}^{2+} > \text{Mg}^{2+}$.^{47,48} It was suggested that in the later case calcimycin acts rather as a neutral carrier than as an anionic species. “A neutral carrier mechanism for the ISE membranes with low concentration of anionic sites and at the fairly low pH of unbuffered sample solutions, on the other hand, and dissociation of the carboxylic group of A23187 followed by $\text{H}^+/\text{Mg}^{2+}$ exchange in the extraction experiments, on the other hand, are likely explanations for these findings.”⁴⁷

Valinomycin is a 12-membered cyclic depsipeptide produced by *Streptomyces* strains. It is composed of alternating amino and hydroxy acids in both L- and D-configurations. The macrocyclic ring contains amino and ester groups.^{4,10} Valinomycin was discovered in 1959.¹⁰ The fact that valinomycin-induced uncoupling of oxidative phosphorylation in mitochondria was related to the uptake of K^+ ion was established by Pressman and Moore in 1964.¹⁰ The mechanism, through which it worked, however, remained unclear. Thus, for instance, it was initially suggested that valinomycin might be an activator of certain membrane transporter.^{10,11} The chemical structure of this natural product was established by Shemyakin and co-workers and confirmed by synthesis in 1965 (USSR).^{4,11} (Notably, the crown ethers were discovered by Pedersen only two years later in 1967.) It was a

remarkable observation that among a variety of isolated natural and synthetic ionophores, selective for monovalent cations and known at that time, only valinomycin was able to strongly discriminate between K^+ and Na^+ ions.^{4,11} To get insight into the nature of the ion selectivity and the chemistry behind this property of the macrocyclic ring, Ovchinnikov and co-workers synthesized 85 analogs of valinomycin and performed physicochemical studies of these compounds.^{4,11} The book “Membrane-active complexones” was published in 1974. The Institute of Bioorganic Chemistry in Moscow was named after Shemyakin and Ovchinnikov.

I-12



I-13

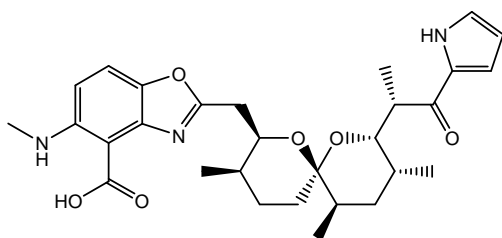


Figure 1.14. Structures of valinomycin (I-12) and calcimycin (I-13).

An interesting example is the SO_4^{2-} -selective receptor reported recently by Custelcean, Hay and Moyer.^{49,50} Separation of SO_4^{2-} from the aqueous solution containing mixtures of different salts is an environmentally important problem. These authors imply that specific recognition of the charge, size, and tetrahedral geometry of SO_4^{2-} anion was achieved by the means of deliberate, computer-aided design of the new receptors; the crystallized metal-organic frameworks are “highly shape specific” (I-14).^{50,51}

In Nature specific binding/recognition is thought to be achieved by utilizing the following general principle: upon interaction with the substrate or beforehand the binding event, the receptor creates a cavity and the “perfect fit” where all the possible interactions, electrostatic, H-bonding, van der Waals, are optimized. A little mismatch arising from the slight difference in geometry, charge, ionic radii, etc. of the substrate is transduced into a large loss in the free energy of binding, arising and amplified due to the steric, electrostatic and other constraints in the receptor molecule. In the case of interaction between the ion and the ionophore (either a small receptor molecule or an ion-binding protein) in aqueous solution the experimentally observed selectivity is primarily due to the small differences between two large effects: the difference in the hydration energies and the difference in the ion binding by the receptor molecule.⁴⁶

In the paper by Custelcean *et al.* the authors report the selective recognition of SO_4^{2-} anion achieved by the TREN-based receptor in the solid state (I-14).^{50,51} In a solution of MSO_4 the ionophore gives rise to the crystals with NaCl topology. The crystals do not grow in the presence of M_2SO_4 or MX where $\text{X} = \text{ClO}_4, \text{NO}_3$, etc. The isostructural lattice with MX is too weak to be formed due to large distances between

only singly charged ions. The isostructural crystals are, however, formed in the presence of CO_3^{2-} and SO_3^{2-} anions, which have a very different geometry. The whole metal-organic framework/ crystal lattice with M^{2+} centers plays a role of selective “anionophore”.

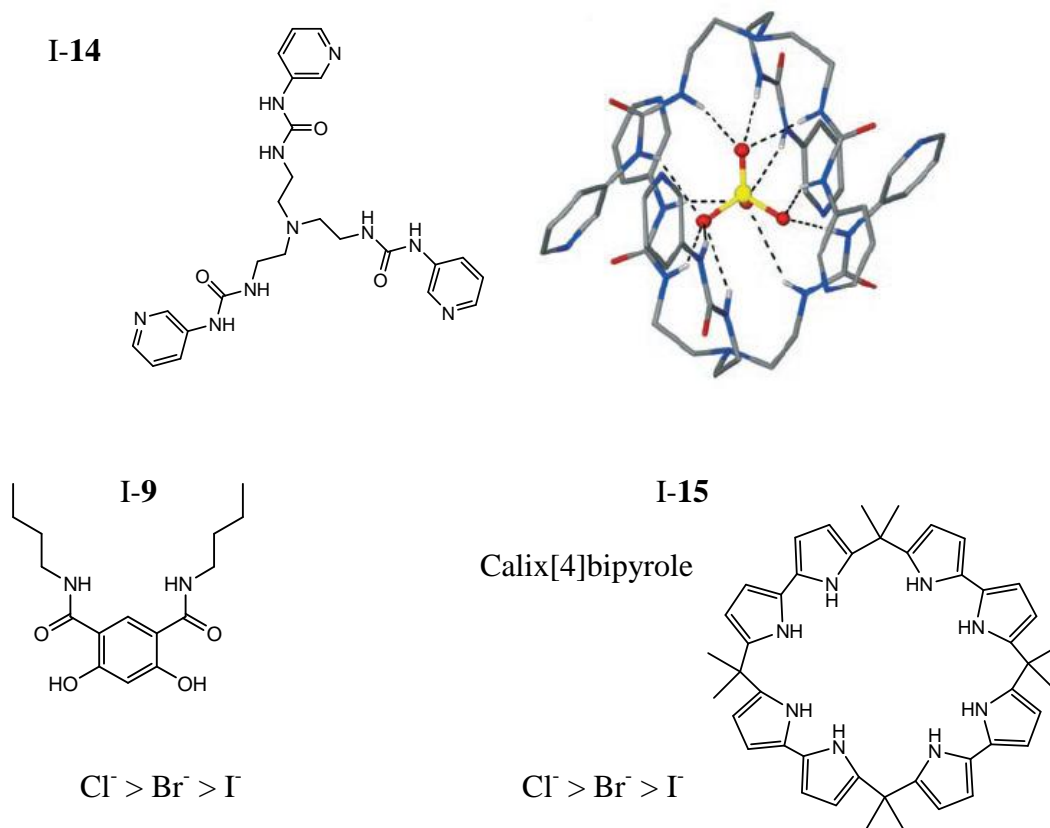


Figure 1.15. Structures of SO_4^{2-} selective receptor **I-14** and fragment of the crystal structure (reproduced from the original publication 50 with permission from the ACS). Selectivity of **I-14** was determined by means of competitive crystallization in the aqueous solution. Structures of Cl^- selective receptors **I-15** and **I-9**; selectivity was determined by ^1H NMR titration and/or ITC in CD_3CN using $(\text{Bu})_4\text{N}^+ \text{X}^-$ ($\text{X}^- = \text{Cl}^-, \text{Br}^-, \text{I}^-$) as a source of anions.

The authors imply that selectivity observed in the competitive crystallization experiment $\text{SO}_4^{2-} > \text{SeO}_4^{2-} > \text{CO}_3^{2-} > \text{SO}_3^{2-}$ does not perfectly correlate with the hydration energies (and with the gas phase proton affinities (PA) for these anions as an equivalent). In contrast, this order reflects/correlates with selectivity as an “intrinsic” property for the receptor (lattice) - anion interaction obtained using the lattice energy calculations (DFT method) and the experimental X-ray data (results of these calculations are not provided). One must argue, however, that by definition the experimentally observed selectivity (if crystallization is, indeed, thermodynamically controlled) must reflect the differences between hydration energy of the anion and the energy of the anion – lattice interaction but not the latter only. As a sum of two effects the experimentally observed selectivity ($\text{SO}_4^{2-} > \text{SeO}_4^{2-} > \text{CO}_3^{2-} > \text{SO}_3^{2-}$) might arise in the case when the “intrinsic binding affinity” changes in the different order, for instance, $\text{CO}_3^{2-} > \text{SO}_3^{2-} > \text{SO}_4^{2-} > \text{SeO}_4^{2-}$ (which better correlates with the PA values and, therefore, might be more reasonable) due to higher hydration for CO_3^{2-} and SO_3^{2-} anions than for the SO_4^{2-} anion. Therefore, to prove the recognition of the anion shape in the aqueous solution, one must solve a different problem: to design a receptor which is selective for CO_3^{2-} or SO_3^{2-} anions in the presence SO_4^{2-} anion.

It is interesting to compare previous example of the recognition in the aqueous solution with the classical anion binding using small organic molecules in solvents with low dielectric constants. Interaction with ionophores is usually studied using ^1H NMR titration and alkylammonium salts as a source of anions in CH_2Cl_2 , CHCl_3 and CH_3CN . In contrast to crystallization that requires complete dehydration of the anion,

in this case the energy of solvation is lower and upon interaction only part of the solvation shell to be replaced with the stronger H-bond donor groups.

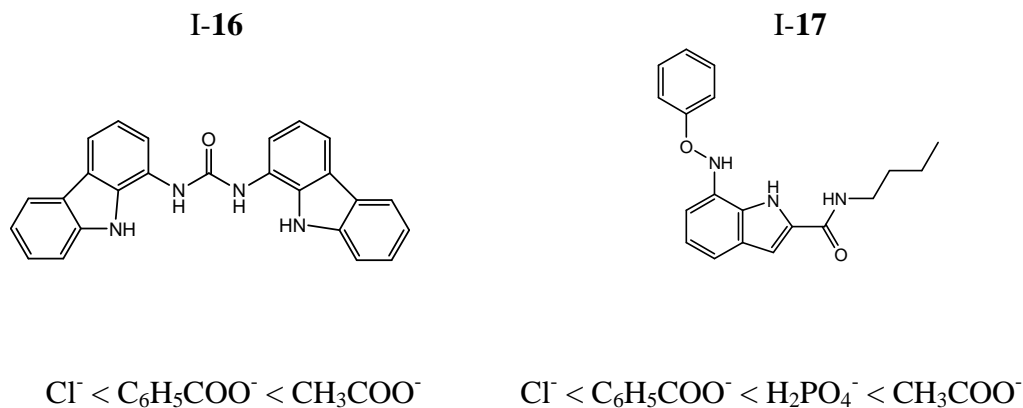


Figure 1.16. Structures of the compounds **I-16** and **I-17**. Selectivity was determined spectroscopically using $(\text{Alk})_4\text{N}^+ \text{X}^-$ salts ($\text{X}^- = \text{Cl}^-, \text{Br}^-, \text{I}^-$) as a source of anions by fluorescence measurements (fluorescence of **I-16** is quenched upon interaction with the anions) and by ^1H NMR titration (**I-16** and **I-17**).

Therefore, the following trend is often observed $\text{Cl}^- > \text{Br}^- > \text{I}^-$. In this case the receptor selectively discriminates between anions and the “intrinsic” affinity of the receptor towards anion (not solvent-anion interaction) to determine the experimentally observed trend. For instance, receptor **I-15**⁵² and **I-9** are selective for Cl^- anion over other halides.

Two cases of anion recognition discussed above illustrate that apparent selectivity of the anion binding might depend on the solvents and does not necessarily correlate with the intrinsic binding affinity of the receptor towards different anions.

In this respect it is interesting to compare the receptors shown in Figure 1.14 with the carbazole and indole based anion receptors **I-16** and receptor **I-17**.⁵³ When investigated in DMSO (0.5% H₂O) as a solvent these compounds exhibited selectivity for oxoanions over Cl⁻. This is likely that in the conditions of the experiment Cl⁻ remains strongly hydrated, while other anions tested do not (or remain hydrated to a lesser extent). Thus, water molecules prefer to interact with each other rather than with the more hydrophobic anions. In turn, the anion receptor binds hydrophobic anions stronger than hydrated chloride.

Another interesting example is the Br⁻-selective rotaxane reported very recently by Beer's group.⁵⁴ In a 1:1 CDCl₃/MeOH solvent mixture this compound has stronger affinity towards Br⁻ than Cl⁻ anion. The difference between the binding constants obtained is an order of magnitude. In contrast, a variety of structurally similar compounds described in the literature are selective for chloride over bromide anion in the same solvent mixture.⁵⁴ This results probably indicates that the cavity afforded by this rotaxane is, indeed, a better match for the Br⁻ anion than the cavity provided by these other compounds. Nevertheless, these experimental observations do not necessarily indicate the selectivity of this rotaxane for Br⁻ over Cl⁻ in terms of intrinsic affinities towards these two anion. To prove selective recognition of the Br⁻, this anion has to be compared with the weaker solvated I⁻.

At a glance, selective anion recognition by means of neutral supramolecular organic receptor appears to be more difficult to achieve than the well studied recognition of the alkali cations. Giving this fact, one might think of the reasons that

stay behind this experimental observation. For instance, being anionic species, by definition, halides are not as “hard” as the isoelectronic cations of alkali metals.

1.3.8. Liposomes as a tool to obtain structural information about the membrane-active ion-conducting complex. A common question is whether the synthetic ion transporter functions as a single molecule or the activity observed requires aggregation of individual molecules within the biomembrane. There are a number of liposomal assays involving ion-sensitive dyes and NMR shift reagents that have been employed to serve this purpose. To determine degree of aggregation one should study the dependence of the transport rate on concentration of the transporter. In the literature, research articles and reviews, the physical picture behind these experiments is often missing or obscured. Apparently, there are two similar but different models that have been used to analyze the observed dependence. First one is related to the case of the channel, when formation of the pore, which instantaneously “equilibrates” intra and extra vesicular solutions, presumably, is the rate-limiting step (Gokel^{18b,34}). Another one describes the case of ionophores-carriers or membrane disruptors when permeation of the ions across hydrophobic barrier is the rate-determining and, presumably, there is no channel mechanism to be involved (Regen^{55a,55b}). In the original publication Regen noticed that sterol-polyamine conjugates are not expected to form pores in the voltage clamp setup since observed ion fluxes in liposomes are slow. Nevertheless, these synthetic conjugates were also defined as synthetic ion channels in “Encyclopedia of supramolecular chemistry”.³⁴ Probably, the most comprehensive description of the liposomes as a tool to obtain the

structural information about ion-conducting complex can be found in the studies published by Regen.^{55a,55b} Some key points of this technique, relevant to the subject of this thesis, are revised below.

Since this section is not devoted to the ion selectivity, let us, for instance, assume the most simple case. In the presence of some hypothetical ionophore in aqueous solution the experimentally recorded rate of Na⁺ influx into the liposomes is, indeed, the rate-limiting process. Studying the dependence of the rate on concentration and implying the following relations:

$$\text{Rate} = k_{\text{obs}} [\text{ion}] \quad (1.8)$$

$$k_{\text{obs}} = k [\text{pore}] \quad (1.9)$$

$$K = [\text{pore}] / [\text{ionophore}]^n \quad (1.10)$$

$$k_{\text{obs}} = k K [\text{ionophore}]^n \quad (1.11)$$

one can, presumably, find the exact number of molecules within a membrane-conducting complex (n).⁵⁵ There is, however, a certain model that this approach (equations (1.8 – 1.11)) relies on, and that is useful to keep in mind.

1. First of all, we assume that there is an equilibrium between the ionophore in the lipid and aqueous phases that establishes instantaneously upon addition of the ionophore into the liposomal solution. Thus, concentration of the active form, ion-conducting complex, does not change over time and ion permeation is the rate-limiting step during.

An argument that this might be the case is the relatively large values of the permeability coefficients for the small molecules reported in the literature, for instance: $P(\text{acetic acid}) = 5.0 - 6.9 \cdot 10^{-3} \text{ cm s}^{-1}$, $P(\text{methylamine}) = 8.0 \cdot 10^{-2} \text{ cm s}^{-1}$, $P(\text{acetamide}) = 1.7 - 2.9 \cdot 10^{-4} \text{ cm s}^{-1}$.⁵⁶ (Examples of neutral inorganic compounds can be found in the Table 1.1., the lowest row.) Using the definition of the time constant (τ) one can determine that the influx of these molecules ($P = 10^{-4} \text{ cm s}^{-1}$) into the 100 μm vesicle happens on a millisecond time scale:

$$\tau = 1/k \quad (1.3)$$

$$P = k \cdot V/A = k \cdot r_{\text{liposome}} / 3 \quad (1.12)$$

where V – volume of the liposome, A – surface area of the liposome,

$$\text{thus } \tau = 1/k = r_{\text{liposome}} / (3 \cdot P) = 0.5 \cdot 10^{-5} / (3 \cdot 10^{-4}) = 0.017 \text{ s.}$$

Therefore, intra and extra vesicular solutions as well as concentration of the compound in the lipid phase should equilibrate on the ms time scale following the injection of a solution of the small molecule.

There is, however, a recent report from the Fyles group suggesting that at least in some cases, the concentration of the ionophore/synthetic ion channel in the lipid phase might change over time.³⁹ Thus, processes defined as partitioning into the bilayer or “pore-opening” become rate-limiting. In that particular case, studied by Fyles, the ionophoretic compound was also shown to have a strong tendency to aggregate in the aqueous phase and form micelles.³⁹

Another relevant example is membrane-active “molecular umbrella” compounds investigated by Regen *et al.* These molecules are derived from a polyamine and several units of the cholic acid. At a glance the “molecular umbrella” is a conjugate of several more simple facial amphiphiles. The experimentally determined rate of the efflux from the “molecular umbrella”-loaded liposomes determined by equilibrium dialysis is very low: it takes hours to achieve equilibrium between lipid and aqueous phases. The permeability coefficients of these conjugates are only about $P \approx 10^{-11} \text{ cm s}^{-1}$. This value is similar to the permeability of inorganic ions.^{55c} ($P \approx 10^{-11} \text{ cm s}^{-1}$ was obtained using equation (1.12) and reported rates of the efflux, $k \approx 0.01 \text{ h}^{-1}$, from 200 μm liposomes^{55c}) These “molecular umbrella” compounds were also recently shown to exhibit some ionophoretic activity.^{55c}

2. Second, the ionophore does not aggregate in the aqueous but only in the “organic” phase. One should expect to see diminished transport rates and apparent value of n due to formation of micelles or micelle-like aggregates.

To show that the amphiphilic compound does not aggregate in the aqueous phase, for instance, Regen provided evidence that he worked in the concentration range below the CMC (critical micelle concentration) of the ionophore. Thus, this technique is based on a negative hypothesis/statement (2) which, by definition, is challenging to prove.

3. If the rate constant were extracted using definition of the initial rates the experimental data should look adequate: concentration of Na^+ ion inside of the liposomes has to be a linear dependence on time (the value of the initial rate should not depend on the time interval where it was determined).

1.4. Amphiphilic Catechols as Potential Anion Receptors and Membrane Transporters.

It is probably safe to say that the majority of anion transporters described in the literature are rich in amide functionalities -NH-CO- .¹⁸ These groups are employed to bind anions as well as to drive self-assembly of the receptor within phospholipid bilayers. In recent reports Winstanley and Smith uncovered catechol (**I-18**) as an anion binding motif exhibiting a selectivity of $\text{Cl}^- > \text{Br}^- > \text{I}^-$.^{57,58,59} Compared to simple amide-based receptors, the affinity of **I-18** toward anions is enhanced, which is consistent with the stronger H-bond donor ability of phenol.⁵⁷ In one of Winstanley and Smith's papers ten new bis-catechol-based receptors (**I-19**) that bind Cl^- anion in organic solvents were described.⁵⁹

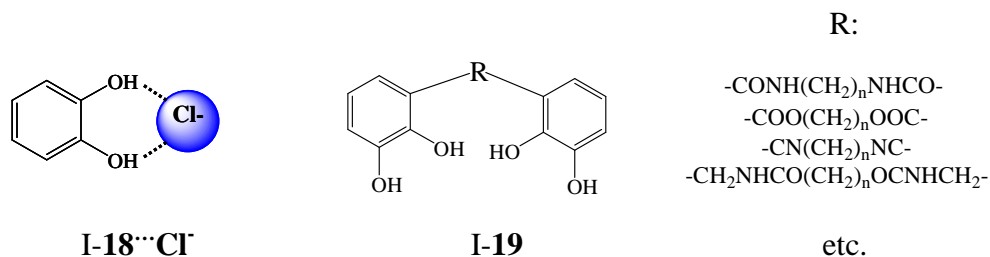


Figure 1.17. Proposed structure of catechol - Cl^- anion complex **I-18**··· Cl^- . General structure of bis-catechol-based anion receptors reported by Winstanley and Smith (**I-19**).

According to the authors, however, CD_3CN solution of $(\text{Bu})_4\text{N}^+\text{Cl}^-$ and catechol contain only a 1:1 complex and only one compound in this series of 10 bis-catechols exhibited an increased affinity towards Cl^- when compared to the monomer **I-18**. Even in this single case, however, the increased Cl^- affinity is due to an increase in effective molarity due to the presence of two catechol units in the molecule that resulted in the doubled value of the binding constant rather than from the “cooperativity”.^{57,59} Reported by McInnes and co-workers in 1985, the crystal structure of $(\text{Bu})_4\text{N}^+\text{Cl}^- \cdots \text{I-18}$ consists of a discrete catechol-halide anion, $\text{Cl}^- \cdots \text{I-18}$, and an alkylammonium cation (Figure 1.17.).⁶⁰ The two H-bonds between catechol and the Cl^- anion in $\text{Cl}^- \cdots \text{I-18}$ are equal. Based on the crystallographic data these authors concluded that catechol forms stronger H-bonding with Cl^- than Br^- anion in the isostructural complex, $(\text{Bu})_4\text{N}^+\text{Br}^- \cdots \text{I-18}$.

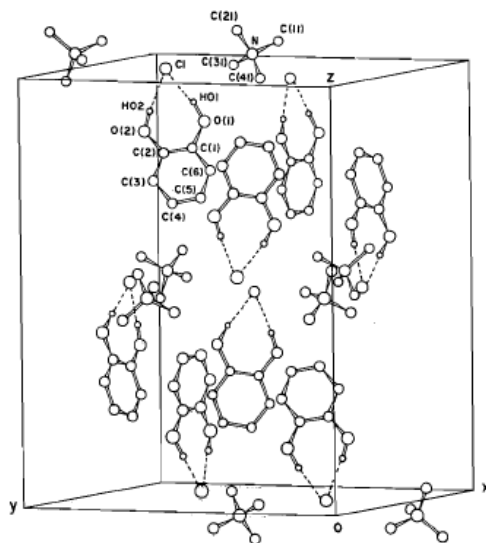


Figure 1.18. Fragment of the crystal structure $(\text{Bu})_4\text{N}^+\text{Cl}^- \cdots \text{I-18}$. Reproduced from the reference 60 by permission from RNC Research Press.

The distances $O^{\cdots}Cl^-$ are at the lower end of the range of the reported literature values, while the $O^{\cdots}Br^-$ distances are in the normal range. As described below and in the following chapters, we decided to use the catechol group to serve as the basis for a transmembrane anion transporter.

Importantly, in contrast with the amide group $-NH-CO-$, which is rather chemically inert at physiological conditions, catechols are often biologically active. As a consequence of their red-ox and metal-complexation properties, different chemical reactions can be initiated by catechols with biomolecules such as DNA, proteins, and phospholipids. In turn, non-covalent interactions are employed by phenols to target biological membranes.⁶¹ Before discussing their anion binding properties some general aspects of these “supramolecular” properties of catechols are discussed below.

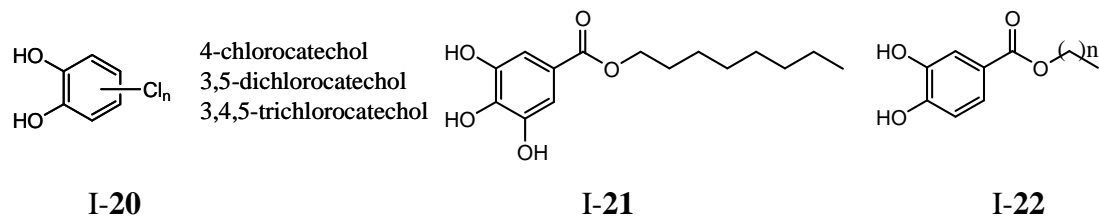


Figure 1.19. Structures of chlorocatechols (I-20), octylgallate (I-21), and 3,4-dihydroxy alkyl benzoates (I-22).

Rather simple weakly acidic (chloro-)catechols (I-20) function as transmembrane H^+ carriers and uncouple electron transport from ATP synthesis in living cells. The protonophoric activity of I-20 increases with degree of chlorination.^{61,62} In turn, lipophilic long-chain catechols can act as nonionic surface-

active agents that nonspecifically disrupt the integrity of cytoplasmic membranes and induce leakage of intracellular content.⁶³

For instance, octylgallate (I-21) is a food additive that expresses a broad spectrum of antimicrobial properties. Structure-activity studies established that its biocidal properties are retained if the catechol moiety is preserved. The antimicrobial activity of alkylgallates and 3,4-dihydroxybenzoates (I-22) is a reversed parabolic function of the length of the alkyl chain, with the maximum between C₈-C₁₂. This dependence on chain length for I-22 is considered to be due to a combination of: 1) its ability to act as a proton carrier so as to inhibit electron transport in energy transducing membranes; and 2) its ability to disrupt the integrity of biomembranes as a nonspecific surface-active agent.⁶³

It is noteworthy that a similar parabolic dependence of activity on the length of the hydrophobic chain or molecular weight was observed for long-chain alcohols, phenols, and quaternary ammonium compounds as well as amphiphile-based antimicrobial polymers.^{64,65,66} Different aggregation behavior of long- and short-chain amphiphiles was suggested as one of the possible explanations for structure-activity relationship.^{65,66} The sequence of events that are thought to lead to cell death under the exposure to such surface-active agents is the following: 1) adsorption on the cell surface; 2) diffusion through the cell wall; 3) adsorption onto the cytoplasmic membrane; 4) critical disruption of the cytoplasmic membrane; 5) leakage of intracellular content; and 6) cell death. This process is monitored by using living cell cultures and such methods as broth dilution, bioluminescence, leakage assays and etc.⁶⁶

Polyphenolic lipids are examples of natural products that are active in biomembranes.^{67,68} Urushiols (I-23) are *n*-alkenyl and alkyl-substituted catechols that are responsible for poison ivy and poison oak dermatitis.⁶⁷ Their allergenic activity depends on the side chain and activity increases with alkyl chain unsaturation.^{67,68} Similarly, some lipophilic resorcinoids (I-24) also induce dermatitis whose severity increases with unsaturation.⁶⁸ Although, allergenicity of these natural products is not attributed to the phenolic moiety directly, but rather its oxidation products (o-quinones), the dependence of activity on the alkyl-chain points toward the importance of interactions with the cell membrane in manifesting the biological effects of these catechols.⁶⁸ Presumably, improved solubility of unsaturated analogs in aqueous media increases their efficiency in partitioning into phospholipid bilayers.^{68,69}

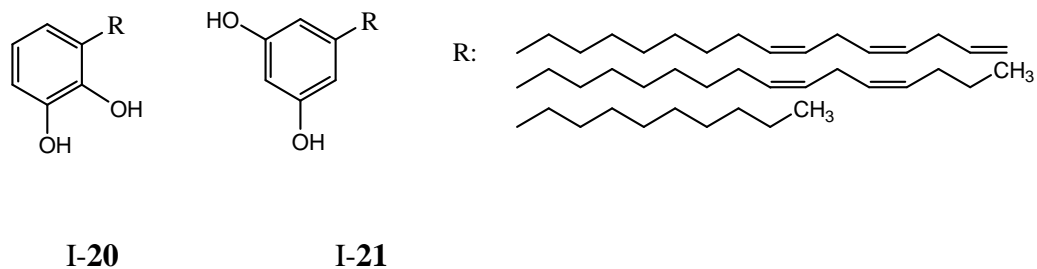


Figure 1.20. Classical examples of urushiols (I-20) and resorcinoid lipids (I-21).

Due to their potent antiparasitic, antibacterial, antifungal properties and non-toxicity to higher animals, resorcinoid lipids have found application as active constituents of medicines and antiseptic lotions.^{68,70} The antitumor property of resorcinoid lipids isolated from the medicinal plants such as *G. Biloba* have also been investigated.⁷¹ In model studies utilizing liposomes, resorcinoid lipids have been

shown to change the thermotropic properties of phospholipid bilayers by increasing the temperature of phase transitions.^{68,71} IR spectroscopy indicated formation of H-bonding between phospholipid head groups and resorcinol rings. It was suggested that this interaction might be responsible for the observed stabilizing/condensing effect.^{68,72} In turn, in liposomes, resorcinoids have been shown to increase permeability toward ions and small non-electrolytes.⁷³ It was hypothesized that this permeabilizing effect might be due to the formation of reversed micelles-like structures.^{68,73,74} Indeed, ³¹P-NMR measurements show the occurrence of an isotropic and hexagonal signal in egg phosphatidylcholine in the presence of about 30 mol% alk(en)yl resorcinol.⁷⁴ In erythrocytes as a model of the cell systems, resorcinolic lipids have been shown to promote clustering of membrane proteins, induce release of K⁺ ions and increase permeability toward small non-electrolytes, therefore eventually leading to cell homolysis.^{68,74} Unsaturation of the n-alkyl chain was found to increase the permeabilizing activity of these compounds.^{70,74} Similar to other amphiphilic agents whose effect on the barrier function of biological membranes is modulated by the presence of divalent cations, Zn²⁺ and other ions protected erythrocytes against the lytic action of resorcinolic lipids.^{68,75} Almost all published research on interaction between resorcinolic lipids and phospholipid membranes (using erythrocytes and liposomes) has been done exclusively by A. Kozubek and co-workers at the University of Wrocław, Poland.

In addition to the amphiphilic catechols discussed above, the high affinity of the receptors with multiple catechol groups toward Fe³⁺ and the membrane transport properties of these complexes have been the subject of intense interest over

the decades.⁷⁶ These synthetic receptors are analogs of bacterial ferric ion sequestering agents - siderophores. According to the definition given by Drechsel and Winkelmann the secondary metabolites can be classified as siderophores if the following applies: 1) iron regulated biosynthesis; 2) ferric iron chelating capability; 3) active transport through the cell membrane.^{76b} The high thermodynamic stability and selectivity toward iron made the siderophores and analogs targets in the search for new medicines. For example, conjugates of antibiotics and siderophores have been made so as to utilize mechanisms of bacterial iron uptake for new drug delivery routes.⁷⁷ If biocompatible, iron chelators also have the potential to treat conditions of iron overload in patients.^{76b,78}

Interesting to notice that such sophisticated molecules as siderophore enterobactin are often genus/specie specific and require genus/specie specific outer membrane receptor.^{2,77b} In addition, the iron transport in this case includes the step when the ferric ion is transferred between the two siderophore molecules embedded in the membrane protein. In turn, some small molecules such as, secreted by bacteria, citric and 2,3-dihydroxybenzoic acids and synthetic bis- and tris-catecholates are known to avoid this particular step but function as siderophores delivering iron directly into the cell. These “primitive” iron chelators are not as genus/specie specific (can be utilized by many bacteria) but due to weaker binding, they often lose in competition for iron to more preorganized hosts.⁷⁷ There is a growing interest, however, in identification of the natural and synthetic siderophores which bypass the above mentioned step of ferric iron exchange between the two molecules and, therefore, can be utilized as a shuttle vector for drug delivery.^{77b} The activity of potential

siderophores and siderophore-antibiotic conjugates is usually evaluated using growth promotion assays.⁷⁷

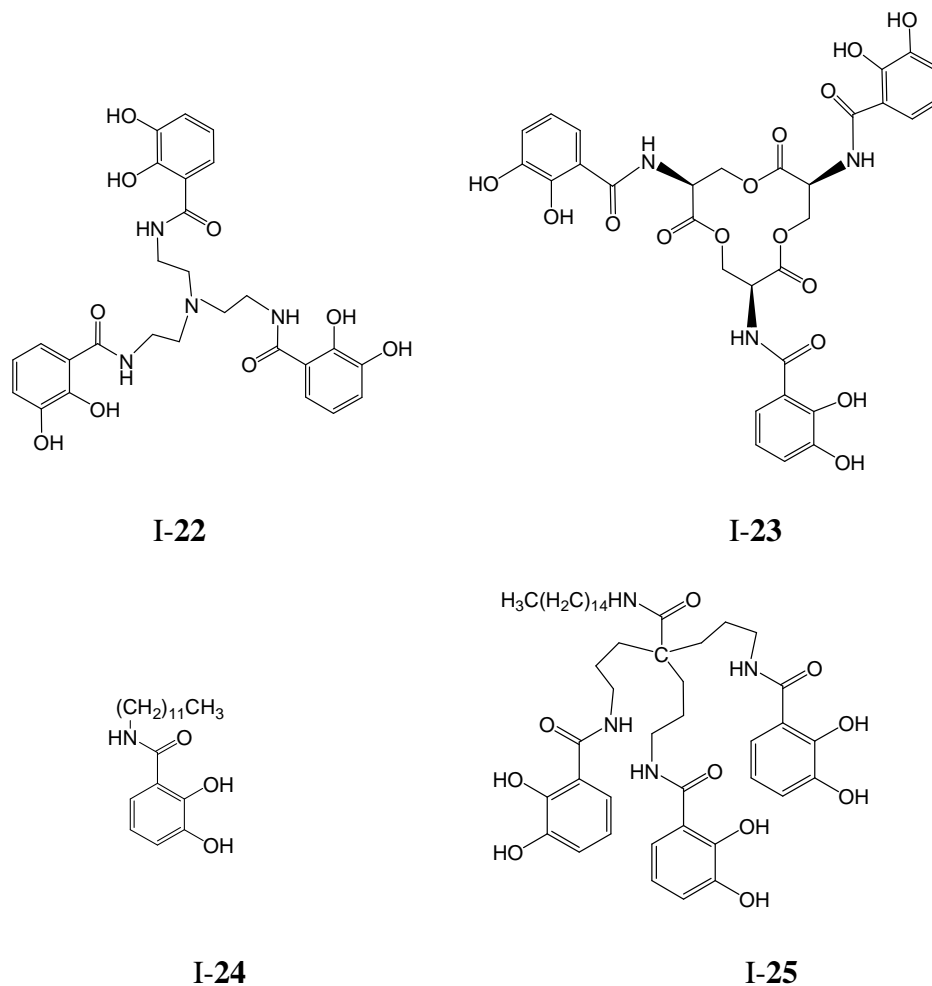


Figure 1.21. Structures of TRENAM (I-22), enterobactin (I-23), synthetic amphiphilic catecholates (I-24, I-25).

Tricatecholates, based on the tris(2-aminoethyl)amine (TREN) scaffold and 2,3-dihydroxybenzoic acid, such as TRENAM (I-22) are known as cationic analogs of the famous enterobactin (I-23).⁷⁹ Natural amphiphilic Fe³⁺ chelators have been recently isolated from marine bacteria.⁸⁰ In contrast to the majority of natural

siderophores, which are water-soluble molecules, these amphiphiles have high affinity toward the phospholipid bilayer and self-assemble into micelles and vesicles in aqueous media.⁸⁰

Catechol-based synthetic analogs (**I-24**, **I-25**) of these natural products have been recently reported.⁸¹ These amphiphilic siderophores (**I-24**, **I-25**) were found to self-assemble in the aqueous media into micelles and vesicles so as to mimic the behavior of the bacteria-produced analogs. Uptake of anionic enterobactin-iron complex requires a protein receptor on the outer membrane of bacteria cells that recognizes the Fe^{3+} -siderophore complex.² In contrast, due to their increased lipophilicity, these amphiphilic iron chelators have the ability to merge with the outer membrane by themselves and to release ferric ion into the periplasm. This hypothesis was tested using **I-24** as a synthetic model of natural amphiphilic Fe^{3+} receptors. This compound self-assembles in aqueous media and induces iron uptake in bacteria mutants. The rather simple analog **I-24** was more active than complexed **I-25**.⁸¹

According to the facts described above, natural and synthetic catechols actively interact with biological membranes. A variety of non-covalent interactions are employed to permeabilize the phospholipid bilayer, either non-specifically or specifically toward H^+ or Fe^{3+} ion. To date, however, there was no evidence that catechols can selectively transport anions across phospholipid bilayer. The main objective of the present study became to design a catechol-derived receptor that could function as a transmembrane anion transporter.

The structures of some hypothetical catechol-based anion transporters are schematically represented in Figure 1.22. Catecholate moieties are linked together through a hydrophobic linker.

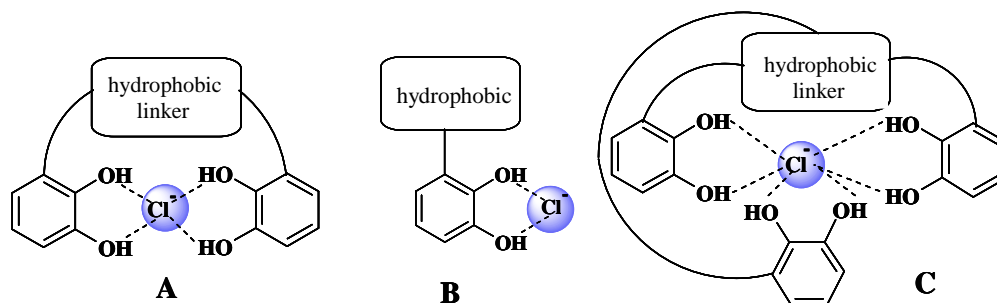


Figure 1.22. Hypothetical catechol-based anion receptors **A**, **B**, and **C**.

To understand the stoichiometry and mechanism of interaction between catechol and Cl^- anion in organic media we initially undertook studies using ^1H NMR spectroscopy and ESI-MS spectrometry and examined the microscopic environment of Cl^- anion in CHCl_3 in the presence of **I-18** and $(\text{Bu})_4\text{N}^+$ as counterion. We also compared catechol with other simple phenolic and amide-based receptors using ^1H NMR, ESI-MS, and computational method. Results of this study are discussed in Chapter 2. Chapter 3 includes investigation of the anion binding properties of newly designed bis-catechol based receptors. The ion transport activity and selectivity of these compounds was evaluated in liposomes. Results of these studies are discussed in Chapter 4. Chapter 4 also includes a description of the future work.

Chapter 2: Complexity of Interaction Between Catechol and $(\text{Bu})_4\text{N}^+\text{Cl}^-$

2.1. Introduction.

There were two main questions to be addressed in this chapter. First, we determine the stoichiometry of interaction between catechol (II-1) and Cl^- ion. Second, we compare the anion binding properties of catechol with other simple phenols and amides (II-2 – II-6).

Interaction between anion receptors containing H-bond donor group(s), X-H, and halide anions is usually investigated using ^1H NMR titration with alkylammonium salts in organic solvents. H-bonding between Cl^- and X-H results in the downfield shift of acidic protons in ^1H NMR spectra. Examples of slow exchange in solution,⁸² as well as fast exchange,⁵⁷ on the NMR chemical shift time scale are described in the literature. The dependence of the apparent association constants (K_a) for the “host-guest” interaction (when the guest is an anion) on the concentration of the salt⁸³ and the nature of the solvent and counterion have been discussed.^{84,85} For example, decreasing polarity of the solvent or replacement of ammonium salts with phosphonium salts increases Cl^- binding ability of amide receptors. In contrast, the addition of halides of alkali metals inhibits the anion-binding ability of neutral hosts.⁸⁶ Extraction of thermodynamic association constants for the relevant system, namely, metal ion - crown ether interactions, using NMR spectroscopy and other

methods was evaluated in a recent IUPAC review. Recommended conditions include relatively polar solvent such as CD_3CN and low concentration of the salt.⁸⁷ This suggestion, however, is difficult to follow in practice, first, because many organic “hosts” are highly hydrophobic and have limited solubility in CD_3CN , as compared to CD_2Cl_2 or CDCl_3 . Second, many organic hosts interact with the anions only in very non-polar aprotic solvents such as CD_2Cl_2 or CDCl_3 .

Would the apparent values of the association constants be satisfactory enough? Let us say, for instance, that we are searching for an anion receptor which has the same ability to discriminate between anions as valinomycin does between K^+ and Na^+ ions. In this case, the binding is strong and the selectivity is such a remarkable property that neither solvent nor counterion effects matter.^{4b}

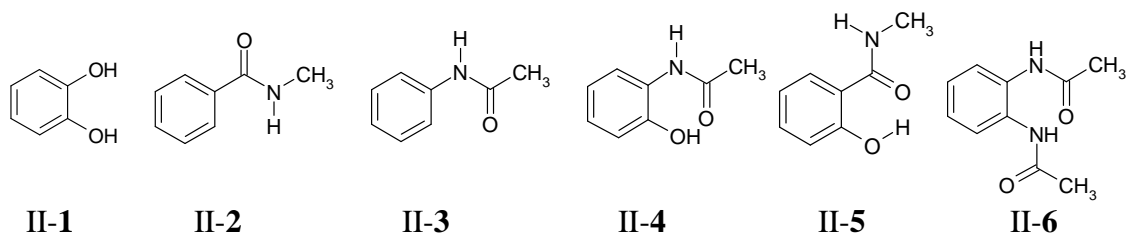


Figure 2.1 Catechol (II-1), N-methylbenzamide (II-2), acetanilide (II-3), 2-acetamidophenol (II-4), N-methylsalicylamide (II-5) and N1-[(acetylamino)phenyl]acetamide (II-6).

According to the experimental results described in this chapter, in the case of the compounds with relatively similar affinities towards Cl^- anion, such as II-1 and

II-6, the counterion effect can become an important factor to take into consideration. Thus, the catechol (**1**) has a stronger affinity towards Cl^- in CHCl_3 but tends to form aggregates of the general structure $(\text{Bu})_4\text{N}^+\text{Cl}^- \cdots \text{II-1}$. In turn, receptor II-6 has a weaker affinity towards Cl^- but, presumably, due to steric reasons, does not form these aggregates but does form $\text{Cl}^- \cdots \text{II-6}$. Tested in the same conditions, receptor II-6 competes with the cation $(\text{Bu})_4\text{N}^+$ for Cl^- anion more efficiently than the catechol as indicated in the ^1H NMR of the salt. Therefore, the question remains: which one, II-1 or II-6, is a stronger anion receptor in CHCl_3 solution of the salt $(\text{Bu})_4\text{N}^+\text{Cl}^-$?

The coordination number for Cl^- anion cocrystallized with the organic hosts containing multiple urea H-bond donor groups reaches eight.⁸⁸ Surprisingly, to the best of our knowledge, the experimental studies in solution between very simple proton donors, like urea, phenols, catechol, and Cl^- anion reported so far indicated only a 1:1 binding stoichiometry.^{57,84,18a}

According to the most recent review, which highlights the progress in the anion recognition chemistry since 2007, there are a number of reports to illustrate the stoichiometry 1 : n ($n = 2, 3$) for the receptor : anion interaction.^{18a} In turn, reports describing the possibility of n : 1 ($n > 1$) stoichiometry are extremely rare. Thus, there is only one paper in this review to suggest formation of the 2 : 1 complex between neutral organic receptor and Cl^- anion in solution.⁸⁹

For instance, the catechol (II-1) was recently described as a surprisingly good Cl^- receptor with a binding constant of $K_a = 10^3 \text{ M}^{-1}$, using classical ^1H NMR titration with $(\text{Bu})_4\text{N}^+\text{Cl}^-$ in CD_3CN . According to the author, however, there was never any evidence for the presence of complexes between II-1 and Cl^- anion of higher

stoichiometry than 1:1. Analogously, there was never any evidence for the presence of mixed complexes like II-3 \cdots Cl \cdots II-1 when catechol (II-1) and acetanilide (II-3) or other simple H-bond donors were simultaneously present in solution.⁵⁷

It appears that the Job plots are usually done in a solution where concentrations of the anion and the anion receptor are relatively low and comparable. In turn, the titration experiment is performed in the presence of an excess of the salt, and the relatively large excess of the salt has to be used when the binding is not particularly strong. It is reasonable to suggest that in the later case, one might want to look at the experimental conditions when not the salt, but the receptor, is present in excess to make sure that the parameters obtained more or less adequately describe this system.

Theoretical methods can open an alternative insight into inorganic anion – organic host interaction. Recently, Hay and colleagues reported the geometries and the binding energies for urea complexes with different shaped anions such as Cl $^-$, NO $_3^-$, SO $_4^{2-}$, etc.⁹⁰ For instance, theoretical calculations indicate that Cl $^-$ anion can bind/coordinate up to four urea units simultaneously, while NO $_3^-$ can bind up to three, and SO $_4^{2-}$ can bind up to six. To the best of our knowledge, there are no reports to indicate that complexes Anion $^-$ *urea $_n$ ($n > 1$) might exist in solution. There are several reports, however, describing metal-directed self-assembly in solution of rather simple urea-based ligands into the cages encapsulating anions such as Cl $^-$ and SO $_4^{2-}$ as templates.^{49,50,51,88}

2.2. Abstract and Summary of Key Findings in this Chapter:

Below, are listed the key findings in this chapter:

a) ^1H NMR chemical shifts of the acidic protons indicate multiple binding of catechol to Cl^- anion when concentrations of the salt and **II-1** are comparable or when the catechol is in excess.

b) ^1H NMR chemical shifts of the cation $(\text{Bu})_4\text{N}^+$ in CHCl_3 are independent of the concentration of the salt unless catechol **II-1** is present in solution. Presumably, ionic clusters $((\text{Bu})_4\text{N}^+\text{Cl}^-)_n$ disaggregate to form free $(\text{Bu})_4\text{N}^+$ cations and H-bonded Cl^- anions, thus the NMR signals of the salt shifts upfield.

c) The combined ^1H NMR data for anion complexation by **II-1** and for dissociation of the salt support multiple binding and suggest formation of “intermediates” in organic media schematically represented as $(\text{Bu})_4\text{N}^+\text{Cl}^- \cdots \text{II-1}$. Presumably, in these aggregates, acidic protons shift downfield due to H-bonding whereas signals of the salt do not change because cations $(\text{Bu})_4\text{N}^+$ remain associated with anions.

d) The ability of catechol to undergo multiple binding into dimers, $\text{II-1}_2 \cdots \text{Cl}^-$, as well as to form ion-paired aggregates, $(\text{Bu})_4\text{N}^+\text{Cl}^-_2 \cdots \text{II-1}$, $((\text{Bu})_4\text{N}^+\text{Cl}^-)_2 \text{Cl}^- \cdots \text{II-1}_2$, etc. was confirmed by electrospray negative ion mass spectrometry (ESI-MS).

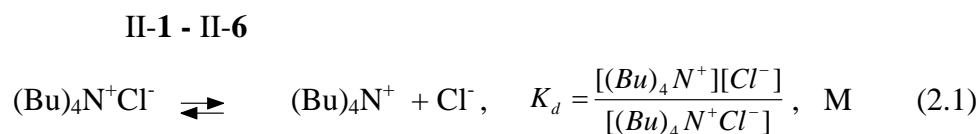
e) The following two ESI-MS observations support findings (a-d) listed above when there is competition between $(\text{Bu})_4\text{N}^+$ and catechol for Cl^- anion:

- Only naked $(\text{Bu})_4\text{N}^+$ appeared in positive ESI-MS in the presence of stoichiometric quantity of **II-1**, whereas in the absence of catechol **II-1** the clusters $((\text{Bu})_4\text{N}^+)_2\text{Cl}^-$ and $(\text{Bu})_4\text{N}^+\text{Cl}_2^-$ are the major species.
- In the negative ESI-MS the distribution of the signal intensities for the clusters $((\text{Bu})_4\text{N}^+)_{m-1}\text{Cl}_m^- \cdots \text{II-1}_n$ ($m \leq n$) and $\text{II-1}_2 \cdots \text{Cl}^-$ is determined by the ratio $[\text{II-1}] : [(\text{Bu})_4\text{N}^+\text{Cl}^-]$ in solution.

f) The mechanistics of interaction between catechol **II-1** and the salt described above can be safely applied to other simple amides and phenols that we investigated such as compounds **II-2** - **II-5**. Only receptor **II-6** is in some way different from the other simple receptors. The ability of **II-6** to form ion-paired aggregates is dramatically diminished, probably due to steric constraints, while the ability to form “dimers” $\text{II-6}_2 \cdots \text{Cl}^-$ and even “trimers” $\text{II-6}_3 \cdots \text{Cl}^-$ arises from the strong tendency of **II-6** to self-aggregate in CHCl_3 solution.

g) Formation of the mixed complexes $\text{R} \cdots \text{Cl}^- \cdots \text{R}'$ (R, R' – different H-bond donors **II-1** - **II-6**) was observed by ESI-MS when different H-bond donors were simultaneously present in excess of the salt.

h) Addition of the anion receptors **II-1** - **II-6** into CHCl_3 solution results in dissociation of the salt clusters and formation of $(\text{Bu})_4\text{N}^+$ cation and “cation-free” anionic species, such as catechol chloride anion, $\text{Cl}^- \cdots \text{II-1}$, thus establishing an equilibrium which for simplicity can be written as the following:



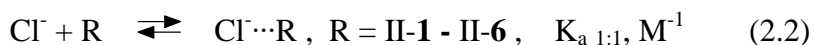
Affinity of $(\text{Bu})_4\text{N}^+$ toward Cl^- anion ($1/K_d$, M^{-1}) depends dramatically on concentration (orders of magnitude in the experimental range) and decreases with increasing concentration of the ions (ionic strength) in CHCl_3 solution. This observation is consistent with the electrostatic model of interaction and opposite charges of the ionic species.

i) *ab initio* (6-31G* basis set) electronic structure calculations were performed to compare binding energies of Cl^- anion to receptors II-1 - II-6. The theoretical predictions were correlated with the experimental values of apparent association constant ($K_{a\ 1:1}$, M^{-1}), estimated by ^1H NMR on a single-point basis, assuming 1:1 binding algorithm and disregarding salt aggregation and multiple binding.

2.3. Results and Discussion

2.3.1. ¹H NMR study.

2.3.1.1. **Relative affinity of the receptors II-1 - II-6 toward Cl⁻ anion in CHCl₃ solution.** Preliminary experimental results indicated that 1) Job plots were asymmetric and 2) binding constants, $K_{a\ 1:1}, M^{-1}$, were concentration dependent. These observations revealed that the mechanism of interaction had to be complex and could not be adequately described using the classical equation (2.2). Therefore, relative affinity of the receptors II-1 - II-6 toward Cl⁻ anion in CDCl₃ was initially evaluated on a single-point basis as described below.



The examined solutions contained equal concentrations of the receptors II-1 - II-6 and the salt, [(Bu)₄N⁺Cl⁻] = [R] = 50 mM. Recorded chemical shifts (δ) of the acidic protons were used to calculate fractions of the free receptor, R, the H-bonded form, Cl⁻⋯R, and the association constant, $K_{a\ 1:1}, M^{-1}$, according to the formula (2.3). Due to simplicity of ¹H NMR spectra the values of chemical shift in the associated form, Cl⁻⋯R, (δ_{\max}) and chemical shift of the free receptor (δ_0) can be obtained independently. The chemical shift of the free receptor was recorded in CDCl₃ solution containing [R] = 100 mM or saturated with the receptor. The values of the chemical shift in the associated form, Cl⁻⋯R, were determined in the presence of an excess of

(Bu)₄N⁺Cl⁻. Upon addition of the salt to the examined solutions ([R] = 50 mM), chemical shift, δ , became independent of the concentration of (Bu)₄N⁺Cl⁻. These maximal values correspond to δ_{\max} .

Table 2.1 Values of $K_{a\ 1:1}$, M⁻¹ for II-1 - II-6 and Cl⁻ in CDCl₃.

Receptor/ ¹ H NMR signal	$K_{a\ 1:1}$, M ⁻¹ *	δ_{\max} , ppm	δ_0 , ppm	δ ,
II-1	1100	8.9 (br) §	5.17	8.43
II-2	9.3	9.42	6.30	7.10
II-3	54	11.20	7.43	9.50
II-4 NH	560	10.72	7.52	10.17
OH	320	10.0 (br) [§]	8.65 (br)	9.7
II-5 NH	61	9.70	6.39	8.27
OH	87	12.9 (br) [§]	12.37 (br)	12.7
II-6	230	10.60	8.52	10.07

[§] Estimated values because signals became very broad.

- $K_{a\ 1:1}$ were calculated
- according to the formula
$$K_{a\ 1:1} = \frac{0.05 \left(\frac{\delta_{\max} - \delta_0}{\delta - \delta_0} \right)}{\left(0.05 - 0.05 \left(\frac{\delta_{\max} - \delta_0}{\delta - \delta_0} \right) \right)^2} \quad (2.3)$$

We were concerned that receptors II-1 - II-6 may self-associate in CDCl₃ so that the position of the acidic protons in ¹H NMR spectra would depend on concentration. Indeed, within the concentration range 100 mM – 10 mM, the strongest dependence was observed for receptor II-6 while acidic protons of catechol

II-1 almost did not shift (SI 2.1). Closer examination, however, established that interaction with Cl^- anion resulted in more dramatic changes in the position of acidic protons, X-H, much higher chemical shift, δ_{max} , as well as $K_{\text{a} 1:1}$ than did any change due to self-association. These facts allowed us to ignore the aggregation of II-1 - II-6. Calculated values of $K_{\text{a} 1:1} = 54 \text{ M}^{-1}$ for acetanilide (II-3) and $K_{\text{a} 1:1} = 1100 \text{ M}^{-1}$ for catechol (II-1) are consistent with the corresponding literature values of $K_{\text{a}} = 31 \text{ M}^{-1}$ and $K_{\text{a}} = 1015 - 1575 \text{ M}^{-1}$ measured by Smith and in CD_3CN solution, assuming a 1:1 binding algorithm.⁵⁷

The results shown in Table 2.1 indicate that the relative affinity of the receptors II-1 - II-6 to Cl^- anion changes in the following order: II-1 > II-4 > II-6 > II-5 \geq II-3 > II-2. At a glance, this trend could be in agreement with the relative ability of the receptors to form strong intermolecular H-bonds. Presumably, the $\text{OH}\cdots\text{Cl}^-$ bond is stronger than $\text{CONH}\cdots\text{Cl}^-$. The catechol (II-1) can bind Cl^- anion using two hydroxy groups. In turn, compound II-4 has only one hydroxy and one amide groups available. Receptor II-6 can employ two amide groups and, therefore, comes as the third strongest binder. Compound II-5 is almost as active as II-3, which has only one amide group. Due to intramolecular H-bonding in the receptor II-5 (six-membered ring), the OH group is “deactivated” and only one amide group remains available.

In conclusion, the anion-binding affinity changes in the order that reflects the ability of the receptors II-1 - II-6 to form strong intermolecular H-bonds with Cl^- anion: II-1 > II-4 > II-6 > II-5 \geq II-3 > II-2.

2.3.1.2. **Signals of the salt (Bu)₄N⁺Cl⁻ shift upfield in presence of H-bond donors. Is there an equilibrium between (Bu)₄N⁺ cation and aggregates ((Bu)₄N⁺Cl⁻)_n?** The dependence of ¹H NMR chemical shifts of organic salts on the concentration and nature of the solvent is described in the literature as a consequence of an equilibrium between free ions and ionic aggregates.⁹¹ For instance, changes in ¹H NMR spectra of quaternary ammonium salts (Bu)₄N⁺X⁻ upon dilution in nitrobenzene are attributed to the following equilibrium:

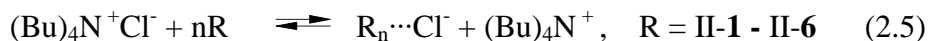


The position of the NMR shifts for the α-CH₂ group of the tetrabutylammonium cation is sensitive to both the concentration and nature of the anion. Dissociation constants, K_d, M, for the salts (Bu)₄N⁺X⁻ in C₆D₅NO₂ extracted from ¹H NMR data are consistent with the values determined using conductometry.⁹²

In contrast to other solvents, in CDCl₃ the ¹H NMR spectrum of the salt (Bu)₄N⁺Cl⁻ did not depend on concentration (SI 2.2). Addition of receptors II-1 - II-6, however, resulted in an upfield shift of all four signals for the salt. The most downfield signal of the salt, α-CH₂ at 3.40 ppm, is the most shifted upon addition of receptors, while the most upfield signal, δ-CH₃ at 1.01 ppm, is the least shifted. The dependence of the chemical shift of the most sensitive α-CH₂ group on the concentration and nature of the receptor is shown in Figure 2.2.

We propose that these ¹H NMR data reflect the following processes happening in the solution. Receptors II-1 - II-6 break apart salt aggregates into discrete ionic species (Bu)₄N⁺ cation and R_n⋯Cl⁻ anion(s) of unknown stoichiometry.

The observed upfield chemical shift is due to the redistribution of electron density along the σ -bonds within the $(\text{Bu})_4\text{N}^+$ cation. This equilibrium can be schematically represented as following:



According to equation (2.5), the concentration of the free $(\text{Bu})_4\text{N}^+$ is equal to concentration of $\text{Cl}^-\cdots\text{R}_n$ anion in solution. In addition, the most active receptor, R, should break apart more salt aggregates and, therefore, induce the most dramatic changes in the ^1H NMR of the salt. The experimental results presented in Figure 2.2 indicate that the ability of compounds II-1 - II-6 to break apart the salt $(\text{Bu})_4\text{N}^+\text{Cl}^-$ in CDCl_3 solution changes in the following order: II-6 > II-1 = II-4 > II-5 = II-3 > II-2.

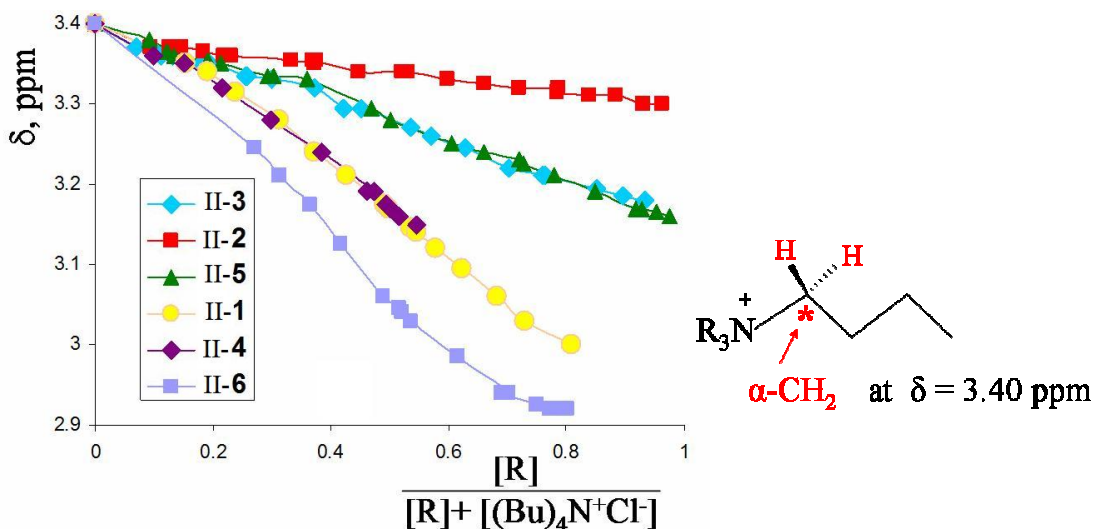



Figure 2.2. Dependence of the chemical shift for $\alpha\text{-CH}_2$ of $(\text{Bu})_4\text{N}^+$ on the fraction of receptors II-1 - II-6 in CDCl_3 solution. Total concentration in the solution is constant: $[\text{R}] + [(\text{Bu})_4\text{N}^+\text{Cl}^-] = 100 \text{ mM}$.

Surprisingly, among the six anion receptors, it is compound **II-6** and not catechol that is the most active. It appears that although catechol (**II-1**) has the strongest affinity for the Cl⁻ anion ($K_{a\ 1:1} = 1040\ \text{M}^{-1}$), it is less likely to induce dissociation of the salt aggregates than does receptor **II-6** ($K_{a\ 1:1} = 230\ \text{M}^{-1}$). According to the equation (2.5), this observation should indicate that it requires more equivalents (n) of the catechol (**II-1**) than receptor **II-6** to break apart the salt (Bu)₄N⁺Cl⁻.

In conclusion, the ability of the receptors to induce dissociation of the salt changes in the following order **II-6** > **II-1** = **II-4** > **II-5** = **II-3** > **II-2**. This sequence should reflect not only the H-bonding ability but also the tendency to “encapsulate” the anion using lower number of the receptor molecules per one Cl⁻ anion (n).

2.3.1.3. Multiple binding of H-bond donors to Cl⁻ anion. Job plots were constructed to get insight into the stoichiometry of interaction between Cl⁻ and anion receptors. Solutions of (Bu)₄N⁺Cl⁻ and receptors **II-1** - **II-6** in CDCl₃ were mixed in different ratios, while the total concentration in the solution remained constant and equal to 100 mM. Initially, we undertook the classical approach toward constructing a Job plot. The chemical shift of the receptors’ acidic protons multiplied by the fraction of the receptor ($\delta\mathbf{x}$) was plotted against the fraction of the receptor in solution (\mathbf{x}) (Figure 2.3, **A**, blue squares ). Data for receptor **II-6** indicated a 1:1 binding algorithm. In contrast, the curves for receptors **II-1** and **II-3** were asymmetric, with maxima around 0.6. These observations suggest that more than one molecule of

II-1 and II-3 might be simultaneously coordinated by a single Cl⁻ anion. For a pure 2:1 complex one should expect the maximum of the Job plot to be at 0.63.

A Chemical shift * fraction, ppm

B Concentration, M⁻¹

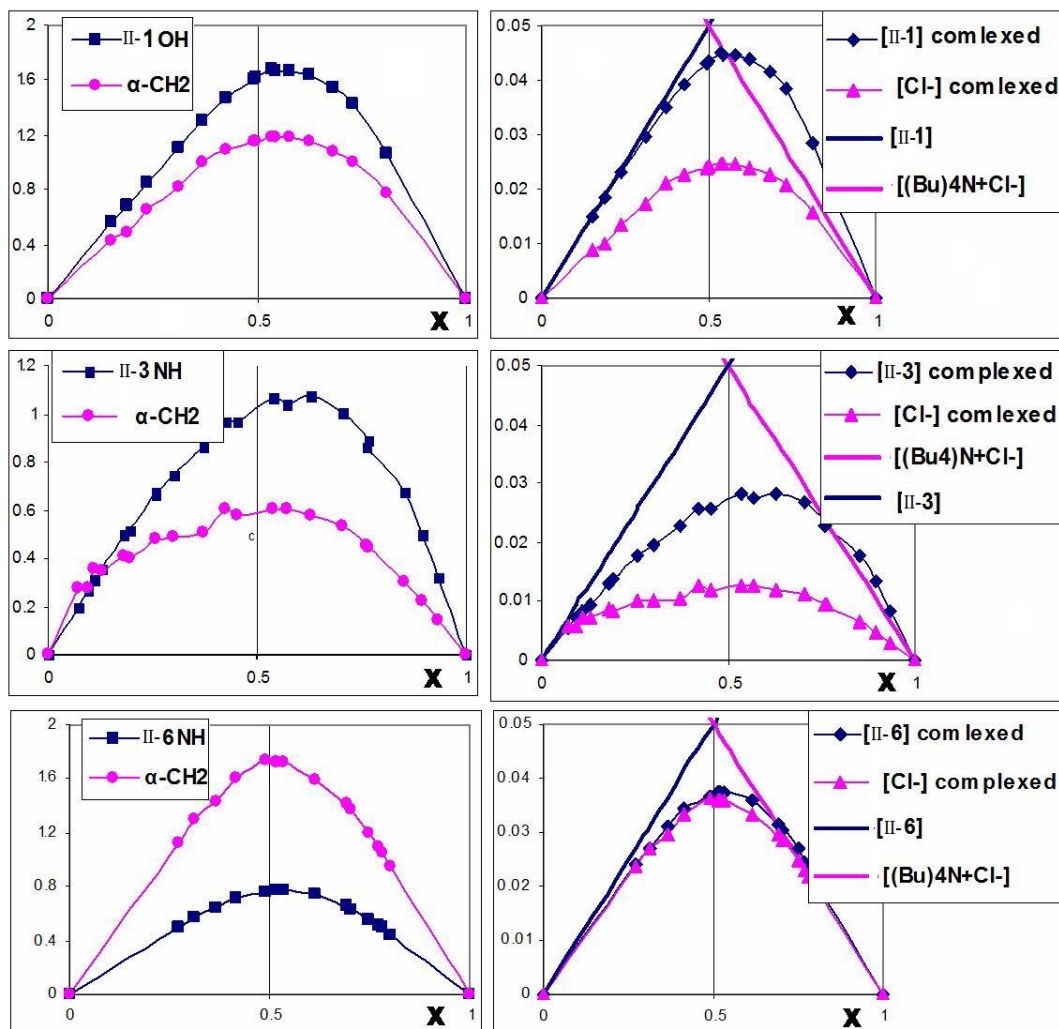




Figure 2.3. Job plots. Horizontal axes (\mathbf{x}) are fractions of the receptors II-1, II-3, II-6 in the solution, while total concentration is constant $[(\text{Bu})_4\text{N}^+\text{Cl}^-] + [\text{R}] = 100 \text{ mM}$. (A) Classical approach. Blue squares \blacksquare : dependence of $\delta\mathbf{x}$, ppm on \mathbf{x} , where δ is chemical shift of the acidic protons as indicated. Pink circles \bullet : dependence of $10\delta\mathbf{x}$, ppm on \mathbf{x} , where δ is chemical shift of $\alpha\text{-CH}_2$ of the salt $(\text{Bu})_4\text{N}^+\text{Cl}^-$. (B) Dependence of concentration of the complexed form of the receptors II-1, II-3, II-6 (blue rhombs \blacklozenge), obtained from the chemical shifts of the receptors' acidic protons as indicated, on \mathbf{x} . Dependence of concentration of the complexed Cl^- anions (pink triangles \blacktriangle) in solution, obtained from the chemical shift of the salt, $\alpha\text{-CH}_2$, on \mathbf{x} . Solid lines indicate total concentration of the salt (pink —) and receptors (blue —) in solution.

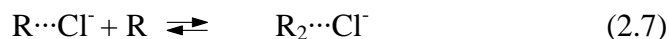
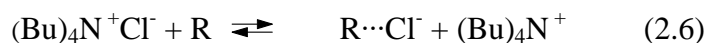
In addition to the classical approach, graphs **B** (blue rhombs \blacklozenge) were constructed using experimental values of δ_{max} and δ_0 to calculate concentrations of free and complexed forms of the receptors in each experimental point. Indeed, the concentration of the complexed form of the receptors **1** and **3** (blue rhombs \blacklozenge) in the solution is higher than the total concentration of the salt $(\text{Bu})_4\text{N}^+\text{Cl}^-$ (solid pink lines —) when these receptors are in excess! This is an unambiguous indication of the ability of II-1 and II-3 to undergo multiple binding to a single Cl^- anion. In contrast, graph **B** constructed for compound II-6 supports a 1 : 1 binding algorithm.

We also decided to take advantage of the fact that the chemical shift of the salt changes upon addition of II-1 - II-6 due to the equilibrium shown in the equation 2.5. We assume that the signal for $\alpha\text{-CH}_2$ at $\delta = 3.40 \text{ ppm}$ corresponds to the aggregated

form $(\text{Bu})_4\text{N}^+\text{Cl}^-$ and that the maximal observed upfield chemical shift of $\alpha\text{-CH}_2$ at $\delta_{\text{max}} = 2.92$ ppm recorded in solution containing 20 mM of $(\text{Bu})_4\text{N}^+\text{Cl}^-$ and 80 mM of **II-6** corresponds to the completely dissociated form. For the free $(\text{Bu})_4\text{N}^+$ cation in a 20 mM solution of $(\text{Bu})_4\text{N}^+\text{Cl}^-$ saturated with the receptors **II-1** and **II-6** the $\alpha\text{-CH}_2$ chemical shift was also at $\delta_{\text{max}} = 2.92$ ppm. Thus, the concentration of Cl^- anion that is H-bonded by the receptors ($\text{R}_n \cdots \text{Cl}^-$), which is according to equation (2.5) equal to the concentration of free $(\text{Bu})_4\text{N}^+$ in solution, can then be obtained ($[\text{Cl}^-]_{\text{complexed}} = [(\text{Bu})_4\text{N}^+]_{\text{free}}$). Remarkably, the concentration of $\text{R}_n \cdots \text{Cl}^-$ (pink triangles ) is about twice as low as the concentration of the complexed receptors **II-1**, **II-3** (blue rhombs ) and equal to the concentration of the complexed form of **II-6**! These observations again support a 1 : 2 Cl^- anion : receptor binding stoichiometry for compounds **II-1** and **II-3** and a 1 : 1 Cl^- anion : receptor binding stoichiometry for receptor **II-6**. Job plots **A** and **B** for the receptors **II-4** and **II-5** are similar to **II-1** and **II-3** (SI 2.3)

In summary, the Job plots indicate a 1 : 2 stoichiometry of interaction with Cl^- for receptors **II-1** - **II-5** and a 1:1 stoichiometry for receptor **II-6**. Two sets of Job plots were constructed: namely, a classical plot (**A**) and a modified (**B**) plot, where concentrations of the complexed form, instead of $\delta\mathbf{x}$, were plotted against \mathbf{x} . The chemical shifts of both acidic protons (blue data) and $\alpha\text{-CH}_2$ of the cation $(\text{Bu})_4\text{N}^+$ (pink data) were used to obtain two curves for each receptor on the graphs **A** and **B**. These presented results indicate that the stoichiometry of interaction can be investigated using not only the chemical shifts of the acidic protons in the receptors but also by monitoring changes in the ^1H NMR spectra of the $(\text{Bu})_4\text{N}^+\text{Cl}^-$ salt.

2.3.1.4. **Dilution experiment: the combined ^1H NMR data for the salt and receptors provides evidence of ion-paired intermediates $(\text{Bu})_4\text{N}^+\text{Cl}^-\cdots\text{R}$ in solution.** If an equilibrium between “free R” and $\text{Cl}^-\cdots\text{R}_n$, with different degrees of complexation (n), takes place:



then dilution should shift this equilibrium toward the form with the least degree of complexation ($n = 1$).

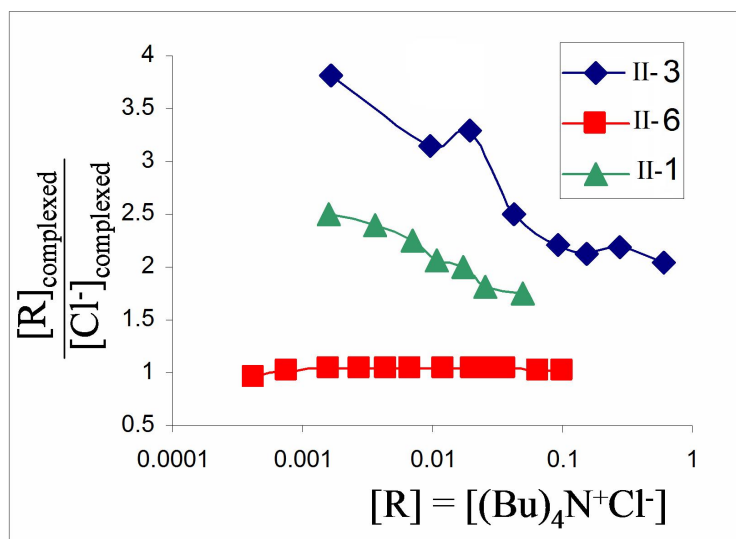
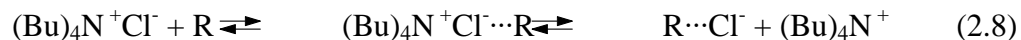


Figure 2.4. Dilution experiment. Three samples that were diluted contained equimolar concentrations of the salt $(\text{Bu})_4\text{N}^+\text{Cl}^-$ and receptors II-1, II-3, and II-6 in CDCl_3 . Concentration of $[\text{R}]_{\text{complexed}}$ was calculated from the chemical shift of the acidic protons. The concentration of Cl^- anion complexed by the receptor ($[\text{Cl}^-]_{\text{complexed}}$) was calculated from the changes in chemical shift of $\alpha\text{-CH}_2$ in the salt assuming $[\text{Cl}^-]_{\text{complexed}} = [(\text{Bu})_4\text{N}^+]_{\text{free}}$.

Solutions containing equimolar concentrations of the salt $(\text{Bu})_4\text{N}^+\text{Cl}^-$ and receptors **II-1**, **II-3**, and **II-6** were diluted. Chemical shifts of the acidic protons and $\alpha\text{-CH}_2$ were recorded in each experimental point so as to calculate the concentrations of the receptor complexed by Cl^- anion ($[\text{R}]_{\text{complexed}}$) and Cl^- anion complexed by the receptor ($[\text{Cl}^-]_{\text{complexed}} = [(\text{Bu})_4\text{N}^+]_{\text{free}}$). The dependence of the ratio $[\text{R}]_{\text{complexed}} : [\text{Cl}^-]_{\text{complexed}}$ on concentration is shown in Figure 2.4. The ratio $[\text{II-6}]_{\text{complexed}} : [\text{Cl}^-]_{\text{complexed}}$ remained constant and equal to about 1:1 across the entire concentration range. In contrast, dilution of the solutions containing compounds **II-1** and **II-3** did not decrease but increased the ratio $[\text{R}]_{\text{complexed}} : [\text{Cl}^-]_{\text{complexed}}$! This observation would be in agreement with the formation of ion paired complexes $(\text{Bu})_4\text{N}^+\text{Cl}^-\cdots\text{R}$ as intermediates:



Presumably, in these aggregates the chemical shift of acidic protons moves downfield due to H-bonding, while the chemical shift of the salt does not change because the $(\text{Bu})_4\text{N}^+$ cation remains associated with the anion.

It can be concluded that study of the salt dissociation versus H-bond formation by receptors **II-1** and **II-3** with Cl^- anion revealed an unexpected trend. This result, however, can be explained if we concede formation of ion-paired intermediates $(\text{Bu})_4\text{N}^+\text{Cl}^-\cdots\text{R}$ in the solution. Thus, the ^1H NMR data for the salt and the receptor in combination provides evidence for the presence of intermediates $(\text{Bu})_4\text{N}^+\text{Cl}^-\cdots\text{R}$.

It is noteworthy, however, that the dilution experiment discussed above was performed in the solution where concentrations of the receptors and the salt were

equal ($[R] = (Bu)_4N^+Cl^-$). When we increased concentration of the receptor relative to concentration of the salt, thus shifting the equilibrium (2.9) strongly to the right, than dilution, indeed, resulted in the initially expected trend for $[R]_{\text{complexed}} : [Cl^-]_{\text{complexed}}$ ratio as illustrated in Figure 2.5.

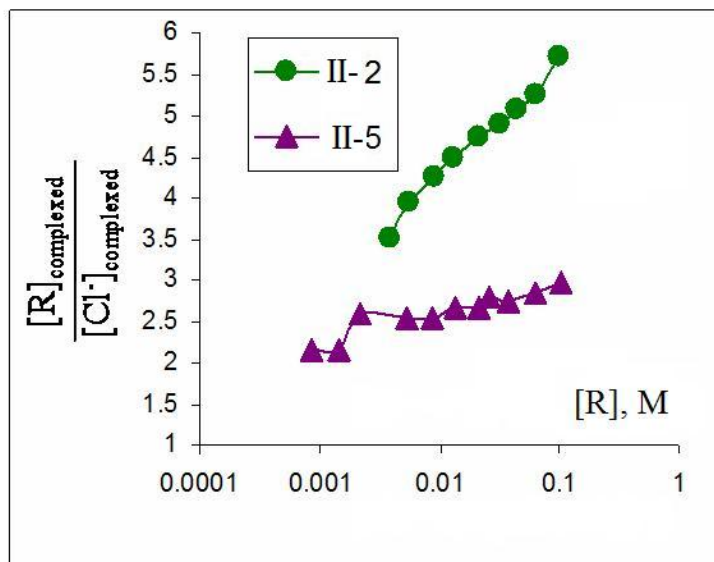
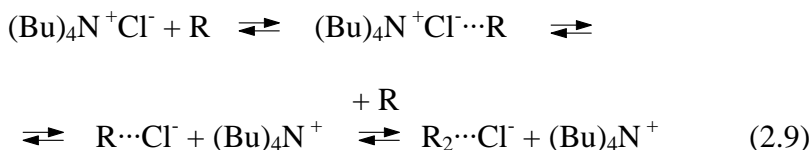


Figure 2.5. Dilution experiment. The samples that were diluted did not contain the equal concentrations of the receptor and the salt but an excess of the receptor: [II-2] = 6*[(Bu)₄N⁺Cl⁻], M and [II-5] = 3*[(Bu)₄N⁺Cl⁻], M.

2.3.1.5. ¹H NMR of the salt supports stepwise interaction mechanism.

Similar to the association constant of the receptor with Cl⁻ anion, $K_{a\ 1:1}$, M⁻¹, defined

from the equation (2.2), the dissociation constant K_d for $(\text{Bu})_4\text{N}^+\text{Cl}^-$ as depicted in scheme (2.10) can be calculated from the chemical shift of $\alpha\text{-CH}_2$ in each experimental point.

II-1 - II-6



Remarkably, even though $K_{a\ 1:1}$ only changed slightly with concentration, we observed dramatic changes in K_d , even of several orders of magnitude within the same concentration range (Table 2.2). This strong dependence of K_d on concentration is consistent with the electrostatic nature of interaction in the aggregates $(\text{Bu})_4\text{N}^+\text{Cl}^-$ in CDCl_3 solution.

Table 2.2. Dependence of the association constant, $K_{a\ 1:1}$, M^{-1} , and dissociation constant of the salt K_d , M on concentration in CDCl_3 solution.

$[(\text{Bu})_4\text{N}^+\text{Cl}^-] = [\text{II-3}]$,

M^{-1}	K_d , M	$K_{a\ 1:1}$, M^{-1}
0.60	0.20	14
0.15	0.034	25
0.043	0.0036	39
0.020	0.00049	47
0.0016	7.275E-07	53

The dependence of the electrical work required to bring two ions together on concentration is determined by the Debye-Huckel law.⁹³ Thus, the dependence of K_d on the function of ionic strength $f(I)$, shown in Figure 2.6, was calculated according to the literature reference.⁹⁴

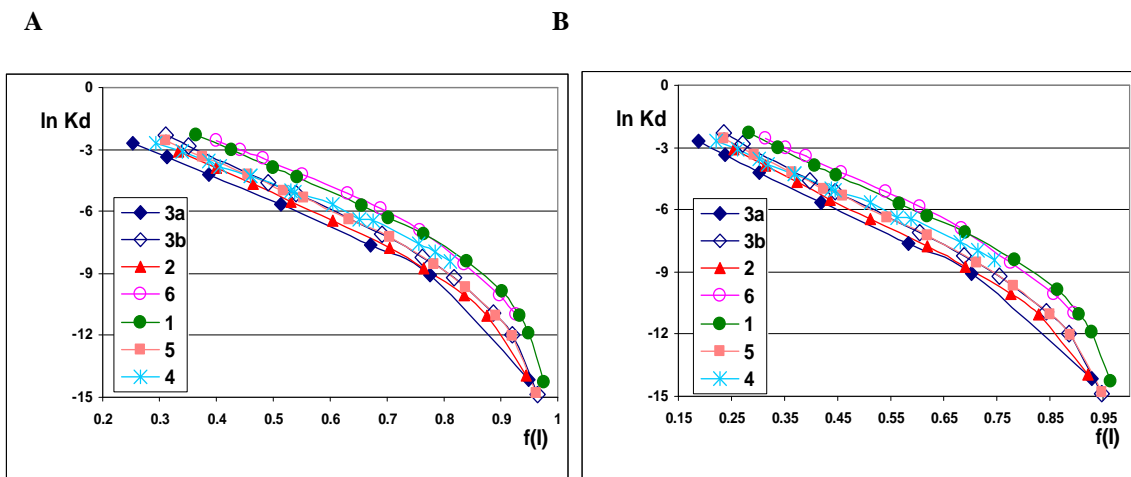
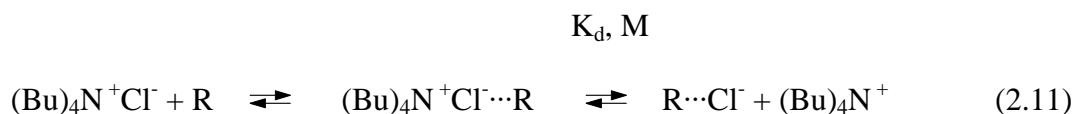


Figure 2.6. The $\ln K_d$ as a function of ionic strength $f(I) = 1/(1+d*\beta*I^{0.5})$, where $I = [(Bu)_4N^+]_{free}$ – ionic strength; $\beta = 1.33 \text{ M}^{-1/2} \text{ \AA}^{-1}$ – the Debye length; **A** $d = 6.86 \text{ \AA}$ – distance between ions in the ion pair $(Bu)_4N^+$, Cl^- ; **B** $d = 10 \text{ \AA}$ – estimated distance between ions in the ion pair $(Bu)_4N^+$, $Cl^- \cdots II-1$. The following solutions were diluted: **1** – [II-1] = $2*[(Bu)_4N^+Cl^-] = 100 \text{ mM}$, **2** – [II-2] = $6*[(Bu)_4N^+Cl^-] = 600 \text{ mM}$, **3a** – [II-3] = $[(Bu)_4N^+Cl^-] = 600 \text{ mM}$, **3b** – [II-3] = $3*[(Bu)_4N^+Cl^-] = 600 \text{ mM}$, **4** – [II-4] = $0.92*[(Bu)_4N^+Cl^-] = 128 \text{ mM}$, **5** – [5] = $3*[(Bu)_4N^+Cl^-] = 105 \text{ mM}$, **6** – [6] = $[(Bu)_4N^+Cl^-] = 100 \text{ mM}$.

Every curve in Figure 2.6 is a linear function at high concentrations (from $I = 10^{-3}$ M, $f(I) = 0.8$ to about $I = 10^{-1}$ M, $f(I) = 0.25$) and values of K_d decrease with decreasing ionic strength as it follows for a cation-anion interaction. Values of K_d , however, decrease faster at low concentrations (below $I = 10^{-1}$ M, $f(I) = 0.25$) than what would arise from a linear dependence. The two-step mechanism represented by the equation (2.11) is in agreement with this observation:



The ^1H NMR of the receptors' acidic protons indicates that at high concentrations almost all of the receptor R in solution is coordinated by Cl^- anion. The same is true for the salt $(\text{Bu})_4\text{N}^+\text{Cl}^-$. Since the concentration of salt in the solutions is the same or lower than the concentration of H-bond donors, almost all the salt is in the form of the aggregates $(\text{Bu})_4\text{N}^+\text{Cl}^-\cdots\text{R}$. Hydrogen-bond donors II-1 - II-6 strengthen the electrolytic properties of clusters $((\text{Bu})_4\text{N}^+\text{Cl}^-)_n$ in CDCl_3 and, thus, the salt is able to disaggregate to form free $(\text{Bu})_4\text{N}^+$ cation and Cl^- anion that is H-bonded to the receptor. Therefore, in a concentrated solution the processes represented by the equation (2.11) is determined by the second step, dissociation of the salt, and a linear dependence of $\ln K_d$ on $f(I)$ is observed.

At low concentrations of the salt the first step in the equation (2.11) becomes limiting. Upon dilution, the concentration of the form $(\text{Bu})_4\text{N}^+\text{Cl}^-$, which does not dissociate, exceeds the concentration of the aggregates $(\text{Bu})_4\text{N}^+\text{Cl}^-\cdots\text{R}$. As a result, the

apparent K_d values decrease faster than what should arise from the expected linear dependence of $\ln K_d$ on $f(I)$.

According to the literature,⁹⁴ equation (2.12), function $f(I) = 1/(1+d*\beta*I^{0.5})$ requires knowledge of the distance d . This parameter can be approximated by the distance between ions in the ion pair $(\text{Bu})_4\text{N}^+, \text{Cl}^- \cdots \text{R}$, which is also unknown. Therefore, initially, as a first approximation, we constructed graph **A** using $d = 6.86 \text{ \AA}$ that equals to the sum of ionic radii for Cl^- and $(\text{Bu})_4\text{N}^+$ ions. Using equation (2.12) and $d = 6.86 \text{ \AA}$, a thermodynamic value of the dissociation constant, $\ln K_d^0$ ($I = 0$, $f(I) = 1$) = -17, was obtained. In the graph **A**, $\ln K_d^0 = -17$, however, would be off scale, that is consistent with the observation that salt $(\text{Bu})_4\text{N}^+\text{Cl}^-$ does not dissociate in CDCl_3 solution. In turn, using the same graph **A**, an experimental value of $\ln K_d^0 = -12$ can be estimated by extrapolation of the linear dependence of K_d on $f(I)$ to $f(I) = 1$ ($I = 0$). According to equation (2.12), this value of thermodynamic constant ($K_d^0 = -12$) corresponds to the distance $d = 10 \text{ \AA}$. Thus, $d = 10 \text{ \AA}$ is an estimated distance between receptor-halide anion and tetrabutylammonium cation in the ion pair $(\text{Bu})_4\text{N}^+, \text{Cl}^- \cdots \text{R}$. Using the parameter $d = 10 \text{ \AA}$ we constructed graph **B**.

The Eigen-Fuoss equation⁹⁴ was used to introduce dependence of electrostatic work required to bring ions together on concentration:

$$K_A = \frac{1}{K_d} = \frac{4\pi N_A d^3}{3000} \exp[-w/RT] \quad w = \frac{z_1 z_2 e^2}{dD_s} \frac{1}{(1 + \beta d \sqrt{I})} \quad (2.12)$$

w – electrostatic work required to bring the ions together,

d – distance between the centers of the ions, z_1 and z_2 - their charges,

$a_1 = a_2 = d/2$ - their radii,

D_s – static dielectric constant,

I – ionic strength, $I = \frac{1}{2} \sum_i c_i z_i^2$ where c_i and z_i concentrations and charges of the

ions in solution: $I = [\text{Cl}^-]_{\text{complexed}} = [(\text{Bu})_4\text{N}^+]_{\text{free}}$.

Calculation of Debye length β in CGS units:

$$\begin{aligned}\beta &= (8 \pi N_A e^2 / 1000 D_s k_B T)^{0.5} = \\ &= (8 * 3.1416 * 6.0221 * 10^{23} * 4.803 * 10^{-10} * 4.803 * 10^{-10} / 10^3 * 4.8 * 1.3806 * 10^{-16} * 298.15)^{0.5} = \\ &= 132939221 \text{ M}^{1/2} \text{ cm}^{-1} = 1.33 \text{ M}^{1/2} \text{ \AA}^{-1}\end{aligned}$$

A. $d = 6.86 \text{ \AA}$ - distance between ions in ionic pair $(\text{Bu})_4\text{N}^+, \text{Cl}^-$ was estimated from the following ionic radii: $r(\text{Cl}^-) = 1.81 \text{ \AA}$, $r((\text{Me})_4\text{N}^+) = 3.40 \text{ \AA}$, $r((\text{Et})_4\text{N}^+) = 3.95 \text{ \AA}$.

B. $d = 10 \text{ \AA}$ - distance between ions in the ion pair between catechol halide anion, $\text{Cl}^- \cdots \text{II-1}$, and $(\text{Bu})_4\text{N}^+$ was estimated using equation (2.9) and the experimental value $\ln K_d^0 = -12$ obtained from the graph **A** in Figure 2.6 by extrapolation to $f(I) = 1$.

2.3.1.6. Why are these results important?

- In the cases when the ^1H NMR spectra of the anion receptor is “unavailable” or “does not change” upon anion binding, the ^1H NMR spectra of the salt can be used to study the stoichiometry of binding and the affinity of the receptor toward Cl^- anion in CDCl_3 .

- The efficient screening of anion receptors, which employs changes in ^1H NMR spectra of the salt as a criteria of the relative affinity towards $(\text{Bu})_4\text{N}^+\text{Cl}^-$ and does not require determination of $K_{a\ 1:1}$, δ_0 , δ_{max} for each compound, can be performed.
- The ^1H NMR spectra of the salt may provide evidence that aggregates of the type $(\text{Bu})_4\text{N}^+\text{Cl}^- \cdots \text{R}$ are formed in solution. These types of intermediates might be formed in CDCl_3 solution in the presence of other H-bond donors/anion receptors.
- Strong dependence of the dissociation constant of the salt $(\text{Bu})_4\text{N}^+\text{Cl}^-$, K_d , on concentration might be an important factor that has to be taken into account when investigating such phenomena as cooperativity of binding, which require knowledge of the thermodynamic values of K_a , as in the case illustrated below in Figure 2.7.

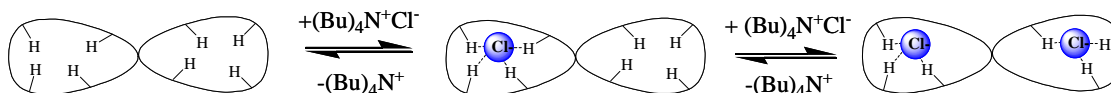


Figure 2.7. Anion binding by cyclic ∞ - shaped receptor in apolar media such as CDCl_3 .⁹⁵

- The dependence of K_d , M on concentration in a polar media (aqueous solution) for an ion pair $\{\text{Cation}^+, \text{Anion}^-\}$ is not strong. However, this dependence becomes dramatic if we move to a solvent with low dielectric constant, like CHCl_3 , or multiply-charged species. In these cases the difference between the thermodynamic value, K_d^0 , M , and the measured, apparent value, K_d , M , can be equal to several orders of magnitude. To obtain the thermodynamic binding constant, independent of

concentration, one needs to keep the ionic strength in the solution constant, while determining the apparent K_d values. Several binding constants, K_d , at different ionic strengths in the solution have to be obtained. Then, thermodynamic K_d^0 , M can be determined by extrapolation of the dependence of K_d , M on concentration to zero ionic strength. Alternatively, one can consider to calculate the activity coefficients (dependence on ionic strength) using empirical formulas.

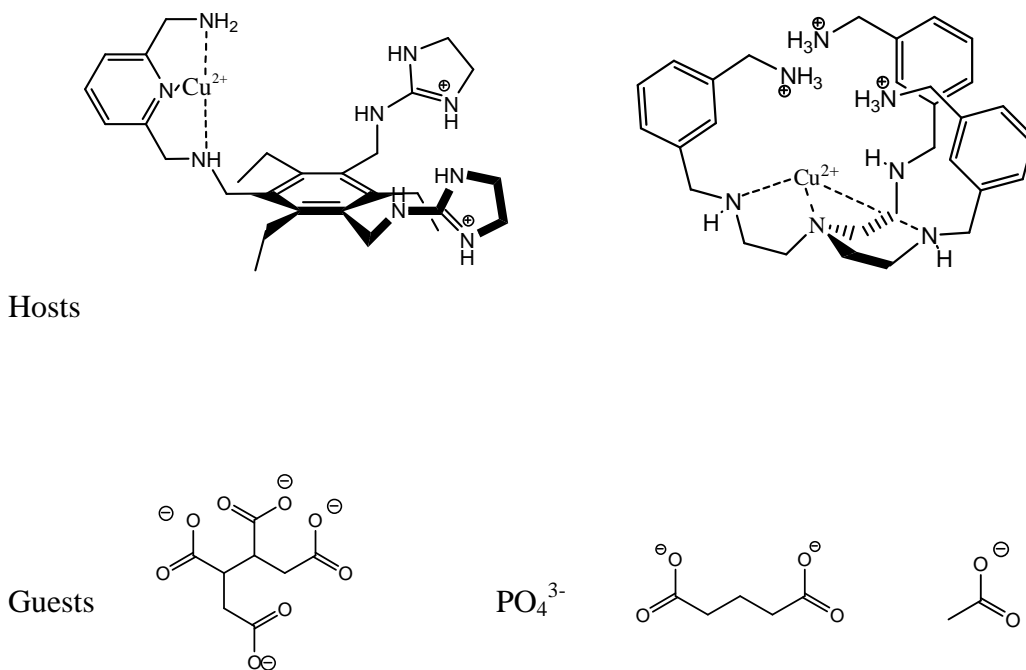


Figure 2.8. Examples of polyanionic guests and polycationic hosts studied in aqueous solution by Anslyn and colleagues.^{96,97}

- Another relevant example is the recent reports by W. H. Gibson *et al.*^{83,98} The authors offered a principally new treatment of the ^1H NMR data for the host-guest interaction involving charged species in the low dielectric constant media

(Figure 2.9. **B**). The experimentally observed dependence of the classical apparent association constant, $K_{a\ 1:1}$, M^{-1} (Figure 2.9. **A**), on the concentration and nature of the counterion defined the necessity in a new approach to the problem.

Therefore, in the aqueous solution for multiply-charged host/guest systems like the ones shown below in Figure 2.8, one has to take into account activity/dependence on ionic strength. Otherwise, the obtained values of the binding constants, and so the “cooperativity of interaction”, would be dependent on concentration. These apparent values would not be desired, independent of concentration, thermodynamic parameters.

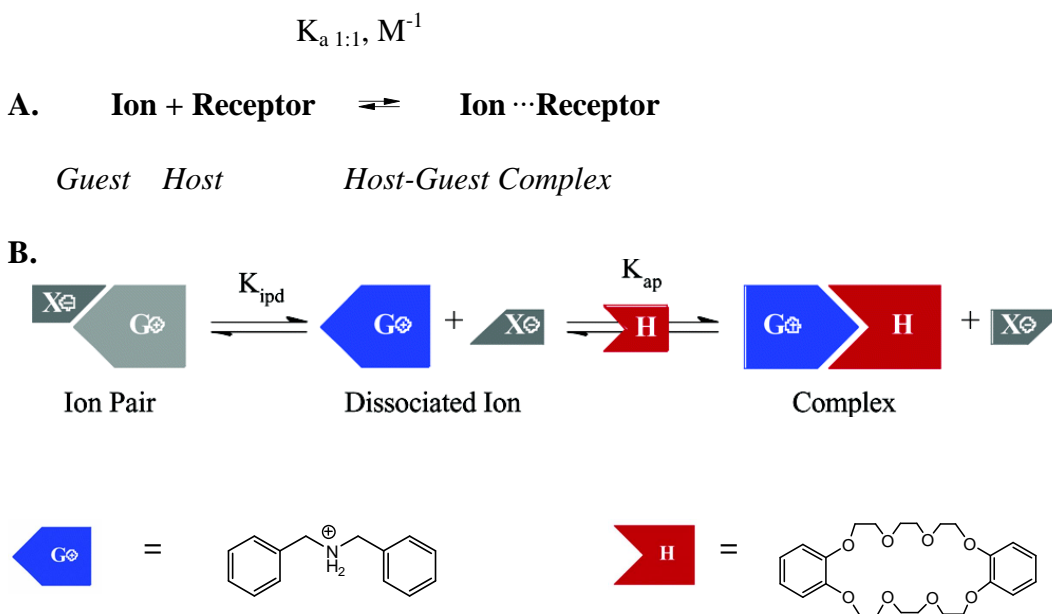


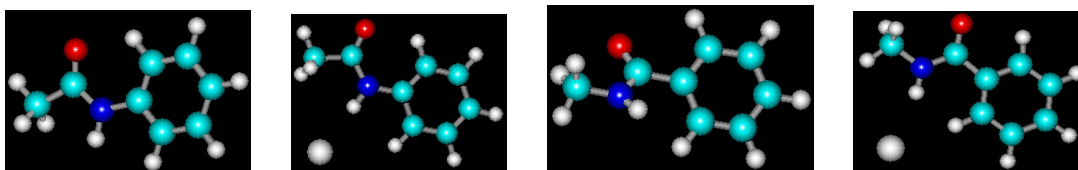
Figure 2.9. A. Classical approach **B.** New approach developed by Gibson and co-workers. Figure **B** is reproduced from the reference 98 with permission from ACS.

As depicted in Figure 2.9. **B**, the new treatment allows one to extract two parameters: K_{ipd} , M, for the ion-pairing equilibrium, and $K_{\text{ap}}M^{-1}$, for the host-guest complexation. The authors noted that chemical signals of the salt in $\text{CD}_3\text{CN}/\text{CHCl}_3$ (2/3) solution were dependent on the concentration and nature of the counterion X^- but, unfortunately, they did not take an advantage of this more simple equilibrium to evaluate K_{ipd} . Instead, both parameters, K_{ipd} and K_{ap} were obtained using “concentration-dependent fluctuations” in the values of the apparent host-guests complexation, $K_{\text{a} 1:1}$, in the presence of the host in solution. This treatment also assumes independence of K_{ipd} on concentration.

It is important to notice the difference between Gibson’s approach (**B**) and our experimental results. First, we established that $(\text{Bu})_4\text{N}^+\text{Cl}^-$ does not dissociate in CDCl_3 unless the host, receptor **II-1** - **II-6**, is present in the solution. Second, we observed formation of the ion-paired intermediates, absent in the scheme **B**. Third, the ion-pairing constant, K_{ipd} (K_{d}), was found to be concentration dependent.

2.3.2. Electronic structure calculations.

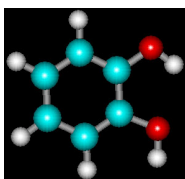
We carried out electronic structure calculations to compare the binding energies for Cl^- anion to receptors II-1 - II-6 and 1,3-dimethyl urea. The geometries of the free receptors and the corresponding complexes with Cl^- anion were optimized using the *ab initio* method, 6-31G* basis set, and the HyperChem software.⁹⁹ The electronic binding energy (ΔE_{elec}) was calculated as the energy difference: $\Delta E_{\text{elec}} = \Delta E_{\text{complex}} - \Delta E_{\text{anion}} - \Delta E_{\text{free receptor}}$. Images of the most stable conformers for the receptors II-1 - II-6 and for the Cl^- anion - receptor complexes with corresponding ΔE_{elec} are shown in Figure 2.10.



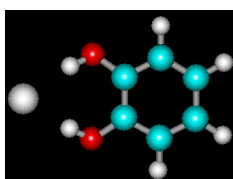
a) free receptor II-3 b) complex II-3... Cl^- c) free receptor II-2 d) complex II-2... Cl^-

$$\Delta E_{\text{elec}} = - 24.3 \text{ kcal mol}^{-1}$$

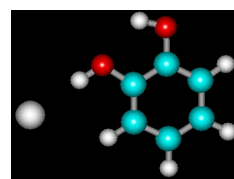
$$\Delta E_{\text{elec}} = - 22.1 \text{ kcal mol}^{-1}$$



e) free receptor II-1



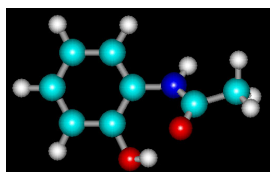
f) complex II-1... Cl^-



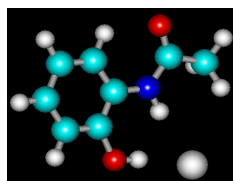
g) intramolecular H-bonded complex II-1... Cl^-

$$\Delta E_{\text{elec}} = - 26.0 \text{ kcal mol}^{-1}$$

$$\Delta E_{\text{elec}} = -24.7 \text{ kcal mol}^{-1}$$

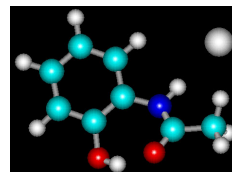


h) free receptor II-4



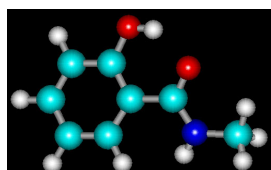
i) complex II-4...Cl⁻

$$\Delta E_{\text{elec}} = -25.4 \text{ kcal mol}^{-1}$$

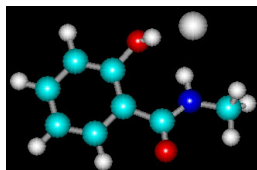


j) intramolecular H-bonded complex II-4...Cl⁻

$$\Delta E_{\text{elec}} = -25.6 \text{ kcal mol}^{-1}$$

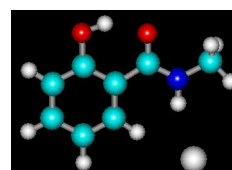


k) free receptor II-5



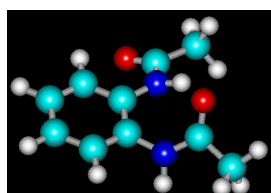
l) complex II-5...Cl⁻

$$\Delta E_{\text{elec}} = -17.0 \text{ kcal mol}^{-1}$$

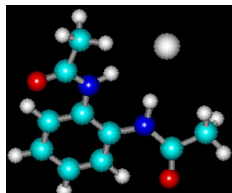


m) intramolecular H-bonded complex II-5...Cl⁻

$$\Delta E_{\text{elec}} = -24.9 \text{ kcal mol}^{-1}$$

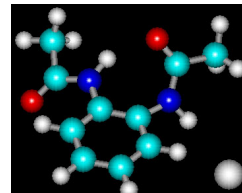


n) free receptor II-6



o) complex II-6...Cl⁻

$$\Delta E_{\text{elec}} = -30.4 \text{ kcal mol}^{-1}$$



p) intramolecular H-bonded complex II-6...Cl⁻

$$\Delta E_{\text{elec}} = -23.1 \text{ kcal mol}^{-1}$$

Figure 2.10. Optimized lowest energy conformations for the free receptors II-1 - II-6 and corresponding complexes with Cl⁻ anion. Calculations were carried out using *ab initio* method, 6-31G* basis set, and HyperChem software.

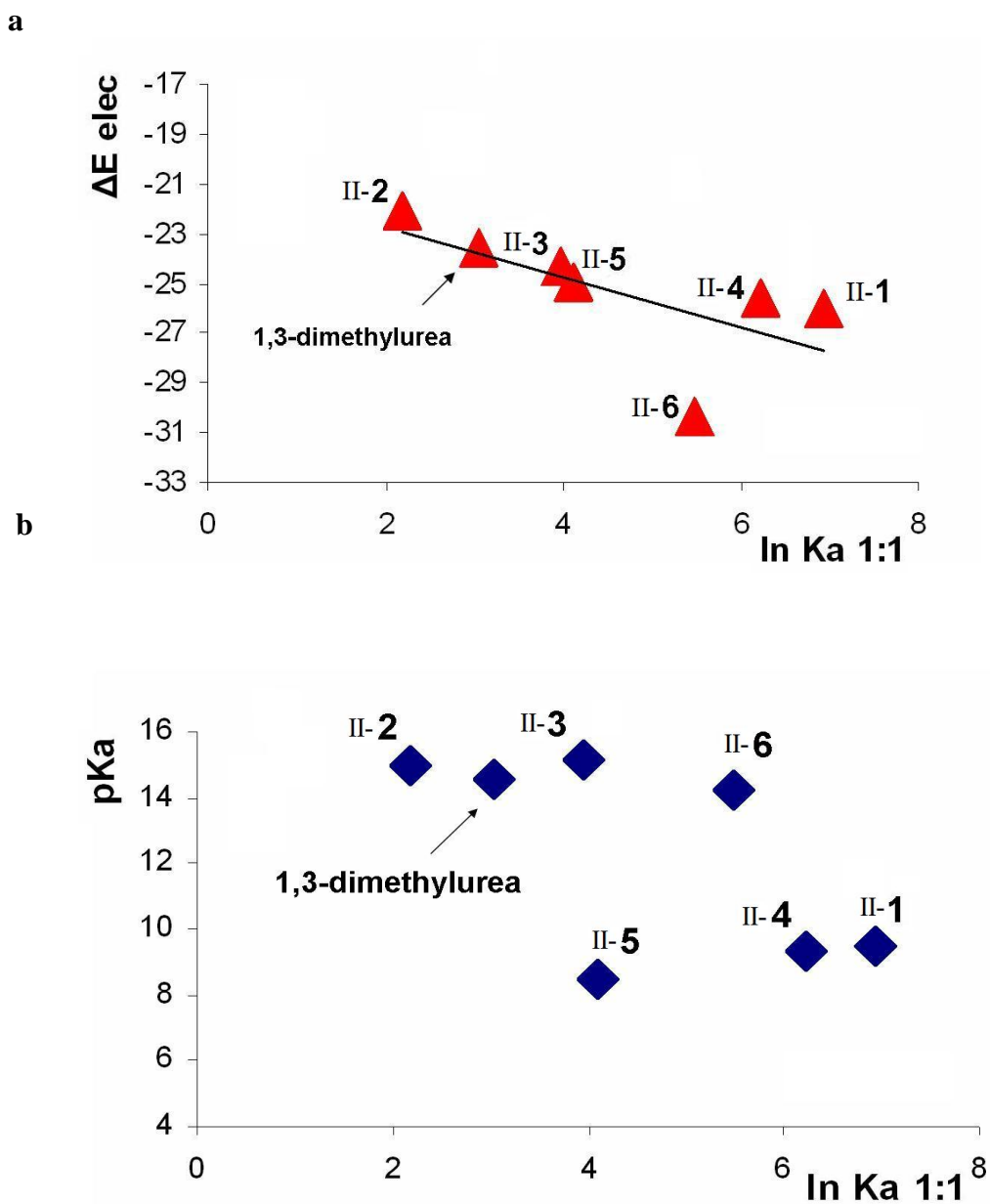


Figure 2.11. Correlation between: $\ln K_{a\ 1:1}$ and ΔE_{elec} (a), $\ln K_{a\ 1:1}$ and pK_a (b).

Energetic data indicate that intramolecular H-bonded complexes of receptors II-4 and II-5 with Cl^- anion (j and m) are of the lower energy than corresponding complexes with $OH \cdots Cl^- \cdots HN$ contact (i and l). For receptors II-1 and II-6, however, formation of

two strong H-bonds with Cl⁻ anion (**f** and **o**) is energetically favorable over intramolecular H-bonded isomers (**g** and **p**). The electronic binding energies obtained, ΔE_{elec} , were correlated with the apparent $K_{a\ 1:1}$ values (Figure 2.11.a). In Figure 2.11.b, pK_a values of H-bond donors II-1 - II-6, evaluated using ACD Lab program,¹⁰⁰ were correlated with the apparent association constants, $K_{a\ 1:1}$. There is a good correlation between the experimental $\ln K_{a\ 1:1}$ and calculated ΔE_{elec} for the most stable isomers if receptor II-6 is excluded. The optimized geometry of the “free” receptor II-6 is rather bent. If compared to II-1 and II-3, receptor II-6 has much stronger tendency to self-aggregate in a CDCl₃ solution (SI 2.1). In the crystal structure, individual molecules of II-6 form four H-bonds with two other molecules below and above the plane of the aromatic ring and thus assemble into columns (SI 2.1).¹⁰¹ We believe that calculations simply overestimate the energy of the “free” receptor II-6, which is stabilized in solution due to intermolecular contacts/self-association.

The presented data demonstrate good agreement between theoretical predictions of intrinsic relative affinity towards Cl⁻ anion and the experiment. Due to similar values of ΔE_{elec} , different structural isomers of R[⋯]Cl⁻ can be present in the solution simultaneously (compare **i** and **j**). *Ab initio* calculations can be applied to elucidate geometries as well as to estimate populations of these structural isomers. These results highlight that theoretical methods can provide new insights into the understanding of the ¹H NMR experiment. To the best of our knowledge, this is the first example where the electronic structure calculations were used to evaluate relative affinity of different H-bond donors towards an inorganic anion.

2.3.3. ESI-MS study.

2.3.3.1. ESI mass spectra indicate formation of the dimers $R_2 \cdots Cl^-$ and $R' \cdots Cl^- \cdots R$ in the presence of an excess of H-bond donors. Mass spectra (MS) depicted in Figure 2.12 were recorded using a $CHCl_3$ solution containing 5 mM of the salt $(Bu)_4N^+Cl^-$, 15 mM of catechol (II-1), 15 mM of acetanilide (II-3), and 15 mM of receptor II-6. A negative-ion MS (A) indicates dominant formation of various dimers coordinated with a single Cl^- anion. Hetero- and homomolecular clusters in all possible combinations are found in the solution. Based just on the MS data, it is not possible to say if the observed 1:1 complexes are formed as a result of ion fragmentation in the spectrometer or if they are present in the original sample solution. This is due to the fact that the intensity of the signals in MS is very sensitive to the experimental conditions; for example, the intensity of the 2:1 cluster relative to the 1:1 complex decreases with either increasing temperature, flow rates, and/or applied voltages (see experimental section for more details).

Remarkably, a small amount of a 3:1 complex was observed only in the case of receptor II-6. Importantly, there is also no indication of any heteromolecular 3:1 clusters! Therefore in $II-6_2 \cdots Cl^-$ and $II-6_3 \cdots Cl^-$, addition of the second and third molecule of the receptor II-6 is likely to be due to strong self-association of II-6 in $CHCl_3$ solution. Possibly, anion-receptor interactions for the second and the third molecule of the receptor II-6 would be diminished due to steric constraints.

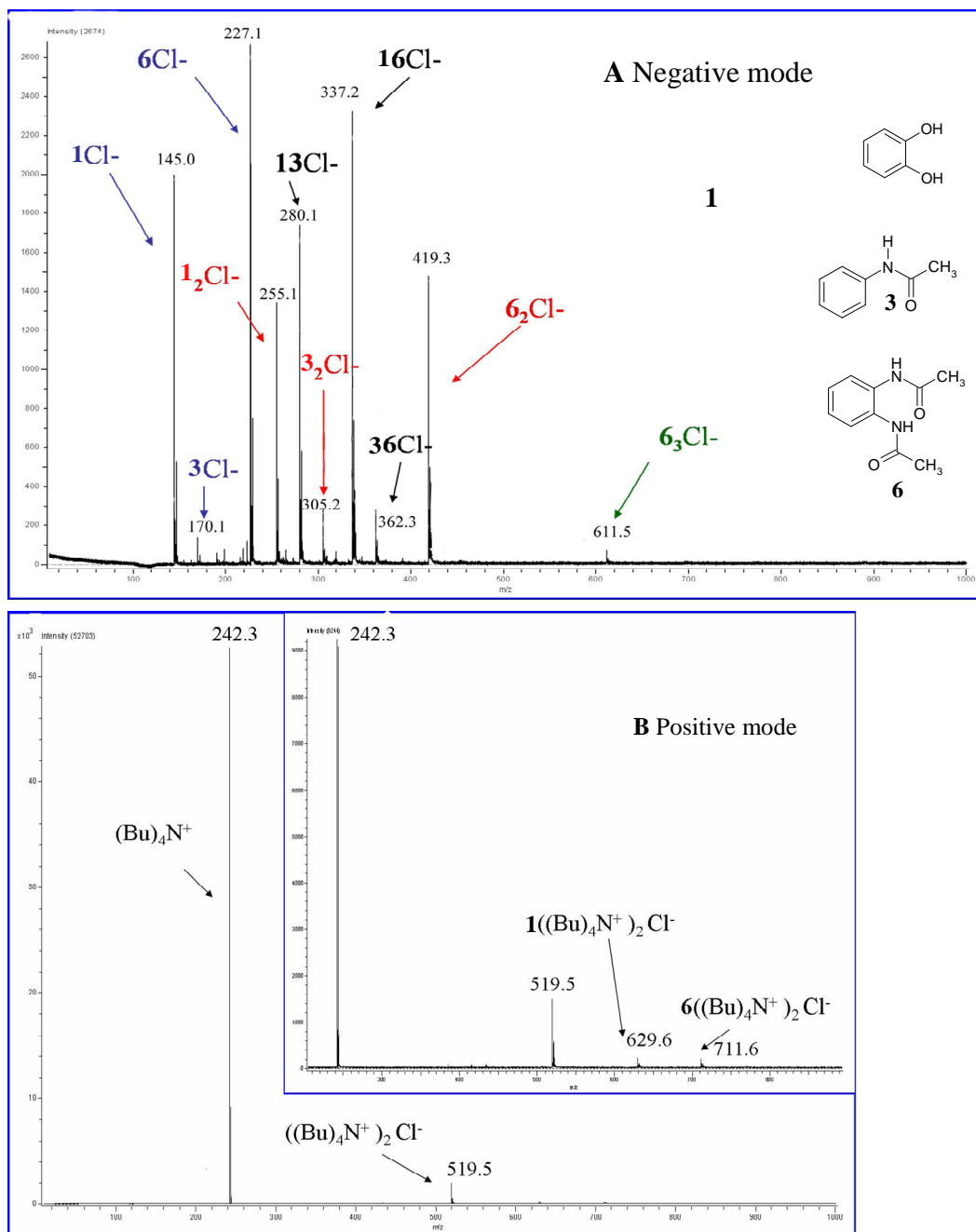


Figure 2.12. Negative ion (A) and positive ion (B) mass spectra of CHCl₃ solution containing 5 mM of the salt (Bu)₄N⁺Cl⁻, 15 mM of catechol (II-1), 15 mM of acetanilide (II-3), and 15 mM of receptor II-6. For clarity the receptors are indicated using only Arabic numbers **1**, **3**, and **6** instead of II-1, II-3, II-6.

The cation $(\text{Bu})_4\text{N}^+$ is the major signal observed in the positive-ion MS (Figure 2.12. **B**). Other aggregates $((\text{Bu})_4\text{N}^+)_2\text{Cl}^-$, **II-3** $\cdots((\text{Bu})_4\text{N}^+)_2\text{Cl}^-$, and **II-6** $\cdots((\text{Bu})_4\text{N}^+)_2\text{Cl}^-$ are found only in relatively tiny amounts. In the absence of H-bond donors in CHCl_3 solution, MS of the pure salt $(\text{Bu})_4\text{N}^+\text{Cl}^-$ indicate formation of the clusters $((\text{Bu})_4\text{N}^+)_2\text{Cl}^-$, instead of free $(\text{Bu})_4\text{N}^+$, and $(\text{Bu})_4\text{N}^+\text{Cl}_2^-$, instead of $((\text{Bu})_4\text{N}^+)_{m-1}\text{Cl}_m^- \cdots \text{R}_n$ ($m \leq n$) and $\text{R}_2 \cdots \text{Cl}^-$, as the major signals in the positive and negative-ion regimes respectively (SI 2.4).

In summary, in a CHCl_3 solution of the salt $(\text{Bu})_4\text{N}^+\text{Cl}^-$ the microscopic environment of the Cl^- anion drastically changes in the presence of H-bond donors. ESI MS indicate formation of the homo- and heterodimers $\text{R}_2 \cdots \text{Cl}^-$ and $\text{R}' \cdots \text{Cl}^- \cdots \text{R}$ when receptors **II-1**, **II-3**, and **II-6** are present in excess.

2.3.3.2. ESI mass spectra indicate presence of the ion-paired intermediates $(\text{Bu})_4\text{N}^+\text{Cl}^- \cdots \text{R}$ when the concentrations of H-bond donors and the salt are comparable in solution. Negative-ion mass spectra shown in Figure 2.13 represent the microscopic environment of Cl^- anion if concentrations of the salt and the anion receptors are comparable in CHCl_3 solution. Signals for ion-paired aggregates **II-1** $\cdots(\text{Bu})_4\text{N}^+\text{Cl}_2^-$, **II-1₂** $\cdots(\text{Bu})_4\text{N}^+\text{Cl}_2^-$, **II-3₂** $\cdots(\text{Bu})_4\text{N}^+\text{Cl}_2^-$, **II-3** $\cdots(\text{Bu})_4\text{N}^+\text{Cl}_2^-$, etc. appear in the spectrum. These anions may also correspond to the neutral aggregates **II-1** $\cdots(\text{Bu})_4\text{N}^+\text{Cl}^-$, **II-1** $\cdots(\text{Bu})_4\text{N}^+\text{Cl}_2^-$, **II-1₂** $\cdots(\text{Bu})_4\text{N}^+\text{Cl}^-$, **II-1₂** $\cdots(\text{Bu})_4\text{N}_2^+\text{Cl}_2^-$, etc. that are not seen in the mass spectra. These type of aggregates (neutral and charged), schematically represented as $(\text{Bu})_4\text{N}^+\text{Cl}^- \cdots \text{R}$, are thought to be “ion-paired intermediates” that are in equilibrium between the free (R)

and the complexed forms ($R_2 \cdots Cl^-$ and $R \cdots Cl^-$). It is also apparent from the spectra depicted in Figure 2.13 that the ability of II-6 to form ion-paired aggregates is diminished if compared to the receptors II-3 and II-1.

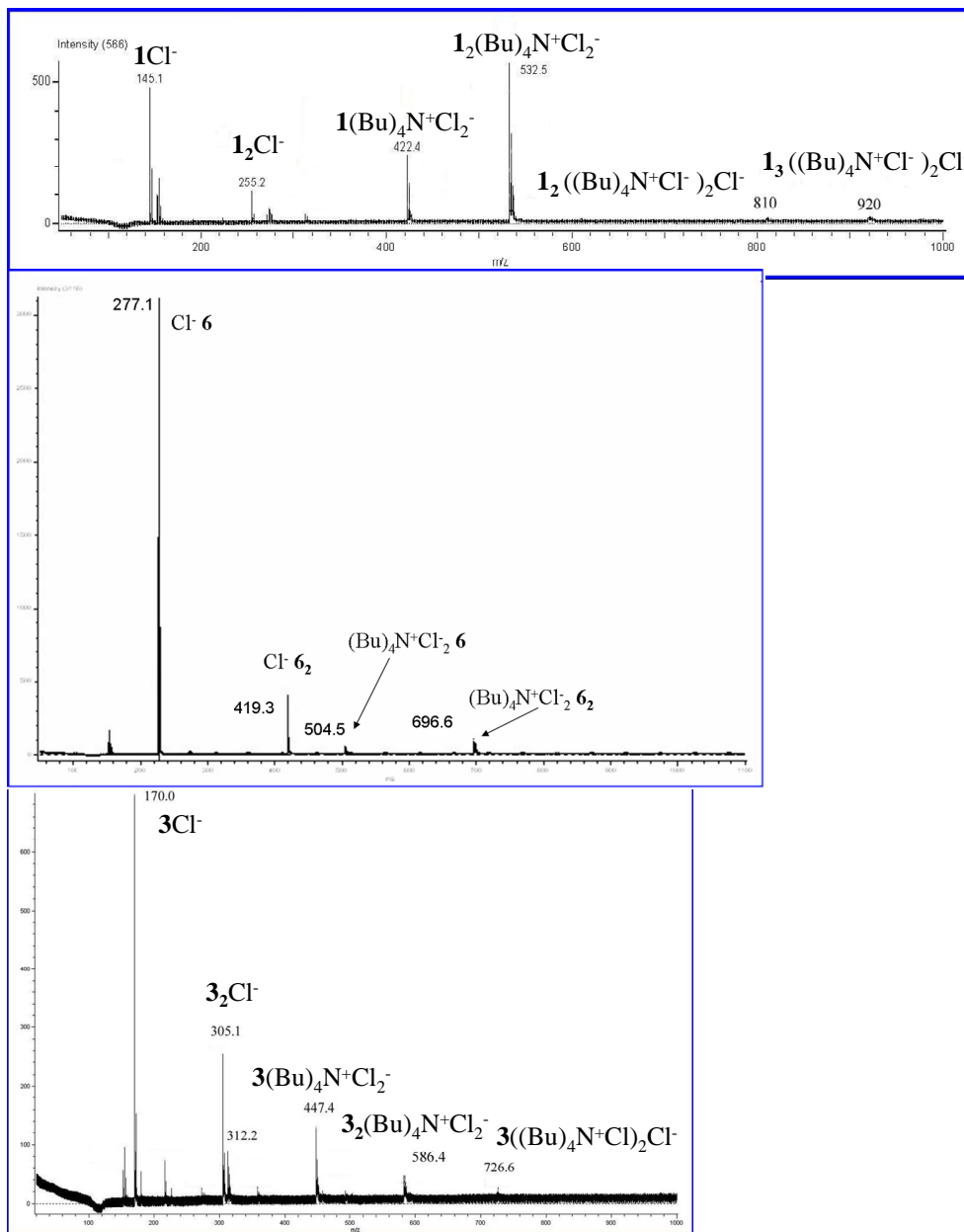


Figure 2.13. Negative-ion mass spectra of the solution containing 20 mM of the salt $(Bu)_4N^+Cl^-$ and 20 mM of H-bond donors II-1, II-3, and II-6. For clarity the receptors are indicated using only Arabic numbers **1,3**, and **6** instead of II-1, II-3, II-6.

2.3.3.3. Relative distribution of the clusters in the negative-ion MS is determined by the salt to receptor ratio. Competition for binding to Cl⁻ anion.

High concentrations of the hydrogen bond donors shift the equilibrium toward the 2:1 complexes, while high concentrations of the salt favor ion-paired aggregates in CHCl₃ solution. For example, Figure 2.14 represents how the distribution of the negative ions depends on the ratio of the salt to receptor for catechol (II-1). When the ratio of salt to receptor is 7 : 1, clusters of the salt (Bu)₄N⁺Cl₂⁻ (m/z = 312), ((Bu)₄N⁺Cl⁻)₂Cl⁻ (m/z = 592), ((Bu)₄N⁺Cl⁻)₃Cl⁻ (m/z = 870) and their ion-paired aggregates II-1⋯(Bu)₄N⁺Cl₂⁻ (m/z = 422), II-1₂⋯(Bu)₄N⁺Cl₂⁻ (m/z = 533), II-1⋯((Bu)₄N⁺Cl⁻)₂Cl⁻ (m/z = 702) are present in CHCl₃ solution. The relative intensities of these salt clusters are higher than the intensities of corresponding aggregates with catechol. It is difficult to say if the complex II-1⋯Cl⁻ observed in the spectra is also present in the original sample solution or if it is formed in the chamber as a result of fragmentation. As the ratio of salt to receptor decreases to 3:1, the relative intensities of the ion-paired aggregates increase (red arrows), compared to the intensities of salt clusters (blue arrows). Moreover, the signal of ((Bu)₄N⁺Cl⁻)₃Cl⁻ (m/z = 870) completely disappears. Instead, the signal of the new cluster II-1₂⋯((Bu)₄N⁺Cl⁻)₂Cl⁻ (m/z = 812) becomes visible in the mass spectrum. As the ratio continues to decrease, the same trend continues to be observed in the distribution of the intensities in the negative MS. Signals of the salt clusters become weaker and finally disappear. The relative intensities of ion-paired aggregates with higher degree of complexation of the receptor gradually increase. The pronounced simplification of the spectra is observed when an excess of catechol II-1 is present in solution.

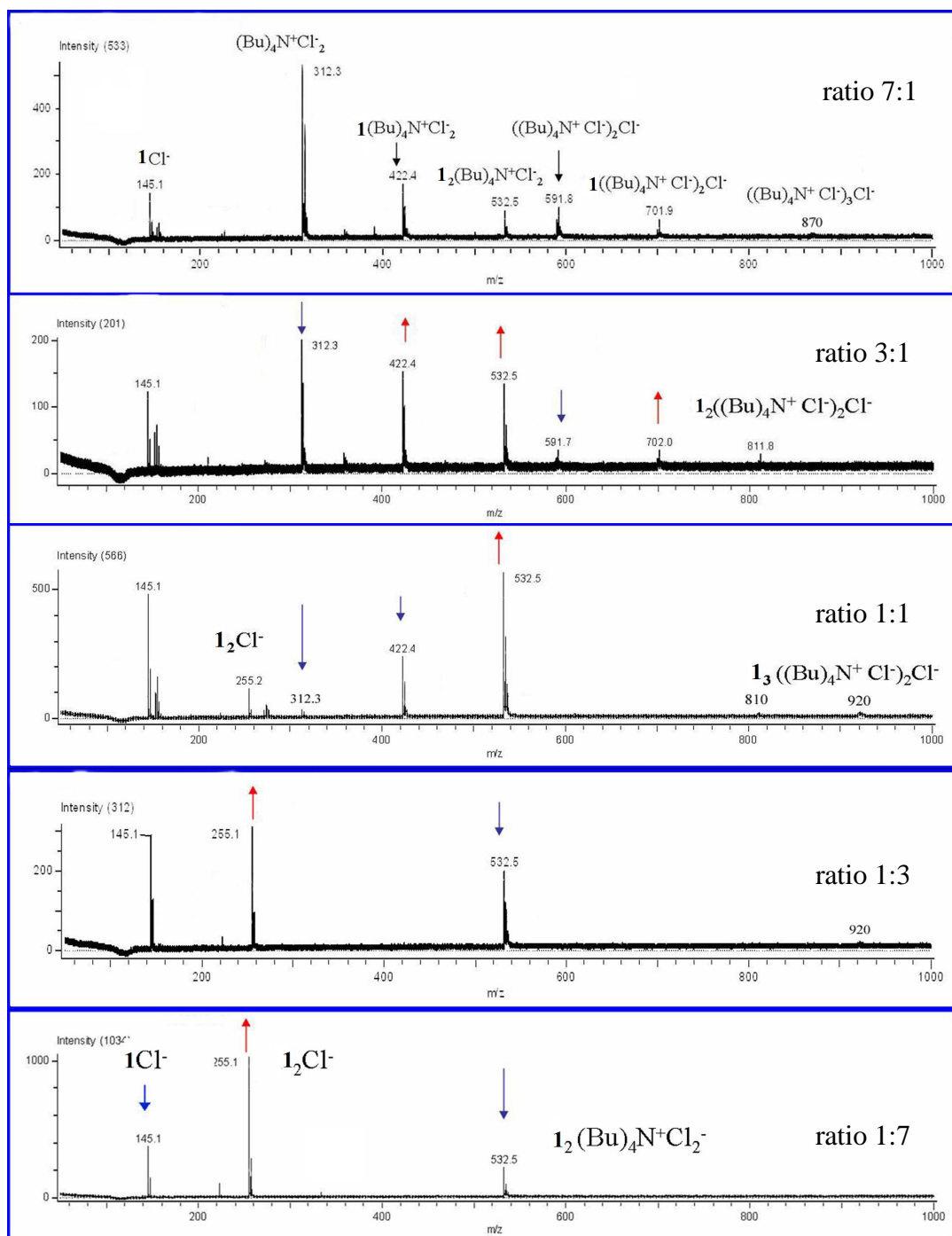


Figure 2.14. Negative-ion clusters in CHCl_3 solution of $(\text{Bu})_4\text{N}^+\text{Cl}^-$ and catechol (II-1). Total concentration is $[(\text{Bu})_4\text{N}^+\text{Cl}^-] + [\text{R}] = 40$ mM. The ratio salt : receptor changes from 7:1 to 1:7. For clarity the receptors are indicated using only Arabic numbers **1,3**, and **6** instead of II-1, II-3, II-6.

The relative intensity of $\text{II-1}_2 \cdots (\text{Bu})_4\text{N}^+\text{Cl}_2^-$ ($m/z = 533$), the only ion-paired aggregate left, drops. The peak of $\text{II-1}_2 \cdots \text{Cl}^-$ ($m/z = 255$), the only aggregate that contains more than one molecule of the receptor per one Cl^- anion, becomes the major signal when the ratio of salt to ligand goes beyond 1 : 3.

Remarkably, the clusters $(\text{Bu})_4\text{N}^+\text{Cl}^- \cdots \text{R}_2$, which contain more than one molecule of receptor per one Cl^- anion, were never observed. This fact indicates that addition of the second molecule of simple H-bond donors **II-1** - **II-6** results in the weakening of the electrostatic forces in the pair $(\text{Bu})_4\text{N}^+\text{Cl}^-$ and the breaking apart of the ionic clusters (see also SI 2.5).

2.3.3.4. **Based on the ESI-MS data the following can be concluded:**

Interaction of the small organic H-bond donors **II-1** - **II-6** with Cl^- anion in CHCl_3 is a rather complicated process. Simple amides and phenols compete with counterions that accompany anions in solution to maintain electric neutrality. As a result, a variety of aggregates that combine both electrostatics and H-bonding in the structure are present in solution.

ESI mass spectra indicate formation of the ion-paired intermediates schematically represented as $(\text{Bu})_4\text{N}^+\text{Cl}^- \cdots \text{R}$, where R is receptor **II-1** - **II-6**. Clusters $(\text{Bu})_4\text{N}^+\text{Cl}^- \cdots \text{R}_2$, which contain more than one molecule of receptor per one Cl^- anion, were never observed. This fact suggests that the addition of the second molecule of simple H-bond donors **II-1** - **II-6** always results in breaking apart of the pair $(\text{Bu})_4\text{N}^+\text{Cl}^-$, as shown in Figure 2.15.

The ESI MS and ^1H NMR data for compounds II-1 - II-5 are in agreement with each other: both techniques evidence formation of the dimers and ion-paired aggregates in CHCl_3 solution. In contrast, ESI MS indicates formation of the dimers $\text{R}_2\cdots\text{Cl}^-$, while ^1H NMR supports a 1:1 stoichiometry of interaction between receptor II-6 and Cl^- anion. This apparent discrepancy can be explained if we take into account the relatively strong ability of II-6 to self-associate. In $\text{II-6}_2\cdots\text{Cl}^-$ and $\text{II-6}_3\cdots\text{Cl}^-$, addition of the second and third molecule of the receptor is thought to arise largely through self-association of II-6 rather than anion-receptor interaction.

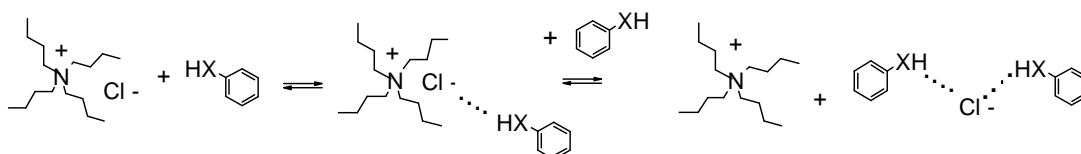


Figure 2.15. Schematic representation of interaction between $(\text{Bu})_4\text{N}^+\text{Cl}^-$ and H-donor in CHCl_3 . X is electronegative oxygen (O) or amide (N-COR group). Ion-paired aggregate formed on the first step dissociates when the second H-bonding unit coordinates to the Cl^- anion.

To the best of our knowledge there are no other reports to indicate the formation of ion-paired aggregates $(\text{Bu})_4\text{N}^+\text{Cl}^- \cdots \text{R}$ or dimers $\text{Cl}^- \cdots \text{R}_2$, $\text{R}' \cdots \text{Cl}^- \cdots \text{R}$ where R, R' are simple amides and/or phenols. The most relevant ^1H NMR study of interaction between $(\text{Bu})_4\text{N}^+\text{Cl}^-$ and simple amides/phenols conducted in CD_3CN

concluded that dimers $\text{Cl}^- \cdots \text{R}_2$, $\text{R}' \cdots \text{Cl}^- \cdots \text{R}$ were never observed in any experimental conditions.⁵⁷

Observation of the dimers $\text{R}_2 \cdots \text{Cl}^-$ using ESI MS at room temperature indicates that these structures are rather stable and can be utilized as a binding motif to design new anion receptors and transporters.

2.4. Supporting Information for Chapter 2.

2.4.1. Self-association of the receptors II-1, II-3, and II-6 in CHCl₃ solution. The concentrated solutions of receptors II-1, II-3, and II-6 in CHCl₃ were diluted. The dependence of chemical shifts of acidic protons (δ , ppm) on concentration [R], M is depicted in Figure S2.1. Within the same concentration range, the data for receptor II-6 reveal the highest degree of concavity. This fact indicates that self-association process is the most pronounced for receptor II-6.

Using Origin 7.0 program¹⁰⁹, the curve fitting method was applied to calculate the constant from the experimental data sets. The dimerization was chosen as the simplest process to model self-association:



The following function was used to create the best fit:

$$\delta = (4 * K_a * [R] + 1 - (1 + 8 * K_a * [R])^{0.5}) / (4 * K_a * [R]) * (\delta_{\max} - \delta_0) + \delta_0 \quad (\text{S2.1})$$

where chemical shift (δ , ppm) is a dependent variable, concentration of the receptor in solution ([R], M) is an independent variable; chemical shift of the free receptor (δ_0 , ppm), chemical shift of the dimer (δ_{\max}), and association constant (K_a) are three parameters to be calculated.

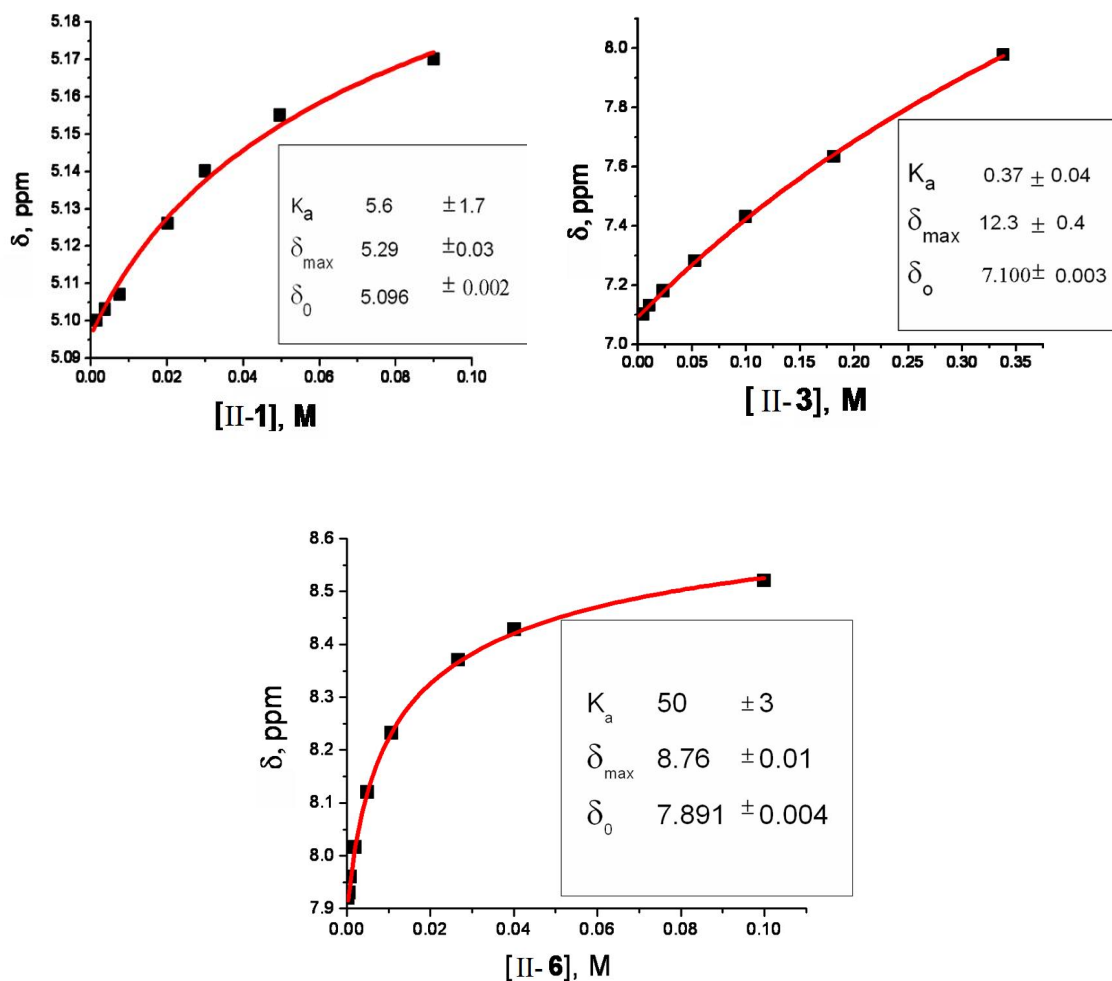


Figure S2.1. Dependence of chemical shifts, δ , ppm, of the receptor's acidic protons on concentration of the receptors II-1, II-3, and II-6 in CHCl_3 solution. Values of the chemical shifts of the free receptor (δ_0 , ppm), chemical shift of the dimer (δ_{\max} , ppm), and association constants for the process of dimerization (K_a , M^{-1}), shown in the box, are derived from the experimental data points using curve fitting method as described. The generated best fit is indicated as a red solid curve.

Calculated values of K_a , M^{-1} indicate that, compared to anion binding, the process of self-association is rather weak for receptors II-1 and II-3 (K_a (II-1) = 5.6 M^{-1} vs $K_{a\ 1:1}$ (II-1) = 1100 M^{-1} and K_a (II-3) = 0.37 M^{-1} vs $K_{a\ 1:1}$ (II-3) = 54 M^{-1}). In contrast, self-association of II-6 ($K_a = 50 M^{-1}$) may compete with the binding of receptor II-6 to Cl^- anion ($K_{a\ 1:1} = 230 M^{-1}$) in $CHCl_3$ solution.

Moreover, in the solid state each molecule of II-6 employs two amide groups to form four intermolecular H-bonds with two neighbors. The picture of the crystal structure of receptor 6 shown in Figure S2.2 is reprinted from the original publication.

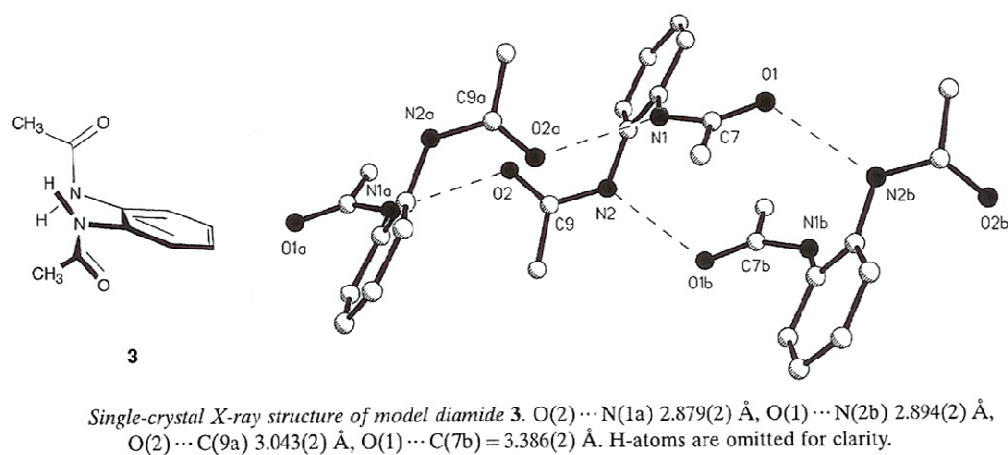


Figure S2.2. Intermolecular H-bonds in the crystal structure of the receptor II-6. This image is reprinted from the original publication 101.

2.4.2. **Chemical shift of (Bu)₄N⁺Cl⁻ in CHCl₃ is independent on concentration.**

Table S2.1. Chemical shift of α -CH₂ in (Bu)₄N⁺Cl⁻ as function of the solvent and concentration.

Solvent	Chemical shift of α -CH ₂ , ppm in X				pK _a	D _s	Chem.	Chem. shift
	M solution [*]						Shift of the	of the
	2 M	1 M	0.1 M	< 0.01 M			solvent signal in 1 M solution of (Bu) ₄ NCl (ppm)	solvent signal without any additives (ppm)
D ₂ O	3.20	-	3.21		14	78.5	4.81	4.80
DMSO	3.23	3.18	3.17		35	46.7	2.52	2.50
CD ₃ CN	3.19	3.12	3.10		25	37.5	1.97	1.93
CDCl ₃	3.46 (sat.)	3.40	3.40	3.40 – 3.38 [@]	17	4.8	7.50	7.25
C ₆ D ₆	3.44 (sat.)	3.38	3.30		43	2.3	7.17	7.16

* - all spectra were calibrated on TMS signal, all concentrations are approximate.

@ - depending on concentration of residual water in the sample.

sat. - saturated.

2.4.3. Job plots A and B for receptors II-2, II-4, and II-5.

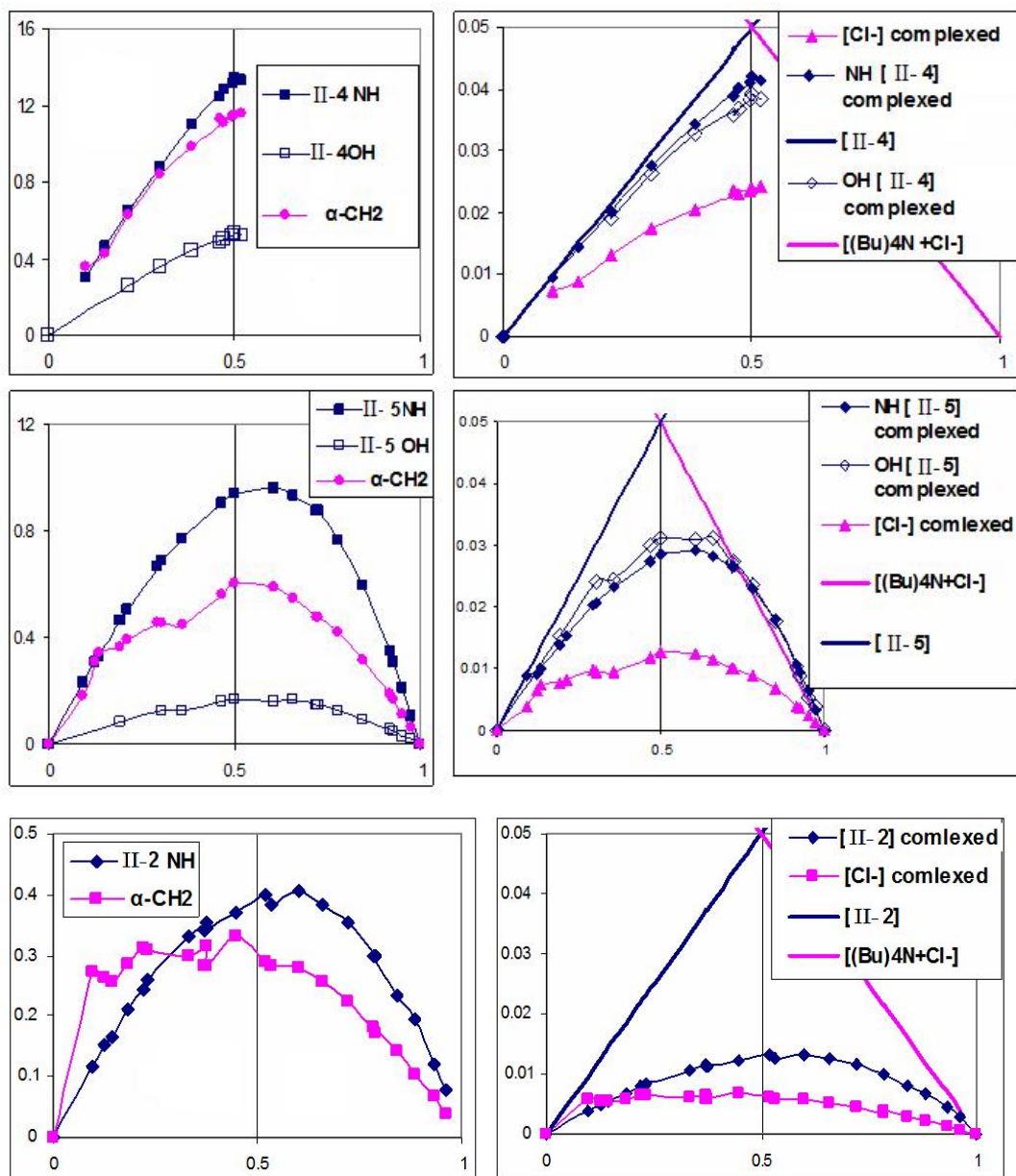


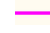



Figure S2.3. Job plots. Horizontal axes (x) are fractions of the receptors II-2, II-4, and II-5, the total concentration in solution is constant $[(\text{Bu})_4\text{N}^+\text{Cl}^-] + [\text{R}] = 100 \text{ mM}$. (A) Classic approach. Blue squares \blacksquare : dependence of δx , ppm on x , where δ is chemical shift of the acidic protons as indicated. Pink circles \bullet : dependence of

$10\delta x$, ppm on x , where δ is chemical shift of α -CH₂ of the salt (Bu)₄N⁺Cl⁻. **(B)**
Dependence of concentration of the complexed form of receptors II-2, II-4, and II-5 (blue rhombs ) and concentration of complexed Cl⁻ anions (pink triangles ) in solution on x . Solid lines indicate total concentration of the salt (pink ) and receptors (blue ) in solution.

2.4.4. **ESI MS of the salt $(\text{Bu})_4\text{N}^+\text{Cl}^-$ in CHCl_3 .** ESI MS of CHCl_3 solution of the salt $(\text{Bu})_4\text{N}^+\text{Cl}^-$ is shown in Figure S3.4. The aggregate $((\text{Bu})_4\text{N}^+)_2\text{Cl}^-$ ($m/z = 519$) is a predominant positive-ion cluster (**A**). In contrast, naked $(\text{Bu})_4\text{N}^+$ ($m/z = 242$) was the major signal in excess in solution of H-bond donors the salt. The aggregates $(\text{Bu})_4\text{N}^+\text{Cl}_2^-$ ($m/z = 312$), $((\text{Bu})_4\text{N}^+\text{Cl}^-)_2\text{Cl}^-$ ($m/z = 592$) as well as solvated Cl^- anions $\text{Cl}^-\cdot\text{CHCl}_3$ ($m/z = 155$) and $\text{Cl}^-\cdot(\text{CHCl}_3)_2$ ($m/z = 275$) are found in the negative-ion MS. Importantly, the relative intensities of the negative-ion clusters strongly depend on the flow rate of the nebulizing gas N_2 . Increasing flow rate of N_2 weakens the signals of the salt clusters $(\text{Bu})_4\text{N}^+\text{Cl}_2^-$ and $((\text{Bu})_4\text{N}^+\text{Cl}^-)_2\text{Cl}^-$ and finally causes them to disappear, whereas signals $\text{Cl}^-\cdot\text{CHCl}_3$ and $\text{Cl}^-\cdot(\text{CHCl}_3)_2$ become dominant (**B**). It is possible that anions $\text{Cl}^-\cdot\text{CHCl}_3$ and $\text{Cl}^-\cdot(\text{CHCl}_3)_2$ are formed in the chamber as a result of fragmentation of the salt aggregates rather than being present in the original sample solution. In turn, decreasing the flow rate of N_2 strengthens the signals of the ion clusters (**C**). Moreover, new aggregates $((\text{Bu})_4\text{N}^+\text{Cl}^-)_3\text{Cl}^-$ ($m/z = 870.8$), $(\text{Bu})_4\text{N}^+\text{Cl}_2^- \cdot \text{C}_2\text{H}_5\text{OH}$ ($m/z = 358$) and $((\text{Bu})_4\text{N}^+\text{Cl}^-)_2\text{Cl}^- \cdots \text{C}_2\text{H}_5\text{OH}$ ($m/z = 638$) appear in the spectrum. (The chloroform, used in the study, contained up to one percent of $\text{C}_2\text{H}_5\text{OH}$ as stabilizer.) This variety of negatively charged salt clusters is replaced by the dimers $\text{R}_2 \cdots \text{Cl}^-$ when receptor R is in excess.

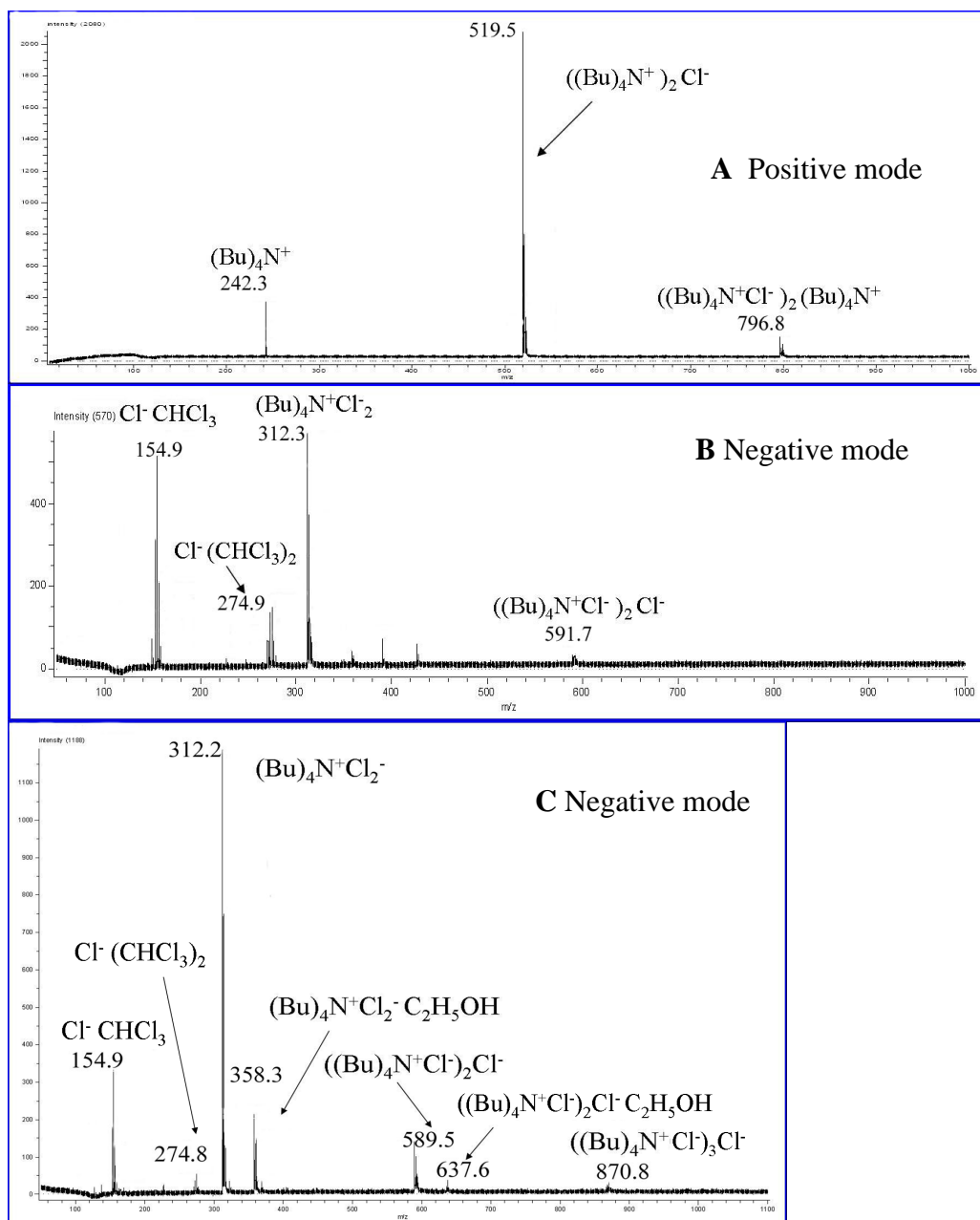
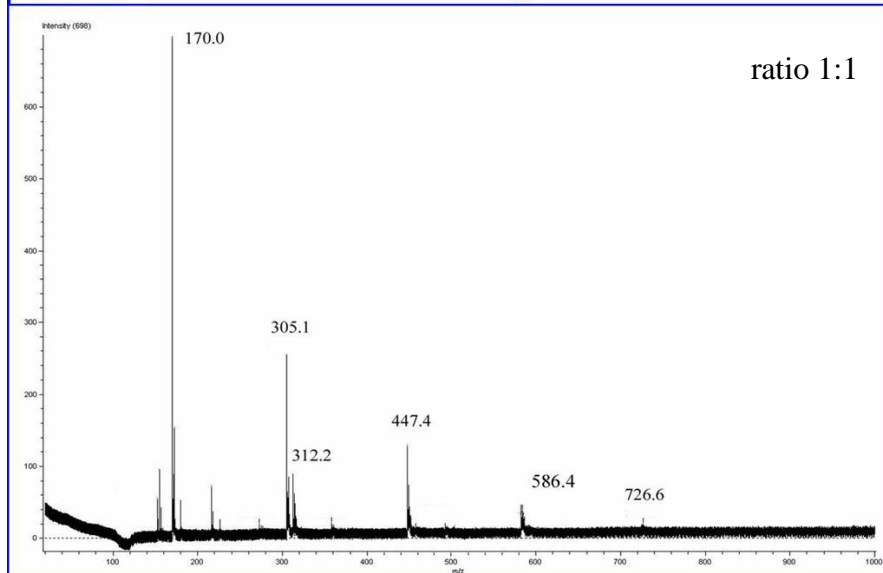
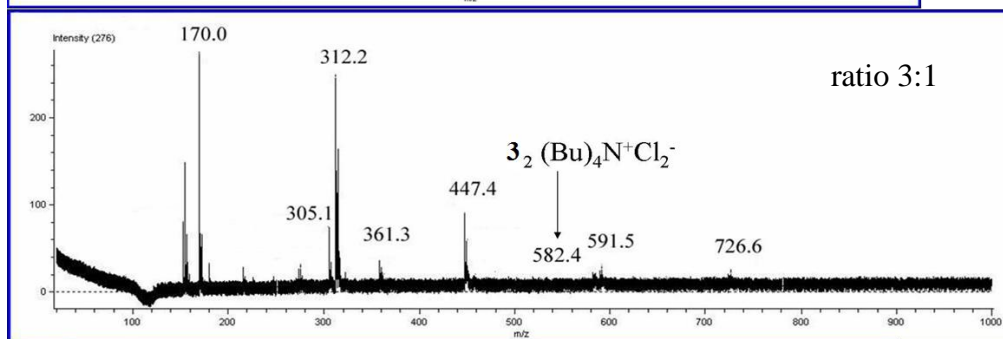
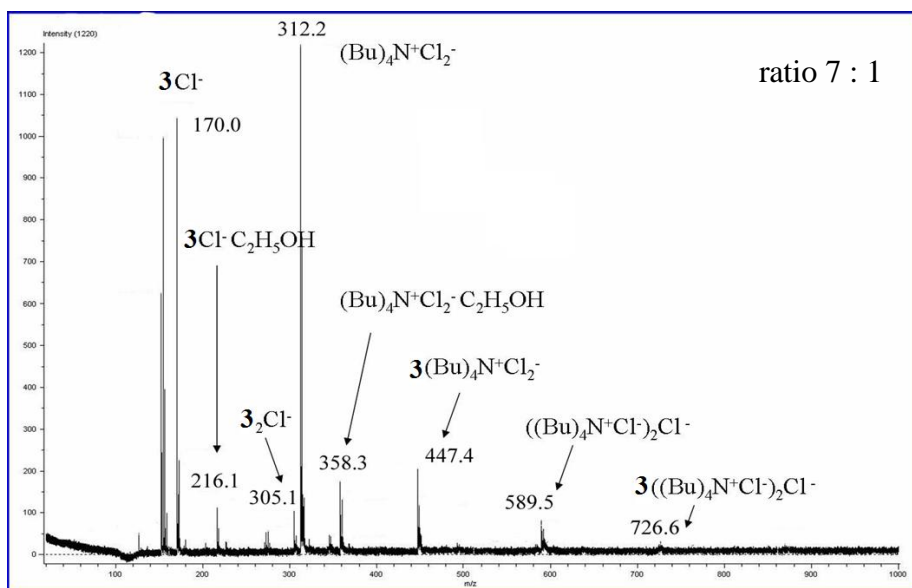


Figure S2.4. Positive- (A) and negative-ion (B and C) mass spectra of the CHCl_3 solution containing 40 mM $(\text{Bu})_4\text{N}^+\text{Cl}^-$. The flow rate of the nebulizing gas N_2 was lower in C than in B.

2.4.5. Dependence of the negative-ion MS on the ratio Salt : Receptor for H-bond donors II-3 and II-6.



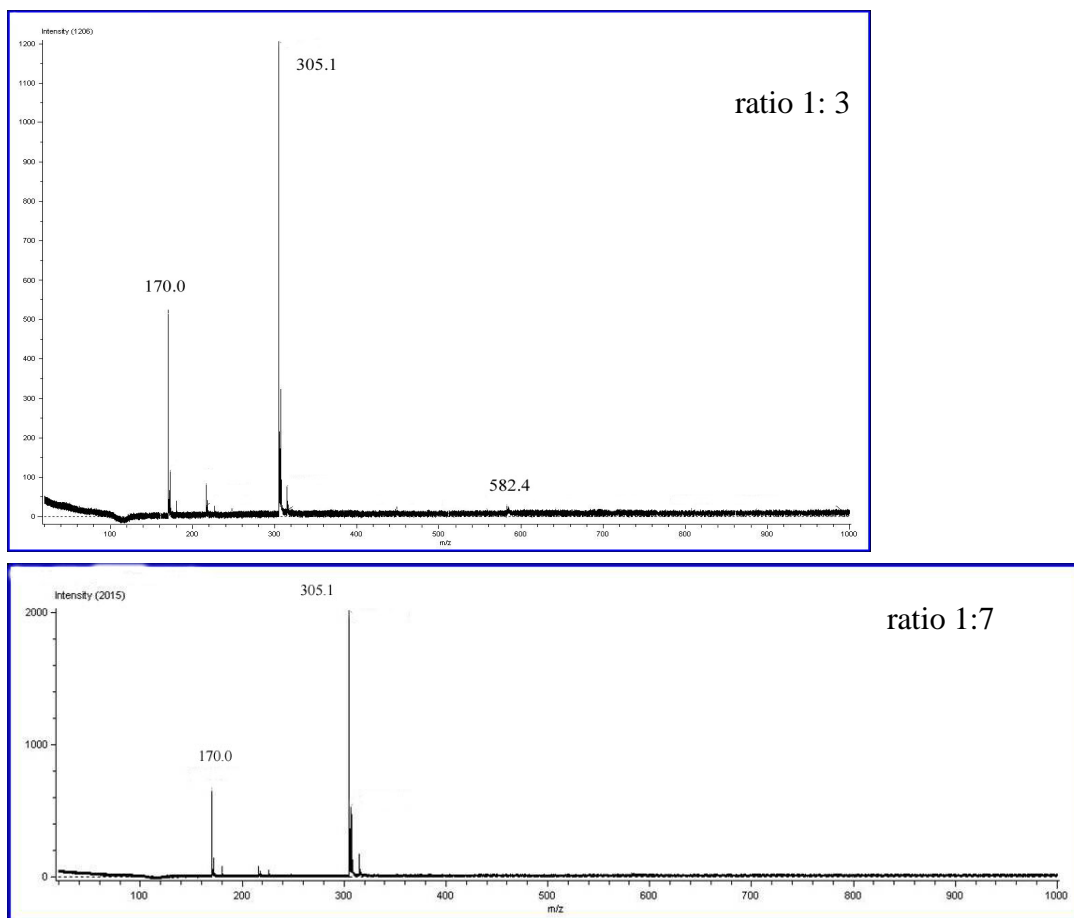
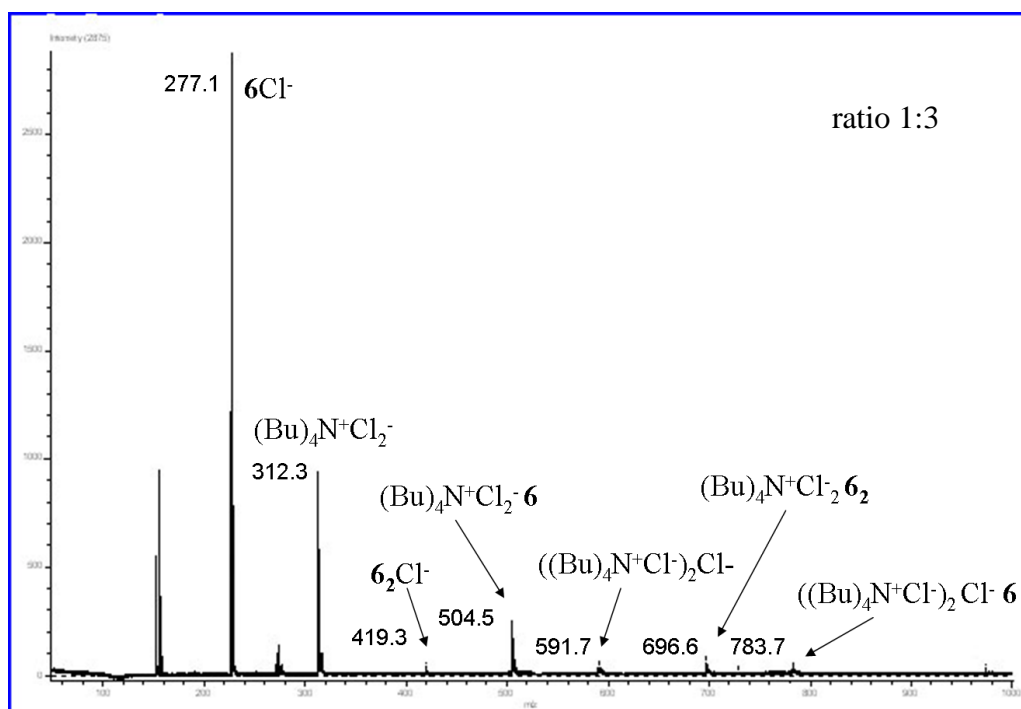
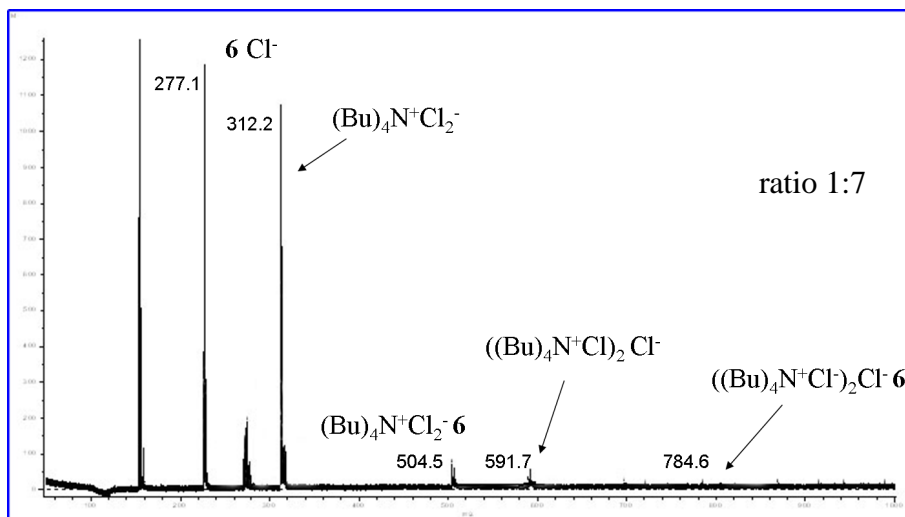


Figure S2.5. Negative-ion clusters in CHCl_3 solution of $(\text{Bu})_4\text{N}^+\text{Cl}^-$ and acetanilide (II-3). Total concentration is $[(\text{Bu})_4\text{NCl}] + [\text{R}] = 40 \text{ mM}$. The ratio salt : receptor changes from 7:1 to 1:7 as indicated. For clarity the receptor is indicated using only Arabic numbers **3** instead of II-3.



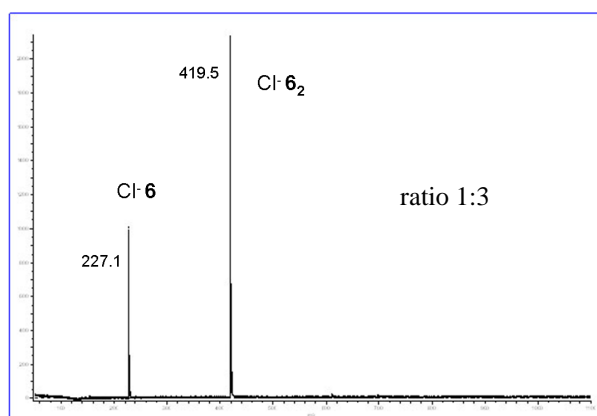
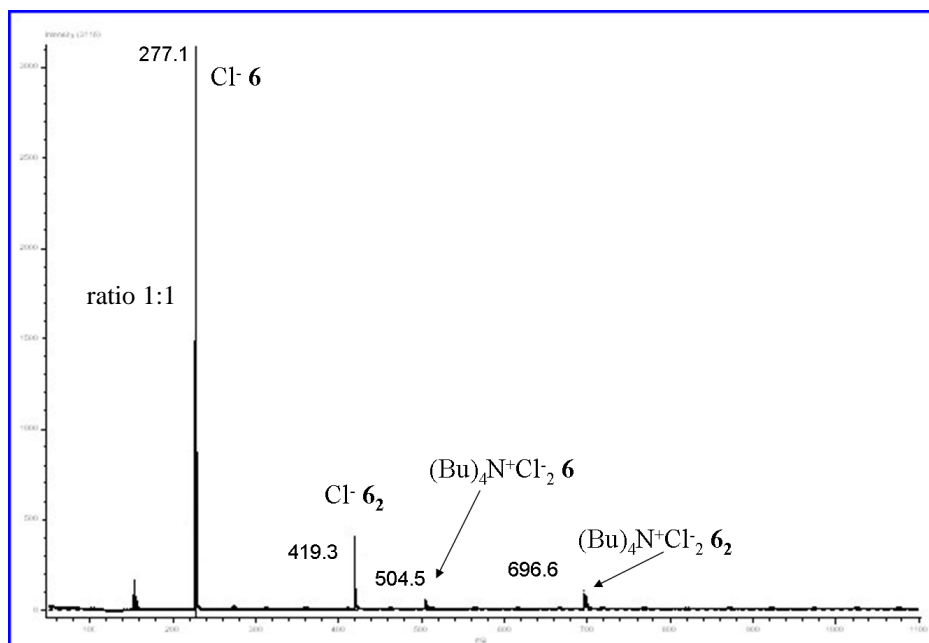


Figure S2.6. Negative-ion clusters in CHCl_3 solution of $(\text{Bu})_4\text{N}^+\text{Cl}^-$ and receptor (II-6). Total concentration is $[(\text{Bu})_4\text{NCl}] + [\text{R}] = 40 \text{ mM}$. The ratio salt : receptor changes from 7:1 to 1:3 as indicated. . For clarity in the figure the receptor is indicated using only Arabic numbers **3** instead of II-3.

Chapter 3: Anion Binding and Self-Assembly. Bis-Catechols and Methylated Analogs.

3.1. Introduction.

3.1.1. **New bis-catechol based anion receptors and their structural analogs.** Based on our initial hypothesis discussed in Chapter 1 and experimental findings described in Chapter 2 we decided to use tris(2-aminoethyl)amine (TREN) and 2,3-dihydroxybenzoic acid to connect together two catechol groups. A hydrophobic tail was linked to the scaffold in the third position to make the receptors lipophilic so as to partition into the membrane (Figure 3.1). We hypothesized that these primitive amphiphilic bis-catechols might be able to transport Cl^- anion and H^+ across a phospholipid bilayer. We suggested that these receptors can coordinate Cl^- anion in solution utilizing four -OH groups to form four equivalent H-bonds.

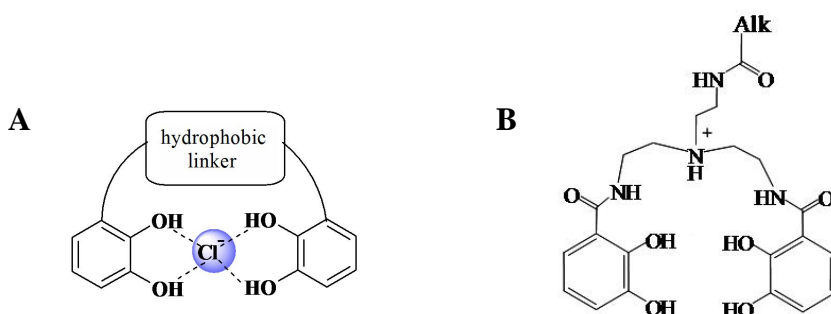


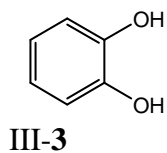
Figure 3.1. **A** – proposed anion binding mode; **B** - amphiphilic anion receptor and membrane transporter.

We considered the fact that intramolecular H-bonding might influence the anion binding mode. The intramolecular H-bonding in 2-hydroxybenzoates is known to survive in polar aprotic DMSO.¹⁰² To investigate the influence of intramolecular H-bonding pattern on the anion binding and transport properties of the new bis-catechols we obtained the isostructural analog containing -OH group in the positions 3 and 4 instead of 2 and 3. Thus, the ability of this 3,4-dihydroxy compound to form intramolecular H-bonds should be diminished if compared to the 2,3-dihydroxy analogs depicted in Figure 3.1. B.

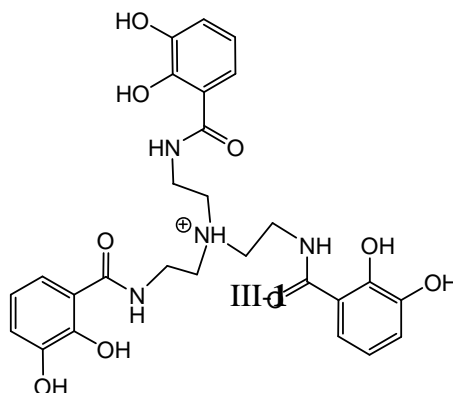
We also became aware that structurally relevant ferric ion sequestering tricatecholate, TRENCAM, (III-1), has a $pK_a = 8.75$ for the tertiary amine group.⁷⁹ Notably, the TRENCAM and structural analogs of this iron chelator are usually isolated as their HBr salts.⁷⁹ Therefore, the amino group in the new bis-catechols depicted in Figure 3.1 B is likely to be protonated at neutral pH. This additional functionality might stabilize the receptor – anion complex through electrostatic interaction and/or H-bonding.

The dependence of the anion binding properties for a number of structurally relevant bis-catechols on the type of the linking group was recently investigated by Winstanley and Smith.⁵⁹ Results of ¹H NMR titration in CD₃CN using alkylammonium salts as an anion source indicate that formation of intramolecular H-bond weakens the anion binding property of bis-catechols. Thus, compound III-2 was found to be a weaker anion receptor than free catechol III-3. Based on this finding, these authors proposed the anion binding mode for the receptor III-2 as depicted in Figure 3.2.

$$K_a = 100 \text{ M}^{-1}$$



$$pK_A(N^+H) = 8.75$$



$$K_a = 25 \text{ M}^{-1}$$

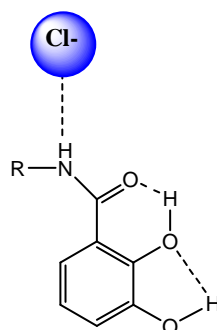
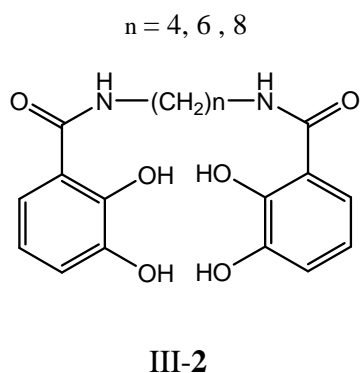


Figure 3.2. TRENAM (III-1); bis-catechols (III-2) obtained by Winstanley and Smith and proposed anion binding mode (III-2...Cl⁻); catechol (III-3). K_a – anion binding constant obtained by ¹H NMR titration in CD₃CN using (Bu)⁺N⁺Cl⁻ as an anion source.⁵⁹

While this thesis was in preparation Smith *et. al* evaluated a number of TREN-based compounds, such as III-4, as anion receptors and potential membrane

transporters (Figure 3.3).¹⁰³ Two different approaches were applied to investigate the anion binding properties. First, the amine **III-4** was titrated into a CD₃CN : DMSO = 9 : 1 mixture using alkylammonium salts as an anion source. Presumably, upon addition of the salt the signal corresponding to three equivalent amide groups shifted downfield. A variety of structurally similar TREN-based anion receptors have been described in the literature.^{18a,18c,57,84} Analogously, the amine **III-4** is thought to form a 1:1 complex⁸⁴ with Cl⁻ anion (**III-5**) as depicted in Figure 3.3.

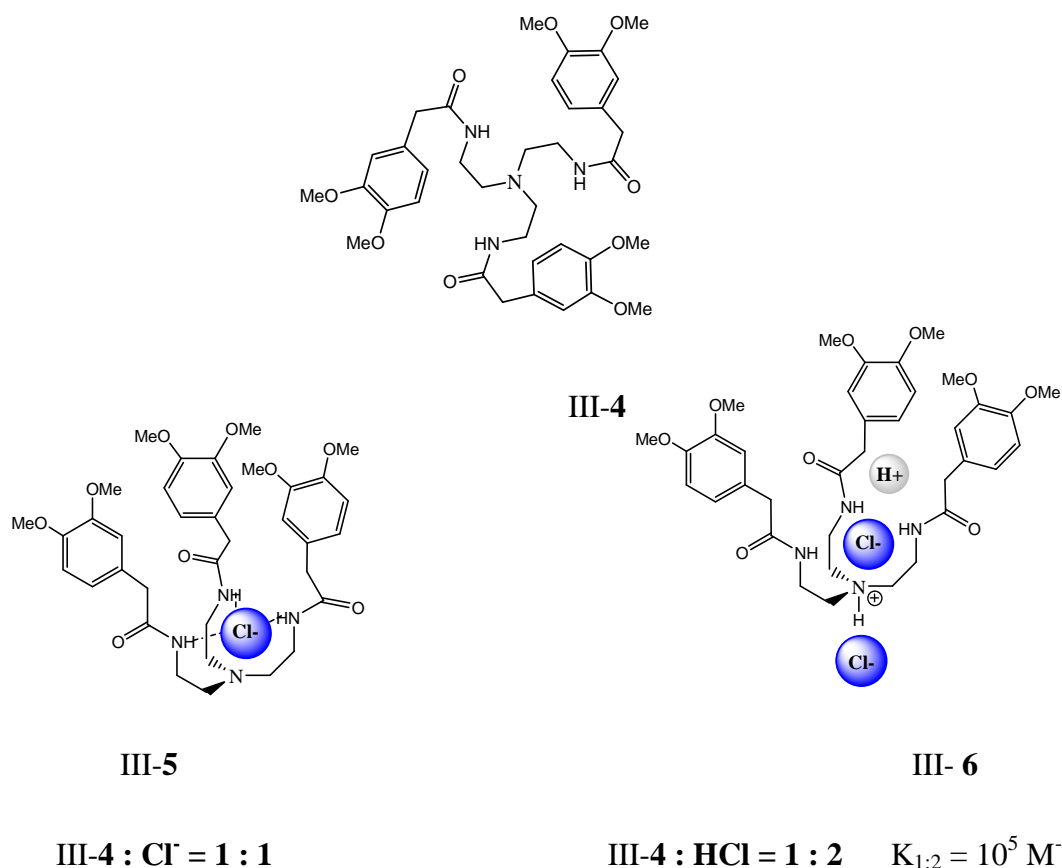


Figure 3.3. TREN based anion receptor **III-4** reported by Smith *et al.* 1:1 complex with Cl⁻ anion (**III-5**) formed in CD₃CN/DMSO mixture. Hypothesized 1:2 complex (**III-6**) formed upon interaction with two HCl molecules in the same solvent mixture.

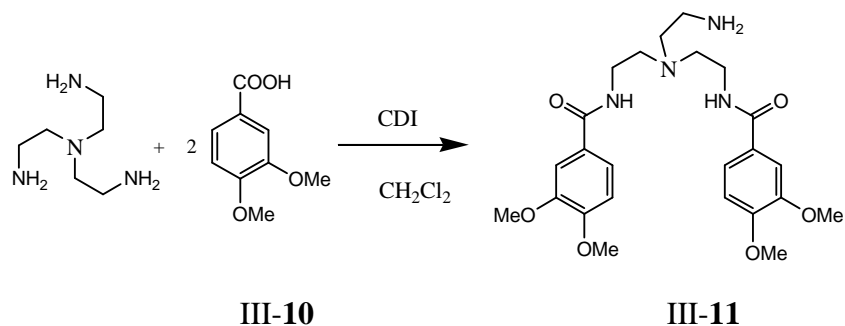
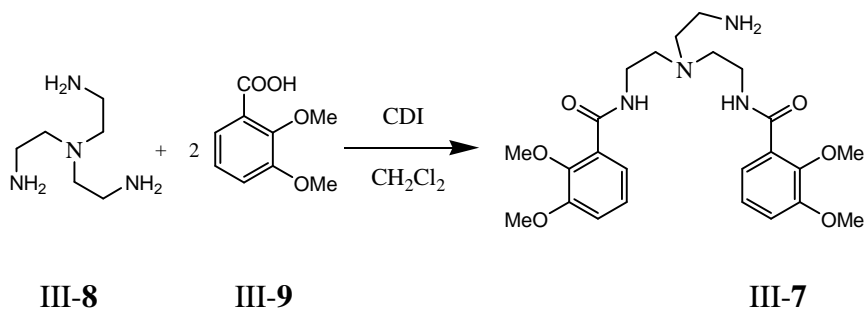
Second, in the following original experiment by Winstanley *et al.*, the interaction between the amine III-4 as a host molecule and HCl as a guest was investigated in the same solvent mixture by ^1H NMR titration using a solution of HCl in ether. Based on the Job plot outcome these authors concluded that a 1:2 complex III-6 was formed in the solution. To obtain the association constant, $K_{1:2}$, the data were fitted using a 1:2 binding algorithm. The hypothesized structure of the 1:2 complex (III-6) is depicted in Figure 3.3. According to the model applied by the authors, complex III-6 is in equilibrium with the free amine III-4 in $\text{CD}_3\text{CN}/\text{DMSO}$ solution.

In conclusion, due to the presence of additional amide and amine functionalities in the linker several different anion binding modes can be proposed for the new bis-catechols depicted in Figure 3.1. B, in addition to the coordination of Cl^- shown in Figure 3.1. A. One can draw an interesting analogy with iron chelator enterobactin and its TREN-based synthetic analogs, such as TRENCAM. These compounds are thought to interact with Fe(III) using two different switchable modes of bonding: catecholate and salicylate.¹⁰⁴

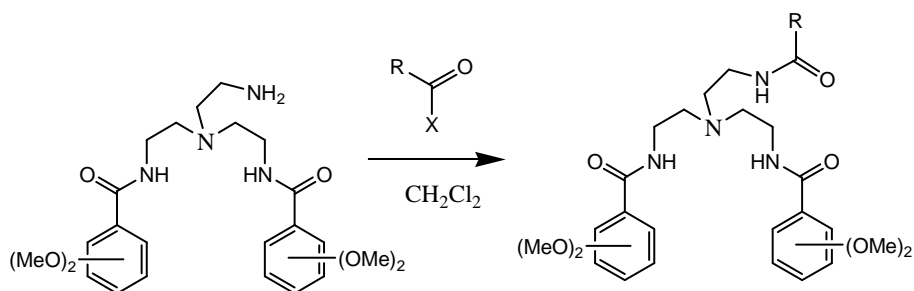
3.2. Results and discussion.

3.2.1. **Synthesis.** Syntheses of bis-catechols and methylated precursors are shown schematically in Figure 3.4. Synthetic route to the amide **7** was recently described in the literature as a key towards constructing the Fe^{3+} receptor with mixed ligands.¹⁰⁵ We used this approach to make methylated precursors and attach the hydrophobic group in the third position. Methyl ethers that protected the nucleophilic oxygens in the first step can be easily removed by means of BBR_3 . For details the syntheses are described in the Experimental Section.

Step I



Step II



III-7 and III-11

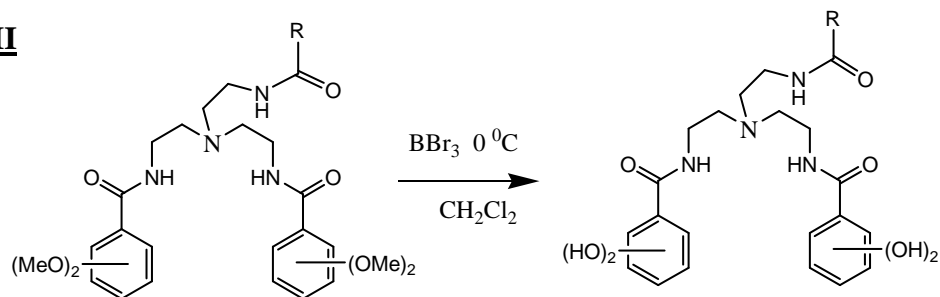
III-7 2,3 (OMe)

R = CH ₃		III-12	2,3-1
R = (CH ₂) ₂ CH ₃		III-13	2,3-3n
R = CH ₂ C(CH ₃) ₃		III-14	2,3-5iso
R = (CH ₂) ₄ CH ₃		III-15	2,3-5n
R = CH ₂ CH(CH ₃)CH ₂ C(CH ₃) ₃		III-16	2,3-8iso
R = (CH ₂) ₈ CH ₃		III-17	2,3-9n
R = (CH ₂) ₁₆ CH ₃		III-18	2,3-17n

III-11 3,4 (OMe)

R = CH ₃		III-19	3,4-3n
R = (CH ₂) ₄ CH ₃		III-20	3,4-5n
R = CH ₂ C(CH ₃) ₃		III-21	3,4-9n
R = (CH ₂) ₁₆ CH ₃		III-22	3,4-17n

Step III



2,3-1	III-12	III-23
2,3-5iso	III-14	III-24
2,3-5n	III-15	III-25
2,3-17n	III-18	III-26
2,3-3n	III-13	III-31
2,3-9n	III-17	III-32
3,4-5n	III-20	III-27
3,4-17n	III-22	III-28

Figure 3.4. Syntheses of bis-catechols and methylated analogs.

3.2.2. ^1H NMR spectra of 2,3-bis-catechols in DMSO-d_6 versus **TRENbAlaCAM and enterobactin**. The ^1H NMR spectrum of the compound **III-26** in DMSO-d_6 is shown in Figure 3.5. There are a number of reports of ^1H NMR spectra for the TRENbAlaCAM (**III-1**) and its structural analogs, such as TRENbAlaCAM (**III-33**), in DMSO-d_6 as a solvent. Although signals in the ^1H NMR of the TRENbAlaCAM were not identified, in some cases, signals in the proton spectra have been partially assigned for its structural analogs (Figure 3.6).¹⁰⁶

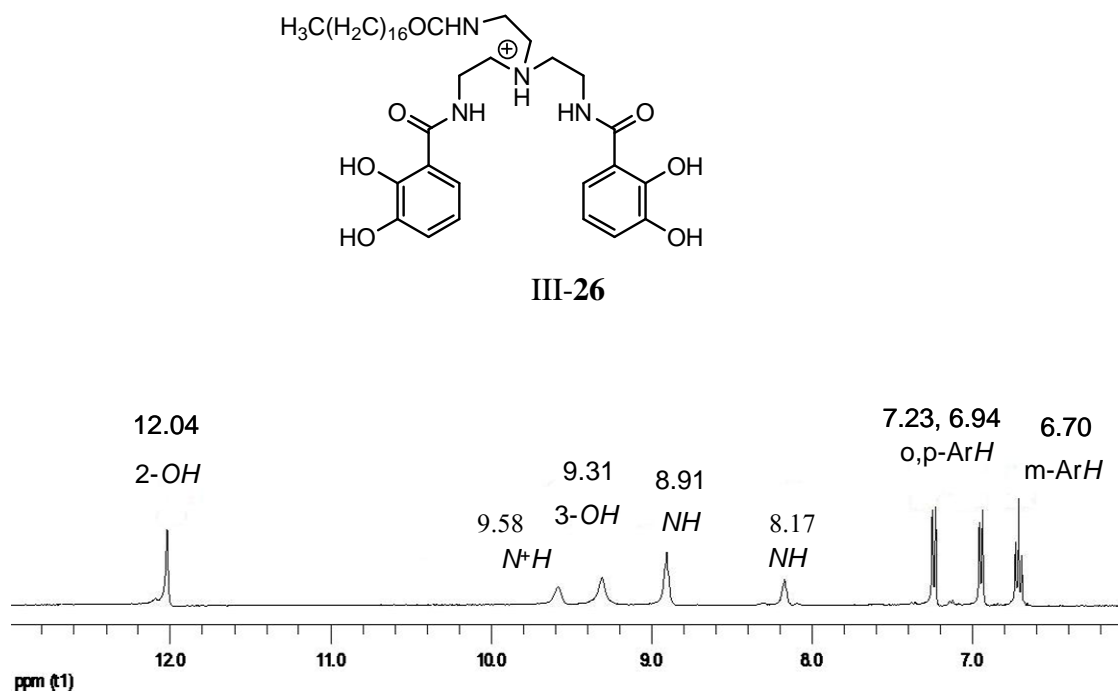


Figure 3.5. The downfield region of the ^1H NMR spectra of the bis-catechol **III-26** in DMSO-d_6 . The assignment of the signal is based on the analogy to known compounds: natural product enterobactin (**III-34**)¹⁰⁷ and its synthetic analog TRENbAlaCAM (**III-33**)¹⁰⁶.

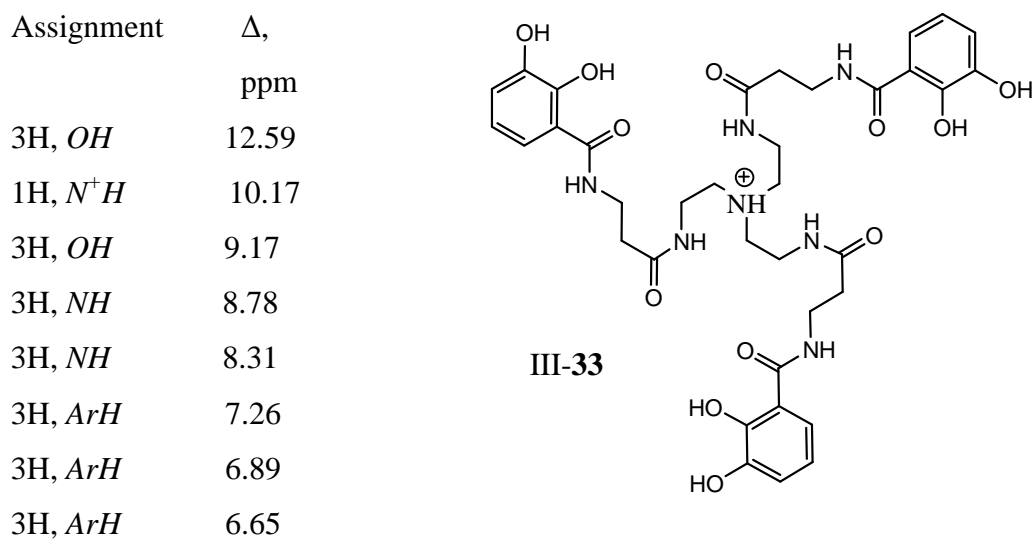


Figure 3.6. TRENbAlaCAM (III-33) and partial assignment of the signals in the downfield region of the ^1H NMR spectra recorded in DMSO- d_6 as reported in reference 106.

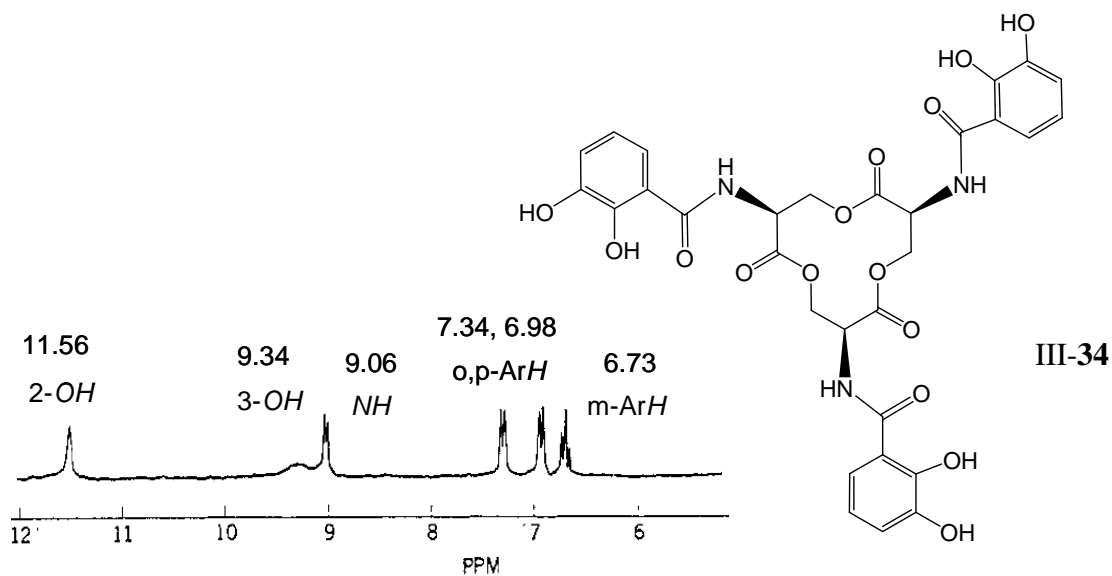


Figure 3.7. Enterobactin (III-34) and the downfield region of the ^1H NMR spectra recorded in DMSO- d_6 . The spectrum is reprinted from the original publication 107 with permission from the ACS.

In addition, the ^1H NMR spectrum of the natural product enterobactin (III-34) has been published and assigned (Figure 3.7)¹⁰⁷ Therefore, we identified the signals in the spectrum of III-26 (Figure 3.5) by analogy to the known compounds III-33 and III-34. It is interesting to note that 2-OH and 3-OH signals for bis-catechol III-26 are separated by more than 2 ppm. Moreover, 2-OH is a sharp signal, while 3-OH is broadened into the base line. This is consistent with Neiland's studies of structurally similar enterobactin wherein he stated: "one would expect the ortho phenol to be electronically more deshielded than the homologous meta proton while being more stabilized toward chemical exchange because of intramolecular H-bond."⁹ The NH groups, adjacent to the tertiary carbon atom in the enterobactin, appear as a doublet in the proton NMR. In contrast, the NH signals in the bis-catechol III-26 ($\delta = 8.91$ ppm and $\delta = 8.17$ ppm) are weakly resolved triplets since these groups are positioned next to the secondary carbon atoms.

The higher pKa values are expected for N^+H and 3-OH than for 2-OH (SI 3.1). Therefore, "thermodynamics", suggests slower exchange with residual water for these two groups than for 2-OH. In the spectrum, however, the protons in N^+H and 3-OH, not involved in strong intramolecular interactions, appear as broader signals than more acidic 2-OH, which is in relatively slow exchange with H_2O due to the "kinetic reason". The well resolved spectrum, like the one shown in Figure 3.5, can be obtained only by using fresh DMSO-d_6 from the ampoules, which presumably contains the minimal amount of residual water. The uptake of H_2O from the air, due to high hygroscopicity of the DMSO-d_6 solution, results into the broadening and disappearance of the NH, OH, and N^+H signals.

3.2.3. Anion binding study. Relative affinities of bis-catechols and methylated precursors toward Cl^- anion in DMSO-d_6 solution.

We compared the relative affinity of our new amphiphiles depicted in Figure 3.8 toward Cl^- anion by classical ^1H NMR titration technique.

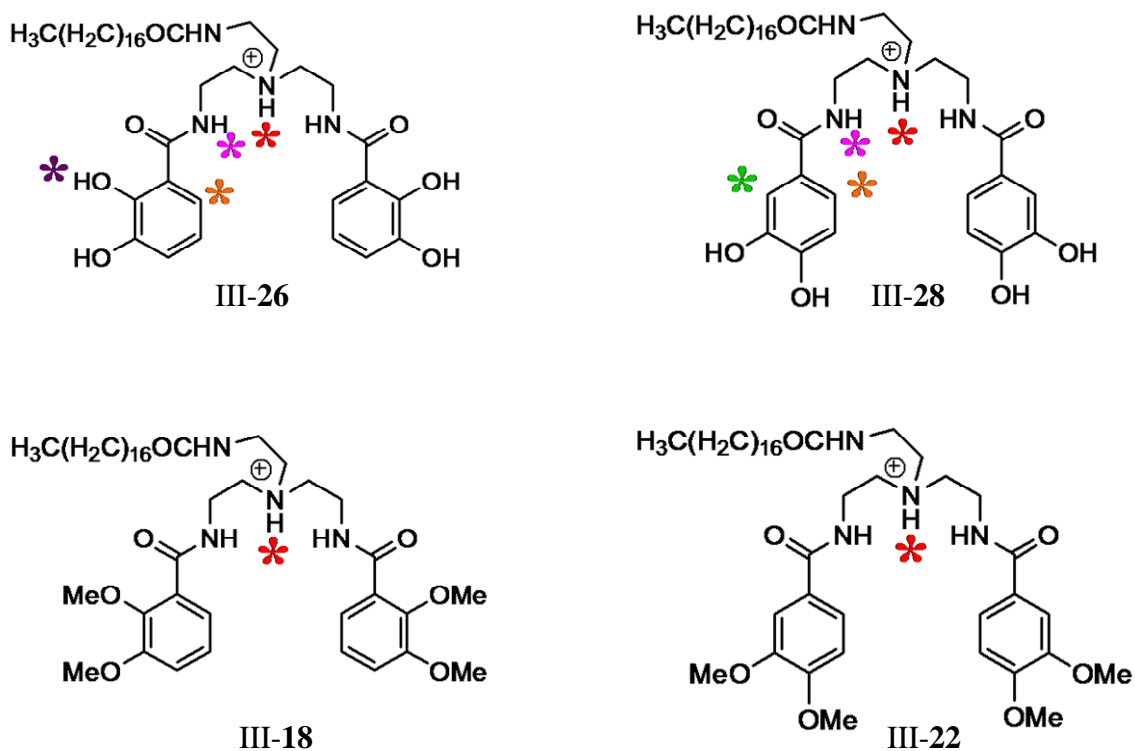


Figure 3.8. Compounds employed to study relative affinity toward Cl^- anion in DMSO-d_6 . The signals, whose changes upon addition of the salt $(\text{Bu})_4\text{N}^+\text{Cl}^-$ were monitored to obtain the binding constants, are indicated by the colored stars.

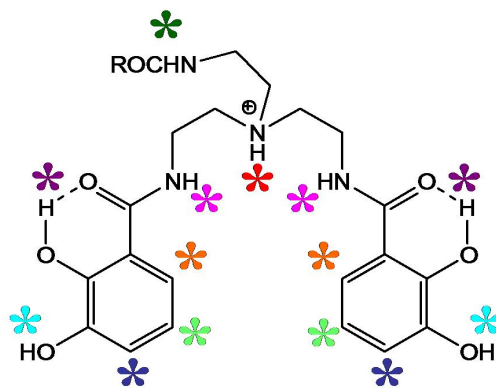
Indeed, both the 2,3- and 3,4-biscatechols as well as their methylated precursors bind Cl⁻ anion in DMSO-d₆ with the association constants in the range $K_a = 50$ to 150 M^{-1} (Table 3.1).

Table 3.1. Relative affinities (K_{a1} , M^{-1}) toward Cl⁻ anion in DMSO-d₆ for bis-catechols III-26, III-28 and HCl salts of their methylated analogs, III-18 and III-22, evaluated using signals of the different acidic protons as indicated below and in Figure 3.8.

	III-18	III-26	III-22	III-28
K_{a1} , M^{-1}	47.6 ± 2.8	150.3 ± 23.0	75.1 ± 11.5	68.7 ± 5.7
	N ⁺ H *	N ⁺ H *	N ⁺ H *	N ⁺ H *
		148.7 ± 11.9		92.5 ± 49.7
		2-OH *		CH(s) *
		145.0 ± 52.1		62.1 ± 12.6
		CH(d) *		CH(d) *
		142.8 ± 63.7		70.3 ± 32.3
		NH(2) *		NH(2) *

Titration were performed using 2.5 mM solutions of the analogs with a stearic acid tail (C17), namely, III-18, III-22, III-26, and III-28. All four compounds were used in their protonated forms as HCl (III-18 and III-22) or HBr salts (III-26 and

III-28). Upon addition of $(\text{Bu})_4\text{N}^+\text{Cl}^-$ signals of the acidic protons shift strongly downfield.



III-26

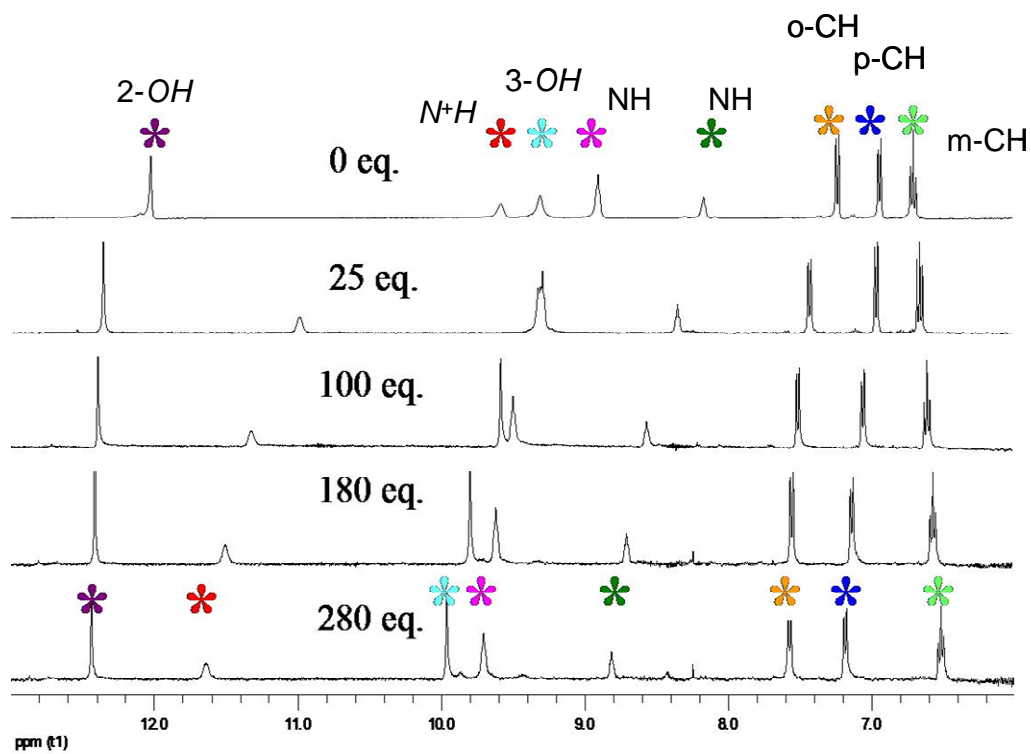


Figure 3.9. Five sample spectra of ^1H NMR titration of the compound III-26 in DMSO-d_6 using $(\text{Bu})_4\text{N}^+\text{Cl}^-$ as a source of Cl^- anions, $[\text{III-26}] = 2.5 \text{ mM}$, $[(\text{Bu})_4\text{N}^+\text{Cl}^-] = 23 \text{ to } 1000 \text{ M}$.

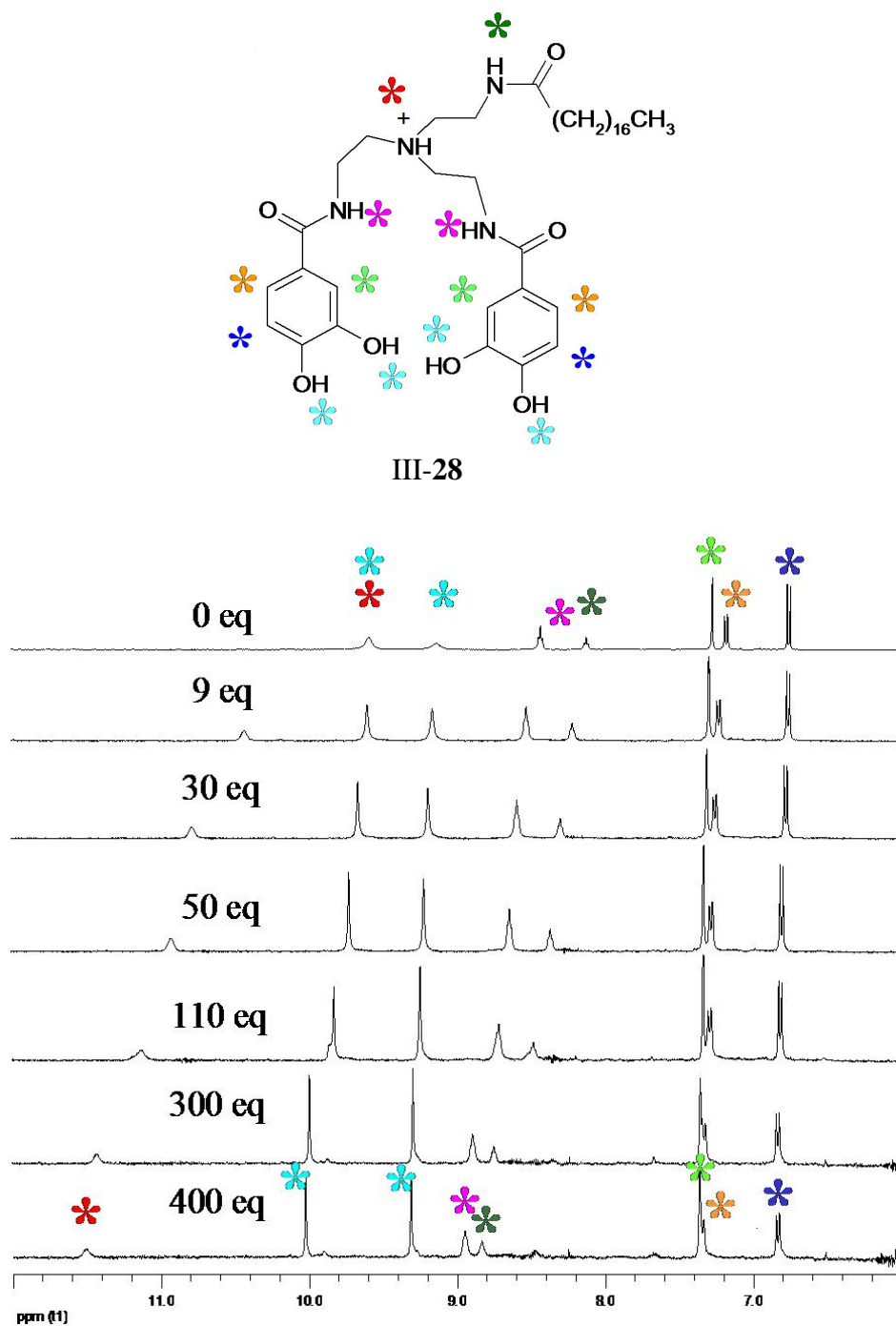


Figure 3.10. Sample spectra of ^1H NMR titration of III-28 in DMSO-d_6 using $(\text{Bu})_4\text{N}^+\text{Cl}^-$ as a source of Cl^- anions, $[\text{III-28}] = 2.5 \text{ mM}$, $[(\text{Bu})_4\text{N}^+\text{Cl}^-] = 0.016$ to 1000 mM .

Presumably, in the 2.5 mM solution the amphiphiles exist mainly as free cations and the changes in the spectra, observed upon addition of the 10 to 400 equivalents of the salt $(\text{Bu})_4\text{N}^+\text{Cl}^-$, are due to Cl^- binding events. It is worth noticing that our approach differs from the two systems employed by Smith to study anion binding properties of the TREN-based anion receptors described in the introduction.¹⁰³ The sample spectra for ^1H NMR titration of the compounds III-26 and III-28 are shown in Figures 3.9 and 3.10.

The largest K_a value was obtained for 2,3-dihydroxy compound III-26. It is reasonable to assume that the alkyl chain length does not influence the anion binding affinity of the amphiphiles.

Surprisingly, the experimental results indicated that the apparent affinity to Cl^- anion was strongly dependent on the signal chosen to evaluate the compound's binding property. For example, two groups of signals could be clearly distinguished in the ^1H NMR spectra of 26: the first group of signals indicated a strong interaction, whereas the second group of signals indicated weak interactions (Figure 3.9.)

For instance, an association constant of $K_a = 1.84 \pm 0.24 \text{ M}^{-1}$ was extracted from the changes observed for 3-OH group (*) using curve fitting method and 1:1 binding algorithm. Such a small value is rather more indicative of a simple collision event than binding. In contrast, the salt-induced downfield shifts for the 2-OH signal (*) gave association constants $K_a = 150 \pm 23 \text{ M}^{-1}$. In this case, however, the experimental data points could not be adequately described unless a two-step binding algorithm was applied. Taking into account the fact that very broad concentration

range of the salt $(\text{Bu})_4\text{N}^+\text{Cl}^-$ was employed to study anion binding, we offer the following interpretation of these experimental findings.

Specific interactions, namely ion-pairing and H-bonding, are responsible for the receptors' binding to Cl^- anion in dilute solution ($K_{a1} \approx 150 \text{ M}^{-1}$). The binding site for Cl^- anion is located close to the positively charged nitrogen atom (*). In addition to electrostatic interaction, H-bond donor groups N^+H (*), $\text{CH}(\text{d})$ (*), $\text{NH}(\text{2})$ (*), and 2-OH (*) stabilize the anion in this binding site. The amphiphile is completely associated with the anion when $[(\text{Bu})_4\text{N}^+\text{Cl}^-] \approx 0.1 \text{ M}$. Increasing concentration of the salt, however, induced a continuous downfield shift of the signals N^+H (*), $\text{CH}(\text{d})$ (*), $\text{NH}(\text{2})$ (*), and 2-OH (*), which we suggest is due to non-specific weak interactions of this 1:1 associate with other anions in solution ($K_{a2} \approx 1, \text{ M}^{-1}$).

Notably, two signals of the aromatic protons $\text{CH}(\text{d})$ at 6.98 and 7.34 ppm indicate different affinity towards Cl^- anion (Figure 3.9.) We assigned the downfield signal, which is indicative of strong binding event with Cl^- anion, to the ortho-CH. In turn, the signal, suggesting weak interaction and likely to be the furthest from the anion binding site, was assigned to be the para-CH.

The following model of interaction with Cl^- anion has been used to describe changes observed in the ^1H NMR spectra upon addition of $(\text{Bu})_4\text{N}^+\text{Cl}^-$. The experimentally observed chemical shifts for the acidic protons (δ_{obs}) consist of three terms: $\delta_0 \cdot x_0$ – chemical shift in the free receptor multiplied by its fraction in DMSO solution, $\delta_1 \cdot x_1$ – chemical shift in the 1:1 complex (strong binding event, $\delta_1 = \delta_0 + \Delta\delta_1$) multiplied by its fraction and $\delta_2 \cdot x_2$ – chemical shift in the “1:2 complex” (weak interaction, $\delta_2 = \delta_1 + \Delta\delta_2$) multiplied by its fraction:

$$\delta_{\text{obs}} = \delta_0 * x_0 + \delta_1 * x_1 + \delta_2 * x_2 \quad (4.1)$$

In the case of the acidic protons which are in direct contact with the Cl⁻ anion in the 1 : 1 complex (and/or protons whose position is the most influenced upon interaction with the first Cl⁻ anion due to electronic effects) all three terms are important and only the two-step binding model can adequately describe the experimental data set.

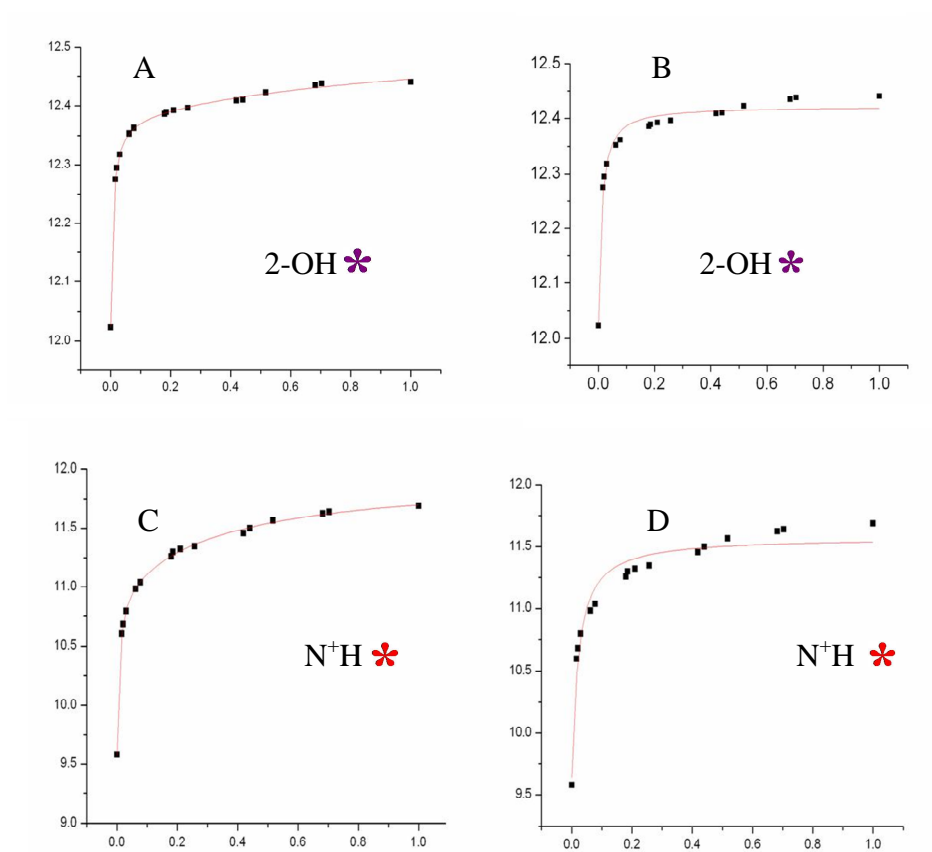


Figure 3.11. Examples of the data sets from the ¹H NMR titration (black squares) and the best curve fits of the experimental data (red lines) for compound III-26. 2-OH (✱) signal: two-step (A) vs single-step (B); N⁺H (✱) signal: two-step (C) vs single-step (D).

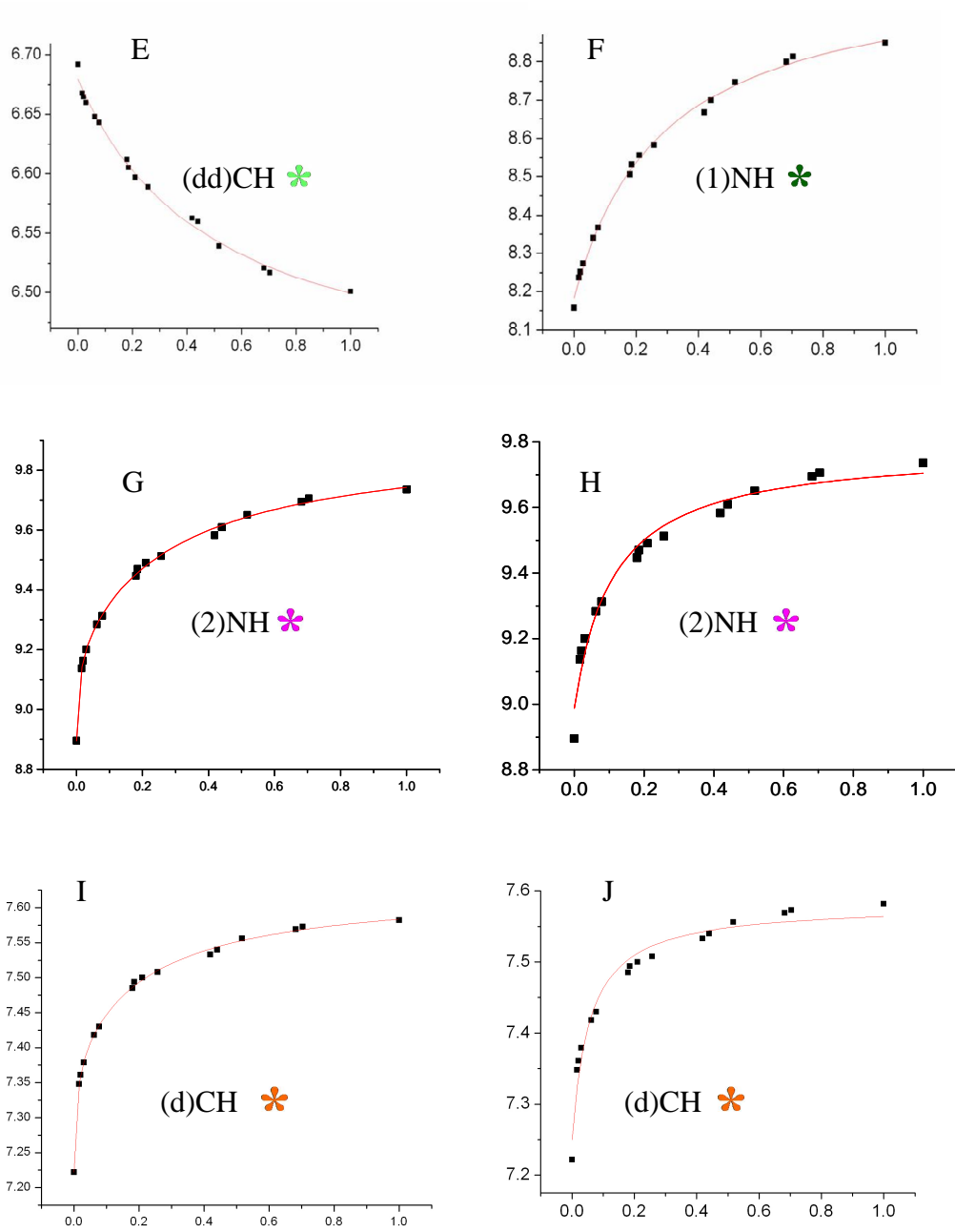


Figure 3.12. Examples of the data sets from the ^1H NMR titration (black squares) and the best curve fits of the experimental data (red lines) for compound III-26. Single-step (dd)CH (✱) and (1)NH (✱) signals; (2)NH (✱) signal: two-step (G) vs single-step (H); (d)CH (✱) signal: two-step (I) vs single-step (J).

In the case of the acidic protons, which are not “in direct contact” with the Cl⁻ anion in the 1 : 1 complex, the major changes in chemical shift come from the weak interactions with the “second” Cl⁻ anion. The first process might result in a very tiny initial jump in the chemical shift (if observed at all). This rather small initial jump is “masked” by the following large change in chemical shift due to “direct” interactions with Cl⁻ anion in the collision complex (weak event). As a result the term $\delta_1 \cdot x_1$ can be ignored and a single step model $\delta_{\text{obs}} = \delta_0 \cdot x_0 + \delta_2 \cdot x_2$ adequately describes the experimental data set (Figures 3.11 and 3.12, see more details and experimental data in SI 3.2).

Therefore, we propose the following model describing the 1:1 complex between Cl⁻ anion and bis-catechol III-**26** in solution. The anion binding pocket is located in close proximity to the tertiary nitrogen atom, N⁺H (✳), which employs both electrostatics and H-bonding to interact with the Cl⁻ anion. Other neighboring acidic protons, CH(d) (✳), NH(2) (✳), and 2-OH (✳), help to stabilize the anion within this binding site. Using semiempirical method AM1 and HyperChem software⁹⁹ three possible conformations of this complex (AA, BB, AB/BA) have been optimized (Figure 3.13). It is undetermined, however, if intramolecular H-bonds are broken (conformer BB) or not (conformer AA) upon anion complexation. Although the binding data for 2-OH (✳) and N⁺H (✳) are alike and strongly differ from 3-OH (✳) group, one might argue that this observation might be due to the certain electronic effects. Thus, 2-OH (✳) group helps to preorganize the anion binding site (conformer AA) but, in contrast to N⁺H (✳), is not directly involved in the anion complexation. One can argue, however, that formation of the stronger H-bond, –

$\text{OH}\cdots\text{Cl}^-$, might drive the breaking apart of the intramolecular H-bonding. Our own *ab initio* calculations suggest that, at least in the case of the structurally relevant but simpler N-methylsalicylamide (II-5), this is not the case. The intramolecular H-bonded complexes of this receptor with Cl^- anion is of the lower energy than corresponding complex with $-\text{OH}\cdots\text{Cl}^-\cdots\text{HN}=\text{O}$ contact (Chapter 2, Figure 2.10). Therefore, we imply that conformers AA, which preserve the intramolecular H-bonds, might yet be of the lowest energy and dominate in solution.

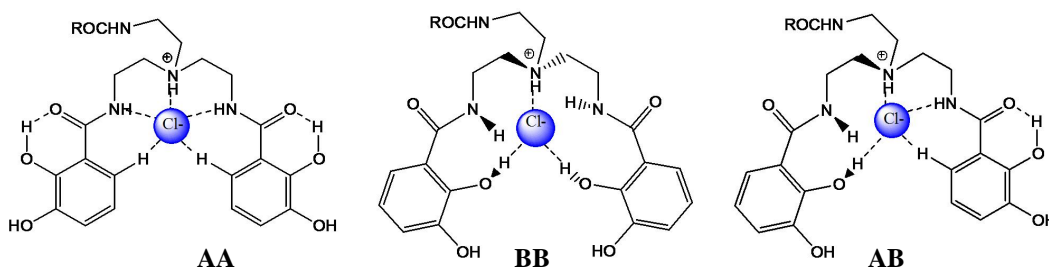


Figure 3.13. Schematic representation of the conformers optimized using AM1 method and HyperChem 7.0 software.

3.2.4. Self-assembly of methylated analogs in organic solution and crystalline state.

3.2.4.1. **Introduction.** In the course of the present study a number of methylated analogs of bis-catechols have been prepared. It was interesting to find out that small changes in chemical structure result in profound difference in the properties of these compounds in the solid state and solution. For example, compound III-**22**, a 3,4-disubstituted analog, is a white solid, self-associates in CHCl₃ and gels a variety of organic solvents while the 2,3-disubstituted isomer III-**18** is an oil, does not self-aggregate or form gels in organic media.

Discovery of a new organogelator and experimental determination of the structural features responsible for this activity are important findings by themselves.¹⁰⁸ In addition, it is reasonable to imply that self-association of the methylated analog in organic solvents might replicate/mimic some of the properties of the corresponding bis-catechol derivatives that are soluble in aqueous media. In turn, self-aggregation in aqueous solution is thought to be an important factor to strongly influence the apparent activity of ion transporters in the liposome based assays as well as in planar bilayer experiments.

The qualitative experimental observations indicate that solubility of the bis-catechols in aqueous solution decreases with increasing length of the alkyl chain and acidity of the media. Moreover, compound III-**26** with -OH groups in 2 and 3 positions is more soluble in aqueous solution than is the 3,4-dihydroxy isomer III-**28**.

Does it indicate that receptor III-28 exhibit stronger tendency to aggregate in the aqueous media than its isomer III-26 and why?

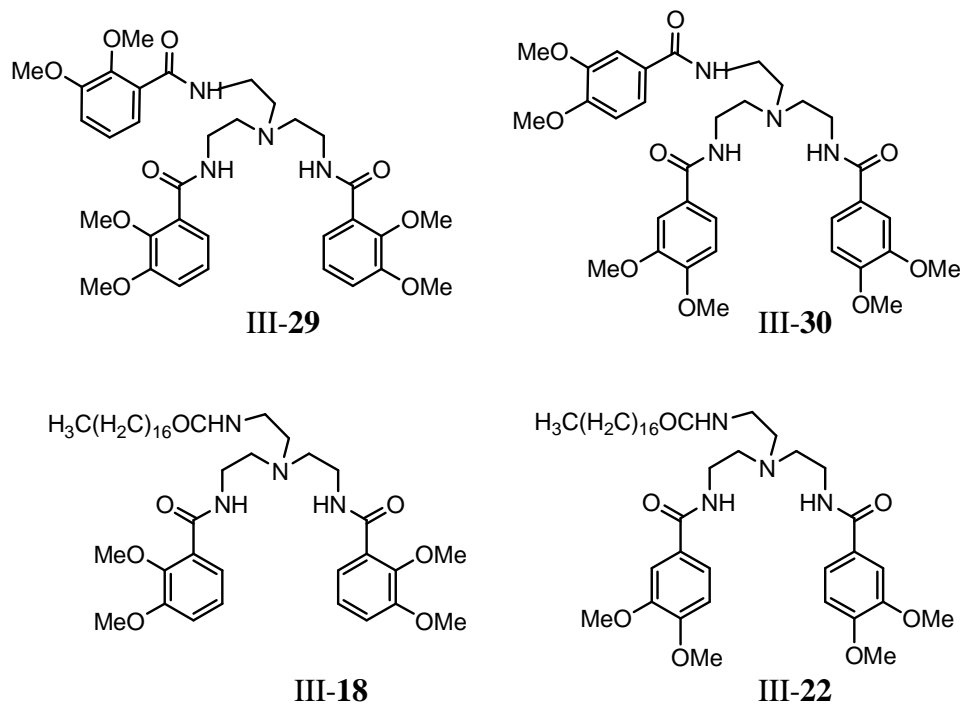
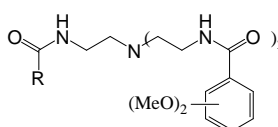
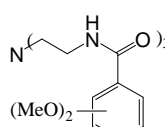


Figure 3.14. Methylated analogs, III-18, III-22, III-29, and III-30, whose property to self-assemble has been evaluated in organic solution and in the crystalline state.

We did not directly investigate the self-aggregation of the bis-catechols in DMSO or in aqueous solution. We imply, however, that the present study of methylated precursors in organic media and solid state might yet provide some insights on the properties of bis-catechols by disclosing the mechanisms of how certain structural changes might influence self-association.

3.2.4.2. **Physical properties of methylated precursors.** The physical properties for methylated analogs, summarized in Table 3.2, indicate the following: 3,4-dimethoxy compounds have tendency for solid/crystalline state, while their structural isomers with 2,3-*O*-dimethyl groups form oils.

Table 3.2. Physical properties of dimethoxy compounds III-12 - III-22, III-29, and III-30.

								
	17n	9n	8iso	5n	5iso	3n	1	
2,3	III-18	III-17	III-16	III-15	III-14	III-13	III-12	III-29 Isolated as white solid, crystallizes from solution to form very thin plates. X-ray
	Oil	Oil	Oil	Oil	Oil	Oil	Oil	
3,4	III-22 White amorphous solid, forms organogels upon attempts to crystallize.	III-21 White amorphous solid, swells in organic solvents, does not crystallize.		III-20 Oil		III-19 Oil		III-30 Isolated as white solid. Sample crystallizes from solution to give big colorless prisms. X-ray

3.2.2.3. **Properties of the compound III-22 as an organogelator.** The dimethoxy analog III-22 was found to gelate ethyl acetate, acetonitrile, acetone, chloroform, hexane-ethyl acetate and acetone-water mixtures. This compound forms organogel at as low as 5 mass % in CD₃CN. This value corresponds to 0.3 mol % in

CD_3CN , 1 molecule of III-22 per 340 molecules of organic solvent, and 0.4 mol % in $\text{CH}_3\text{COCH}_2\text{CH}_3$, 1 molecule of III-22 per 240 molecules of organic solvent.

The organogels were prepared using the following procedures: a) dilution of III-22 in a hot solvent (5 mass %) and cooling to the room temperature on ice; b) slow rotoevaporation of the solvent from the diluted solution of III-22 (under reduced pressure); c) slow evaporation of the diluted solution of III-22 from the open container (atm. pressure).

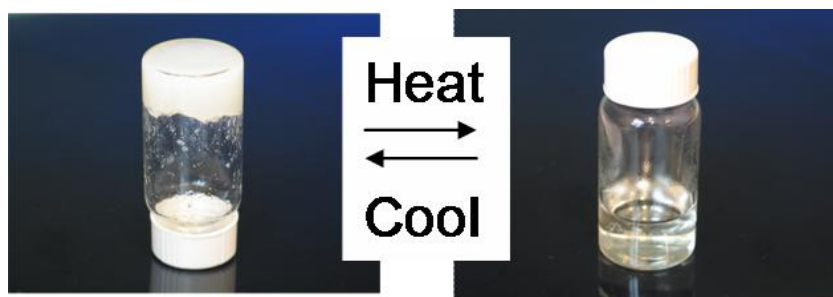


Figure 3.15. Reversible formation of the organogel in CD_3CN in the presence of 5 mass % of III-22.

These organogels are stable if stored in a sealed container. Stored in an open container, the organogel slowly loses the solvent and dries forming a white powder. The acetone-based gel dries very fast. The formation of the organogel by receptor III-22 is reversible (Figure 3.15). The sealed vial containing acetone-based gel was

heated up to 56 °C (b.p. of acetone) to get transparent solution. The following cooling on ice resulted in formation of the gel phase. This procedure was repeated twice, no degradation was observed.

3.2.4.4. **¹H NMR study of dimethoxy compounds in CHCl₃ solution.** The ¹H NMR indicates that compound III-22 forms intermolecular H-bonds and self-aggregates in CHCl₃ solution. The -NH- signals of two amide groups shift downfield in concentrated solution (Figure 3.16). Compared to the organogelator III-22, the -NH- signals in the ¹H NMR spectra of the 2,3-disubstituted III-18, which contains -OMe groups in 2 and 3 positions, are located downfield in diluted solution and these chemical shifts do not change at high concentration (Figure 3.17). These observations indicate that amide groups in receptor III-18 should be involved in strong intramolecular interactions and this compound does not self-associate in CHCl₃.

It is interesting to note, that the apparent polarities of III-18 and III-22 are also remarkably different: the 3,4-dimethoxy (III-22) compound is more “polar” than the 2,3-analog (III-18). In the eluent mixture EtAc 90%, TEA 10% the R_f(III-22) = 0.15 while R_f(III-18) = 0.50. Apparently, the -NH- groups in III-22 strongly interact with the silica gel, while the same groups in the 2,3-analog III-18 are “protected” due to intramolecular interactions.

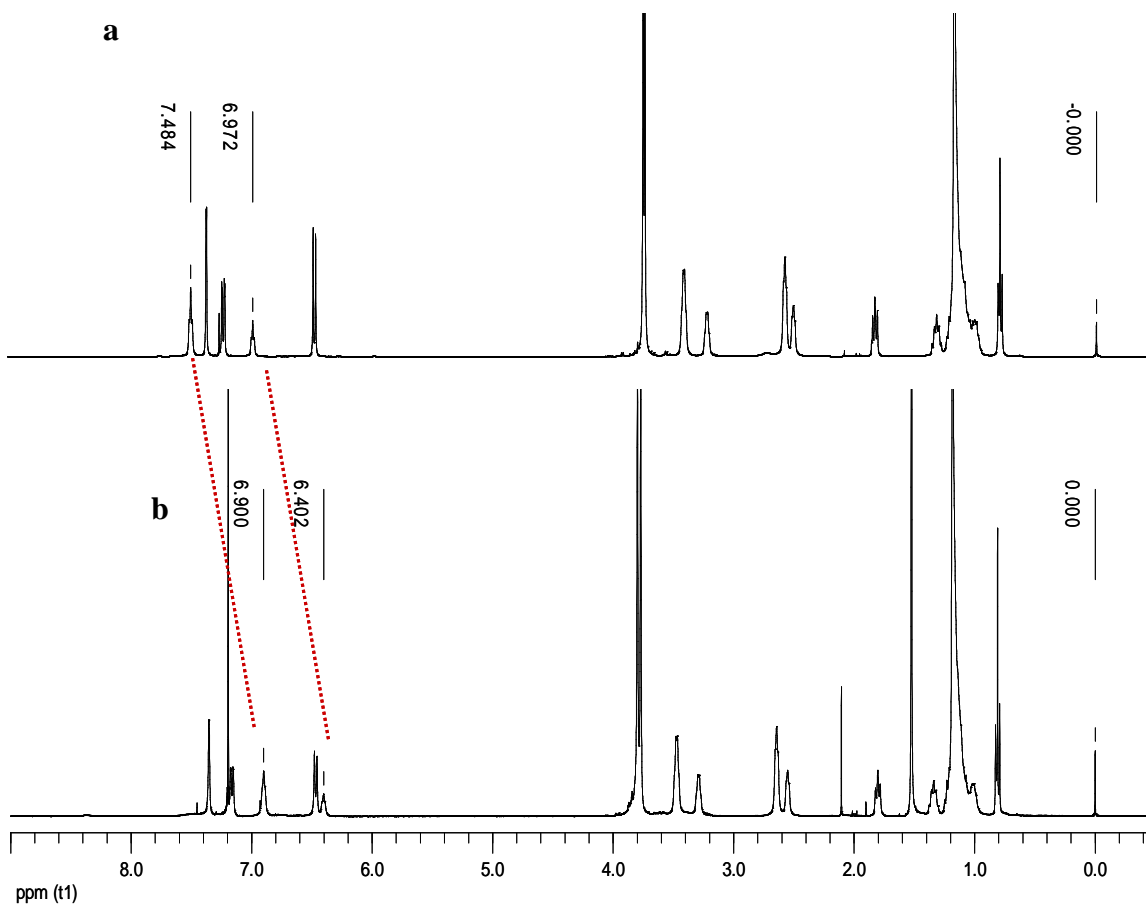


Figure 3.16. ^1H NMR of receptor III-22 in CDCl_3 solution at concentrations: **a)** 250 mM and **b)** 4 mM. Signals of the $-\text{NH}-$ groups shift downfield in concentrated solution.

Self-association of dimethoxy compounds in CDCl_3 solution was studied by ^1H NMR. Dimerization was chosen as the simplest approach to model self-assembly in organic media. Interestingly that compounds III-30 ($K_a = 2.9, \text{M}^{-1}$) and III-22 ($K_a = 2.2, \text{M}^{-1}$) have identical aggregation properties in CDCl_3 (Figure 3.18). (The experimental data on self-aggregation of the compound III-30 in CDCl_3 can be

found in SI 3.3.) Similarly, both III-29 and III-18 do not aggregate in organic solvents.

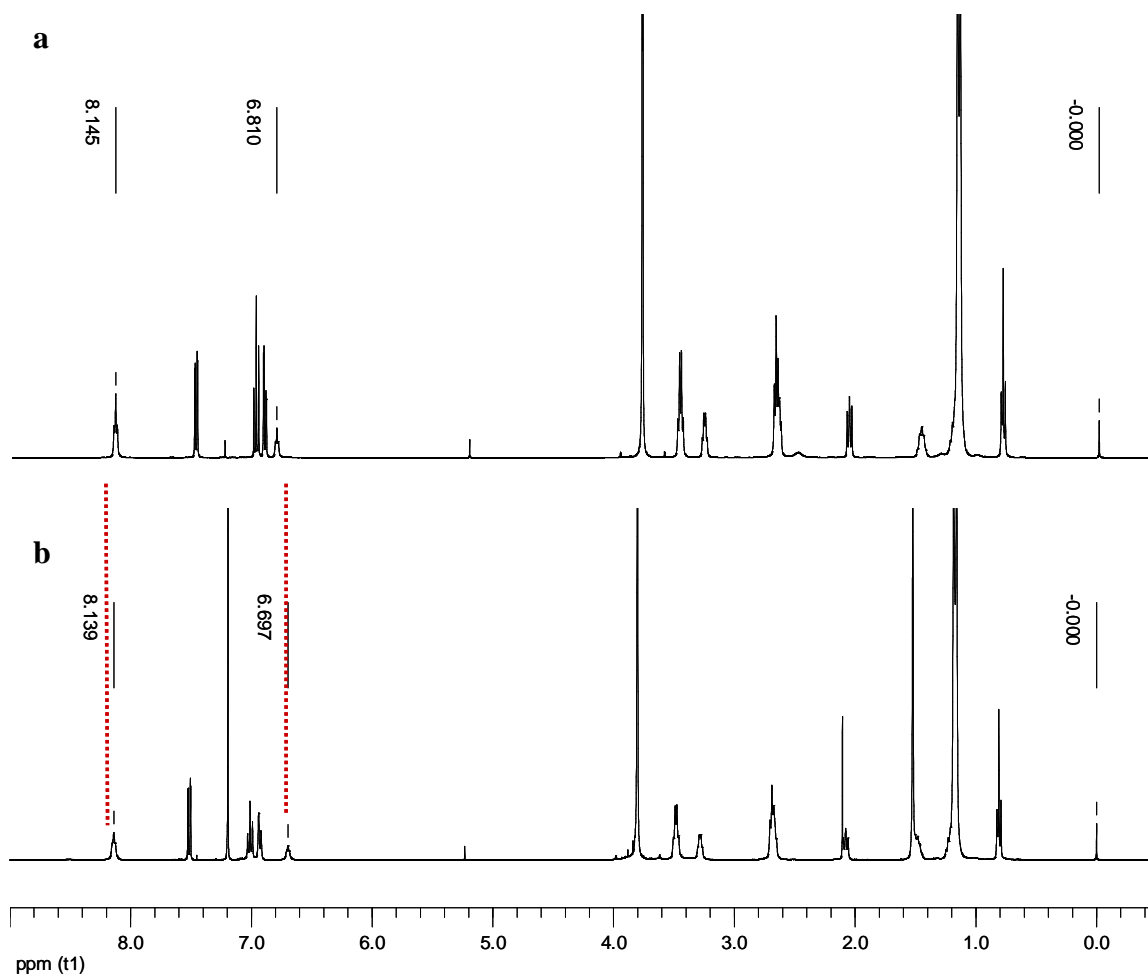


Figure 3.17. ^1H NMR of III-18 in CDCl_3 at concentrations a) 250 mM and b) 4 mM. Signals of the -NH- groups are shifted downfield in diluted as well as concentrated solutions.

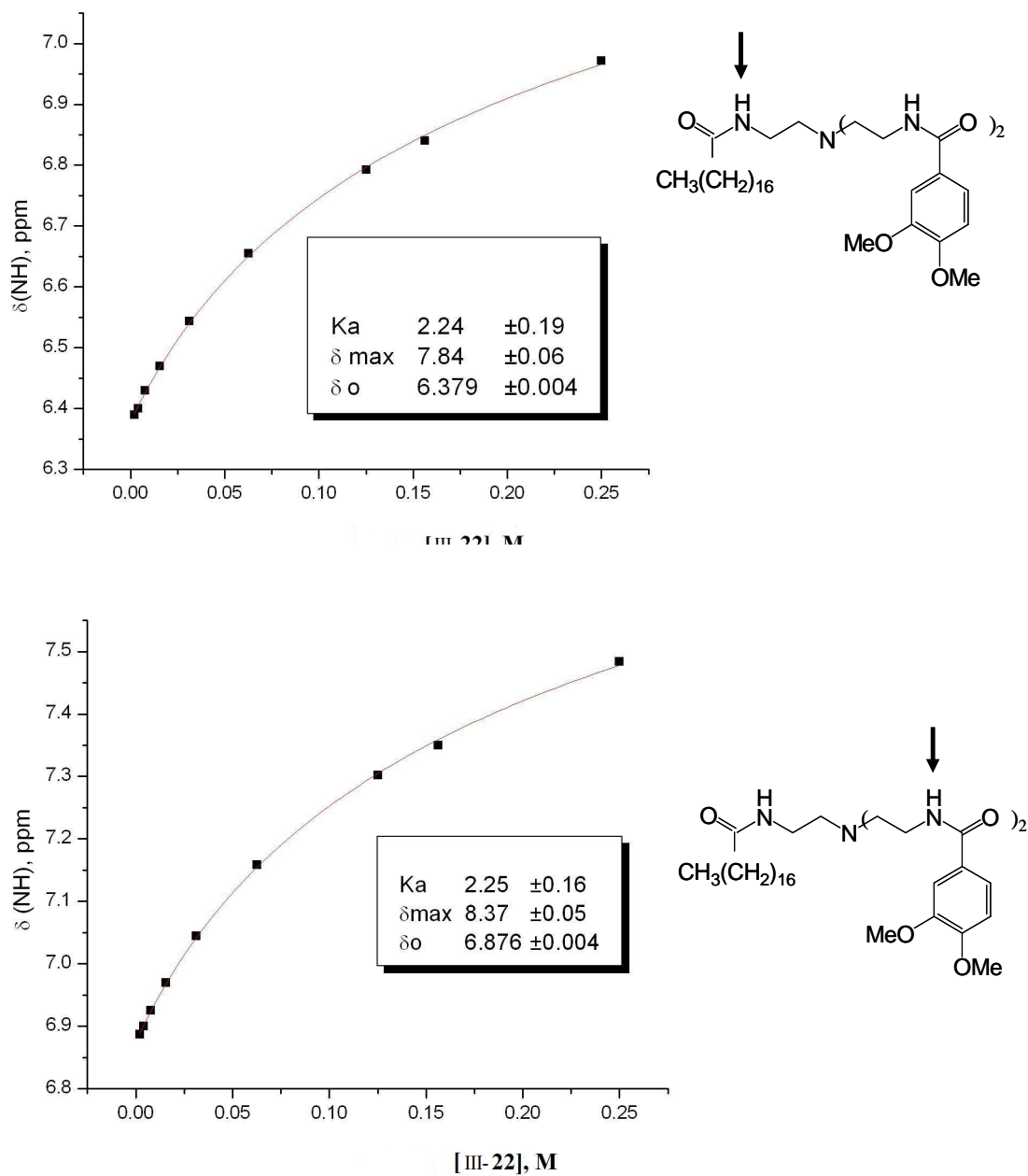
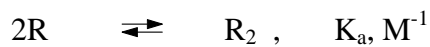


Figure 3.18. Dependence of the chemical shifts of the two amide signals in ^1H NMR of III-22 on concentration in CDCl_3 solution. The red curve is the best fit obtained using equation (S2.1) to model the dimerization.

3.2.4.5. Conformational control of gelation. Structure of the organogel.

There are strong intramolecular H-bonds (six-membered rings) in the receptor **III-18**, while only weak intramolecular interactions are possible between the amide groups in the analog **III-22** (Figure 3.19 (a)).

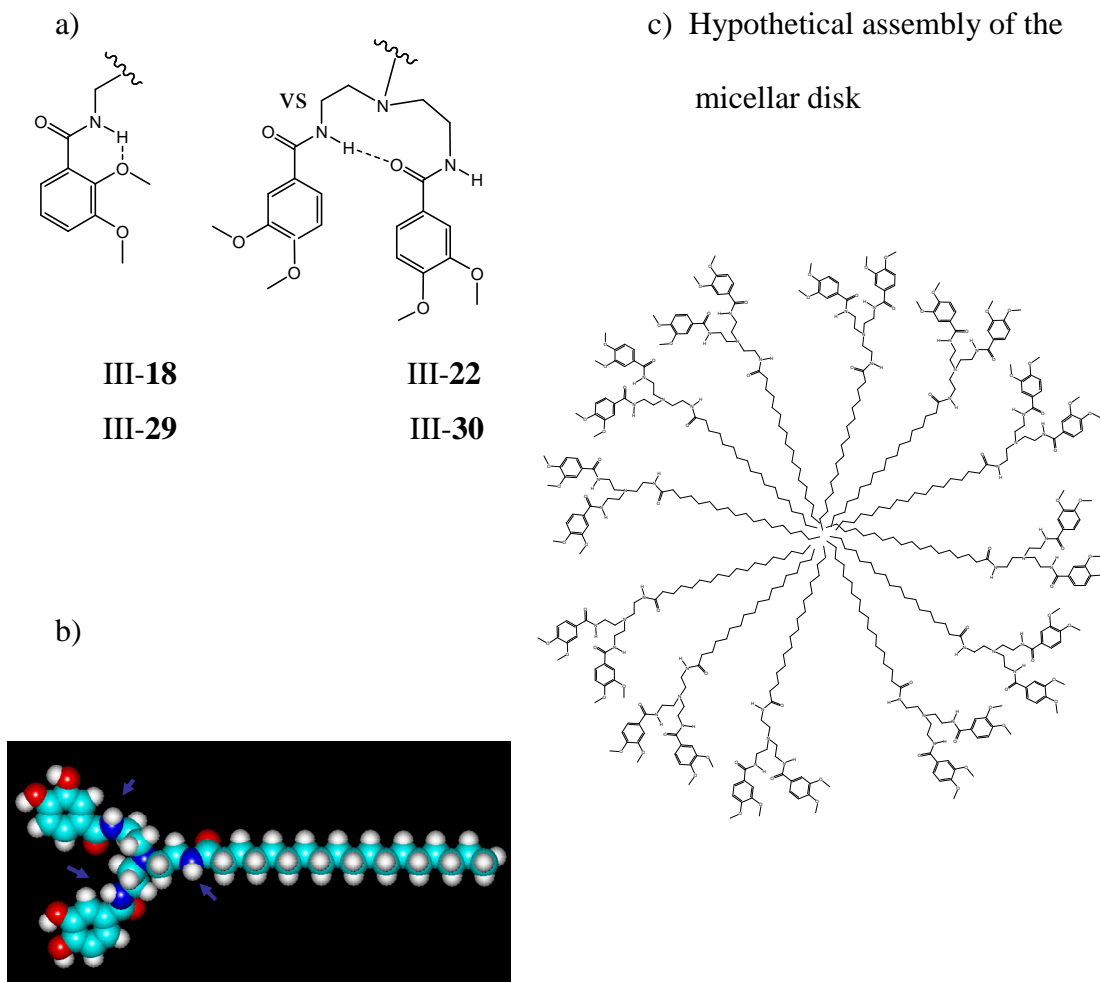


Figure 3.19. a) Intramolecular interactions in the receptors **III-18**, **III-22**, **III-29**, and **III-30**. b) One of the possible conformations of **III-22** optimized by AM1 method using HyperChem software. c) The cross-section of hypothetical fiber formed by the assembly of **III-22** in organic media.

Therefore, the conformations, adopted by the dimethoxy analogs in solution, define the “supramolecular” properties of these compounds in organic media. It also can be concluded that it is necessary to have a long alkyl chain to make this assembly efficient since short-chain 3,4-dimethoxy analogs do not form organogels (Table 3.2). One of the possible conformations of **III-22** optimized by AM1 method using HyperChem software is shown in Figure 3.19 (b). Each molecule of **III-22** can form up to six H-bonds: three with the molecule above and three with the molecule below the plane. The cross-section of the hypothetical fiber formed by the self-aggregation of **III-22** in organic media is shown in Figure 3.19. (c). Hypothetically, due to the intermolecular interactions depicted, micellar disks can stack on the top of each other to form elongated assembly – an elemental fiber. Presumably, these fibers further aggregate/interact to form a fibrilous network – the structural basis of the organogel.

3.2.4.6. Crystal structures of compounds III-29 and III-30. Compounds **III-30** and **III-22** have identical aggregation properties in CDCl_3 solution (K_a (**III-22**) = 2.2, M^{-1} , Figure 3.18 and K_a (**III-30**) = 2.9, M^{-1} , SI 3.2). Similarly, both **III-29** and **III-18** do not self-associate in organic solvents: the amide signals in the ^1H NMR of these compounds are independent on concentration and shifted far downfield due to intramolecular interactions. We imply that crystal structures of the compounds **III-29** and **III-30**, discussed below, should provide useful insight on the possible intra- and intermolecular interactions in the analogs **III-18** and **III-22**.

In the crystal structure each molecule of **III-30** forms four intermolecular H-bonds as it is indicated in Figure 3.20, and there are no intramolecular interactions

between -NHCO- groups. One of the amide groups, marked yellow, is not involved in H-bonding interactions in the crystalline state, likely, due to the space filling reasons. Intramolecular interactions shown in Figure 3.19 (a), which might be possible in solution, were not observed in the crystalline state of the receptor III-30.

There are two unequivalent molecules of III-29 in the crystal structure. One of them forms three intramolecular H-bonds and no intermolecular interactions (Figure 3.19 (a) and Figure 3.21). Another unequivalent molecule of III-29, in addition to three intramolecular H-bonding interactions, indeed, forms two intermolecular H-bonds (Figure 3.22).

Therefore, as it was expected, crystal structures revealed strong intramolecular interactions in III-29, while receptor III-30 forms only intermolecular H-bonds.

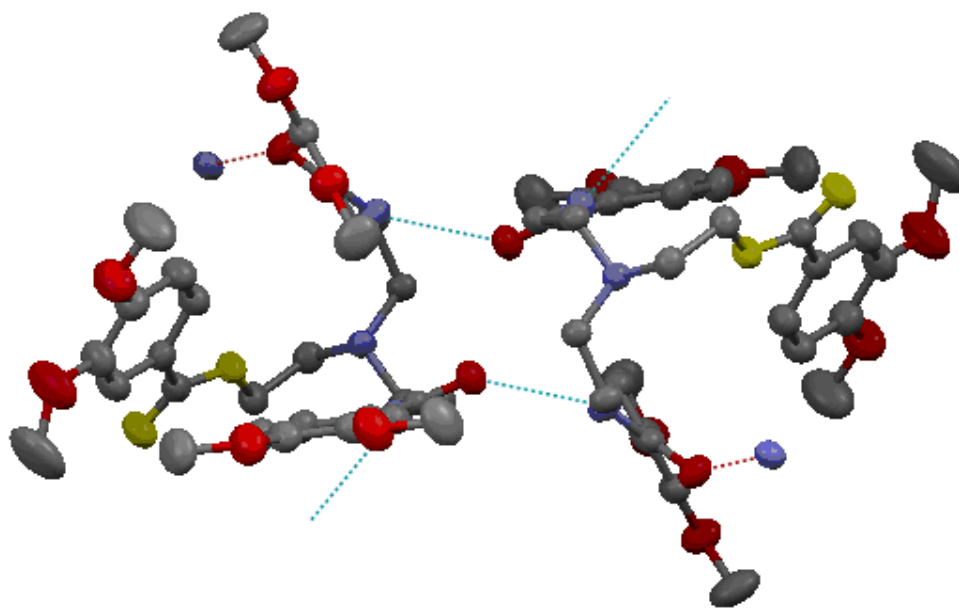


Figure 3.20. Fragment of the crystal lattice of compound III-30. H-bonds are indicated by the dotted lines. Amide groups -NHCO- which are not involved in H-bonding interactions are marked yellow.

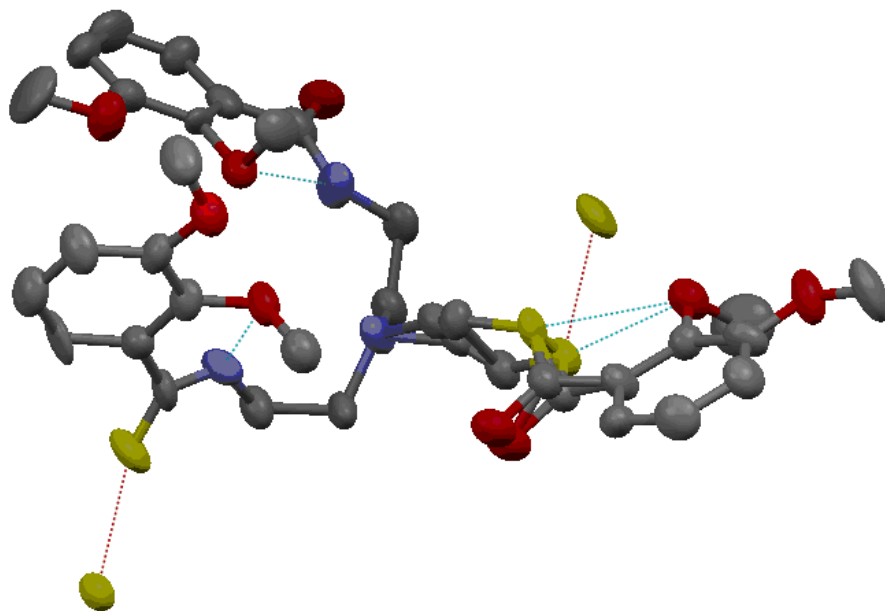


Figure 3.21. One of the two unequivalent molecules in the crystal structure of III-29. H-bonds are indicated by the dotted lines. CO and NH groups involved in intermolecular interactions are marked yellow.

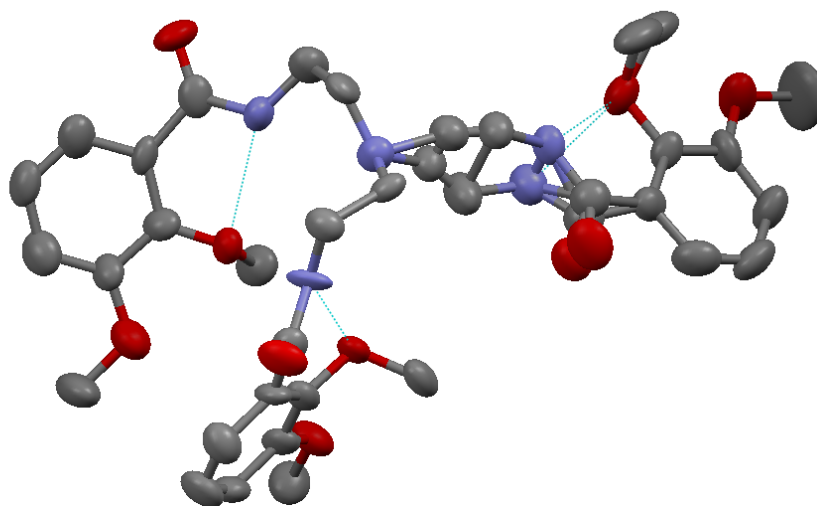


Figure 3.22. One of the two unequivalent molecules in the crystal structure of III-29, which does not form intermolecular interactions. Intramolecular H-bonds are indicated by the dotted lines.

3.2.4.7. **Conclusion.** First of all, due to the simplicity of the structure and easy access compound III-22 might encode a new family of organogelators with tunable properties. For instance, due to the presence of the tertiary amine functionality gelation of acetone by III-22 should be pH-dependent. One can also think of making these gelators chiral molecules. Different methods of electron microscopy (EM), small angle X-ray powder diffraction, etc. might be applied to study structure of these organogels. Different questions can be addressed using these new compounds.

Second, properties of the *O*-methylated analogs are indirect evidence to support hypothesis that, in contrast to the 2,3-catechols, the 3,4-catechols have a stronger tendency to self-aggregate in aqueous media. Thus, 3,4-dimethoxy compound III-22 can form up to six intermolecular H-bonds, self-associates in CDCl₃, and gels organic solvents. In contrast, due to intramolecular MeO...NH contacts the self-aggregation property of the analog III-18 is diminished. Similarly, in the 3,4-catechols three amide groups are perfectly suited for self-association, while the 2,3-catechols form intramolecular H-bonds that “prevent” the -CO-NH- groups from intermolecular interactions. Indeed, this structural difference might be sufficient to explain the difference in solubility properties of the bis-catechols III-26 and III-28 in aqueous media. Compound III-28 is more likely to self-aggregate in aqueous media and, therefore, is less soluble.

3.3. Supporting Information for Chapter 3.

3.3.1. The pK_a values of the TRENAM analog and some other relevant compounds.

	pK _A
(2,3-(HO) ₂ (C ₆ H ₃)CONHCH ₂ CH ₂) ₃ NH ⁺	5.88 (OH), 6.71 (OH), 8.61 (OH), 8.75
TRENAM	(N ⁺ H) ⁷⁹
1,2-(OH) ₂ C ₆ H ₄ catechol	9.5
NH ₄ ⁺	9.2
HN ⁺ (C ₂ H ₅) ₃	10.8
H ₂ N ⁺ (C ₂ H ₅) ₂	11
2,4 (NO ₂) ₂ (C ₆ H ₃)OH	4.0
2,4-Dinitrophenol(DNP)	
H ₂ O	16
HN ₃	4.72
HCl	-8

3.3.2. Anion binding studies.

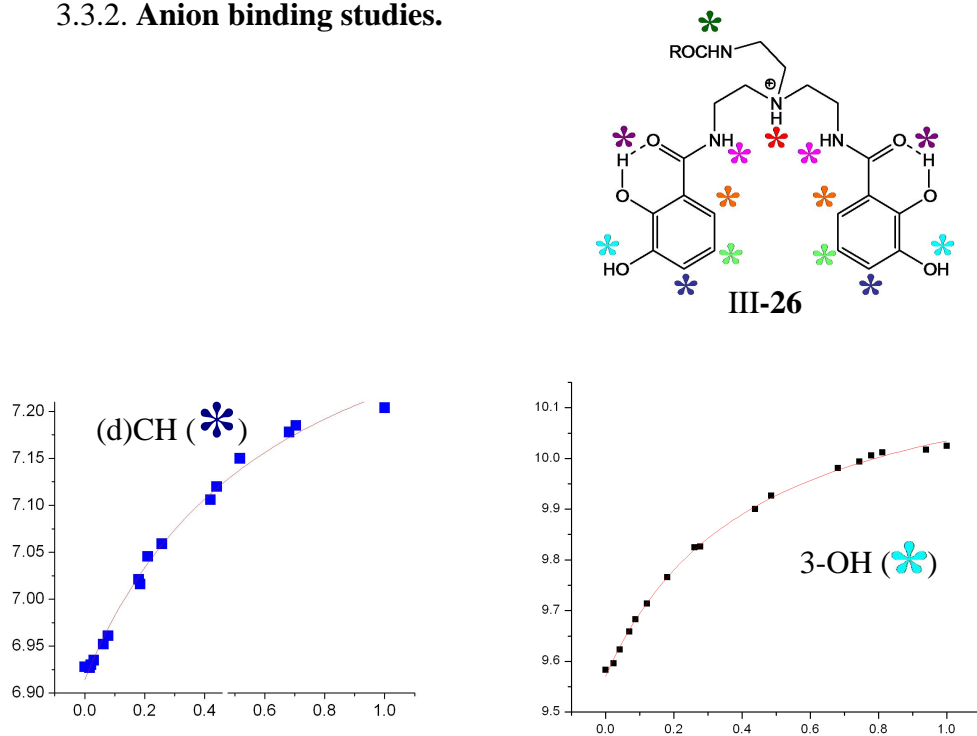


Figure S3.1. Example of the experimental data set from the ¹H NMR titration experiment (blue squares) and best curve fits (red line) of the receptor III-26: d(CH) (✱) signal single step, 3-OH (✱) signal single step.

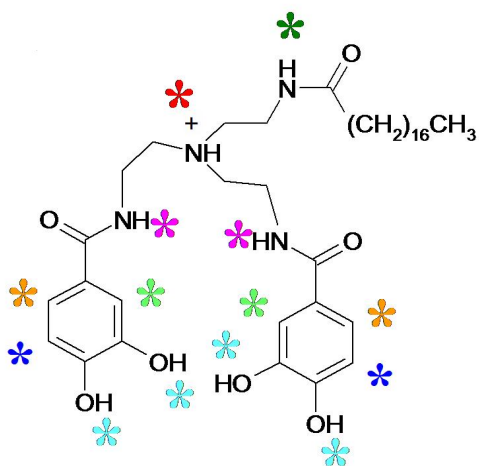


Figure S3.2. Compound III-28.

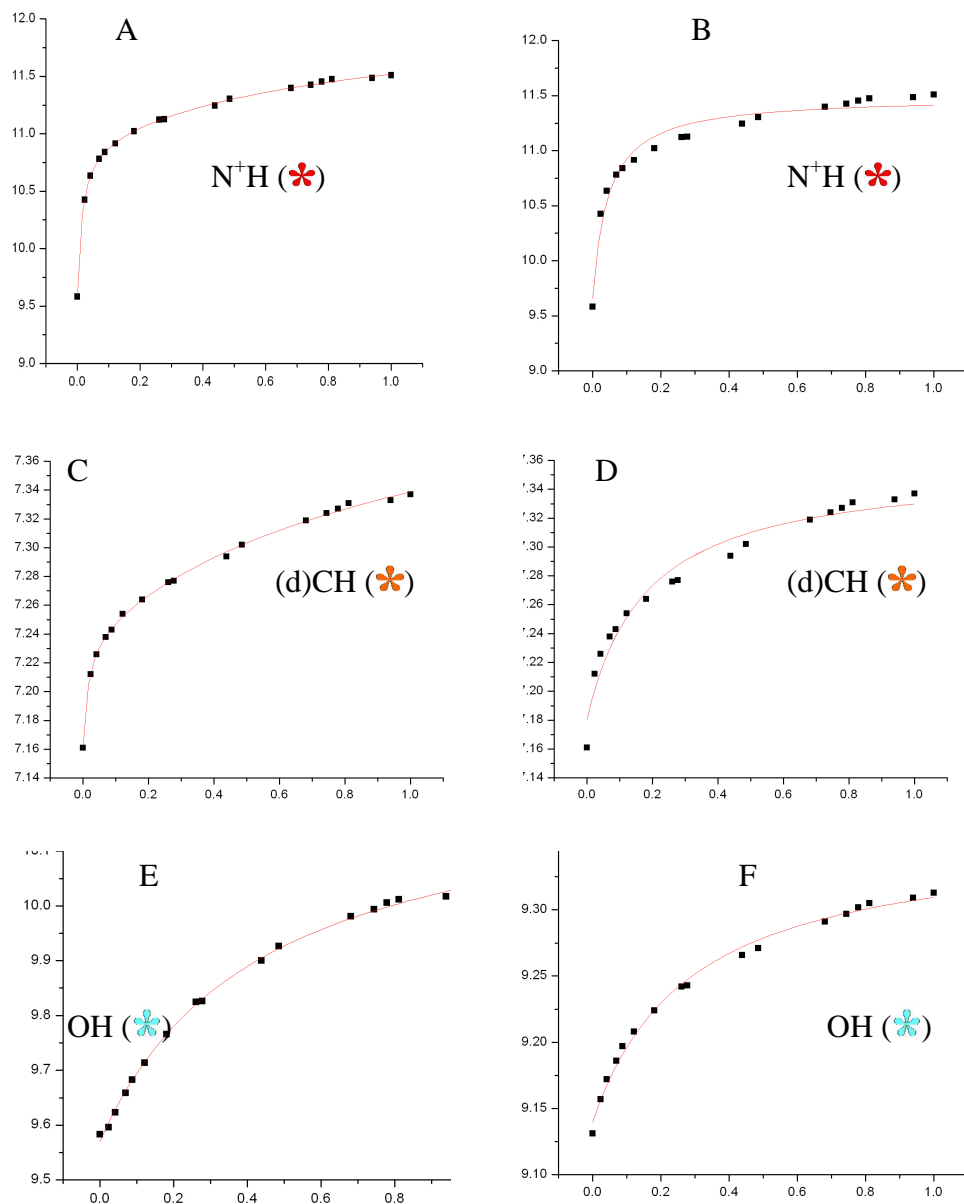
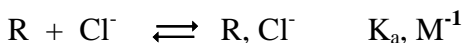


Figure S3.3. Examples of experimental data sets from the ^1H NMR titration experiment (black squares) and best curve fits (red line) for compound III-28. N^+H (*) signal: two-step (A) vs single-step (B); $(\text{d})\text{CH}$ (*) signal: two-step (C) vs single-step (D); two OH (*) signals: single step (E, F).

3.3.3. **Modeling of anion binding.** Solutions of the receptors R, III-22, III-26, III-28, and III-18, were titrated in DMSO-d₆ using (Bu)₄N⁺Cl⁻ as a source of Cl⁻ anions. Two solutions, first contained 2.5 mM of amphiphile, second contained 2.5 mM of amphiphile and [(Bu)₄N⁺Cl⁻] = 1 M, were mixed in different ratio. To obtain the binding constant the following algorithms were considered:

Single-step model

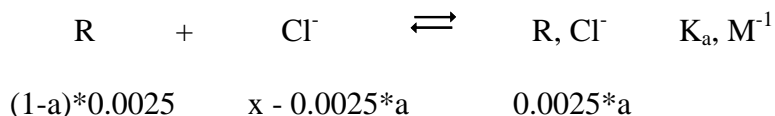


Using Origin 7.0 program¹⁰⁹, the curve fitting method was applied to obtain K_a, M⁻¹ from the experimental data. The following function was used to create the best fit of experimental data:

$$\delta = \delta_0 + (\delta_{\max} - \delta_0) * (0.0025 * K_a + K_a * x + 1 - ((K_a * 0.0025 + K_a * x + 1)^2 - 4 * 0.0025 * x * K_a^2)^{0.5}) / (2 * K_a * 0.0025) \quad (S4.1)$$

where the recorded chemical shift, δ , is the dependent variable; concentration of the salt (Bu)₄N⁺Cl⁻ in solution, x , is the independent variable; and the chemical shift of the free receptor, δ_0 , chemical shift of the associate with Cl⁻ anion, δ_{\max} , and association constant, K_a, are three parameters to be calculated.

In turn, the function (S4.1) was constructed according to the following:



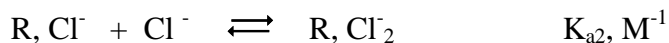
The following relations take place:

$$\delta = \delta_0*(1 - a) + \delta_{\max} * a \quad (\text{S4.2})$$

$$K_a = a/((1 - a)*(x - 0.0025* a)) \quad (\text{S4.3})$$

where “a” is the fraction of the receptor in the form of the associate with Cl⁻ anion. In combination, equations (S4.2) and (S4.3) gave the desired function (S4.1) that was used to fit the experimental data sets.

Two-step model

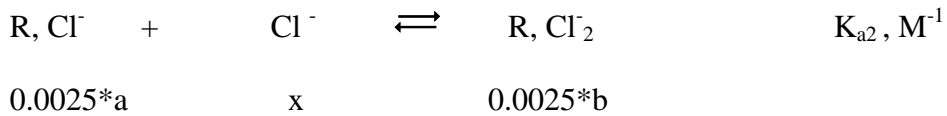
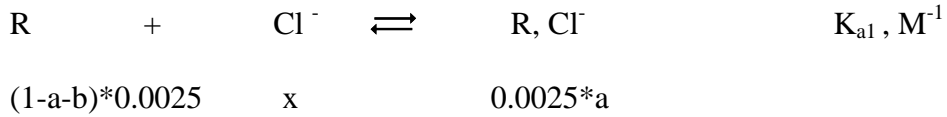


Using Origin 7.0 program¹⁰⁹, the curve fitting method was applied to calculate the constants, K_{a1} and K_{a2}, from the experimental data. The following function was used to create the best fit:

$$\delta = \delta_0 + (\delta_{\max 1} - \delta_0) * K_{a1} * x / (K_{a1} * K_{a2} * x^2 + K_{a1} * x + 1) + (\delta_{\max 2} - \delta_0) * K_{a1} * K_{a2} * x^2 / (K_{a1} * K_{a2} * x^2 + K_{a1} * x + 1) \quad (S4.4)$$

where the chemical shift, δ , is the dependent variable; concentration of the salt $(\text{Bu})_4\text{N}^+\text{Cl}^-$ in solution, x , is the independent variable; and the chemical shift of the free receptor, δ_0 , chemical shift of the associate with one Cl^- anion, $\delta_{\max 1}$, chemical shift of the associate with two Cl^- anions, $\delta_{\max 2}$, and the corresponding binding constants K_{a1} and K_{a2} are five parameters to be determined.

In turn, the function (S4.4) was constructed according to the following:



The following relations take place:

$$x \gg 0.0025,$$

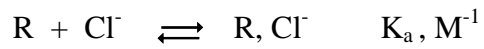
$$\delta = \delta_0 * (1 - a - b) + \delta_{\max 1} * a + \delta_{\max 2} * b \quad (S4.5)$$

$$K_{a1} = a / (x * (1 - a - b)) \quad (S4.6)$$

$$K_{a2} = b / (x * a) \quad (S4.7)$$

where “a” is the fraction of the receptor in the form of the associate with a single anion R, Cl⁻, “b” is the fraction of the receptor associated with two anions R, Cl₂⁻. In combination, equations (S4.5), (S4.6), and (S4.7) gave the desired function (S4.4) which was used to fit the experimental data sets.

Single-step model



Two-step model

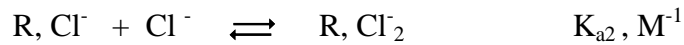


Table S3.1. Single-step model. The following parameters K_a , M^{-1} , $\Delta\delta = \delta_{\max} - \delta_0$, ppm, and R^2 were obtained from the best fit of experimental data sets for compounds III-26 and III-28. The cases, when the single step model could not adequately describe the experimental data sets ($R^2 < 0.99$), are marked bold.

		K_a, M^{-1}	R^2	$\Delta\delta$, ppm	
III-28	N⁺H	22.74 ± 33.65	0.9714	1.831	± 0.127
	OH	2.31 ± 0.15	0.9984	0.667	± 0.020
	OH	3.53 ± 0.56	0.9947	0.218	± 0.010
	NH(2)	1.99 ± 0.40	0.9858	0.694	± 0.068
	NH(1)	1.43 ± 0.23	0.9931	1.127	± 0.095
	CH(s)	4.80 ± 0.78	0.9843	0.105	± 0.007
	CH(d)	5.57 ± 1.25	0.9685	0.176	± 0.017
	CH(d)	5.48 ± 0.39	0.9968	0.116	± 0.003
III-26	N⁺H	49.19 ± 8.94	0.9657	1.936	± 0.150
	2-OH	101.5 ± 12.8	0.9827	0.397	± 0.020
	3-OH	1.84 ± 0.24	0.9943	1.312	± 0.091
	NH(2)	9.19 ± 1.90	0.9749	0.795	± 0.066
	NH(1)	3.50 ± 0.29	0.9966	0.864	± 0.033
	CH(d)	18.19 ± 3.54	0.9736	0.331	± 0.056
	CH(d)	1.58 ± 0.22	0.9935	0.497	± 0.039
	CH(dd)	1.99 ± 0.26	0.9935	0.271	± 0.019

Table S3.2. Two-step model. The following parameters K_{a1} , K_{a2} , $\Delta\delta_1 = \delta_{\max 1} - \delta_0$, $\Delta\delta_2 = \delta_{\max 2} - \delta_{\max 1}$ and R^2 were obtained from the best fit of experimental data for compounds **III-26** and **III-28** using data sets which could not be described adequately by a single step model.

	R^2	K_{a1}, M^{-1}	$\Delta\delta_1, \text{ppm}$	K_{a2}, M^{-1}	$\Delta\delta_2, \text{ppm}$
III-28					
N ⁺ H	0.9996	68.69 ± 5.66	1.342 ± 0.049	1.11 ± 0.25	1.152 ± 0.141
NH(2)	0.9986	70.28 ± 32.26	0.144 ± 0.029	0.79 ± 0.19	0.884 ± 0.126
CH(s)	0.9985	92.48 ± 49.72	0.310 ± 0.007	1.94 ± 0.40	0.102 ± 0.011
CH(d)	0.9990	62.08 ± 12.62	0.082 ± 0.007	0.88 ± 0.21	0.208 ± 0.029
III-26					
N ⁺ H	0.9992	150.3 ± 23.0	1.386 ± 0.080	2.89 ± 0.64	0.993 ± 0.115
2-OH	0.9992	148.7 ± 11.9	0.356 ± 0.011	0.84 ± 0.48	0.149 ± 0.052
NH(2)	0.9986	142.8 ± 63.7	0.307 ± 0.055	3.31 ± 0.63	0.706 ± 0.073
CH(d)	0.9989	145.0 ± 52.1	0.161 ± 0.024	4.40 ± 0.88	0.247 ± 0.028

Similarly, HCl salts of methylated analogs **III-18** and **III-22** were titrated in DMSO. The data obtained are summarized below.

Table S3.3. Single-step model. The following parameters K_a and $\Delta\delta = \delta_{\max} - \delta_0$ were obtained from the best fit of experimental data for compounds **III-18** and **III-22**.

	K_a, M^{-1}	$\Delta\delta, \text{ppm}$
III-18		
N ⁺ H	22.74 ± 3.65	1.831 ± 0.127
NH(2)	<<<1	
NH(1)	4.4 ± 0.2	0.67 ± 0.01
III-22		
N ⁺ H	35.5 ± 5.9	1.4 ± 0.1
NH(2)	6.5 ± 0.8	0.79 ± 0.04
NH(1)	3.5 ± 0.4	0.88 ± 0.04
CH(s)	10.5 ± 1.6	0.270 ± 0.02
CH(d)	35.1 ± 2.4	0.128 ± 0.004
CH(d)	2.92 ± 0.42	0.076 ± 0.005

Table S3.4. Two-step model. The following parameters K_{a1} , K_{a2} , $\Delta\delta_1 = \delta_{\max 1} - \delta_0$ and $\Delta\delta_2 = \delta_{\max 2} - \delta_{\max 1}$ and R^2 were obtained from the best fit of the experimental data for compounds **III-18** and **III-22**.

	K_{a1}, M^{-1}	$\Delta\delta, \text{ppm}$	K_{a2}, M^{-1}	$\Delta\delta, \text{ppm}$
III-18				
N ⁺ H	47.6 ± 2.8	1.53 ± 0.05	0.65 ± 0.37	0.8 ± 0.3
III-22				
N ⁺ H	75.1 ± 11.5	1.2 ± 0.1	0.9 ± 0.6	1.0 ± 0.4

3.3.4. Self-aggregation of the compound III-30 in CDCl₃.

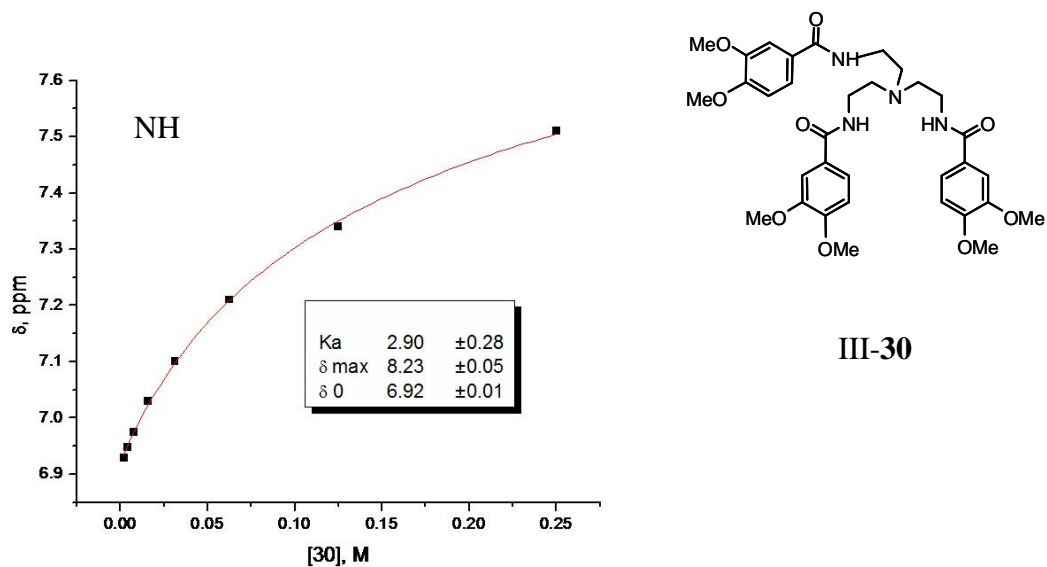


Figure S3.4. Dependence of the chemical shifts of the amide signals (NH) in compound III-30 on concentration in CDCl₃ solution. Red curve is the best fit obtained using Origin 7.0 program¹⁰⁹ and equations (S2.1) to model the dimerization.

Chapter 4: Bis-Catechols as Anion Transporters.

4.1. Results of the Transport Experiments and Discussion.

Much of this chapter has been published in the reference 41d:

- S. K. Berezin, J. T. Davis “Catechols as Membrane Anion Transporters” *J. Am. Chem. Soc.*, **2009**, *131*, 2458 – 2459.

4.1.1. Relative activity of the bis-catechols and methylated analogs in liposomal assay. The activity of new anion receptors was evaluated using an anion transport assay described by Sidorov *et al.*¹¹⁰ The pH-sensitive dye HPTS was encapsulated within the phospholipid vesicles with intravesicular NaNO₃ and Na₂SO₄ as an external electrolyte. The amphiphile-induced alkalinization of these liposomes, above the pH of the extravesicular solution, indicated that the apparent efflux of the acid H⁺NO₃⁻ was driven by the anion gradient while the multiply charged SO₄²⁻ and HPTS anions remained relatively impermeable. Bis-catechol (III-25) with alkyl chain of medium length was found to be the most active compound. The control compounds, the 3,4-dihydroxy (III-27) and methylated (III-15) analogs, were inactive (Figure 4.1 and Figure 4.2). In Figure 4.2 the Y-axis “Ratio” refers to the ratio of HPTS fluorescence emission at 510 nm (I_0/I_1) where I_0 is excitation at 460 nm (basic form of HPTS) and I_1 is excitation at 403 nm (acidic form of HPTS).¹¹⁰ The dependence of the Ratio on pH can be found in SI 4.1. Structure of HPTS dye

and the basics of liposomal assays have been reviewed in detail in the introductory Chapter 1.

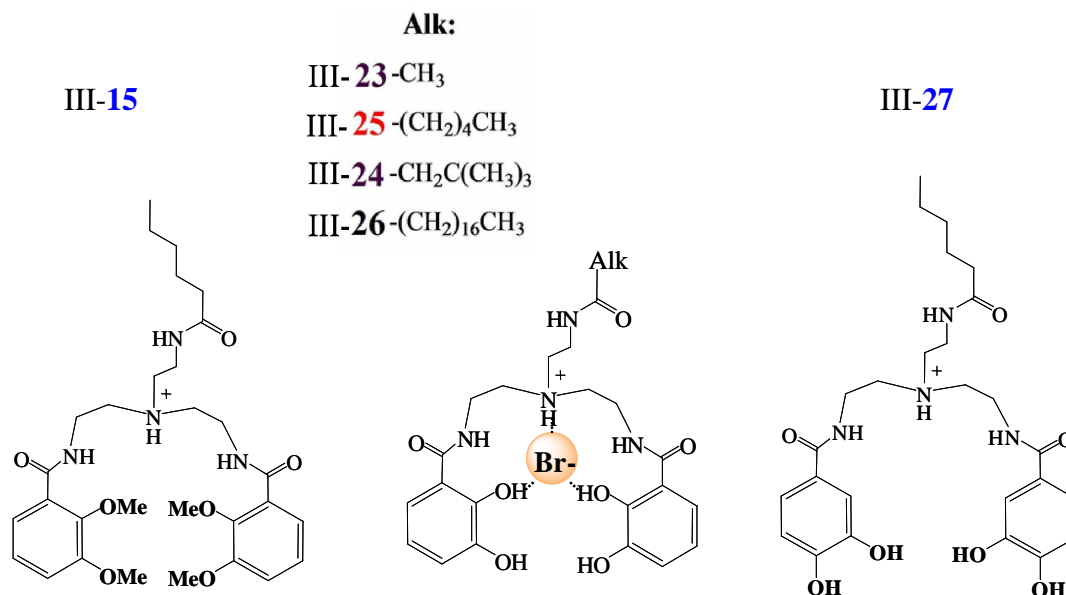


Figure 4.1. Amphiphilic anion transporter III-**25**, analogs with different alkyl chain length (III-**23** - III-**26**) and inactive structural analogs III-**15** and III-**27**.

The observation that the analogs III-**23** - III-**26** differ in activity (Figure 4.2b) suggests that the ion transport property likely depends on the ability of these anion receptors to partition into the membrane. Compound III-**26**, with a longest C17 alkyl chain, likely aggregates in water, limiting its partitioning into the liposomes due to “low solubility” of individual molecules. Compound III-**2**, with the shortest chain, was the least active analog, as it may not be hydrophobic enough to partition into the membrane. Presumably, the most active analog III-**25** does not aggregate significantly and is hydrophobic enough to efficiently partition into liposomes. The bis-catechol's alkyl chain length was not the only structural determinant of membrane transport

function. As indicated in Figures 5.2c, the catechol's substitution pattern is also crucial for ion transport. Thus, the 3,4-dihydroxy analog (III-27) was completely inactive in this anion transport assay.

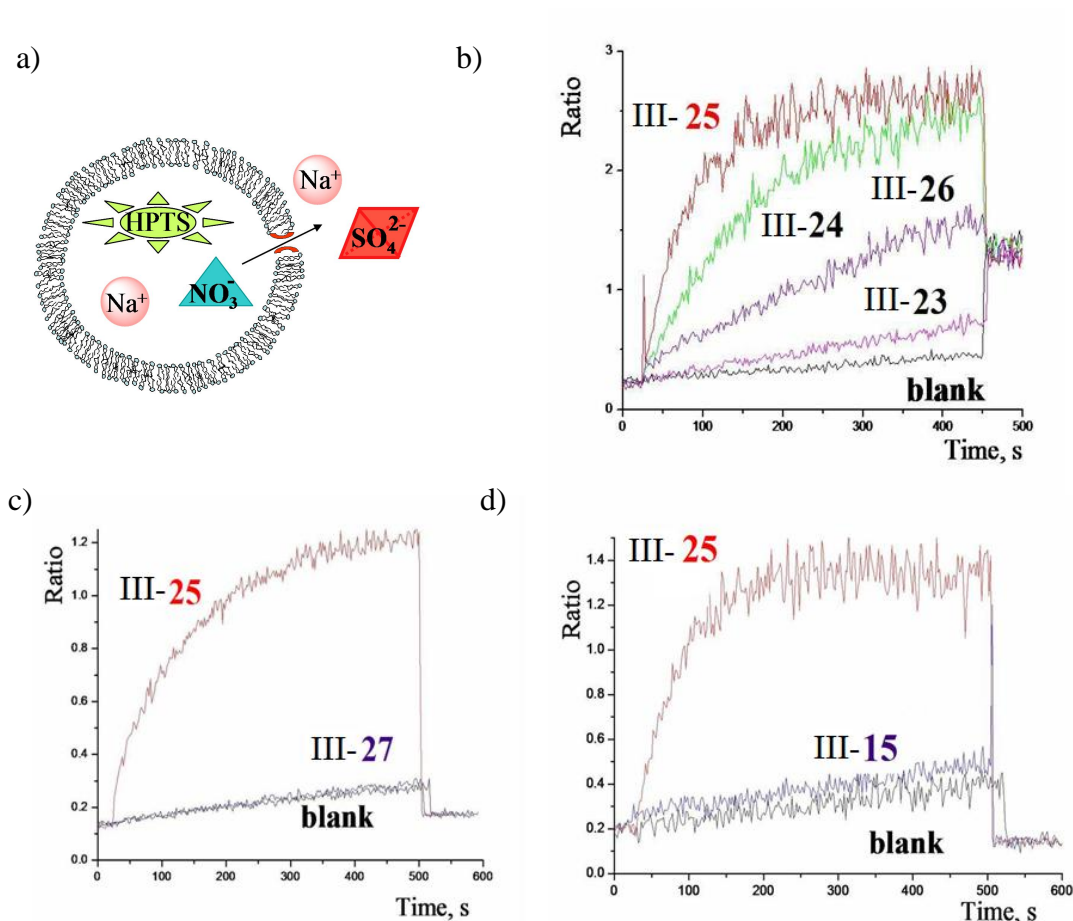


Figure 4.2. Schematic representation of the anion transport assay (a). Intravesicular 100 mM NaNO₃, 10 mM phosphate pH = 6.4, extravesicular 75 mM Na₂SO₄, 10 mM phosphate pH = 7.5[§] (b), pH = 6.3 (c and d). Solutions of the amphiphiles in MeOH were injected at $t = 25$ s (or just MeOH was injected in the case of **blank**), ratio PC : amphiphile = 10 : 1. Aqueous 10% Triton-X was injected at $t = 450$ or 500 s. [§] The extravesicular pH had to be basic to avoid precipitation and ensure solubility of the long-chain analog III-26.

Why is the 2,3-catechol (III-25) active while the 3,4-catechol (III-27) is not? To function as an anion transporter a given receptor should be able to interact with both the anion and the phospholipid bilayer. Indeed, the anion-binding properties of 2,3-catechol (III-25) and 3,4-catechol (III-27) analogs in DMSO-d₆ solution are almost the same (see Table 3.1). Therefore, we hypothesize that the observed difference in anion transport is defined by the different self-association property of these two receptors in the aqueous media. Experimental observations indicate that 3,4-catechol (III-27) has a lower solubility in aqueous solution than does 2,3-catechol (III-25) and that the solubility of both compounds increases in basic solution. Based on these qualitative observations, we conclude that, compared to the 2,3-catechol (III-25), the 3,4-catechol (III-27), similarly to the long alkyl chain analog III-26, has a stronger tendency to self-aggregate in the aqueous media. Therefore, the solubility of individual molecules of these compounds that can partition into the bilayer dramatically diminishes due to formation of water-soluble aggregates. Indeed, in the 3,4-catechol derivative three amide groups are perfectly suited for self-association, while in 2,3-catechol strong intramolecular H-bonds “prevent” the -CO-NH- groups from intermolecular interactions (see Chapter 3). The properties of the *O*-methylated analogs, reviewed in the previous chapter, are indirect evidence to support this hypothesis. In brief, the 3,4-dimethoxy compound III-22 self-associates in CDCl₃ while the 2,3-dimethoxy analog III-18 does not. Moreover, III-22 is an organogelator while III-18 is not. It is likely that due to the intramolecular MeO...HN H-bonds the self-aggregation property of the analog III-18 is diminished. Similarly, compared to 3,4-catechol (III-27), the self-aggregation properties of 2,3-catechol (III-25) is

diminished due to strong intramolecular OH \cdots CONH H-bonds.

4.1.2. Study of the anion selectivity. To determine the selectivity of the observed anion transport we used different Na $^+$ salts as external and internal electrolytes, creating a concentration gradient for anions across phospholipid bilayer. Fluorescence measurements allowed us to monitor the increase in intravesicular pH in response to the imposed concentration gradients. (The dependence of the Ratio on pH can be found in SI 4.1. The basics of liposomal assays have been reviewed in detail in the introductory Chapter 1). Surprisingly, alkalization of liposomes initiated by the most active bis-catechol **III-25** was observed only when the extravesicular anion was on the left of the intravesicular anion in the Hofmeister sequence, ClO $_4^-$ > I $^-$ > NO $_3^-$ > Br $^-$ > Cl $^-$ > SO $_4^{2-}$ (Figure 4.3).¹¹¹ This experimental observation can be explained as follows. Because of the difference in relative permeability of intra- and extravesicular anions, the amphiphile-induced anion efflux exceeds anion influx. As an extremely thin insulating layer, the biomembrane acts as a parallel-plates capacitor and allows separation of charges. Therefore, the initial leakage of the negative charge out of the vesicles results in a rising positive electrical potential inside and a negative potential outside of the liposomes. This transmembrane electrical potential does not stabilize. Instead, it reaches a maximum and then diminishes as the concentration of the anions in intravesicular and extravesicular solutions slowly equilibrates. Permeation of protons across the phospholipid bilayer is rapid on the experiment time scale. Thus, protons are in equilibrium with the established electrical potential and initially move out of the vesicles against their own chemical gradient. This translocation of H $^+$

appears as acid efflux from the liposomes but does not alter the transmembrane electrical potential because of the rather low concentrations of $\text{H}^+/\text{OH}^-/\text{buffer}$ in solution as compared to the concentration of electrolytes $\text{Na}^+ \text{Anion}^-$.

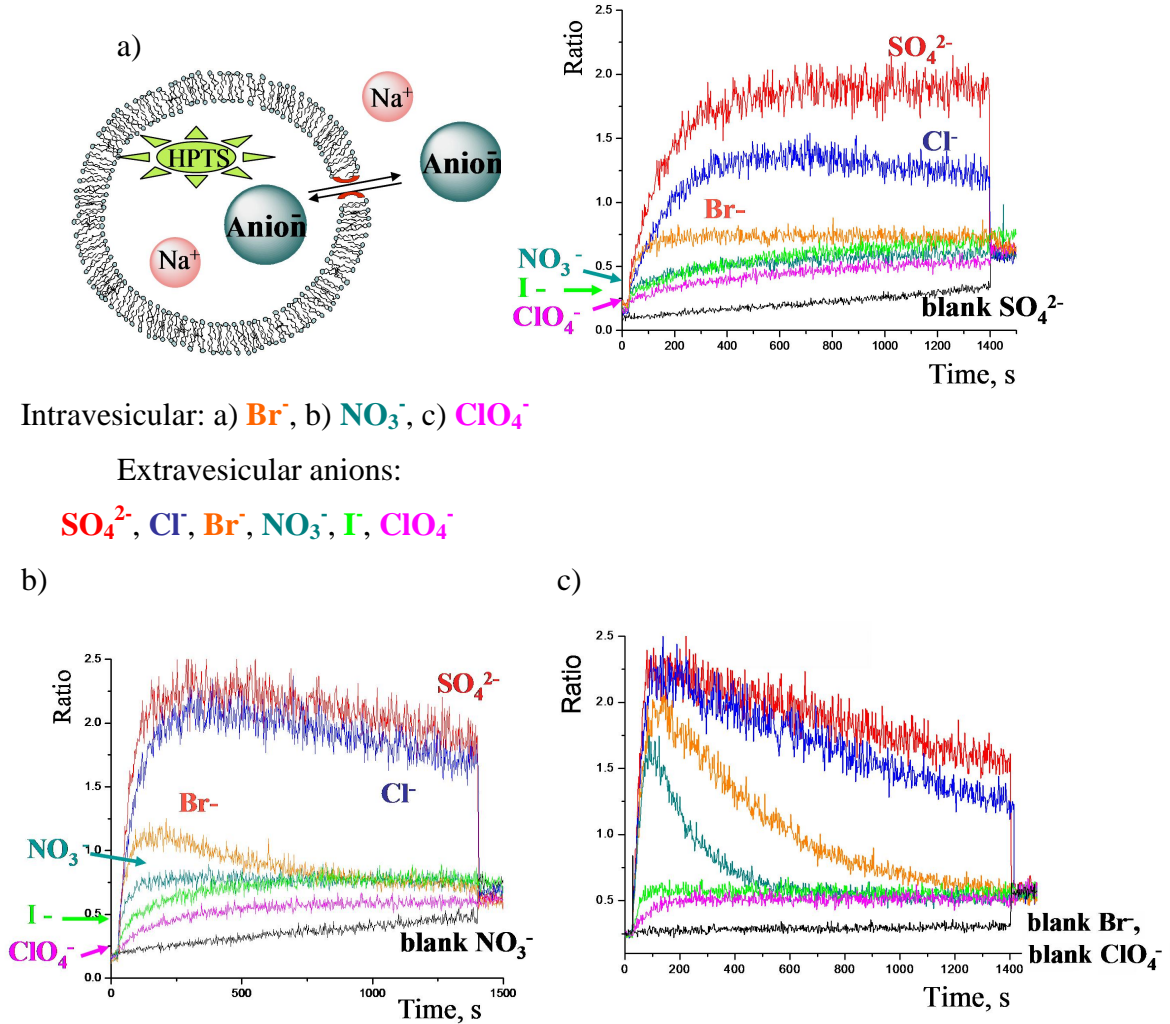


Figure 4.3. Anion transport assays. Extravesicular 100 mM $\text{Na}^+ \text{Anion}^-$ ($\text{Anion}^- = \text{Cl}^-$, Br^- , NO_3^- , I^- , ClO_4^-) or 75 mM Na_2SO_4 , 10 mM phosphate pH = 7.15. Intravesicular 10 mM phosphate pH = 5.5, a) 100 mM NaBr , b) 100 mM NaNO_3 , c) 100 mM NaClO_4 . Solution of III-25 in MeOH (or MeOH in the case of **blank**) was injected at $t = 25$ s, ratio PC : III-25 = 10 : 1. Aqueous 10% Triton-X was injected at $t = 1400$ s.

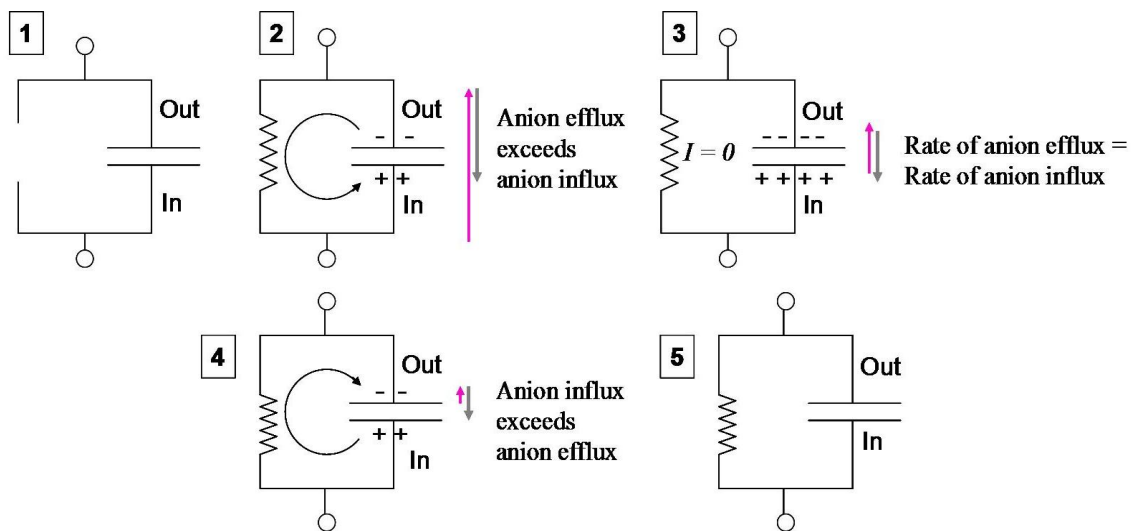
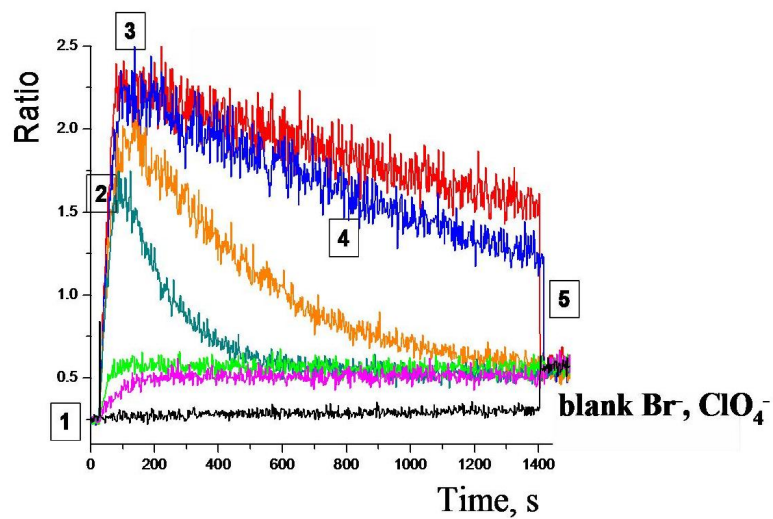


Figure 4.4. Anion transport assay with intravesicular ClO_4^- and set of electric circuit diagrams to represent mechanistics of the transport process.

Acid efflux is followed by the relatively slow acid influx which, in turn, reflects the dissipation of the electrical potential. The rates of this second process are defined by the transport rates of extravesicular anions and are in accordance with the Hofmeister sequence. It is noteworthy that the time and pH when the inward and outward “acid fluxes” achieved the same rate ($d \text{ Ratio}/dt = 0$, pH_{max}) were also anion dependent. For instance, in the case of perchlorate as an intravesicular anion, the transmembrane electric potential was lower and the intravesicular pH was less basic when the extravesicular anion was more permeable and anion exchange was more rapid. The mechanistics of the ion transport can be illustrated as a set of electric circuit diagrams (Figure 4.4).

In the case of strong electrolytes no change in intravesicular pH was observed in the absence of the amphiphile because of the low permeability of anions across the phospholipid bilayer. In contrast, when liposomes loaded with the salt of a weak acid such as NaN_3 were exposed to an anion gradient, the intravesicular pH immediately rose as a result of the outward diffusion of the neutral acid HN_3 . Two alternatives should be considered. If H^+ permeation across the bilayer is rapid, even in the absence of the receptor III-25, then the observed intravesicular alkalization is accompanied by the instantly established transmembrane electrical potential that is stable and opposed to the N_3^- chemical potential. The H^+ ions equilibrate with this transmembrane electrical potential but are unable to lower it due to rather low concentration of $\text{H}^+/\text{OH}^-/\text{buffer}$ in the solution.

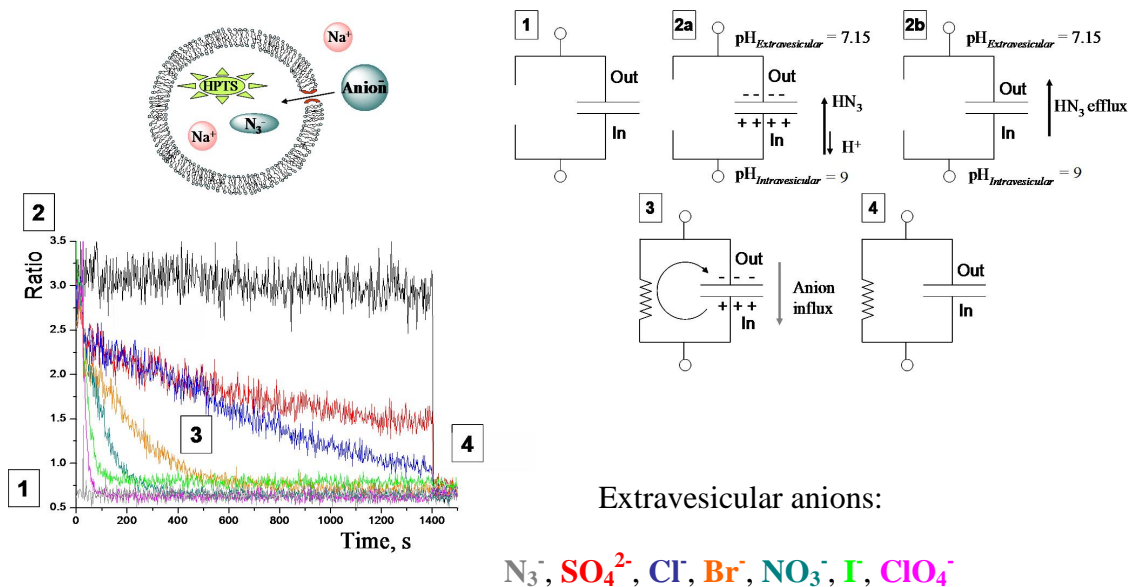
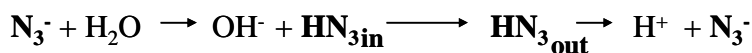


Figure 4.5. Anion transport assay. Extravesicular 100 mM Na^+ Anion $^-$ (Anion $^-$ = N_3^- , Cl^- , Br^- , NO_3^- , I^- , ClO_4^-) or 75 mM Na_2SO_4 , 10 mM phosphate pH = 7.15. Intravesicular 100 mM NaN_3 , 10 mM phosphate pH = 6.4. Solution of III-25 in MeOH (or MeOH in the case of **blank**) was injected at $t = 25$ s, ratio PC : III-25 = 10 : 1; aqueous 10% Triton-X was injected at $t = 1400$ s. Electric circuit diagrams illustrating mechanistics of the ion transport process. 1 – extravesicular NaN_3 ($t = 0 - 25$ s); 2a, 2b - extravesicular NaX ($X \neq \text{N}_3$) ($t = 0 - 25$ s); 3 – process following the injection of III-25 in MeOH at $t = 25$ s; 4 – endpoint of the ion transport: intra and extravesicular solutions are identical. There are two alternatives to consider: H^+ transport across phospholipid bilayer is rapid even in the absence of the amphiphile (2a) or there is no H^+ /charge transport/electric potential across phospholipid bilayer until III-25 is introduced into solution (2b).

Alternatively, there is no transmembrane electrical potential to be established because H^+ does not permeate across the bilayer in the absence of the amphiphile III-25. Efflux of HN_3 happens on a millisecond time scale and shuts down at high intravesicular pH. Transmembrane electrical potential is established instantaneously on the millisecond time scale only during the next step when the receptor that catalyzes proton/charge transport is introduced into the solution. Addition of the amphiphile III-25 allows slow influx of extravesicular anions. The anion exchange across the phospholipid bilayer as the net effect is observed on the minute time scale. The gradual decrease in intravesicular pH reflects changes in the chemical gradients of N_3^- and $Anion^-$ across the phospholipid bilayer. The experimental dependence of Ratio on time can be described using first-order kinetics. Curve fitting using equation (4.1) allows extraction of the rate constants k_{Anion}, s^{-1} .

$$Ratio = Ratio_0 - (Ratio_0 - Ratio_{\infty}) * (\exp(k_{Anion} * t) - 1) / \exp(k_{Anion} * t) \quad (4.1)$$

$Ratio_0$ and $Ratio_{\infty}$ are values at the time of injection $t = 0$ and $t = \infty$. In our calculations we ignored the initial drop in pH that was anion independent and most likely not due to anion transport. Using anion transport rates, k_{Anion}, s^{-1} , the turnover numbers, n_{Anion}, s^{-1} , defined as the number of anions transported across the bilayer per single liposome per second, and the permeability coefficients, $P, cm s^{-1}$, can be calculated and compared to the literature (Table 4.1, see details in SI 4.2).^{8a}

Table 4.1. Anion transport rates, k_{Anion} , s^{-1} , turnover numbers per single liposome, n , s^{-1} , and permeability coefficients, P , $cm\ s^{-1}$.

	<i>Ion</i>	k_{Anion} , s^{-1} $*10^3$	n , s^{-1}	$P *10^9$, $cm\ s^{-1}$
Bis-catechol amphiphile				
III-25	SO_4^{2-}	0.61	20	1.0
	Cl^-	1.29	44	2.2
PC : III-25 = 10 : 1	Br^-	4.40	150	7.3
	NO_3^-	11.3	384	19
	Γ	36.2	1,231	60
	ClO_4^-	69.5	2,400	116
Pure phospholipid bilayer: no transporter (blank experiment, 10 μ l MeOH) [@]	NO_3^-	0.09	3	0.15 [@]
Pure phospholipid bilayer ⁶ (literature)	NO_3^-			0.05
Valinomycin carrier* ¹¹²	K^+		10,000	
	Na^+		0.5	
Potassium ion channel*	K^+		10 ⁸	
Pure phospholipid bilayer ⁶ (literature)	K^+			0.003
	Na^+			0.001
	Rb^+			0.0033

*Assuming there is one molecule of the natural transporter per liposome.

[@] Experimental value obtained from the N_3^- - based liposomal assay depicted in Figure 4.11 (N_3^- in, NO_3^- out), see for detail SI 4.3, Figure S4.6.

4.2. Modeling of the Ion Transport Kinetics.

4.2.1. **Modeling of ion transport in the N_3^- -based assay.** The mechanism of anion exchange depicted in Figure 4.6 is based on the following assumptions: 1) we imply that H^+ influx (**3**) is rapid and does not limit (or partially limit) the rate of the anion influx. To provide an experimental evidence, we might want to show that addition of the H^+ carrier, such as FCCP,^{33,40,4b} does not influence (speed up) the observed anion transport rates in N_3^- -based the assay. Similarly to other catechols, known to “shuttle” H^+ across phospholipid bilayer in the cells and cellular organelles,^{61,62} receptor III-**25** is expected to act as a proton transporter; 2) according to the diagram, the rate is independent of the nature of intravesicular weak-acid anion, which can be confirmed experimentally (for instance, CH_3COO^- versus N_3^-);

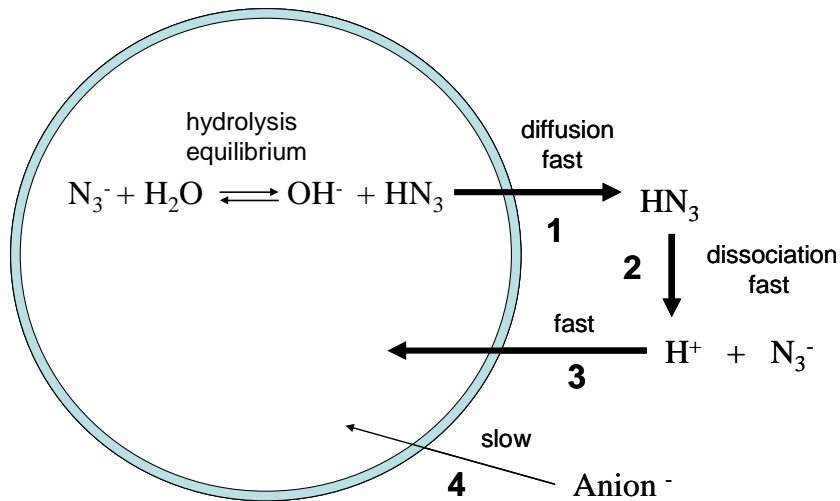


Figure 4.6. Mechanism of anion exchange in the N_3^- -based assay.

3) the model neglects the influence of the electrical potential on the anion transport rates, k_{Anion} . Negative outside and positive inside, the electrical field is developed due to fast net N_3^- efflux. The $k_{Anion In}$ should exceed $k_{Anion Out}$ due to favored/opposed transmembrane electrical potential (Figure 4.7). Similarly, the model neglects the influence of the osmosis.

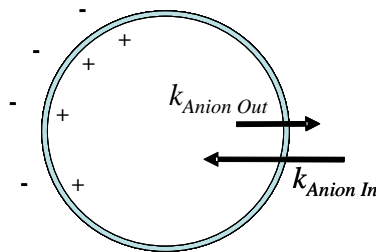


Figure 4.7. Influence of the electrical field on the anion transport rate in and out of the liposomes, $k_{Anion In}$ and $k_{Anion Out}$.

To qualitatively describe the transport, the dependence of the intravesicular anion concentration, $[Anion]_{In}$, on time, $f(t)$, has to be obtained. Giving the above assumptions, the following description of the Anion flux can be derived:

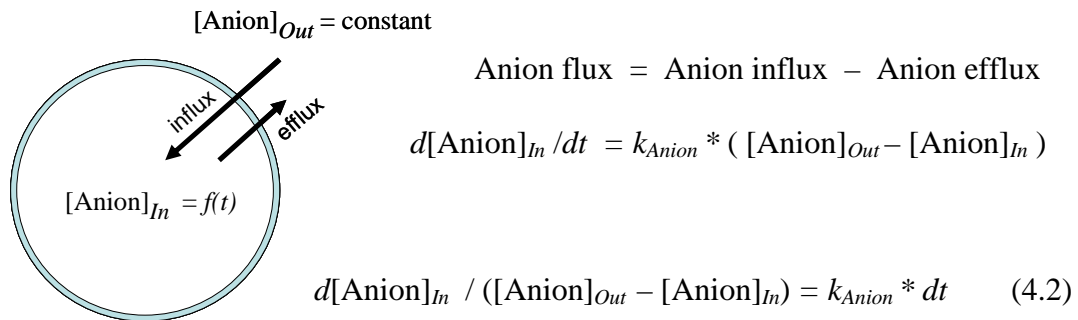


Figure 4.8. Schematic representation of the Anion flux.

Integrating the left side of equation (4.2) from $[\text{Anion}]_{In} = 0$ to $[\text{Anion}]_{In} = [\text{Anion}]_t$ and the right side from $t = 0$ to $t = t$ the following expression for $f(t)$ is obtained:

$$[\text{Anion}]_t = f(t) = [\text{Anion}]_{Out} * (\exp(k_{Anion} * t) - 1) / \exp(k_{Anion} * t) \quad (4.3)$$

We imply that there is a linear relation between experimentally determined parameter Ratio and intravesicular concentration $[\text{Anion}]_t$:

$$\text{Ratio} = k * [\text{Anion}]_t + b \quad (4.4)$$

Then coefficients k and b can be defined as following:

Ratio = Ratio₀ when $[\text{Anion}]_t = 0$ (at $t = 0$) thus $b = \text{Ratio}_0$

Ratio = Ratio_∞ when $[\text{Anion}]_t = [\text{Anion}]_{Out}$ (at $t = \infty$) and equation (4.4) can be rewritten as following:

$$\text{Ratio}_\infty = k * [\text{Anion}]_{Out} + \text{Ratio}_0 \quad (4.5)$$

thus $k = (\text{Ratio}_\infty - \text{Ratio}_0) / [\text{Anion}]_{Out}$ and equation (4.4) can be rewritten as following:

$$\text{Ratio} = \text{Ratio}_0 + (\text{Ratio}_\infty - \text{Ratio}_0) * [\text{Anion}]_{In} / [\text{Anion}]_{Out} \quad (4.6)$$

In combination, equations (4.6) and (4.2) gave the desired function (4.1), which was used to fit the experimental data of Ratio on time dependence:

$$\text{Ratio} = \text{Ratio}_0 + (\text{Ratio}_\infty - \text{Ratio}_0) * (\exp(k_{\text{Anion}} * t) - 1) / \exp(k_{\text{Anion}} * t) \quad (4.1)$$

4.2.2. **Modeling of the ion transport. The assay with intravesicular ClO_4^- anion.** The experimental dependence of Ratio on time (Figure 4.3c) has a characteristic profile/shape. It is noteworthy that this shape is remarkably similar to the kinetic profile for a chemical reaction “A” \rightarrow “C” proceeding through the formation of an intermediate “B”, as schematically shown below.

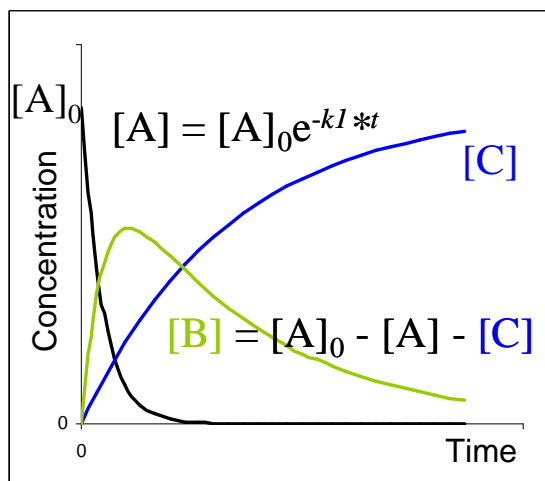
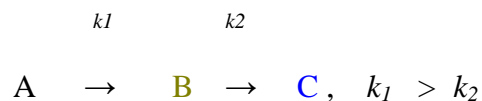


Figure 4.9. Kinetic profile for a chemical reaction “A” \rightarrow “C” proceeding through the formation of an intermediate “B”.

Using this analogously, the profile of Ratio on time dependence in Figure 5.3c also can be described qualitatively to obtain the kinetic parameters.

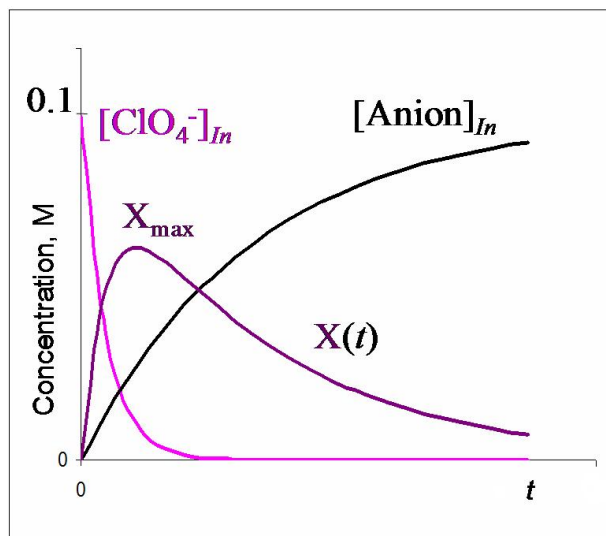


Figure 4.10. Kinetic profile of anion exchange in the perchlorate - filled liposomes. $[\text{ClO}_4^-]_{In}$ – concentration of perchlorate anion in liposomes. $[\text{Anion}]_{In}$ – concentration of the Anion⁻ in the liposomes. $[\text{Anion}]_{Out} = 0.1 \text{ M} = \text{constant}$. $X(t) = 0.1 - [\text{ClO}_4^-]_{In} - [\text{Anion}]_{In}$. (See also Figure 4.3c and the description of the experiment for more details).

For simplicity, we can assume that flux of perchlorate and Anion flux are independent of each other: the rate of perchlorate flux does not influence the rate of Anion flux and *vice versa*. We can also consider only perchlorate efflux, equation (4.6), because $[\text{ClO}_4^-]_{Out}$ is close to zero. In contrast, we have to consider Anion flux as a sum of influx and efflux, equation (4.2).

$$[\text{ClO}_4]_{In} = 0.1 * \exp(-k_{\text{ClO}_4} * t) \quad (4.6)$$

$$[\text{Anion}]_{In} = [\text{Anion}]_{Out} * (\exp(k_{\text{Anion}} * t) - 1) / \exp(k_{\text{Anion}} * t) \quad (4.2)$$

A new function $X(t)$ can be defined as following:

$$\begin{aligned} X(t) &= 0.1 - [\text{ClO}_4]_{In} - [\text{Anion}]_{In} = \\ &= 0.1 - 0.1 * \exp(-k_{\text{ClO}_4} * t) - 0.1 * (\exp(k_{\text{Anion}} * t) - 1) / \exp(k_{\text{Anion}} * t) \quad (4.3) \end{aligned}$$

We imply that there is a linear relation between Ratio and $X(t)$:

$$\text{Ratio} = k * X(t) + b \quad (4.7)$$

The coefficients k and b can be defined as following:

$$\text{Ratio} = \text{Ratio}_0 \text{ when } X(t) = 0 \text{ (at } t = 0) \text{ thus } b = \text{Ratio}_0$$

$$\text{Ratio} = \text{Ratio}_0 \text{ when } X(t) = 0 \text{ (at } t = \infty)$$

Ratio = Ratio_{max} when $X(t) = X_{\text{max}}$ (at $t = t_{\text{max}}$) and equation (4.7) can be rewritten as following:

$$\text{Ratio}_{\text{max}} = k * X_{\text{max}} + \text{Ratio}_0 \quad (4.8)$$

thus $k = (\text{Ratio}_{\text{max}} - \text{Ratio}_0) / X_{\text{max}}$ and equation (4.7) can be rewritten as following:

$$\text{Ratio} = \text{Ratio}_0 + (\text{Ratio}_{\text{max}} - \text{Ratio}_0) / X_{\text{max}} * X(t) \quad (4.9)$$

where Ratio_{max} – maximum in the experimental Ratio on time dependence, X_{max} – to be obtained using $X(t)$ dependence.

Once X_{\max} is obtained, equation (4.9) can be used to fit the experimental data set to obtain $k_{\text{ClO}_4^-}$ and k_{Anion} using perchlorate-based assay. Therefore, as an alternative to the N_3^- - based assay experimental traces in Figure 4.3c can also be used to obtain k_{Anion} .

4.3. Molecular Models of the Anion Transport.

4.3.1. **Dependence of the anion transport rate on concentration of the bis-catechol.** The dependence of the rate, $k_{NO_3^-}$, on the concentration of bis-catechol **III-25** revealed a non-linear relationship indicating that transport becomes more efficient when this compound aggregates within the bilayer (Figure 4.11, SI 4.3).

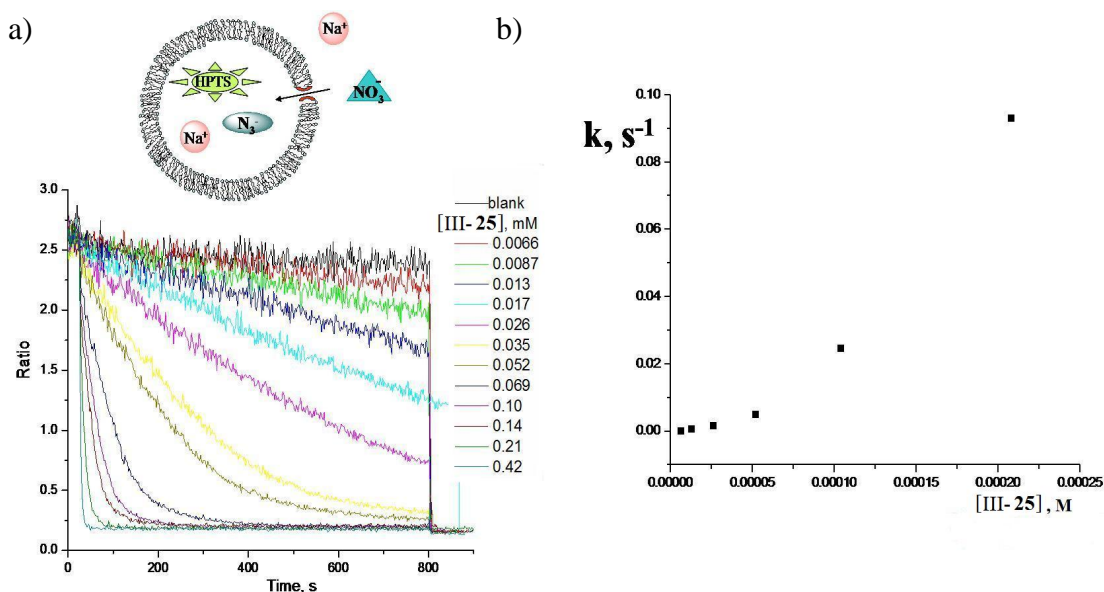


Figure 4.11. a) NO_3^- anion transport assay. Intravesicular 100 mM NaN_3 , 10 mM phosphate pH = 6.4. Extravesicular 100 mM Na_2SO_4 , 10 mM phosphate pH = 6.4. The combined data sets for two independent experiments. $[PC] = 0.585$ mM. A solution of the amphiphile **III-25** in MeOH was injected at $t = 25$ s (just MeOH (20 μ l) was injected in the case of blank). Aqueous 10% Triton-X was injected at $t = 800$ s. b) Dependence of NO_3^- transport rate on concentration of the amphiphile **III-25**.

We propose that H-bonding drives the self-association of the bis-catechol amphiphiles in the phospholipid membranes. These aggregates provide new pathways for ion transport, thereby increasing the permeability of the bilayer toward anions (Figure 4.12). The amphiphilic structures of bis-catechol based anion receptors, which encode the ability to form a water-soluble phase, should explain the relatively low activity (ratio PC : amphiphile = 10 : 1). This low activity is likely because only a small fraction of potentially active molecules partitions into the PC bilayer, while the majority forms a water-soluble phase on its own (Figure 4.12). The active analogs III-23, III-24, III-25, and III-26 should have the same affinity toward the anion. Nevertheless, a difference in transport properties of these amphiphiles was observed (Figure 4.2b). Therefore, the apparent relative activity is a combination of at least two effects: i) the efficiency of partitioning into the membrane; and ii) the anion binding properties. We imply that the compound with the long hydrophobic chain ($n = 17$) forms a water-soluble phase (such as micelles or “micellar-like” aggregates) and cannot effectively partition into the liposomes due to the low solubility of individual molecules. In contrast, the compound with the short chain ($n = 1$) is not hydrophobic enough (rather soluble in water) and does not interact with the bilayer, and thus is strong enough to induce effective transmembrane ion exchange. Compound III-25 is the most active among the five compounds that were evaluated. It is soluble enough to partition into the liposomes and it is hydrophobic enough to interact with the bilayer and form ion-conducting aggregates.

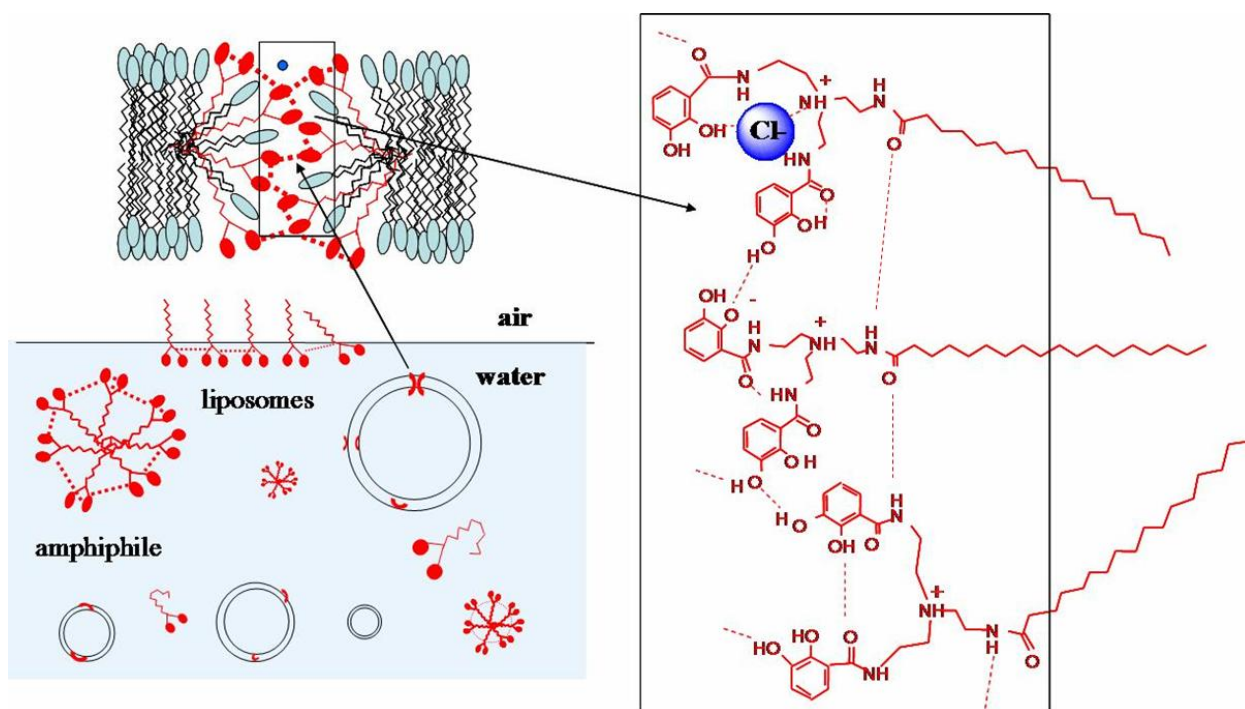


Figure 4.12. Schematic representation of the anion conducting aggregates and the processes that might take place in the solution.

We imply that on the experimental time scale the liposomes are stable structures and do not disassemble. In turn, there is an equilibrium between different forms of bis-catechol amphiphile in aqueous solution that establishes itself within several milliseconds following the injection of III-25 as a diffusion-controlled process. At first approximation the concentration of the amphiphile in the liposomes should be proportional to the concentration of the “monomeric” bis-catechol amphiphile in aqueous solution. In turn, this concentration is unknown due to unknown degree of self-aggregation in the aqueous media.

Figure 4.12 can also provide insight as to why the methylated analog III-15 might be inactive. Compounds III-15 and III-25 have very similar anion-binding properties in DMSO. To form ion-conducting aggregates, molecules of III-25 self-associate in the PC bilayer. The head groups of III-25 interact with each other in the plane perpendicular to the surface of the liposome to form a “hydrophilic pathway”. Only OH groups are suited for this purpose. It is likely that the methylated analog III-15 cannot provide the latter structure and is, therefore, an inactive anion transporter.

4.3.2. **Mechanism of transport from the point of view of an anion. Energy profile for the bis-catechol assisted anion permeation.** At a glance, amphiphile-assisted membrane transport of the anion consists of at least two events that are not necessarily separable from each other: dehydration (at least partial) and translocation across the biomembrane, as is schematically represented in Figure 4.13.

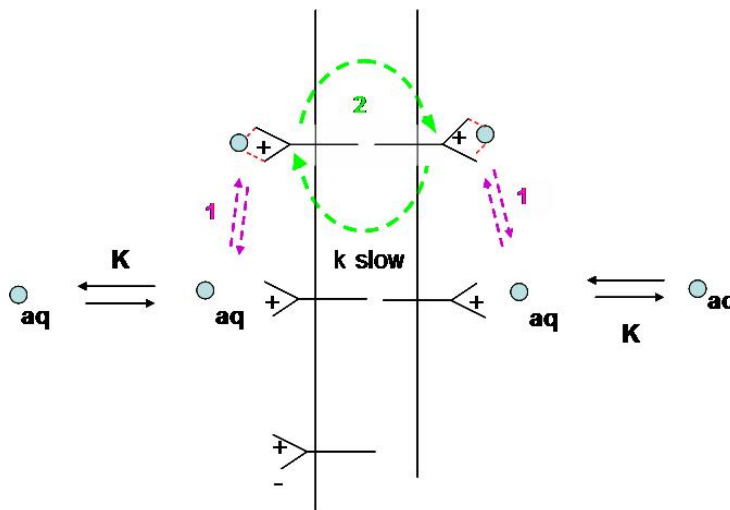


Figure 4.13. Permeation across phospholipid bilayer from the point of view of an anion: 1. Dehydration 2. Translocation.

Another way of thinking about the mechanism of transport would be to represent the energy profile for anion permeation facilitated by the bis-catechol. For instance, Figure 4.14 illustrates the anion permeation in the Cl⁻-selective ion channel CFTR.

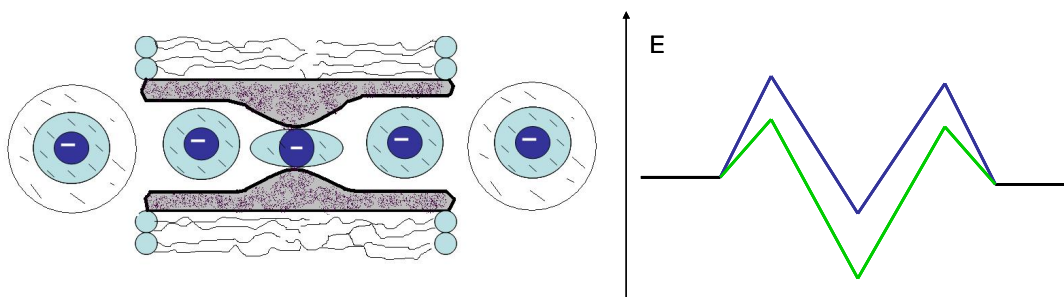


Figure 4.14. Energetics of permeation through CFTR ion channel Cl⁻ vs SCN⁻, adapted from the reference 30.

This energy profile was derived based on the anion selectivity studies in planar lipid bilayer membrane.^{30,113,114} Some of the key findings are shown in Table 4.2. The permeation through CFTR is described in terms of the two barrier one binding site model. In brief, the permeating anions lose only a bit of water as they enter the pore and hence remain largely hydrated. Thus, the anion permeabilities change in the expected order $I^- > Br^- > Cl^-$ but the absolute values are very similar: $P_{Br^-}/P_{Cl^-} = 1.2$, $P_{I^-}/P_{Cl^-} = 2.0$. In turn, the anion conductances are also very similar $g_{Br^-}/g_{Cl^-} = 1.2$, $g_{I^-}/g_{Cl^-} = 2.0$ but the selectivity is reversed: $Cl^- > Br^- > I^-$. It is thought that weakly hydrated anions are easier to permeate but also are more likely to tightly bind to the channel. The affinity towards the “binding site” follows the sequence: $I^- > Br^- > Cl^-$. The Cl⁻ anion (probably, yet strongly hydrated) is “excluded” from the interaction

with the pore interior. This selectivity mechanism is thought to determine the function of CFTR as a Cl⁻ filter.

Table 4.2. Energetics of the anion transport in the presence of the compound III-25 in comparison with the transport “through” and “into” a pore of CFTR Cl⁻ channel.

Anion	III-25		CFTR				$\Delta G_{Hydr}/$
	k_{Anion}/k_{Cl^-}	$\Delta\Delta G^{\ddagger\ddagger}$, kJ*M ⁻¹	P_{Anion}/P_{Cl^-} [£]	g_{Anion}/g_{Cl^-} [£]	$\Delta\Delta G^{\ddagger}(P)$ §, kJ*M ⁻¹	$\Delta\Delta G^{\ddagger}(g)$ §, kJ*M ⁻¹	$\Delta\Delta G_{Hydr}$, kJ*mol ⁻¹
SO ₄ ²⁻	0.5	-1.7					
Cl ⁻	1	0	1	1	0	0	-358 / 0
Br ⁻	3.4	3.0	1.2	0.64	0.45	-1.1	-332 / 26
NO ₃ ⁻	8.8	5.4	1.4	0.75	0.83	-0.71	-327 / 31
I ⁻	28	8.3	2.0	0.18	1.71	-4.2	-297 / 61
			(0.4)		(-2.3)		
ClO ₄ ⁻	54	9.9	(0.3)	0.2	(-3.0)	-4.0	-271 / 87

§ - calculated according to the formulas

$$\Delta\Delta G^{\ddagger} = 8.31*298*\ln k_{Anion}/k_{Cl^-}/1000 \quad (4.10),$$

$$\Delta\Delta G^{\ddagger} = 8.31*298*\ln P_{Anion}/P_{Cl^-}/1000 \text{ or}$$

$$\Delta\Delta G^{\ddagger} = 8.31*298*\ln g_{Anion}/g_{Cl^-}/1000.$$

£ - permeability selectivity ratio P_{Anion}/P_{Cl^-} and relative conductance g_{Anion}/g_{Cl^-} in CFTR Cl⁻ channel are taken from the review 30.

□ - calculated according to the formula $\Delta\Delta G_{Hydr} = \Delta G_{Hydr}(Anion) - \Delta G_{Hydr}(Cl^-)$ using values ΔG_{Hydr} taken from the reference ¹¹⁵.

In turn, the profile for anion permeation mediated by the receptor III-25 should illustrate the following experimental results obtained from the N₃⁻-based

assay: anions that are easier to dehydrate are made more permeable by this transporter. According to the estimates shown in Table 4.2, the observed changes in the anion transport rates (k_{Anion}/k_{Cl^-}) follow the trend in the Hofmeister sequence but do not nearly reflect the absolute value of changes in hydration energy ($\Delta\Delta G_{Hydr}$).

An increase in the hydration energy for inorganic anions ($\Delta\Delta G_{Hydr}$), if equivalent to the change in activation energy for the anion transport ($\Delta\Delta G^\ddagger$) in the N_3^- -based assay, should result in a more dramatic drop in the relative transport rates (k_{Anion}/k_{Cl^-}) by compound III-25 and *vice versa*.

For instance, according to the data in Table 4.2, the difference in hydration energy for Cl^- and Br^- anion equals $\Delta\Delta G_{Hydr} = 26 \text{ kJ}\cdot\text{mol}^{-1}$. This difference should correspond to the rate increase $k_{Anion}/k_{Cl^-} = 3.7\cdot 10^4$, calculated using formula (4.10). The experimentally observed rate increase using bis-catechol III-25, however, is much lower, being only $k_{Anion}/k_{Cl^-} = 3.4$, and this value corresponds to $\Delta\Delta G^\ddagger = 3.0 \text{ kJ}\cdot\text{M}^{-1}$ which is much less than the change in the hydration energy, $\Delta\Delta G_{Hydr}$ for Cl^- and Br^- anions.

For simplicity we can think that the energy profile for anion permeation contains only one barrier. At a glance, the hypothesis that permeation facilitated by the transporter III-25 does not require complete dehydration of the anions would be in agreement with the data discussed above (values of $\Delta\Delta G^\ddagger < \Delta\Delta G_{Hydr}$). Therefore, we can propose that dehydration of inorganic ions determines the activation energy of transport, but the anions have to be only partially dehydrated to pass through the “transient pore”, which is schematically represented in Figure 4.12. In addition, to explain the experimental results, we also have to say that the “apparent change in

hydration energy” should be “proportional” to the absolute value of the hydration energy for a given anion: the change in hydration energy would be greater for the stronger hydrated anion. This principle is schematically illustrated in Figure 4.15. Assume that “apparent hydration energy”, which is equal to our activation energy, ΔG^\ddagger , for each anion is lower than actual hydration energy, ΔG_{Hydr} , for the same number of kJ mol^{-1} . Given this assumption, the values of $\Delta\Delta G^\ddagger$ would be the same as $\Delta\Delta G_{Hydr}$ regardless if we “dehydrated” given pair of anions fully or partially.

As illustrated in Figure 4.15, the same principle is behind the selectivity of anion permeation into the CFTR Cl^- channel as follows from the data in Table 4.2. How was this discrimination between inorganic anions achieved by the natural transporter? According to the description above, within the mouth of the CFTR pore only the outer hydration sphere for the small anions is replaced upon interaction with the channel (the anion’s inner sphere waters remain intact). Therefore, the relative permeation of the anion of interest (Cl^-) into the pore increases. Consider permeation of an anion into a rigid cylinder of fixed diameter. To get into this pore the weakly hydrated iodide does not have to undergo dehydration. Bromide ion has a smaller ionic radius than iodide, thus its hydration sphere will be better organized and tighter than for iodide. The radius of the hydrated Br^- ion is, however, larger than that for the iodide. Therefore, the Br^- anion should undergo dehydration to get into the same pore as I^- . The Cl^- anion has a larger radius for its hydrated ion than does Br^- and, therefore, Cl^- will undergo more substantial dehydration than will Br^- .

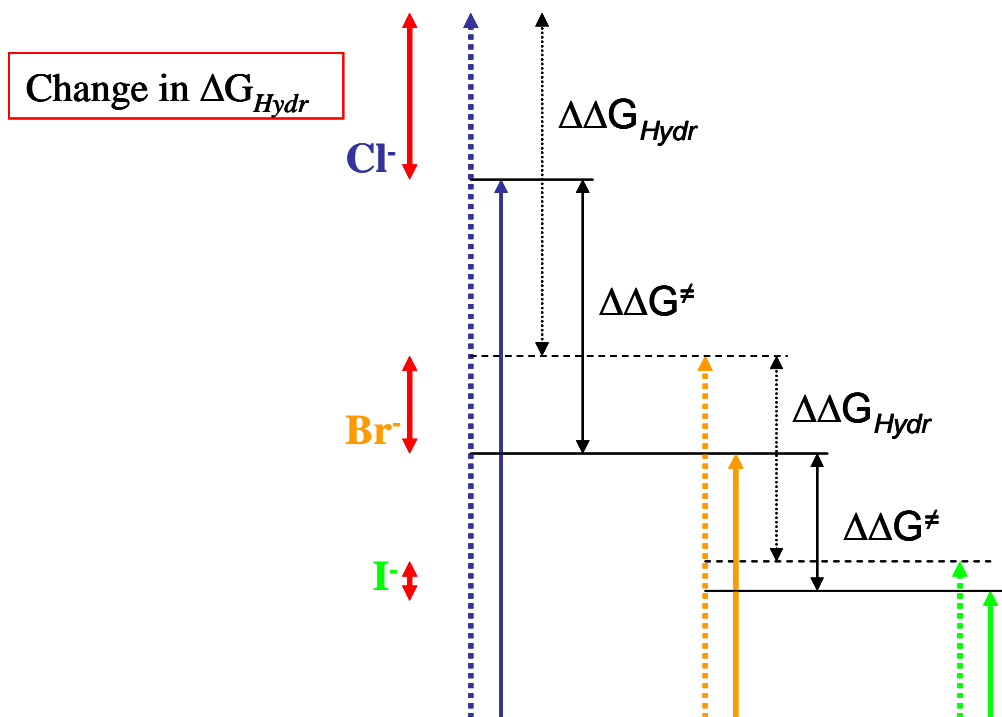


Figure 4.15. Schematic representation of the relations between thermodynamic parameters. Dashed colored arrows represent the hydration energy, ΔG_{Hydr} , for the anions **Cl⁻**, **Br⁻**, **I⁻**. Dashed black arrows indicate the change in the hydration energy, $\Delta\Delta G_{Hydr}$, for a given pair of anions. Solid colored arrows represent “apparent hydration energies”, which are equal to the activation energy of the transport process, ΔG^\ddagger . Solid black arrows represent the change in activation energy for a given pair of anions, $\Delta\Delta G^\ddagger$. Solid red arrows represent “apparent change in hydration energy” - the difference between the hydration energy, ΔG_{Hydr} , and activation energy of transport (“apparent hydration energy”), ΔG^\ddagger , for a given anion.

Unassisted permeation of halides across the phospholipid bilayer also follows the same selectivity principle (Table 1.1). In this case, we might think of a transient pore mechanism. The cost for permeation of the completely dehydrated anion is too high. Partial dehydration provides a more energetically favorable route. It requires less energy to create a larger cavity in the phospholipid bilayer than to remove an excess of the hydration sphere. Thus, permeation through the transient pore of the “fixed diameter” would follow the same rules as permeation through the stable pore, discussed above using CFTR as an example. In turn, more energy is required to create a larger cavity. Thus, even if we consider the transient pore with a “flexible diameter”, the same principle takes place: the larger the diameter of the hydrated ion, the less permeable it becomes.

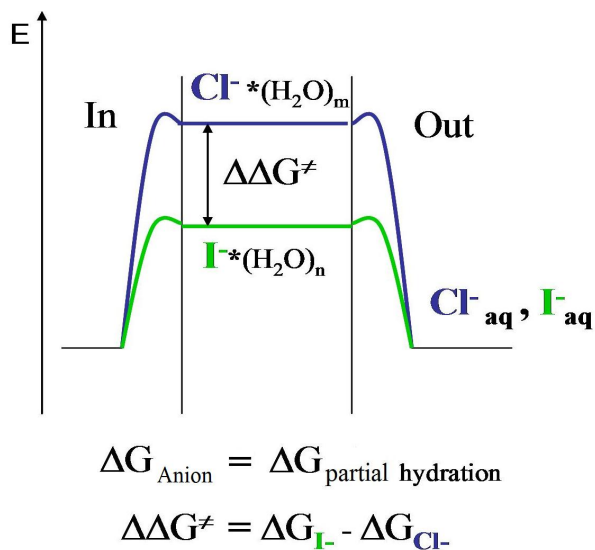


Figure 4.16. Energetics of the amphiphile-assisted anion transport Cl^- vs I^- .

It is likely that the same rules are in place in the case of assisted permeation by bis-catechol III-25. The mechanism can be discussed as the passage of the partially hydrated anion through a transient pore formed by the bis-catechol aggregates, and the energy profile can be schematically represented as shown in Figure 4.16. It is important to note that the present description of the mechanism does not exclude the possibility that alternative mechanistic models/descriptions of permeation process can be applied to this system.

4.4. Conclusion.

In conclusion, we have shown that bis-catechol based anion receptor **III-25** functions as membrane transporter. Although the closest structural analogs of **25**, 2,3-dimethoxy (**III-15**) and 3,4-dihydroxy (**III-27**) compounds, have similar binding affinity toward Cl⁻ in DMSO, they were inactive in the anion transport assays. The structure-activity relationships that would explain this difference remain hypothetical and require further investigation. The latter could include synthetic efforts, study of self-aggregation properties of bis-catechols in aqueous and organic media, and development of new liposomal assays.

In addition, the anion transport activity of **III-25** is a function of hydrophobicity. The amphiphilic structure of the analogs **III-23** – **III-26** with alkyl chain of different length encodes the ability to form a water-soluble phase. Compared to the compounds with branched and unsaturated alkyl chains or facial amphiphiles, the analogs with the linear alkyl groups are known to exhibit a stronger tendency to form micelles or “micelle-like aggregates” in aqueous media.⁶⁹ Thus, we suspected bis-catechol **III-25** to aggregate in aqueous media and therefore, we did not determine the exact number of the molecules within the membrane-conducting aggregates using common technique.^{55a,55b}

We propose that H-bonding drives self-association of the amphiphile in the bilayer. These aggregates of molecules function as transient pathways and increase membrane permeability toward anions. The ionic permeability in the presence of **III-25** follows the Hofmeister sequence: anions that are easier to dehydrate are made

more permeable by this transporter. The dependence of the rate on dehydration energy indicates that to pass through the membrane the anions must be partially dehydrated. The analysis of pKa values suggests that at neutral pH in aqueous solution the bis-catechol would exist as zwitterions (SI3.1). It is reasonable that in a non-polar environment of the bilayer this zwitterion becomes cationic and binds anion. We also imply that similarly to other catechols,^{61,62} receptor III-25 transports H⁺ across bilayer and that H⁺ permeation is extremely rapid on the time scale of the anion transport experiments.

The selectivity of bis-catechol 25 in the ion transport assays was determined by employing a newly devised method.^{41d} Although the transport experiments look logical and self-consistent, connections made between experimentally measured parameters and intravesicular concentration are rather empirical and lack a comprehensive description. For instance, why should the relationship between the experimentally determined parameter, “Ratio”, and the concentration of the transported Anion liposomes, [Anion]_{in} be linear? We also neglect the influence of the electrical potential and osmosis phenomena on the transport rates.

Further study of the mechanism and selectivity of the receptor-mediated ion transport requires knowledge of permeability coefficients, P , cm s⁻¹. To validate the permeability, P , obtained from N₃⁻ - based assay, a comparison with the literature data would be helpful. Remarkably, the $P(NO_3^-)$ in the “blank experiment” (addition of MeOH) was only three times lower than that of reported values for permeation across pure phospholipid bilayer (see Table 4.1). At the same time, permeabilities for the halides and H⁺ across PC bilayer vary in the literature by several orders of

magnitude.^{6,8a} Therefore, presently, there is no agreement in the literature regarding ion permeability coefficients and the “right” ways to compute them. It appears that due to complexity of the ion transport one can only wish to obtain the very best experimental estimate rather than “the only true value”. Another way to test the method would be to study active transporters whose selectivity and efficiency in the biomembranes have been established by independent techniques. The naturally-occurring ionophore, valinomycin, whose activity and selectivity has been intensively investigated in liposomes, using radioactive isotopes of alkali metals, and electrochemically in planar lipid bilayer could potentially serve this purpose.^{4b,116}

4.5. Why are these Results Important? Future Directions.

The finding that simple bis-catechol such as III-25 are anion-selective membrane transporters suggests that a variety of the known compounds might also initiate selective ion transport upon interaction with biomembranes. The observation that small structural changes alter the activity indicates that this function can be controlled on the molecular level. The newly devised liposomal assay described in this thesis could serve in the search for new ion-selective membrane transporters and new ways to regulate/study the ion selectivity/mechanism in phospholipid bilayer.

On the other hand, ion transport across biological membranes has strong connections with the problems of ion sensing and separation. Selective binding and transport of inorganic anions across bio- and synthetic membranes by means of the “supramolecular host” is a present-day challenge in organic chemistry. For instance, to the date there is no functional carrier-based NO_3^- or ClO_4^- -selective sensor.⁴⁶

Synthetic transporters also help us to better understand how natural systems move ions across the hydrophobic barrier presented by the biomembranes. First, consider synthetic hydrophobic compound or an assembly of molecules inserted into phospholipid bilayer that increase its permeability toward ionic species. Permeability of some ions changes while permeability of other anions does not. Structural modifications on the molecular level alter activity and selectivity. This is a model of a primitive transmembrane transport system. Something initially rather simple upon interaction with phospholipid bilayer, the cell and its environment has evolved into ion channels and transporters the way they function in Nature. Second, the anion-

selective membrane transporters could be used in biomedical/biochemical studies of membrane transport in the living cell and cellular organelles.¹¹⁷

Lastly, the newly devised approach to study ion selectivity can be applied to investigate the function of the natural ion transporters such as ClC Cl⁻ channels and valinomycin as an alternative to the existing liposome-based technique that employs radioactive isotopes.^{7,116}

Listed below are possible systems of interest and questions that might be addressed:

1. Structural modification of the bis-catechol amphiphile III-25.

a. Dependence of the anion transport activity on the structure of alkyl chain.

Identification of the most active 2,3-alkyl analog.

b. Is the catechol unit necessary?

c. Would a simple replacement of the amine group with “carbon” make bis-catechol cation-selective transporters at neutral pH?

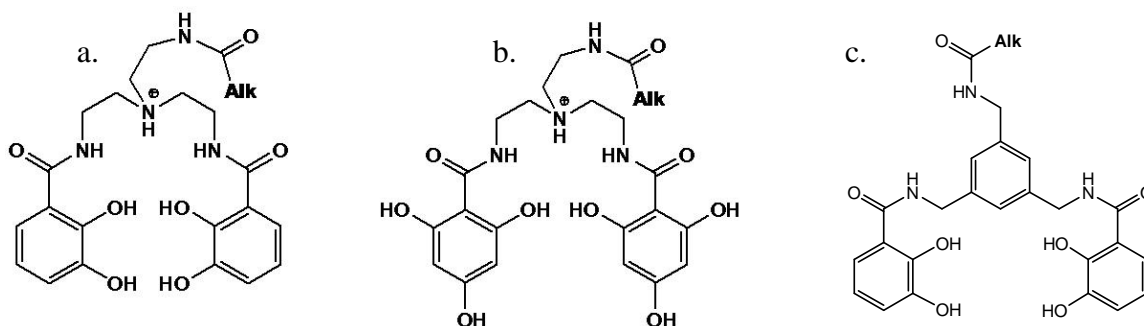


Figure 4.17. Synthetic targets: a, b, c.

2. In 2005 A. P. Davis reported a remarkable observation of contra-Hofmeister anion extraction by cyclosteroidal receptors (III-35).¹¹⁸ Using this example, we propose to obtain receptor III-36. We suggest to study the anion binding and selectivity of this compound and compare them to the original bis-catechol (III-25) using classical ¹H NMR titration and liquid-liquid extraction techniques. We also suggest a comparative evaluation of these two compounds (III-36 and III-25) in the newly devised anion transport assay. We do not necessarily expect to overcome the Hofmeister bias but to detect some attenuation in the relative rates k_{Anion}/k_{Cl^-} due to different anion affinity/selectivity and/or mechanism of the anion transport.

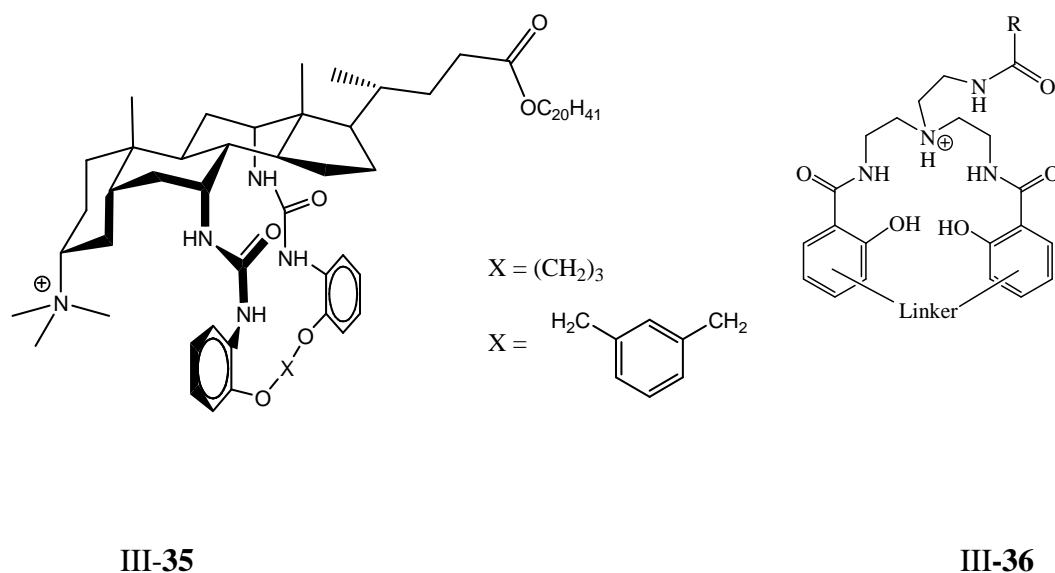


Figure 4.18. Cyclosteroidal receptors III-35 investigated by A. P. Davis. Compound III-36 as cyclic analog of the bis-catechol III-25.

3. Although according to our findings the bis-catechol ligand appeared to be optimum for the chloride anion, it is definitely not an optimum for the ferric ion which coordination number is six. Number of TREN-based scaffolds of interest, hydrophobic and easy to obtain,⁷⁶ are shown below. Hypothetically, some of these iron chelators might transfer Fe^{3+} across phospholipid bilayer. These synthetic siderophores are not expected, however, to easily release the ferric ion into the aqueous media due to the very strong binding. In contrast, the same compounds should bind anions such as Cl^- reversibly in the aqueous solution. It can be also expected from some of these synthetic siderophores to transport Cl^- anion across phospholipid bilayer. From the certain perspective these compounds are facial amphiphiles and remind Regens' "molecular umbrellas".¹¹⁹ Therefore, we might expect the mechanism of ion transport for III-37 and III-38 to be somewhat similar to the mechanism described for the molecular umbrella compounds and different from the one described for our amphiphilic bis-catechol III-25.^{55c,119}

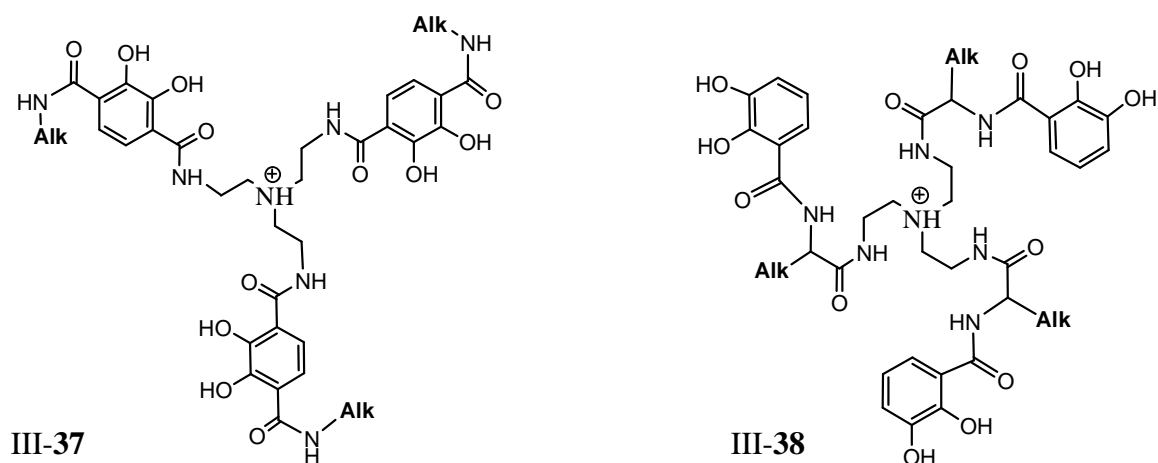


Figure 4.19. Hydrophobic siderophores.

From the some perspective the “antimicrobial agents without resistance” studied by R. Engel (Queens College, CUNY) can be described as supramolecules. They are also structurally similar to our bis-catechol anion transporter III-25. Therefore, it might be interesting to evaluate the anion binding and transport properties of these compounds using classical ^1H NMR titration technique and newly devised liposomal assay.

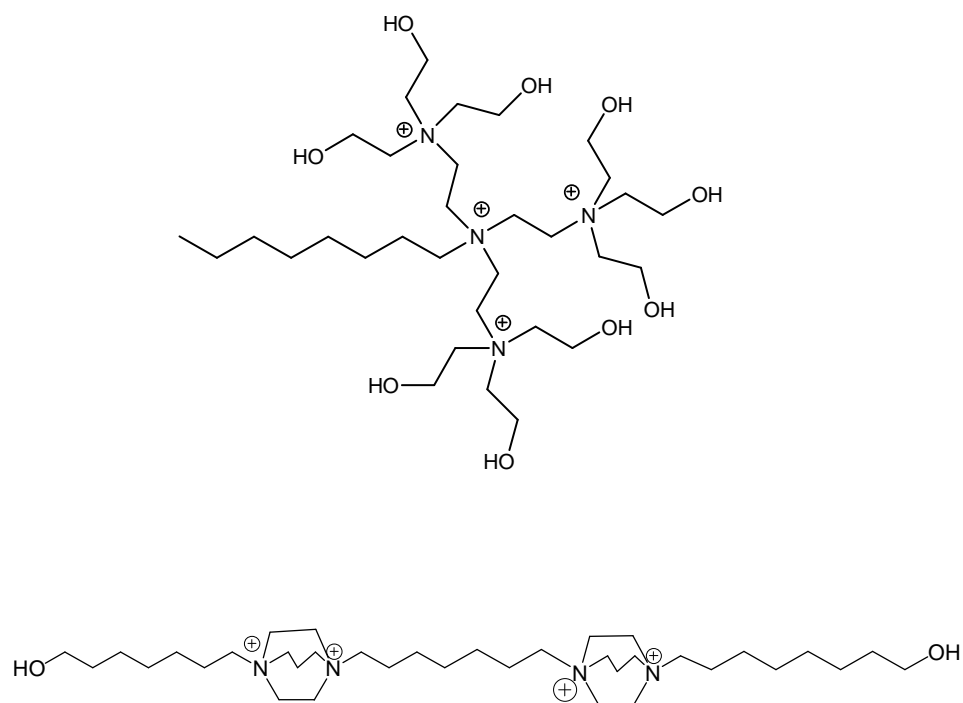


Figure 4.20. Biologically active quaternary ammonium compounds.

4.6. Supporting Information for Chapter 4.

4.6.1. **Dependence of the HPTS response on pH.** The original 0.1 mM HPTS solution used to prepare NO_3^- -filled liposomes was diluted to achieve the same fluorescence intensity as observed in the ion transport assay and was estimated to be only 0.00025 mM in HPTS. Fluorescence of HPTS dye in this solution containing 100 mM NaNO_3 and 10 mM sodium phosphate buffer was measured as function on pH. Dependence of the Ratio and log Ratio on pH is shown in Fig. S8. Ratio refers to the ratio of HPTS fluorescence emissions at 510 nm (I_0/I_1), where I_0 is excitation at 460 nm (basic form of HPTS) and I_1 is excitation at 403 nm (acidic form of HPTS).

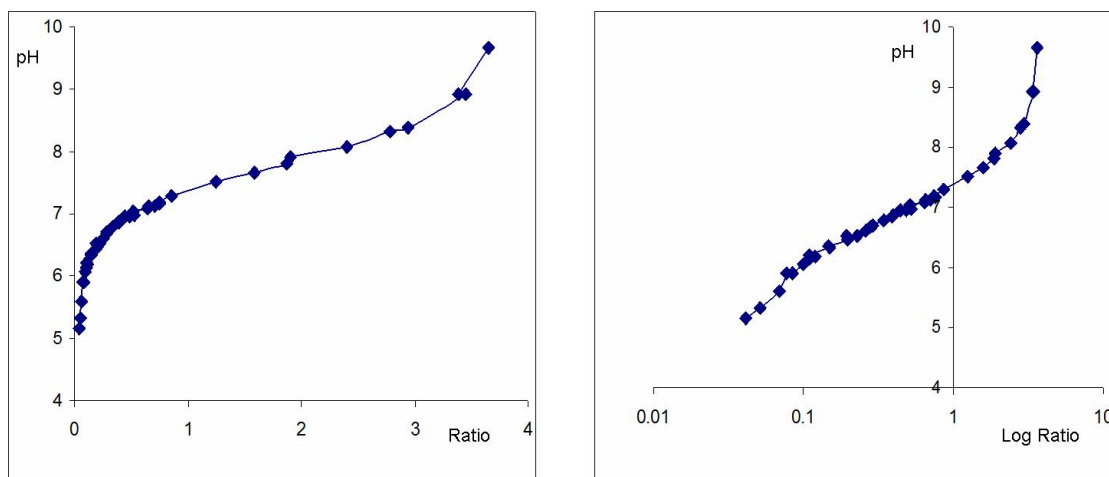


Figure S4.1. Dependence of the Ratio and log Ratio on pH. Ratio refers to the ratio of HPTS fluorescence emissions at 510 nm (I_0/I_1), where I_0 is excitation at 460 nm (basic form of HPTS) and I_1 is excitation at 403 nm (acidic form of HPTS).

Origin 7.0 program curve fitting method was applied to create the best fit of experimental data set and to obtain the polynomial equation that describes the calibration curve:

$$\text{pH} = 5.26985 + 10.46661x - 28.99327x^2 + 47.56252x^3 - 46.85351x^4 + 28.61186x^5 - 10.89064x^6 + 2.51018x^7 - 0.3202x^8 + 0.01734x^9 \quad (\text{S4.1})$$

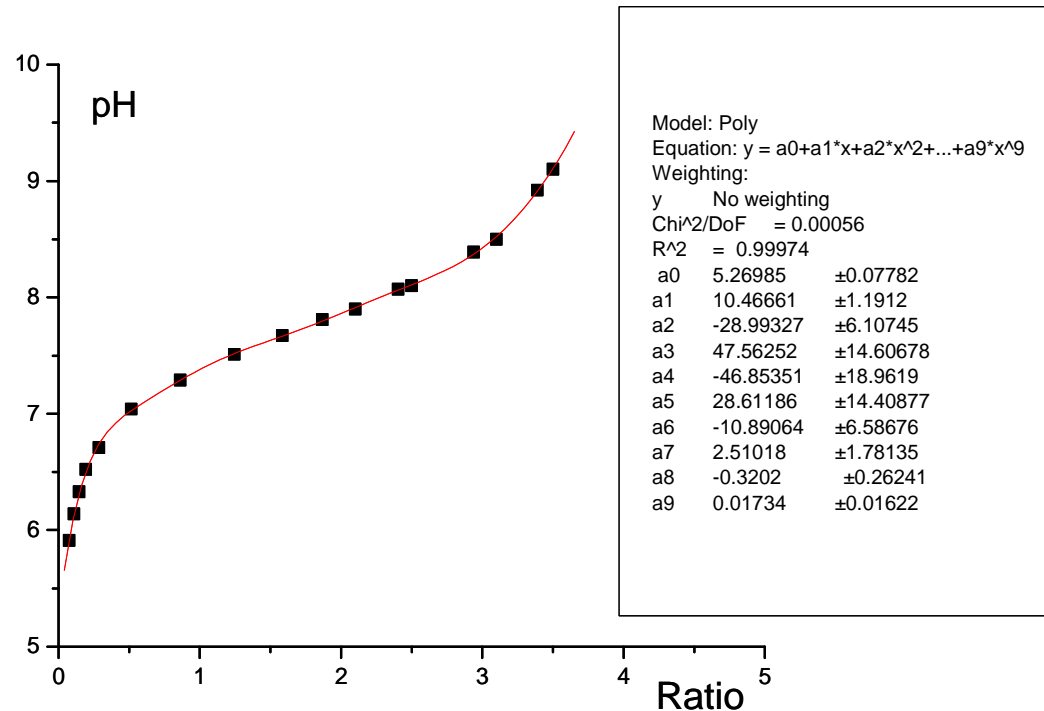


Figure S4.2. pH as function of the emission intensities ratio x . Calibration data set (black squares) and best curve fit (red line) generated using Origin 7.0 program.

4.6.2. Extraction of the anion transport parameters from the experimental data.

Rate constants, k, s^{-1}

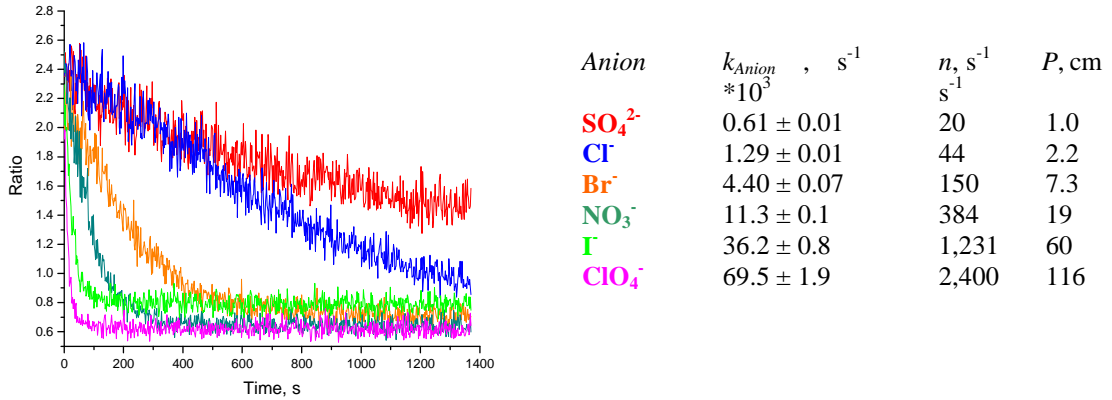
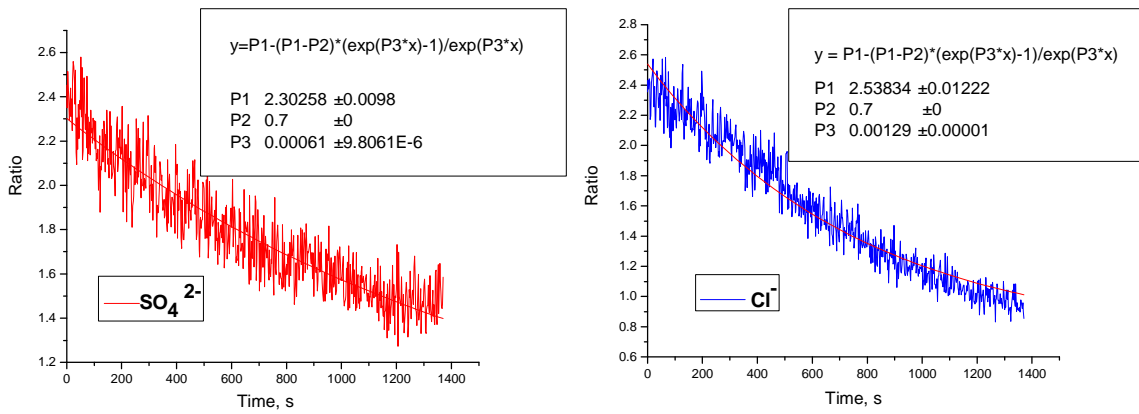


Figure S4.3. Raw data of the Ratio on time dependence and obtained ion transport rates k_{Anion}, s^{-1} , turnover numbers and permeability coefficients.



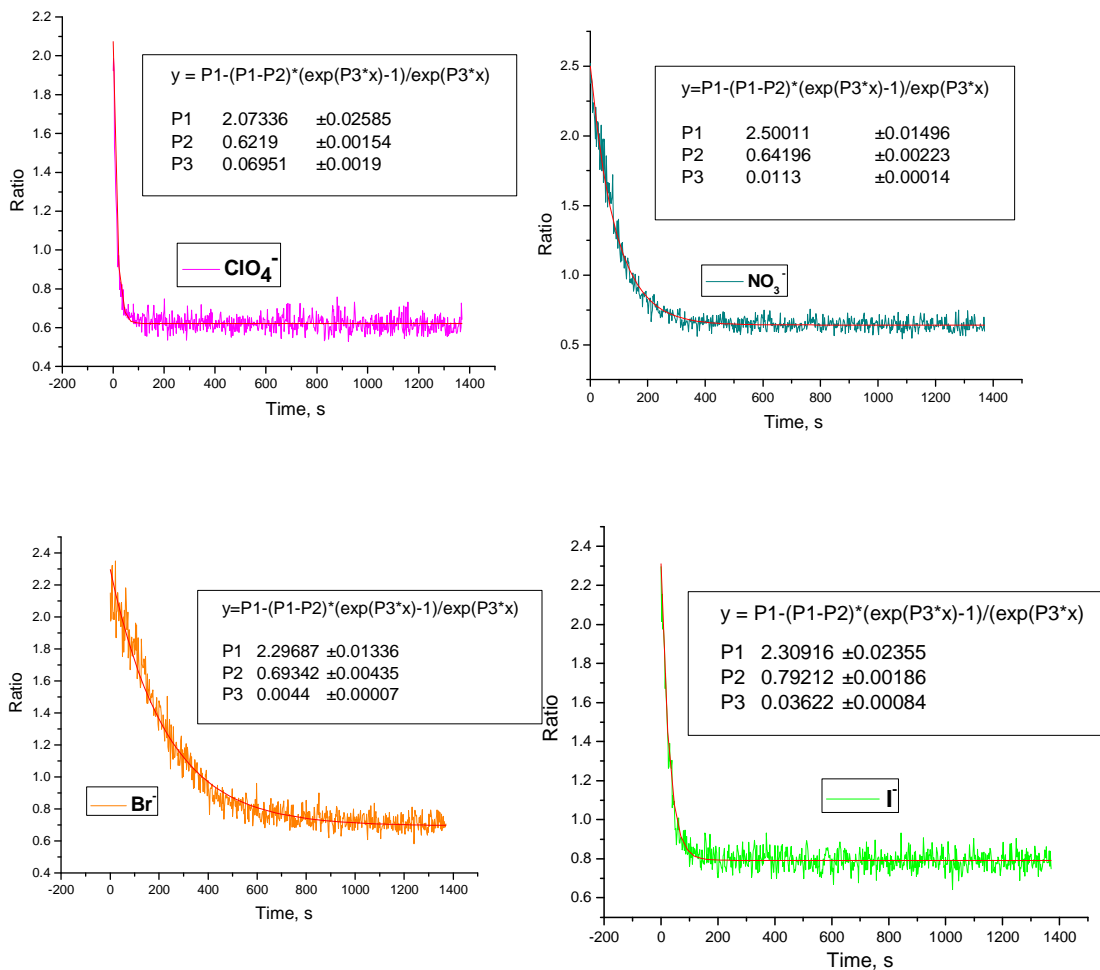


Figure S4.4. Curve fitting of the experimental data sets with the equation:

$$y = P1 - (P2 - P1) * (exp(P3 * x) - 1) / exp(P3 * x) \quad (S4.2)$$

where $x = t$ - independent variable, $y = \text{Ratio}$ - dependent variable, $P1 = \text{Ratio}_0$, $P3 = \text{Ratio}_\infty$, $P3 = k_{Anion}$ - parameters to obtain. Red line is the best fit obtained using Origin 7.0 program.

Turnover numbers, n , s^{-1}

Turnover number is defined as the number of ions transported across the membrane per liposome. Values for n were obtained using the definition of the initial rate, ion transport rates k_{Anion} , s^{-1} and the estimated volume of the liposome:

$$n = d[Anion]_{In} / dt * V_{liposome} * N_a = \text{mol L}^{-1} \text{ s}^{-1} * \text{L} * \text{mol}^{-1}$$

Initial rate = anion influx

$$d[Anion]_{In} / dt = k_{Anion} [Anion]_{Out} = k_{Anion} * 0.1 = x * 10^{-4} \text{ M s}^{-1},$$

$$\text{where } x = k_{Anion} * 10^3$$

The diameter of the EYPC liposomes used in ion transport experiments was estimated as $d = 0.1 \mu\text{m} = 10^{-7} \text{ m}$ (as diameter of the pore in the filter used for extrusion of the liposomes). Thickness of the bilayer was estimated to be $3.0 \text{ nm} = 3 * 10^{-9} \text{ m}$.

$$V_{liposome} = 4/3 \pi r_{liposome}^3 = 4/3 * 3.14 * (0.5 * 10^{-7} - 3 * 10^{-9})^3 = 5.7 * 10^{-22} \text{ m}^3 = \\ = 5.7 * 10^{-19} \text{ L}$$

$$n = x * 10^{-4} * (5.7 * 10^{-19}) * (6.02 * 10^{23}) = x * 34, \text{ s}^{-1} \text{ again where } x = k_{Anion} * 10^3$$

Permeability coefficients, P , cm s^{-1}

Rate k_{Anion} , s^{-1} and P_{Anion} , $\text{cm} * \text{s}^{-1}$ are related as following:

$P = k * V/A$, where V – volume of the liposome, A – surface area of the liposome.

$$P = k_{Anion} * r_{liposome} / 3 = k_{Anion} * 0.5 * 10^{-5} / 3, \text{ cm s}^{-1}$$

4.6.3. Concentration dependence study.

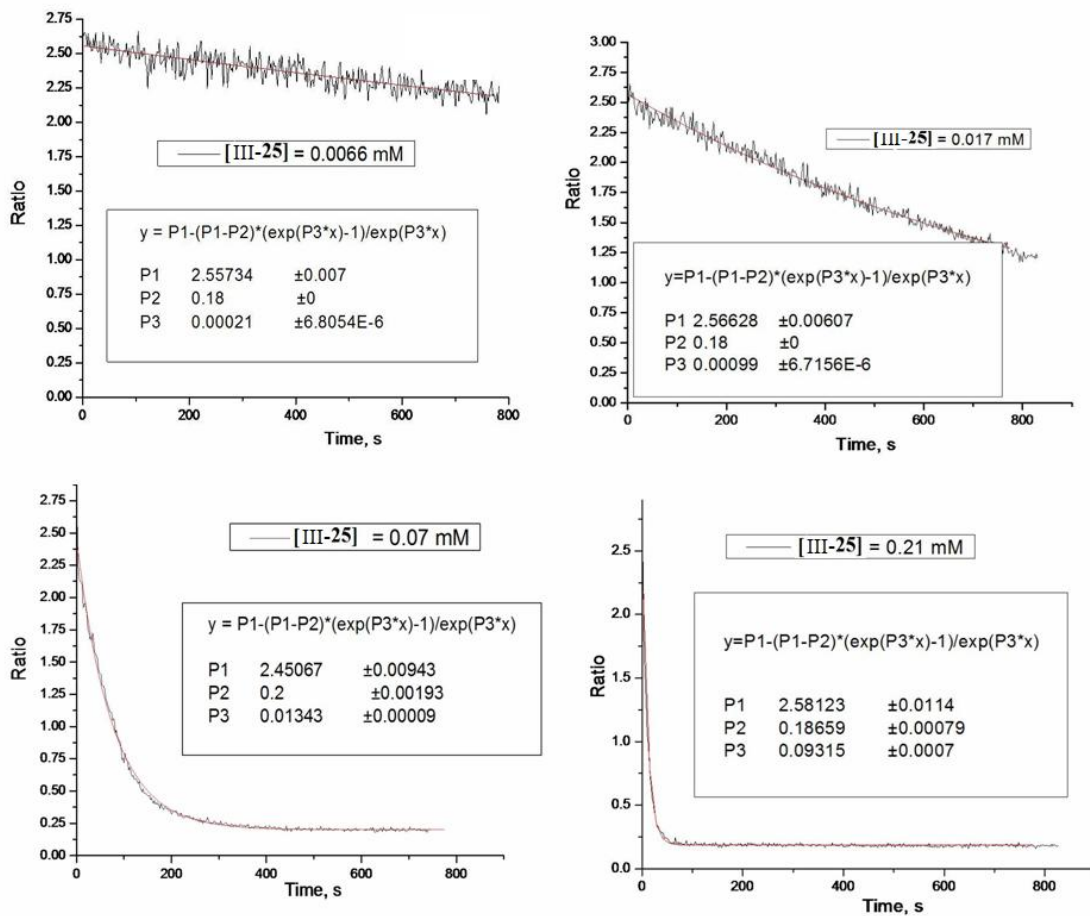


Figure S4.5. Examples of the curve fitting of the experimental data sets using equation (S4.2) where x - independent variable, y - dependent variable, P1, P2, P3 - parameters to obtain. Red line is the best fit obtained using Origin 7.0 program.

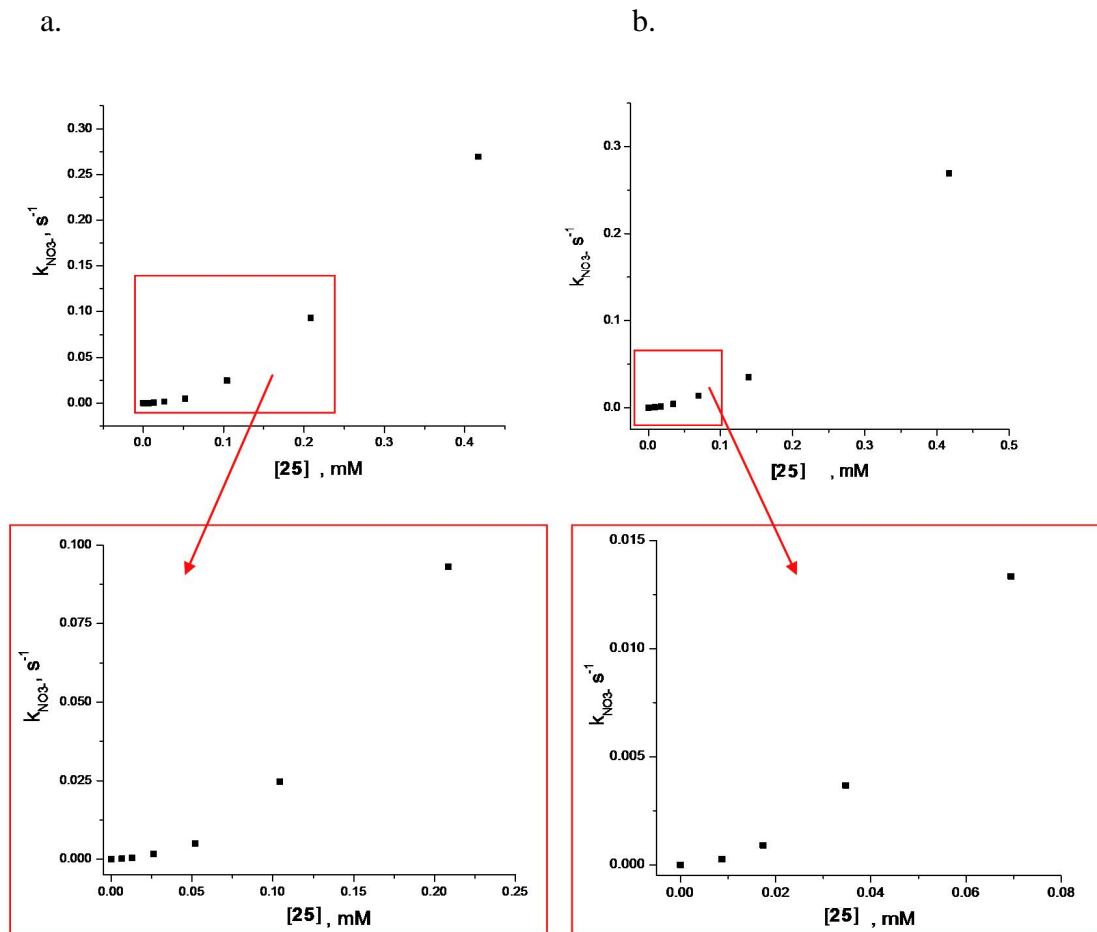


Figure S4.6. Dependence of the NO_3^- anion transport rate $k_{\text{NO}_3^-} = P3 - k_0$, s^{-1} on concentration of the bis-catechol III-25. Two independent experiments **a** and **b**. ($k_0 = 0.00009 \text{ s}^{-1}$ - blank leakage at $[\text{III-25}] = 0 \text{ mM}$).

5. Experimental Section.

5.1. Experimental Section for Chapter 2.

5.1.1. **¹H NMR.** The ¹H NMR spectra were recorded at room temperature on a Bruker DRX400 spectrometer at 400 MHz. Chemical shifts are reported in ppm relative to the TMS signal as an internal standard.

5.1.2. *Ab initio* calculations.

Table E1.1. Geometric parameters for urea and 1:1 Cl⁻ : urea complex.

Compound/ Symmetry	Theory	N-C-N	C-N-H ^{&}	H...H ^{&}	H-N...N-H	H...Cl ⁻	N-H...Cl ⁻
urea (<i>anti</i>)	MP2/TZ [@]	113.6	117.2	2.405	52.5		
	DFT [@]	114.0	117.0	2.455	55.2		
	<i>ab initio</i> [§]	114.0	117.7	2.414	52.5		
1:1 complex	MP2/TZ [@]	112.4	113.0	2.078	0.0	2.251	158.2
	DFT [@]	113.7	115.5	2.143	0.0	2.288	156.8
	<i>ab initio</i> [§]	114.2	117.6	2.189	0.0	2.461	155.7

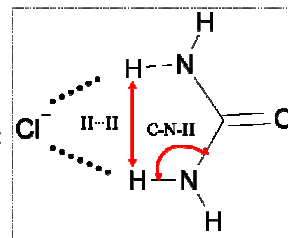
[@]Literature data from the reference 90.

MP2/TZ = MP2/aug-cc-pVTZ, DFT = B3LYP/DZVP2

[§]Present study *ab initio* (6-31G*)

[&]Angle C-N-H and distance H...H are indicated in the following diagram:

Distances are given in angstroms. Angles are given in degrees.



The electronic structure calculations were carried out using the software program, HyperChem 7.0. Geometries were optimized using *ab initio* method and the 6-31G* basis set. To validate the performance of the method, the geometric parameters for optimized urea molecule and 1:1 Cl⁻ : urea complex were compared with the prior theoretical studies. The data in the Table E2.1. indicate acceptable agreement between parameters obtained in the present study using *ab initio* (6-31G*) and the literature.

5.1.3. **ESI-MS.** Conditions of ESI-MS experiments were adjusted as following to observe ion clusters. Mass spectra of the clusters formed from (Bu)₄N⁺Cl⁻ and receptors **1-6** in CHCl₃ were recorded using a JEOL AccuTOF ESI-MS. The CHCl₃ solution was injected into a 5-stage vacuum system through a capillary tube using a syringe pump with flow rate of 60-120 μL/h. The pressure in the chambers was 760 Pa, 200 Pa, 0.2 Pa, 5*10⁻³ Pa, and 7*10⁻⁵ Pa. In the sprayer, the sample solution was combined with a nebulizing gas N₂ to form a spray of liquid droplets. The flow rate of N₂ was kept below 1 L/min. Both the sample and the nebulizing gas were at rt. An electric voltage of ± 2500 V was applied to the tip of the sprayer. Clusters were led from chamber to chamber through a pressure difference and electric field gradient. The signal intensities of the observed clusters depended on the applied voltages on orifices 1 and 2. Lower voltages on the orifices resulted in a less fragmentation. Voltages on the orifices were set to 0 V to support the gentlest conditions possible, while the ring lens voltage was varied over 0-10 V to improve sensitivity. Increasing the temperature, flow rates of either N₂ or the sample, or orifice voltages resulted in fragmentation and decreasing intensity of the signals for the “ion clusters”. In turn,

the intensity of signals for Cl^-CHCl_3 and $\text{Cl}^-(\text{CHCl}_3)_2$ increased and, eventually, became the only signals observed in negative MS.

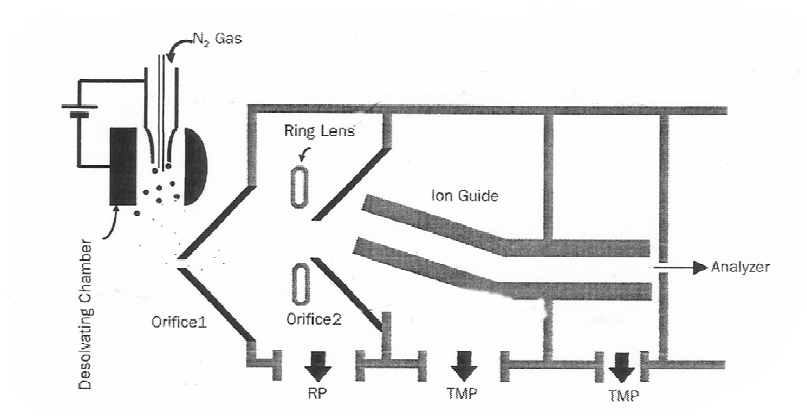


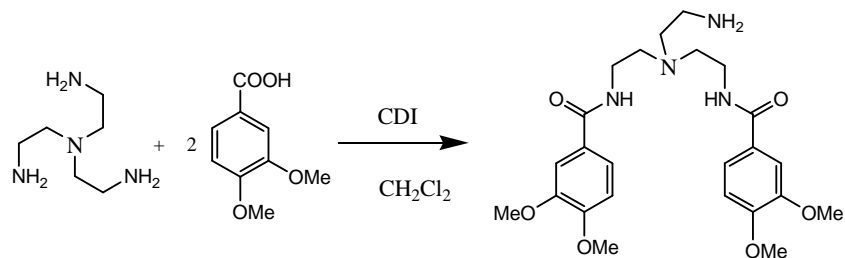
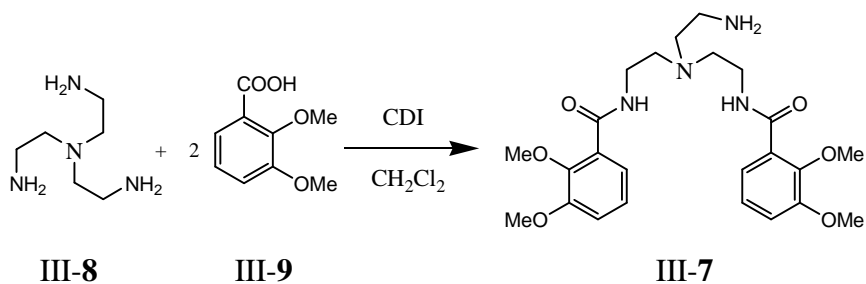
Figure E1.1. Principle of the ion source (*picture is reprinted from the instrument manual*).

5.2. Experimental Section for Chapter 3.

5.2.1. **General experimental.** NMR spectra were obtained using a Bruker DRX-400 spectrometer. ^1H NMR spectra were recorded at 400.13 MHz and ^{13}C NMR spectra were recorded at 100.61 MHz. ESI-MS experiments were done with a JEOL AccuTOF spectrometer. Chromatography was performed using 60-200 mesh silica gel from Baker. Thin layer chromatography was performed on Kieselgel 60 F254 silica-coated glass plates. Deuterated solvents were purchased from Cambridge Isotope Labs. Other chemicals and solvents were purchased from Aldrich, Fisher or Fluka.

5.2.2. Synthesis of bis-catechol amphiphiles.

Step I



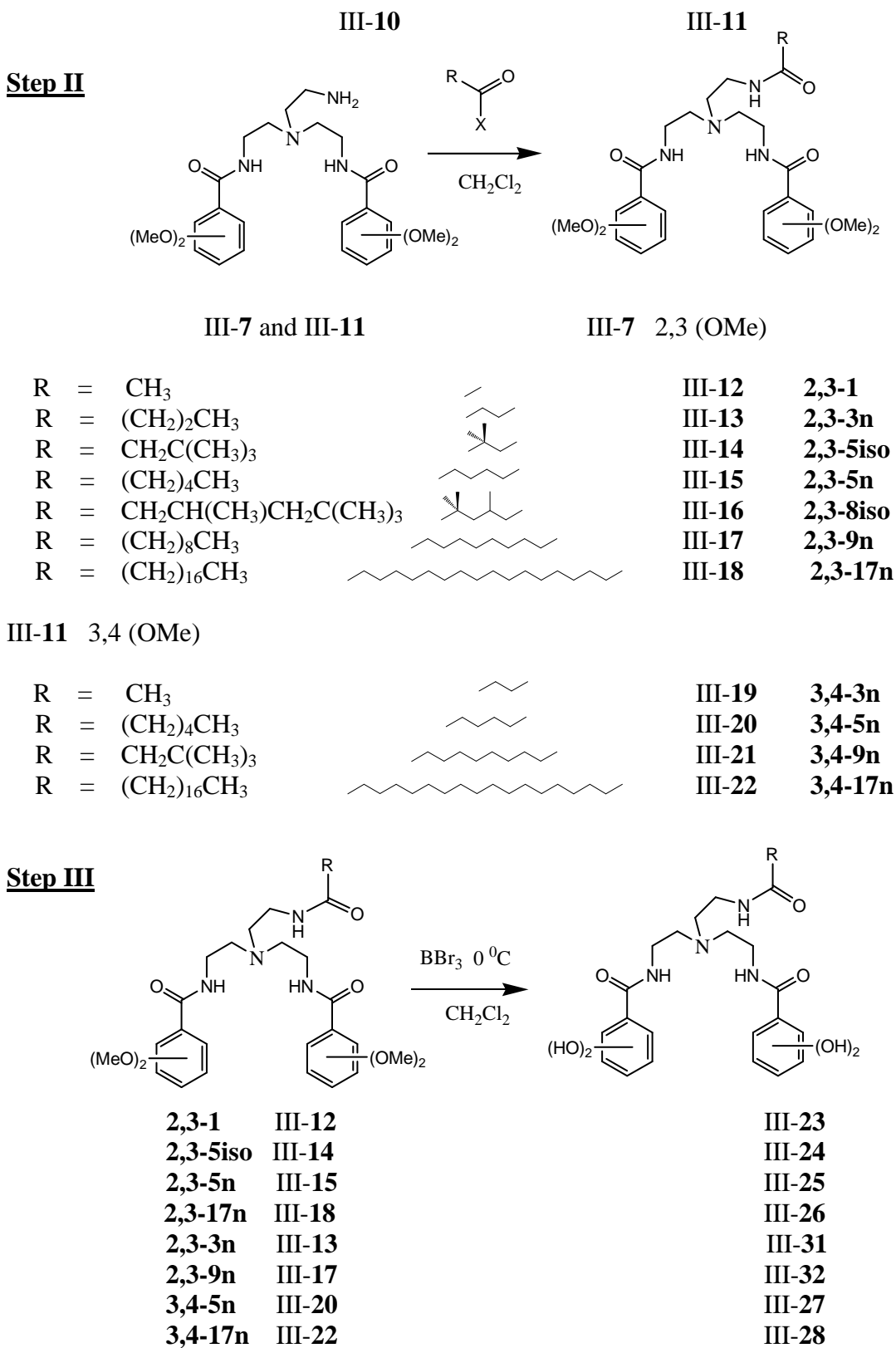


Figure E1.2. Syntheses of bis-catechols and methylated analogs.

Step I. Compound III-9. Compound 7, a known compound, was synthesized following a literature procedure.¹ A solution of 2,3-dimethoxybenzoic acid III-9 (10.0 g, 55 mmol) and carbonyl diimidazole (CDI) (9.23 g, 55.9 mmol) in dry CH₂Cl₂ (500 mL) was refluxed for 2 h under N₂. To this mixture was added dropwise a solution of tris(2-aminoethyl)amine III-8 (TREN) (4.3 mL, 27 mmol) and the reaction mixture was refluxed overnight. The next day the reaction mixture was cooled to rt and washed with 4 M NaOH (1 L). The organic phase was separated, dried over anhydrous MgSO₄ and filtered. Removal of the solvent yielded 13.6 g of crude material as a yellow oil. TLC and ¹H NMR indicated the presence of 3 products: mono-, di- and tri-substituted TREN derivatives. Chromatography on silica gel (ethyl acetate, TEA 3% and CH₃OH 1-10%) gave **9** as a pale yellow oil (6.0 g, 12.7 mM, 46% yield). ¹H NMR (CDCl₃) δ 8.23 (t, *J* = 2 Hz, 2H, NH), 7.58 (d, *J* = 8 Hz, 2H, CH), 7.08 (dd, *J*₁ = *J*₂ = 8 Hz, 2H, CH), 6.99 (d, *J* = 8 Hz, 2H, CH), 3.85 (s, 12H, CH₃), 3.55 (m, 4H, CH₂), 2.77 (m, 6H, CH₂), 2.65 (m, 2H, CH₂), 2.02 (br. s, 2H, NH₂); ¹³C NMR (CHCl₃) δ 165.8, 152.9, 147.9, 127.3, 124.7, 123.0, 115.6, 61.7, 57.7, 56.4, 54.0, 40.4, 38.6.

Compound III-29 was isolated as a side product (first spot on TLC) following the procedure described above. ¹H NMR (CDCl₃) δ 8.23, (t, *J* = 4 Hz, 2H, NH), 7.67 (d, 2H, CH), 7.14 (dd, *J*₁ = *J*₂ = 8 Hz, 2H, CH), 7.05 (d, *J* = 8 Hz, 2H, CH), 3.91 (s, 9H, CH₃), 3.92 (s, 9H, CH₃), 3.66 (m, 6H, CH₂), 2.94 (t, *J* = 4 Hz, 6H, CH₂); ¹³C NMR (CHCl₃) δ 165.9, 153.0, 148.0, 127.2, 124.6, 123.0, 115.7, 61.7, 56.4, 53.9, 38.3. Mass calculated for C₃₃H₄₂N₄₀O₉: 638, found ESI-MS [M+H⁺] 639.2.

Compound III-11. The same procedure as above, with 3,4-dimethoxybenzoic acid III-10 and TREN III-8, gave III-11 as pale yellow oil after chromatography (33% yield). $^1\text{H NMR}$ (CDCl_3) δ 7.63 (t, $J = 2.0$, Hz, 2H, NH), 7.36 (s, 2H, CH), 7.22 (d, $J = 8.4$ Hz, 2H, CH), 7.53 (d, $J = 8.8$ Hz, 2H, CH), 3.78 (s, 12H, CH_3), 3.46 (m, 4H, CH_2), 2.95 (br s, 2H, NH_2), 2.75 (m, 2H, CH_2), 2.67 (m, 4H, CH_2), 2.57 (m, 2H, CH_2); $^{13}\text{C NMR}$ (CHCl_3) δ 167.9, 151.8, 149.0, 127.2, 120.2, 111.0, 110.4, 56.3, 56.2, 55.2, 54.0, 39.6, 38.6.

Compound III-30 was isolated as a side product (first spot on TLC) following the procedure described above. $^1\text{H NMR}$ (CH_3OH) δ 7.19 (s, 2H, CH), 7.08 (d, $J = 8$ Hz, 2H, CH), 6.44 (d, $J = 8$ Hz, 2H, CH), 3.68 (s, 6H, CH_3), 3.66 (s, 6H, CH_3), 3.42 (t, $J = 8$ Hz, 6H, CH_2), 2.69 (t, $J = 4$ Hz 3H, CH_3); $^{13}\text{C NMR}$ (CHCl_3) δ 168.8, 152.2, 148.9, 126.5, 120.7, 111.0, 110.5, 55.3, 56.2, 35.6, 38.0. Mass calculated for $\text{C}_{33}\text{H}_{42}\text{N}_{40}\text{O}_9$: 638, found ESI-MS [$\text{M}+\text{H}^+$] 639.25.

Step II. Compound III-18, 2,3-17n. Stearoyl chloride (2.5 ml, 7.4 mmol) was added dropwise to a solution of III-9 3.04 g, 6.4 mmol) in 200 mL of CH_2Cl_2 . After stirring overnight at rt the reaction mixture was washed with NaOH, dried over anhydrous MgSO_4 and filtered. Evaporation of the solvent gave a yellow oil. Column chromatography on silica gel (ethyl acetate, TEA 3% and CH_3OH 0-5%) yielded III-18 as a colorless oil (1.8 g, 38%). $^1\text{H NMR}$ (CDCl_3) δ 8.21 (t, $J = 4$ Hz, 2H, NH), 7.56 (d, $J = 8$ Hz, 2H, CH), 7.05 (dd, $J_1 = J_2 = 8$ Hz, 2H, CH), 6.98 (d, $J = 8$ Hz, 2H, CH), 6.84 (t, 1H, NH), 3.85 (s, 12H, CH_3), 3.54 (m, 4H, CH_2), 3.34 (m, 2H,

CH₂), 2.74 (m, 6H, CH₂), 2.14 (t, $J = 8.0$ Hz, 2H, CH₂), 1.55 (m, 2H, CH₂), 1.24 (m, 28H, CH₂), 0.86 (t, $J = 8$ Hz, 3H, CH₃); ¹³C NMR (CHCl₃) δ 174.6, 168.0, 152.0, 149.1, 126.9, 120.3, 111.1, 110.3, 56.3, 56.2, 54.7, 54.3, 38.4, 37.8, 32.3, 30.5, 30.1, 29.9, 29.8, 29.7, 26.2, 23.1, 14.5. Mass calculated for C₄₂H₆₈N₄O₇: 740.5, found ESI-MS [M+H⁺] 741.5.

Compound III-12, 2,3-1. The same procedure as described above, using acetyl chloride, gave III-12 as a colorless oil (¹H NMR (CDCl₃) δ 8.22 (br. s, 2H, NH), 7.52 (d, $J = 7.6$ Hz, 2H, CH), 6.13 (br. s, 1H, NH), 7.04 (dd, $J_1 = J_2 = 8.0$ Hz, 2H, CH), 7.00 (d, $J = 8.0$ Hz, 2H, CH), 3.86 (s, 12H, CH₃), 3.60 (m, 4H, CH₂), 3.40 (m, 2H, CH₂), 2.76 (m, 6H, CH₂), 1.97 (s, 3H, CH₃); ¹³C NMR in CHCl₃ δ 171.5, 166.1, 152.9, 147.9, 126.8, 124.7, 122.9, 115.7, 61.7, 56.4, 54.2, 54.1, 53.8, 37.9, 37.8, 23.0. Mass calculated for C₂₆H₃₆N₄O₇: 516.3, found ESI-MS [M+H⁺] 517.2, [M+Na⁺] 539.3.

Compound III-13, 2,3-3n. The same procedure as described above, using butyryl chloride, gave **13** as a colorless oil (¹H NMR (CDCl₃) δ 8.20 (br. t., $J = 4$ Hz, 2H, NH), 7.57 (d, $J = 8$ Hz, 2H, CH), 7.07 (dd, $J_1 = J_2 = 8$ Hz, 2H, CH), 7.00 (d, $J = 8$ Hz, 2H, CH), 6.8 (br. s, 1H, NH), 3.87 (s, 12H, CH₃), 3.57 (m, 4H, CH₂), 3.35 (m, 2H, CH₂), 2.75 (m, 6H, CH₂), 2.13 (t, $J = 8$ Hz, 2H, CH₂), 1.59 (m, 2H, CH₂), 0.86 (t, 3H, CH₃); ¹³C NMR in CHCl₃ δ 174.1, 165.9, 152.9, 147.8, 126.9, 124.7, 122.9, 115.7, 61.7, 56.4, 54.0, 53.8, 38.5, 37.9, 37.6, 19.6, 14.2. Mass calculated for C₂₈H₄₀N₄O₇: 544.3.

Compound III-15, 2,3-5n. The same procedure as described above, using hexanoic anhydride, provided III-15 as a colorless oil. ^1H NMR (CDCl_3) δ 8.26 (br. s, 2H, NH), 7.61 (d, $J = 8$ Hz, 2H, CH), 7.11 (dd, $J_1 = J_2 = 8$ Hz, 2H, CH), 7.03 (d, $J = 8$ Hz, 2H, CH), 6.75 (br. s, 1H, NH), 3.90 (s, 12H, CH_3), 3.60 (m, 4H, CH_2), 3.40 (m, 2H, CH_2), 2.79 (m, 6H, CH_2), 2.18 (t, $J = 8$ Hz, 2H, CH_2), 1.60 (m, 2H, CH_2), 1.25 (m, 4H, CH_2), 0.88 (t, $J = 8$ Hz, 3H, CH_3); ^{13}C NMR (CHCl_3) δ 174.4, 166.1, 152.9, 147.9, 126.8, 124.7, 123.0, 115.7, 61.7, 56.4, 54.1, 53.9, 37.8, 37.7, 36.6, 32.0, 25.9, 22.9, 14.4. Mass calculated for $\text{C}_{30}\text{H}_{44}\text{N}_4\text{O}_7$: 572.3, found ESI-MS $[\text{M}+\text{H}^+]$ 573.3, $[\text{M}+\text{Na}^+]$ 595.4.

Compound III-16, 2,3-8iso. The same procedure as described above, using 3,5,5-trimethylhexanoil chloride, provided III-16 as a colorless oil. ^1H NMR (CDCl_3) δ 8.22 (br. t, $J = 4$ Hz, 2H, NH), 7.61 (d, $J = 8$ Hz, 2H, CH), 7.10 (dd, $J_1 = J_2 = 8$ Hz, 2H, CH), 7.01 (d, $J = 8$ Hz, 2H, CH), 6.70 (br. s, 1H, NH), 3.90 (s, 12H, CH_3), 3.56 (m, 4H, CH_2), 3.35 (m, 2H, CH_2), 2.75 (m, 6H, CH_2), 1.96 (m, 3H, CH_2 , CH), 0.90 (m, 14H, CH_2 , 4 CH_3); ^{13}C NMR (CHCl_3) δ 173.5, 165.9, 152.9, 147.8, 126.9, 124.8, 123.0, 115.7, 61.7, 56.5, 53.9, 53.6, 51.0, 46.3, 38.6, 37.8, 37.5, 31.4, 30.4, 27.5, 22.8. Mass calculated for $\text{C}_{33}\text{H}_{50}\text{N}_4\text{O}_7$: 614.3.

Compound III-17, 2,3-9n. The same procedure as described above, using decanoyl chloride, provided III-17 as a colorless oil. ^1H NMR (CDCl_3) δ 8.21 (br. t, $J = 8$ Hz, 2H, NH), 7.57 (d, $J = 8$ Hz, 2H, CH), 7.08 (dd, $J_1 = J_2 = 8$ Hz, 2H, CH), 6.78 (d, $J = 8$ Hz, 2H, CH), 6.77 (br. s, 1H, NH), 3.87 (s, 12H, CH_3), 3.56 (m, 4H, CH_2), 3.35 (m,

2H, CH₂), 2.74 (m, 6H, CH₂), 2.15 (t, $J = 8$ Hz, 2H, CH₂), 1.56 (m, 2H, CH₂), 1.25 (m, 12H, CH₂), 0.87 (t, $J = 8$ Hz, 3H, CH₃); ¹³C NMR (CHCl₃) δ 174.3, 165.9, 152.9, 147.8, 126.9, 124.7, 123.0, 115.6, 61.7, 56.4, 54.0, 53.8, 37.9, 37.6, 36.6, 32.3, 30.0, 29.9, 29.8, 29.7, 26.3, 23.1, 14.5. Mass calculated for C₃₄H₅₂N₄O₇: 628.3.

Compound III-14, 2,3-5iso. The same procedure as above, using tert-butyl-acetyl chloride, provided III-14 as a colorless oil. ¹H NMR (CD₃OD) δ 7.32 (d, $J = 7.6$ Hz, 2H, CH), 7.14 (d, $J = 6.4$ Hz, 2H, CH), 7.10 (dd, $J_1 = J_2 = 7.6$ Hz, 2H, CH), 3.88 (s, 6H, CH₃), 3.86 (s, 6H, CH₃), 3.54 (t, $J = 6.0$ Hz, 4H, CH₂), 3.34 (m, 2H, H₂), 2.83 (t, $J = 6.0$ Hz, 4H, CH₂), 2.76 (t, $J = 6.0$ Hz, 2H, CH₂), 2.05 (s, 2H, CH₂), 0.99 (s, 9H, CH₃); ¹³C NMR (CD₃OD) δ 173.9, 167.3, 153.2, 147.7, 127.8, 124.4, 121.5, 115.6, 60.9, 55.5, 53.3, 53.1, 49.5, 37.8, 37.3, 30.6, 29.2. Mass calculated for C₃₀H₄₄N₄O₇: 572.3, found ESI-MS [M+H⁺] 574.4, [M+Na⁺] 596.4.

Compound III-19, 3,4-3n. The same procedure, using butyryl chloride and III-11, yielded III-19 as a colorless oil. ¹H NMR (CDCl₃) ; ¹³C NMR (CHCl₃) δ 174.4, 168.1, 152.0, 149.1, 126.9, 120.4, 111.1, 110.4, 56.3, 56.2, 54.6, 54.3, 38.5, 38.3, 37.7, 19.4, 14.2, Mass calculated for C₂₈H₄₀N₄O₇: 544.3.

Compound III-20, 3,4-5n. The same procedure, using hexanoic anhydride and III-11, yielded III-20 as a colorless oil. ¹H NMR (CDCl₃) δ 7.40 (s, 2H, CH), 7.24 (d, $J = 4$ Hz, 2H, CH), 7.13 (br. s, 2H, NH), 6.60 (br. s, 1H, NH), 6.52 (d, $J = 8$ Hz, 2H, CH), 3.82 (s, 6H, CH₃), 3.80 (s, 6H, CH₃), 3.51 (m, 4H, CH₂), 3.32 (m, 2H, CH₂), 2.67 (m,

4H, CH₂), 2.59 (m, 2H, CH₂), 1.86 (t, $J = 8$ Hz, 2H, CH₂), 1.36 (m, 2H, CH₂), 1.26 (m, 2H, CH₂), 1.14 (m, 2H, CH₂), 0.78 (t, $J = 8$ Hz, 3H, CH₃); ¹³C NMR (CHCl₃) δ 174.6, 168.0, 152.0, 149.1, 126.9, 120.3, 111.1, 110.3, 56.3, 56.2, 54.8, 54.3, 38.4, 37.7, 36.6, 31.9, 25.7, 22.8, 14.3. Mass calculated for C₃₀H₄₄N₄O₇: 572.3, found ESI-MS [M+H⁺] 573.3.

Compound III-22, 3,4-17n. The same procedure, using stearoyl chloride and III-11, yielded III-22 as a white solid. ¹H NMR (CHCl₃) δ 7.45 (s, 2H, CH), 7.26 (d, $J = 8.8$ Hz, 2H, CH), 7.00 (t, $J = 5.2$ Hz, 2H, NH), 6.55 (d, $J = 8.0$ Hz, 2H, CH), 6.52 (t, $J = 5.0$ Hz, 1H, NH), 3.89 (s, 6H, CH₃), 3.86 (s, 6H, CH₃), 3.57 (m, 4H, CH₂), 3.38 (m, 2H, CH₂), 2.74 (m, 4H, CH₂), 2.65 (m, 2H, CH₂), 1.90 (t, $J = 8.0$ Hz, 2H, CH₂), 1.43 (m, 2H, CH₂), 1.31 (m, 28H, CH₂), 0.91 (t, $J = 8.0$ Hz, 3H, CH₃); ¹³C NMR (CHCl₃) δ 174.5, 167.9, 152.0, 149.2, 127.0, 120.2, 111.1, 110.3, 56.3, 56.2, 54.9, 54.3, 38.4, 37.8, 36.8, 32.3, 30.1, 30.0, 29.9, 29.8, 26.1, 23.1, 14.6. Mass calculated for C₃₀H₄₄N₄O₇: 740.5, found ESI-MS [M+H⁺] 741.6.

Step III. Demethylation. General Procedure. Under nitrogen, a solution of *O*-methylated precursor (200 mg) dissolved in dry CH₂Cl₂ (200 mL) was cooled to 0 °C. To this mixture was added dropwise a 0.1 M solution of BBr₃ (about 30 equiv) in dry CH₂Cl₂. The reaction mixture was left overnight so as to warm slowly to rt. During and after addition of BBr₃ the reaction mixture was kept under the efficient N₂ flow to facilitate removal of water-reactive volatiles and protect from air and moisture. The next day, ¹H NMR was used to monitor the reaction's progress. If necessary, 10 more

equiv of BBr₃ was added and the reaction mixture was left to stir for one more day. When the reaction was judged to be complete, dry MeOH (500 mL) was added dropwise to the reaction mixture at 0 °C. The solution was then allowed to warm to rt overnight. The reaction mixture was carefully concentrated *in vacuo*, initially at a low temperature to remove volatile boron complexes and then at 50 °C to remove MeOH. Addition and removal of MeOH was repeated (ice bath, 0 °C, N₂ flow) twice more. After the final concentration the desired bis-catechol product, as its HBr salt, was collected as a brown hygroscopic powder in quantitative yield.

Compound III-26. ¹H NMR (DMSO-d₆) δ 12.04 (s, 2H, OH), 9.58 (s, 1H, N⁺H), 9.31 (s, 2H, OH), 8.91 (t, *J* = 2 Hz, 2H, NH), 8.17 (t, *J* = 2 Hz, 1H, NH), 7.23 (d, *J* = 8 Hz, 2H, CH), 6.94 (d, *J* = 8 Hz, 2H, CH), 6.70 (dd, *J*₁ = *J*₂ = 8 Hz, 2H, CH), 3.69 (m, 4H, CH₂), 3.46 (m, 8H, CH₂), 2.07 (t, *J* = 4 Hz, 2H, CH₂), 1.42 (m, 2H, CH₂), 1.23 (s, 28H, CH₂), 0.85 (t, *J* = 8 Hz, 3H, CH₃); ¹³C NMR in DMSO δ 174.6, 171.0, 149.9, 147.1, 119.9, 119.0, 118.6, 116.1, 53.0, 52.4, 36.0, 34.8, 34.6, 32.2, 29.9, 29.8, 29.7, 29.6, 25.8, 23.0, 14.8. Mass calculated for C₃₈H₆₁N₄O₇⁺: 685.5, found ESI-MS [M⁺] 685.4.

Compound III-23. ¹H NMR (CD₃OD) δ 7.21 (d, 2H, *J* = 8.4 Hz, CH), 6.96 (d, 2H, *J* = 7.6 Hz, CH), 6.72 (dd, 2H, *J*₁ = *J*₂ = 8.0 Hz, CH), 3.87 (m, 4H, CH₂), 3.65 (m, 6H, CH₂), 3.58 (m, 2H, CH₂), 1.95 (s, 3H, CH₃); ¹³C NMR in CD₃OD δ 174.4, 171.7, 148.7, 146.3, 119.1, 118.9, 118.6, 115.5, 54.8, 54.7, 35.1, 35.0, 21.4. Mass calculated for C₂₂H₂₉N₄O₇⁺: 461.2, found ESI-MS [M⁺] 462.2.

Compound III-25. ^1H NMR (CD_3OD) δ 7.23 (d, $J = 8.0$ Hz, 2H, CH), 6.97 (d, $J = 7.6$ Hz, 2H, CH), 6.72 (dd, 2H, $J_1 = J_2 = 8.0$ Hz, CH), 3.87 (m, 4H, CH_2), 3.66 (m, 6H, CH_2), 3.57 (m, 2H, CH_2), 2.14 (t, $J = 7.6$, H, CH_2), 1.25 (m, 6H, CH_2), 0.88 (t, $J = 7.2$, 3H, CH_3); ^{13}C NMR in CD_3OD δ 177.6, 171.7, 148.8, 146.3, 119.0, 118.9, 118.6, 115.6, 55.3, 54.5, 35.4, 35.3, 35.0, 31.5, 25.0, 22.4, 13.3. Mass calculated for $\text{C}_{26}\text{H}_{37}\text{N}_4\text{O}_7^+$: 517.3, found ESI-MS [M^+] 518.3.

Compound III-24. ^1H NMR (CD_3OD) δ 7.23 (d, $J = 8.0$ Hz, 2H, CH), 6.97 (d, $J = 7.6$ Hz, 2H, CH), 6.72 (dd, $J_1 = J_2 = 8.0$ Hz, 2H, CH), 3.87 (m, 4H, CH_2), 3.66 (m, 6H, CH_2), 3.58 (m, 2H, CH_2), 2.00 (s, 2H, CH_2), 0.905 (s, 9H, CH_3); ^{13}C NMR in CD_3OD δ 176.2, 171.7, 148.9, 146.3, 119.0, 118.9, 118.5, 115.6, 55.6, 54.5, 35.3, 34.9, 30.6, 29.1. Mass calculated for $\text{C}_{26}\text{H}_{37}\text{N}_4\text{O}_7^+$: 517.3, found ESI-MS [M^+] 518.2, [$\text{M}^+ - \text{H}^+ + \text{Na}^+$] 540.3.

Compound III-27. ^1H NMR (CD_3OD) δ 7.28 (s, 2H, CH), 7.18 (d, $J = 8.3$ Hz, 2H, CH), 6.73 (d, $J = 8.4$ Hz, 2H, CH), 3.73 (m, 4H, CH_2), 3.55 (m, 6H, CH_2), 3.49 (m, 2H, CH_2), 2.09 (t, $J = 7.6$ Hz, 2H, CH_2), 1.39 (m, 2H, CH_2), 1.15 (m, 4H, CH_2), 0.82 (t, $J = 7.0$ Hz, 3H, CH_3); ^{13}C NMR in CD_3OD δ 177.3, 170.5, 149.7, 145.3, 124.6, 120.3, 115.0, 114.8, 54.9, 54.7, 35.6, 35.5, 35.0, 31.5, 25.0, 22.4, 13.3. Mass calculated for $\text{C}_{26}\text{H}_{37}\text{N}_4\text{O}_7^+$: 517.3, found ESI-MS [M^+] 517.3.

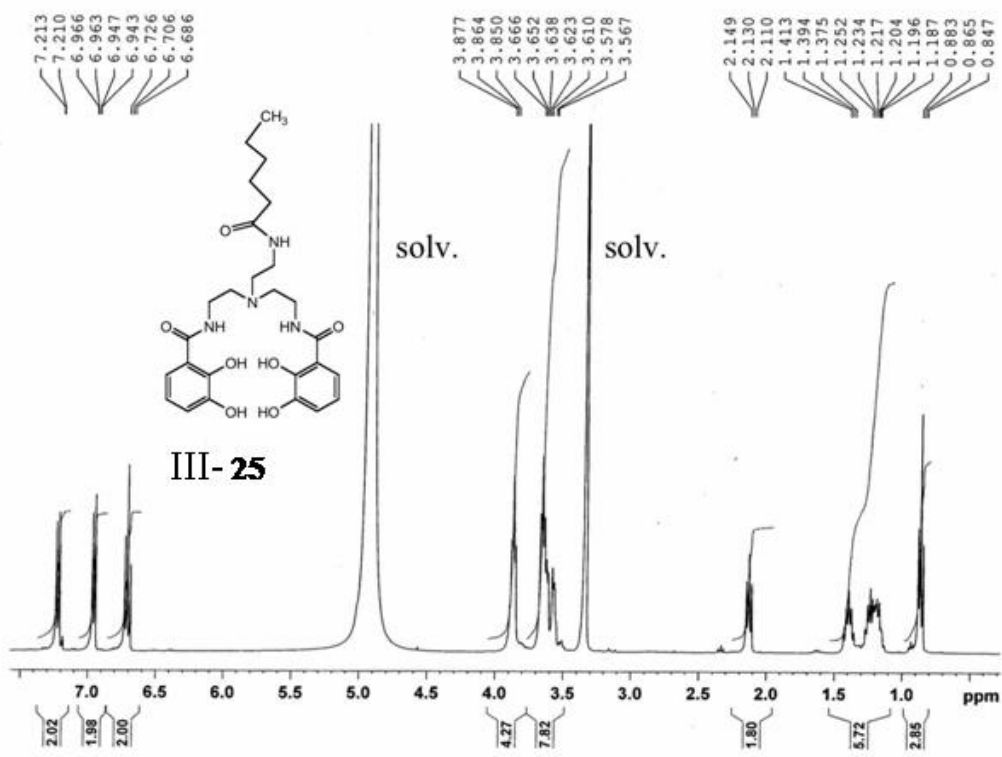
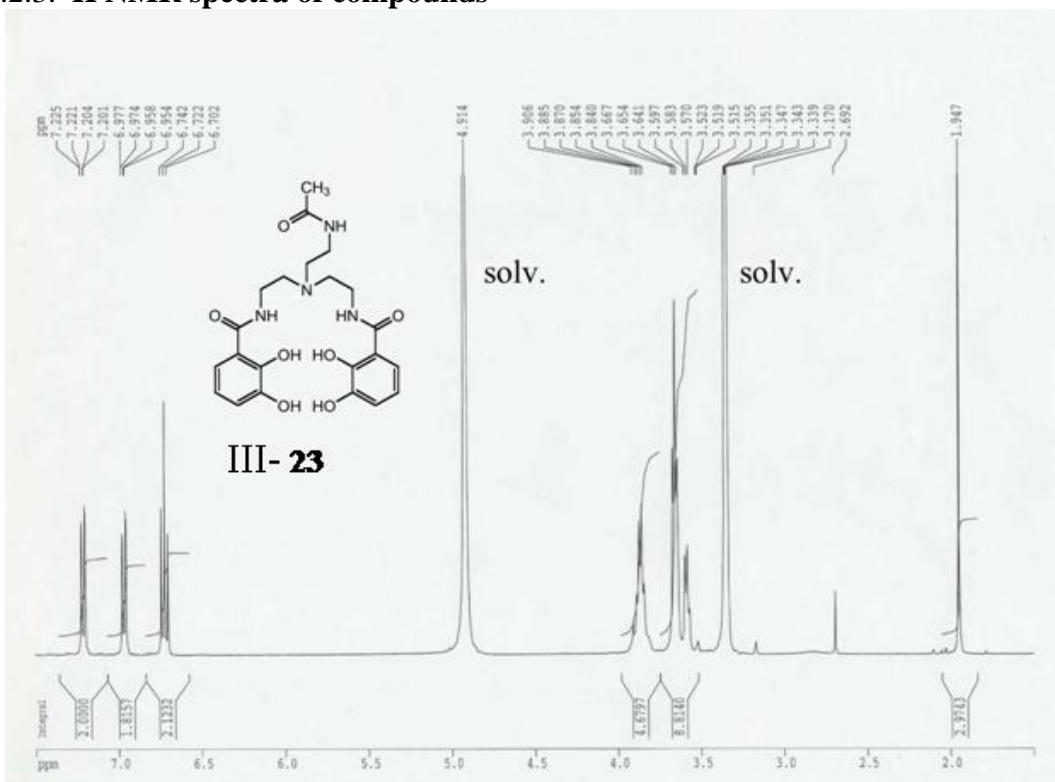
Compound III-28. ^1H NMR (DMSO-d_6) δ 9.60 (br. s, 3H, N^+H , 2OH), 9.13 (br. s, 2H, OH), 8.44 (t, $J = 5.6$ Hz, 2H, NH), 8.13 (t, $J = 5.2$ Hz, 1H, NH), 7.28 (s, 2H, CH),

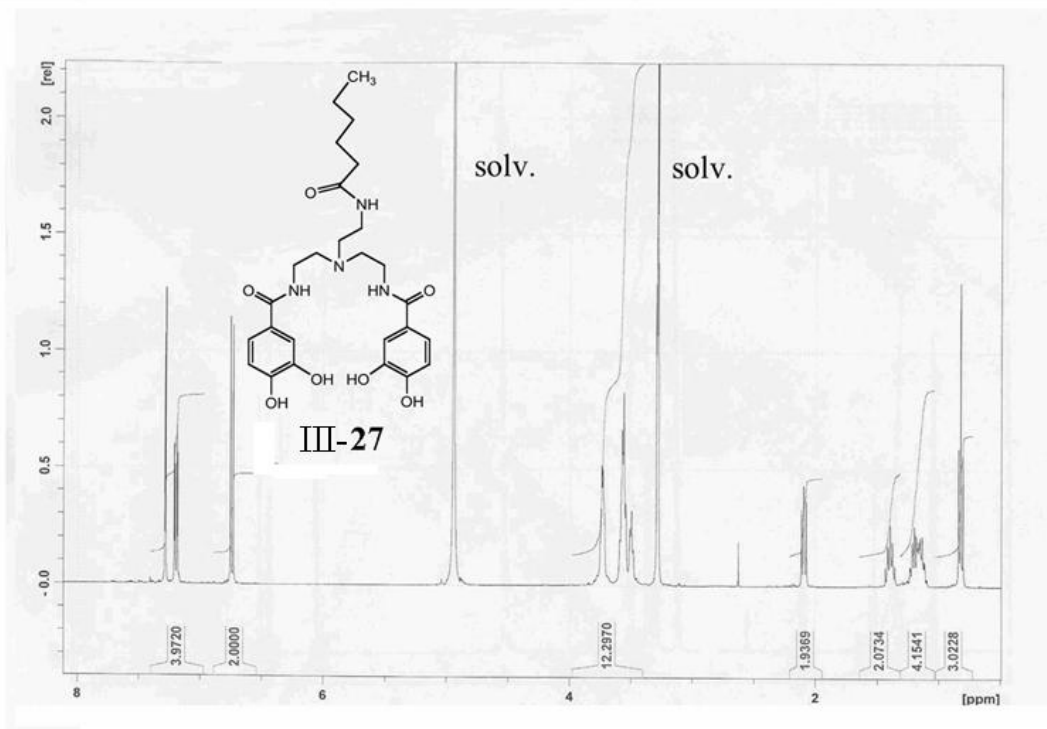
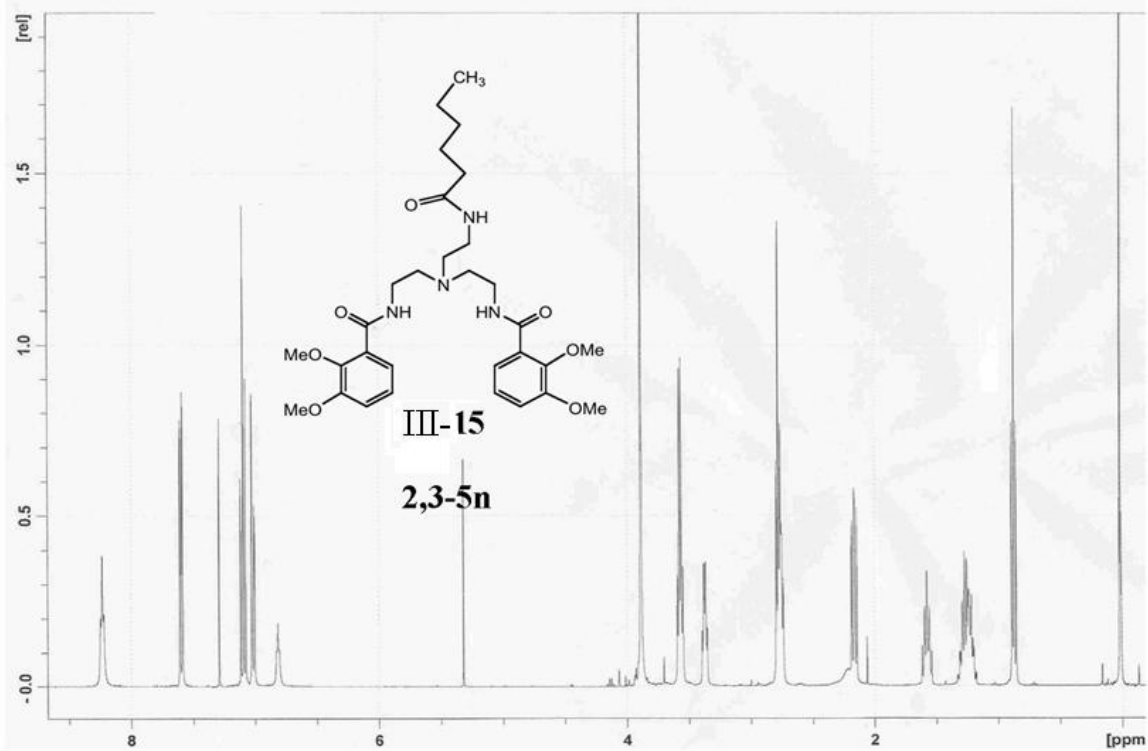
7.18 (d, $J = 8.0$ Hz, 2H, CH), 6.76 (d, $J = 8.0$ Hz, 2H, CH), 3.60 (m, 4H, CH₂), 3.41 (m, 4H, CH₂), 3.33 (m, 2H, CH₂), 2.08 (t, $J = 4.0$ Hz, 2H, CH₂), 1.45 (m, 2H, CH₂), 1.27 (s, 28H, CH₂), 0.85 (t, $J = 7.2$ Hz, 3H, CH₃); ¹³C NMR in MeOH δ 177.3, 170.5, 149.7, 145.3, 124.6, 120.4, 115.0, 114.8, 54.9, 54.7, 35.7, 35.5, 34.9, 32.1, 29.8, 29.7, 29.5, 29.4, 25.4, 22.8, 13.8. Mass calculated for C₃₈H₆₁N₄O₇⁺: 685.5, found ESI-MS [M⁺] 685.4.

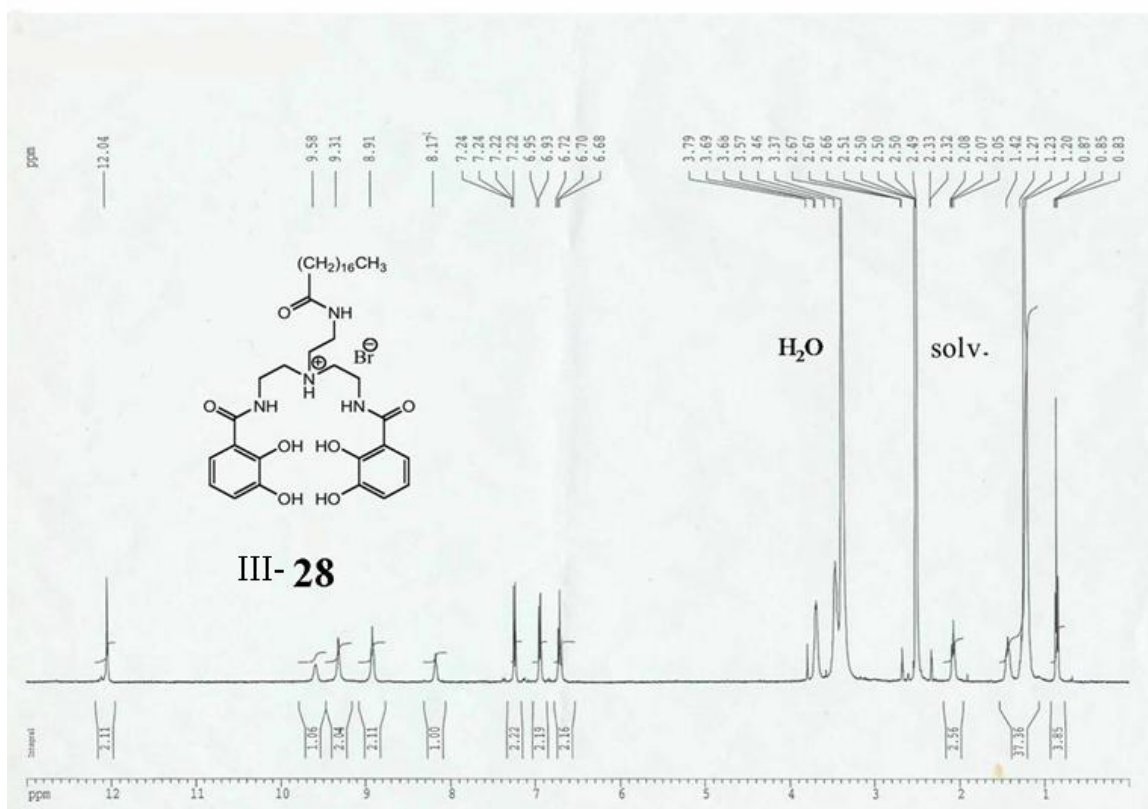
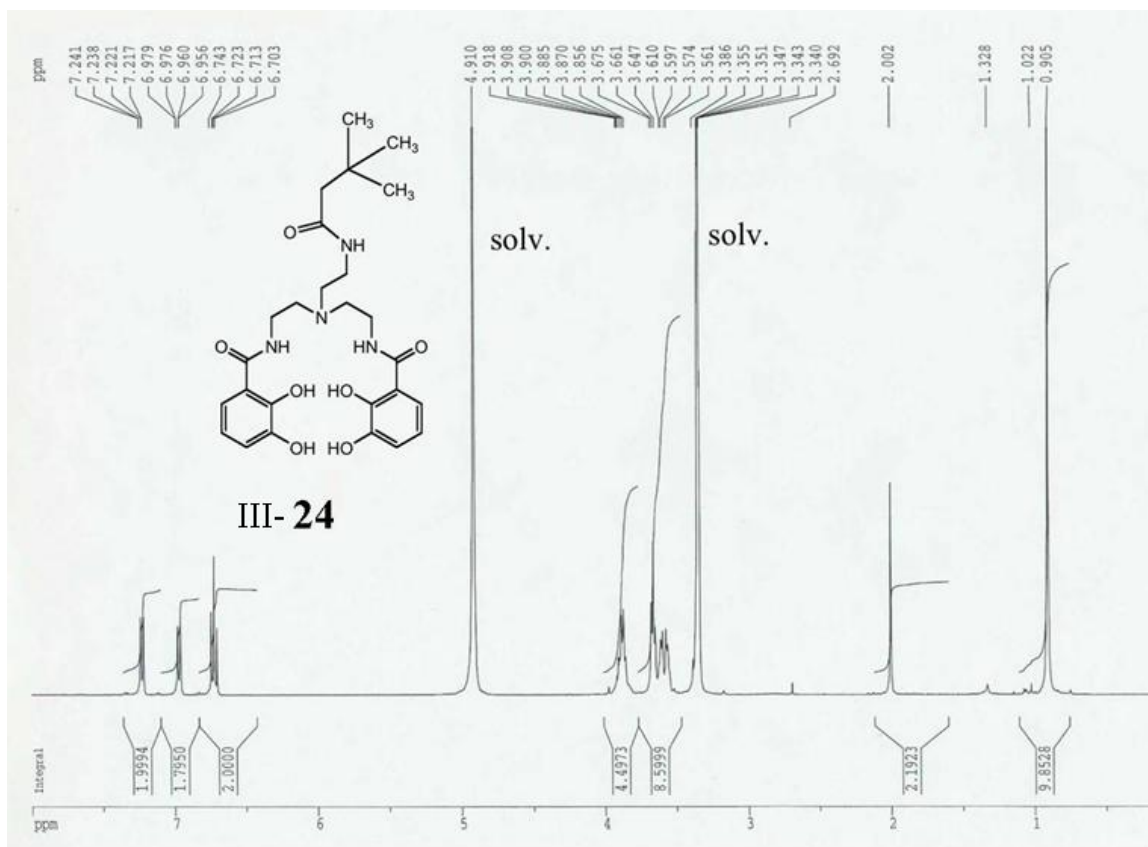
Compound III-31. ¹H NMR (CD₃OD) δ 7.22 (d, 2H, $J = 8$ Hz, CH), 6.97 (d, 2H, $J = 8$ Hz, CH), 6.71 (dd, 2H, $J_1 = J_2 = 8$ Hz, CH), 3.86 (m, 4H, CH₂), 3.64 (m, 6H, CH₂), 3.58 (m, 2H, CH₂), 2.13 (t, $J = 8$ Hz, 2H, CH₂), 1.44 (m, 2H, CH₂), 0.83 (t, $J = 4$ Hz, 3H, CH₃); ¹³C NMR in CD₃OD δ 177.3, 171.7, 148.8, 146.3, 119.0, 118.8, 118.5, 115.5, 55.2, 54.4, 37.4, 35.2, 35.0, 18.7, 13.0. Mass calculated for C₂₄H₃₃N₄O₇⁺: 489.2.

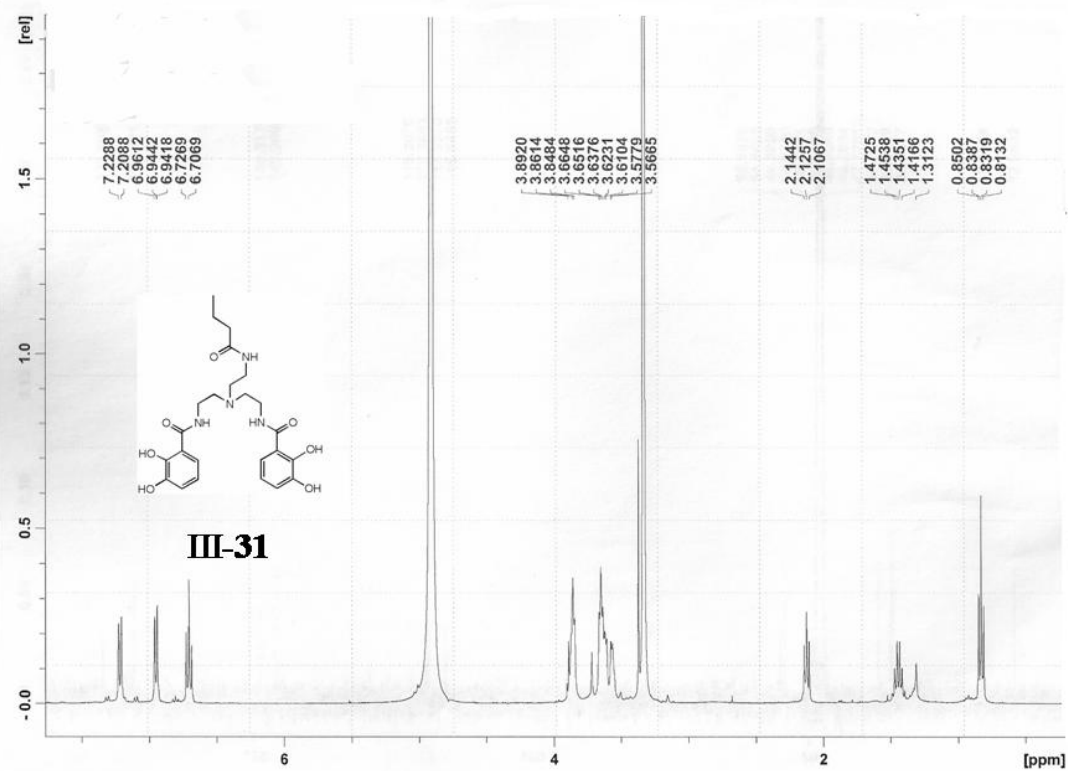
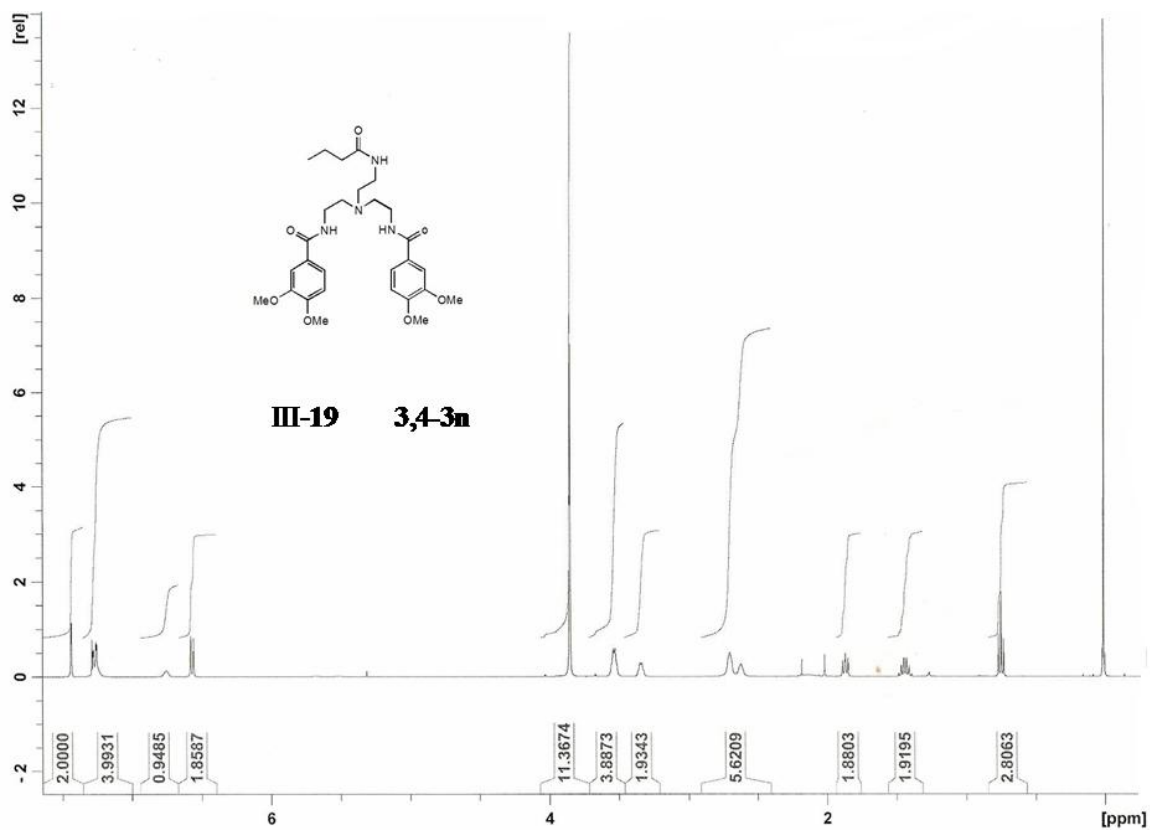
Compound III-32. ¹H NMR (CD₃OD) δ 7.19 (d, $J = 8.0$ Hz, 2H, CH), 6.93 (d, $J = 7.6$ Hz, 2H, CH), 6.68 (dd, 2H, $J_1 = J_2 = 4.0$ Hz, CH), 3.87 (m, 4H, CH₂), 3.63 (m, 6H, CH₂), 3.55 (m, 2H, CH₂), 2.11 (t, $J = 7.6$ Hz, H, CH₂), 1.38 (m., 2H, CH₂), 1.25 (m, 2H), 0.88 (t, $J = 4.0$ Hz, 3H, CH₃); ¹³C NMR in CD₃OD δ 177.5, 171.7, 148.8, 146.3, 119.0, 118.8, 118.5, 115.5, 55.3, 54.4, 35.5, 35.3, 34.9, 32.0, 29.6, 29.4, 29.3, 25.3, 22.7, 13.4. Mass calculated for C₂₆H₃₇N₄O₇⁺: 576.3.

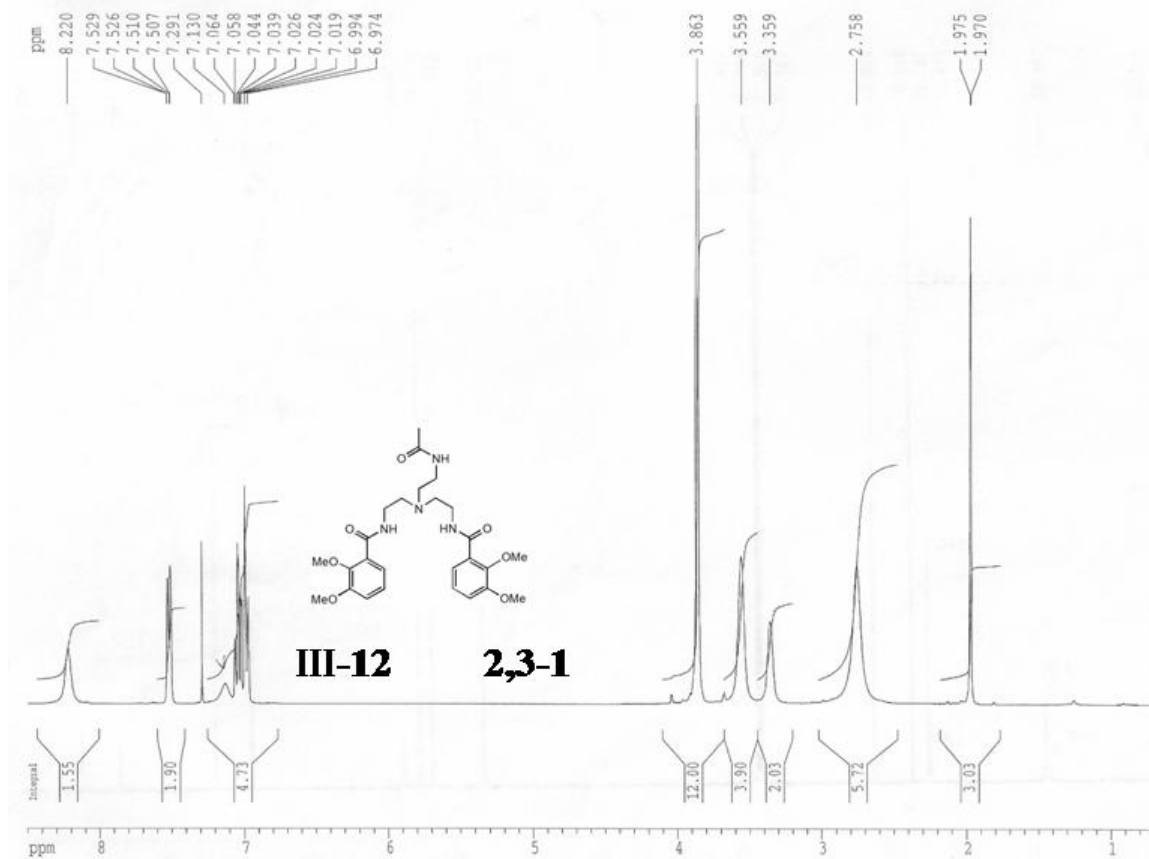
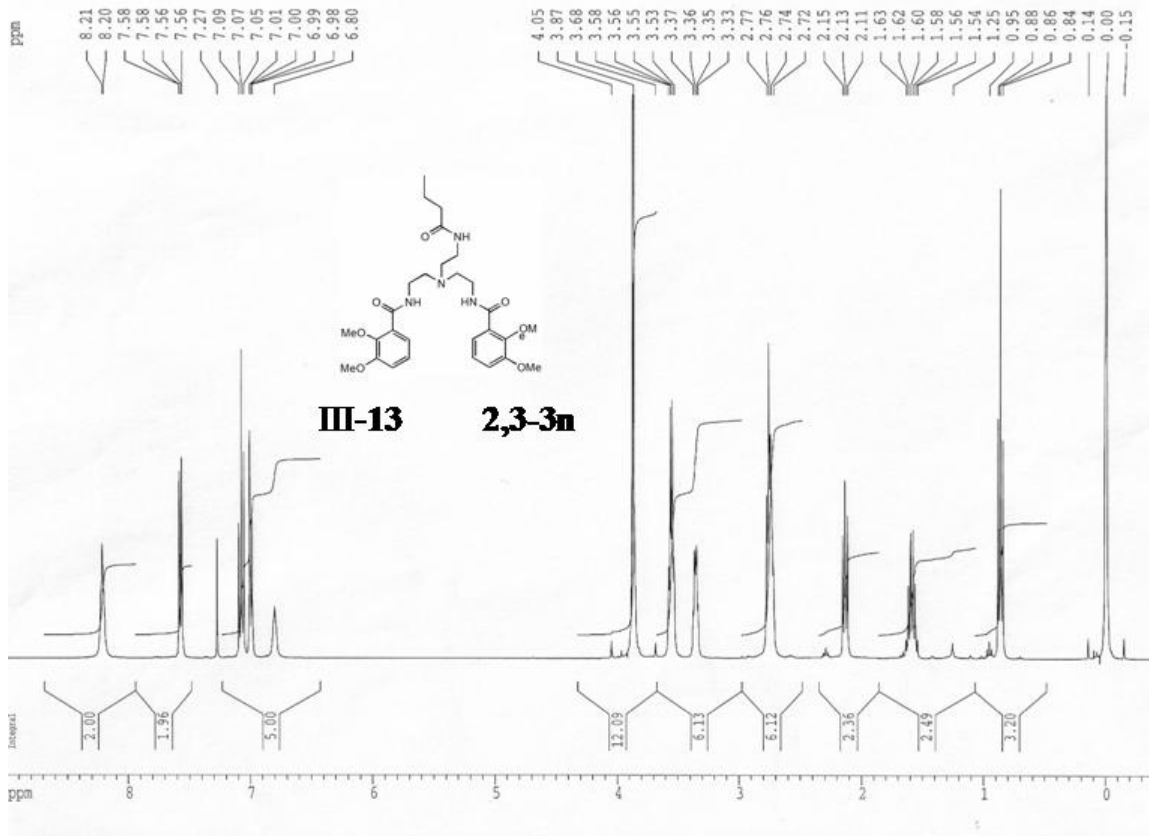
5.2.3. ^1H NMR spectra of compounds

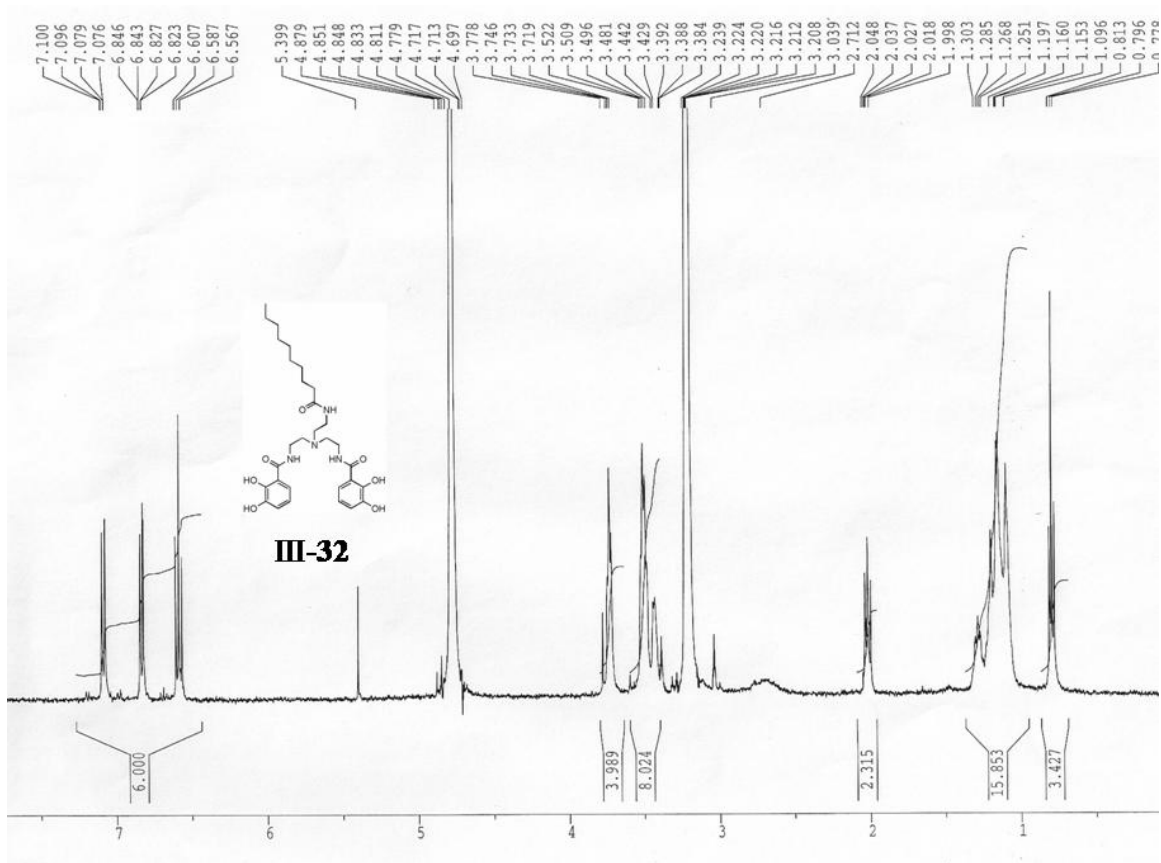
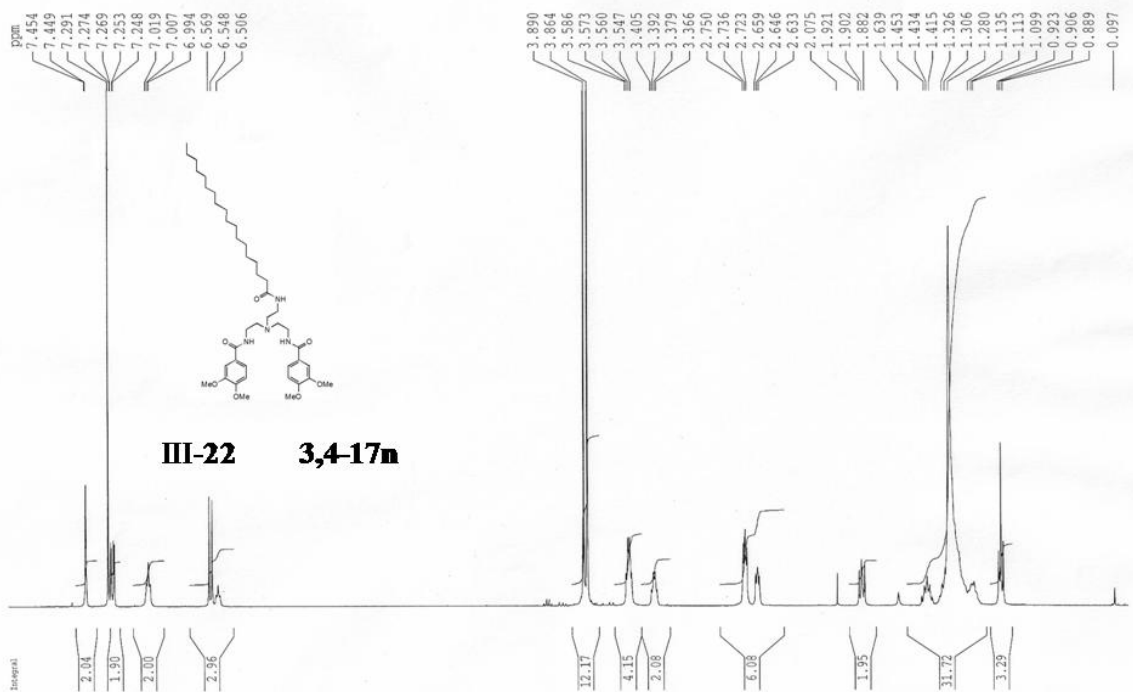


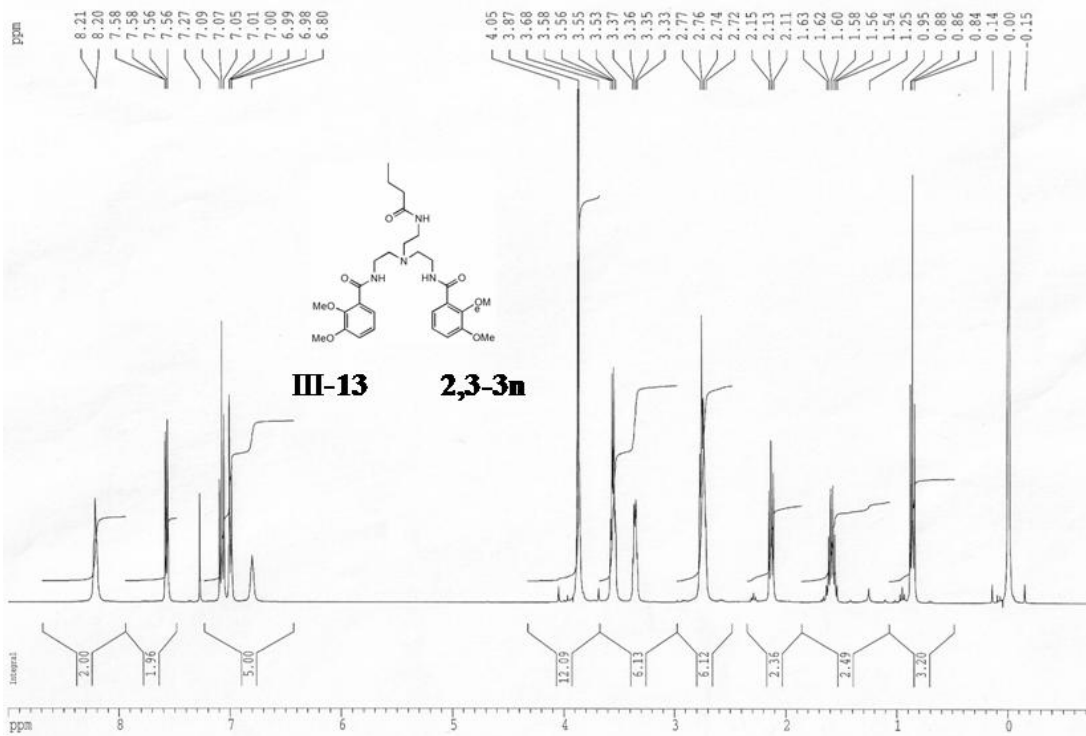
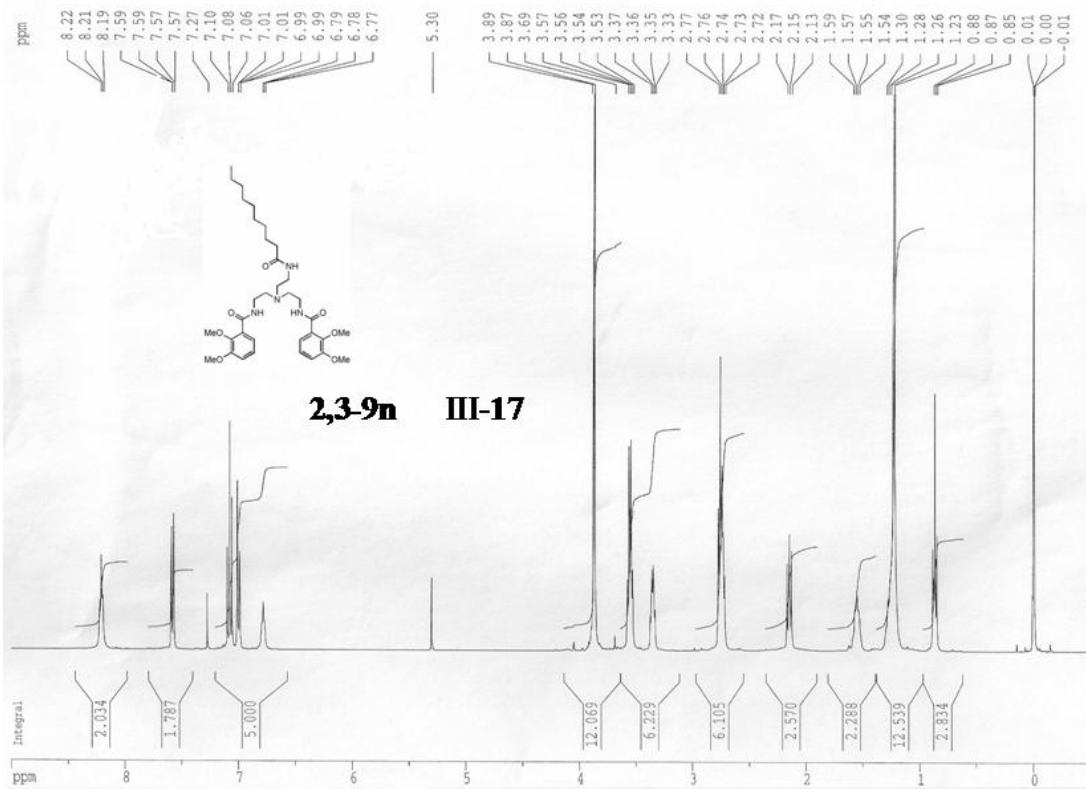


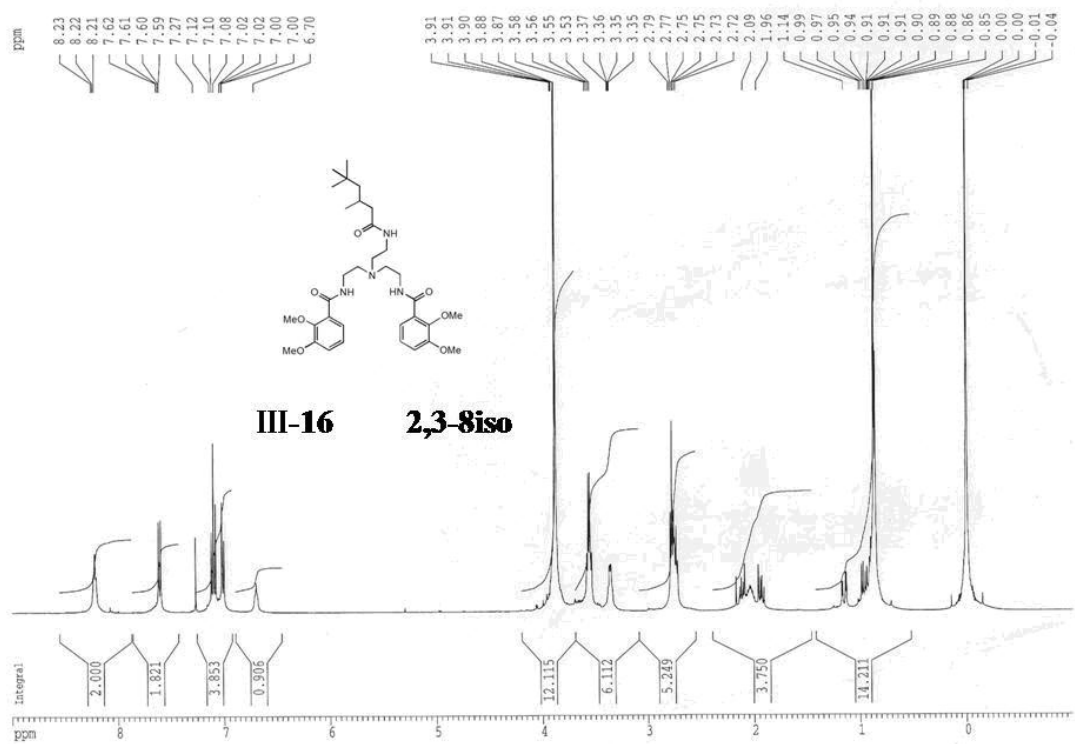
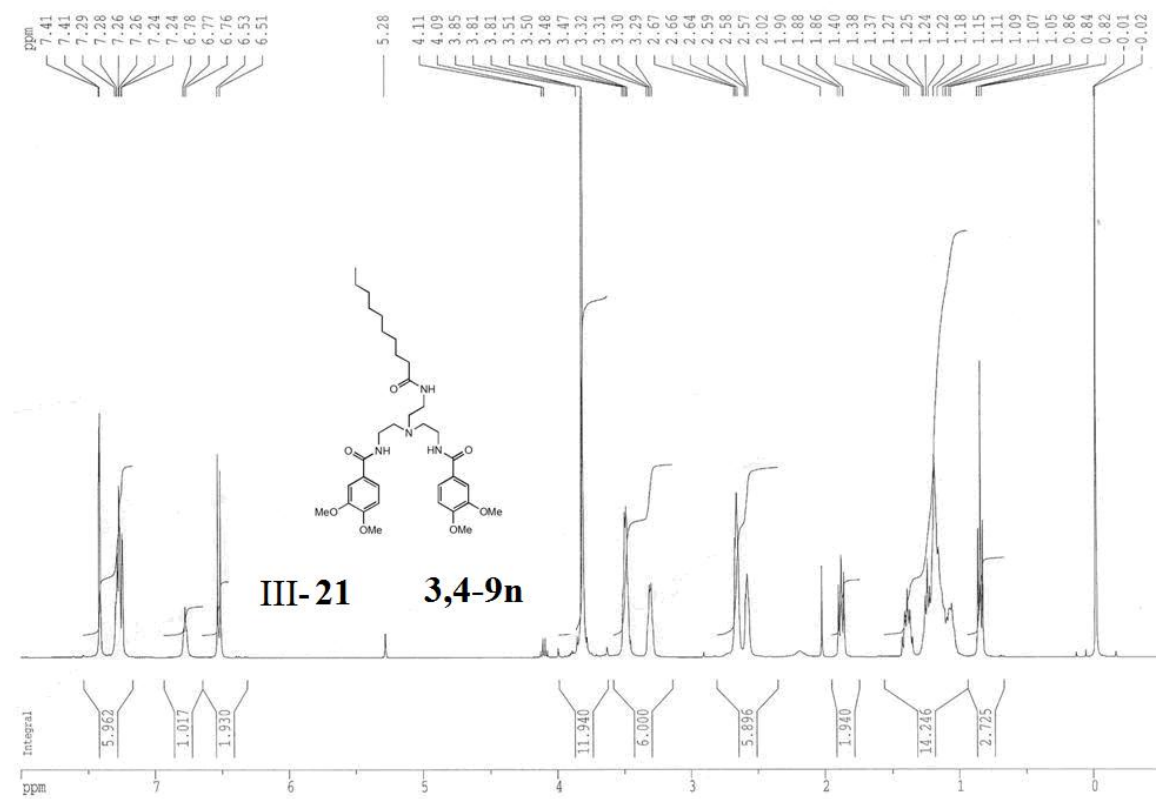


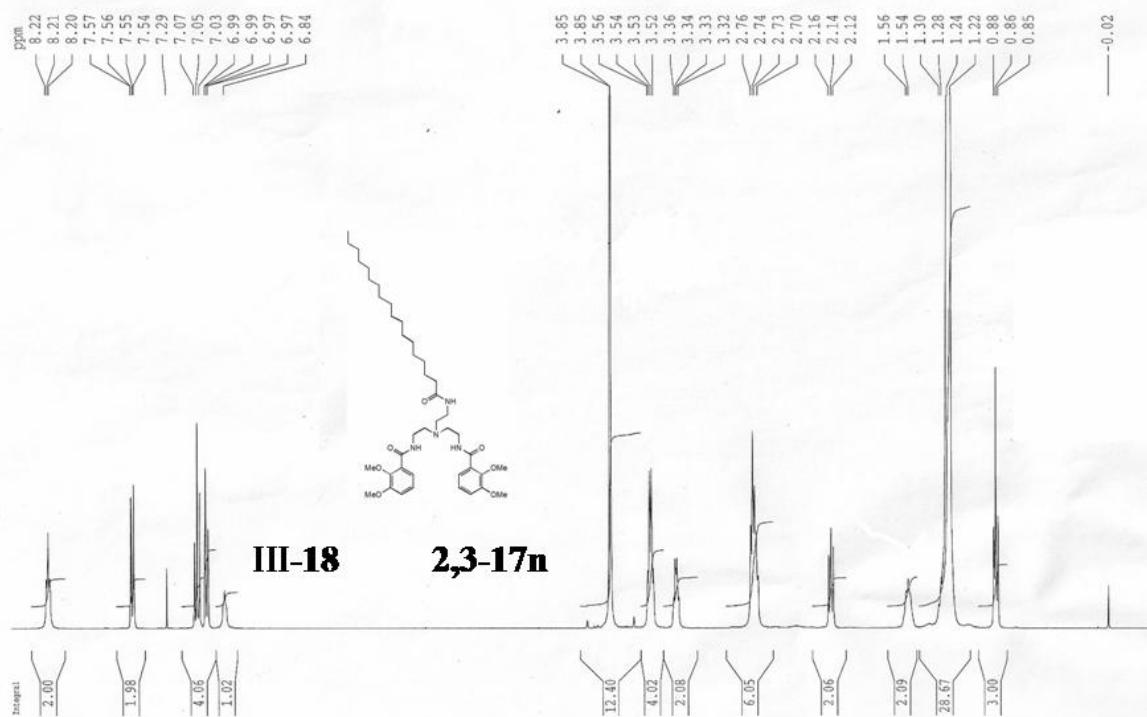
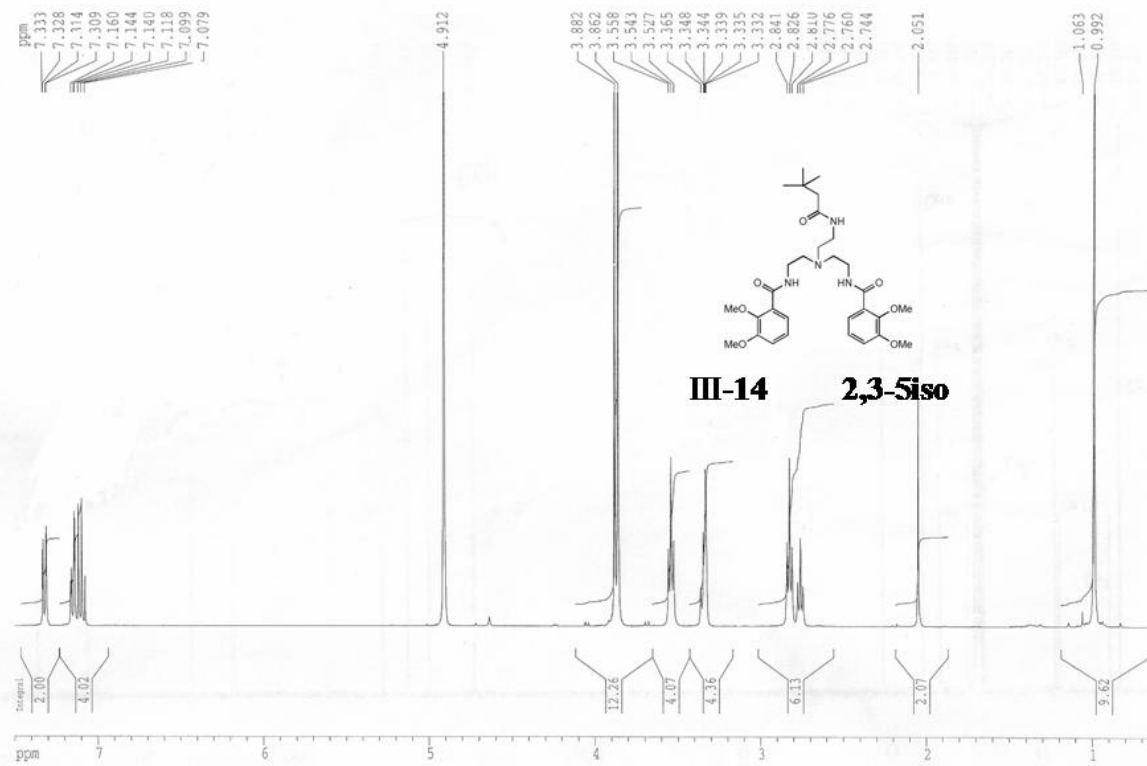












5.3. Experimental Section for Chapter 4.

5.3.1. **General experimental.** The chemicals and solvents were purchased from Aldrich, Fisher or Fluka. Phospholipids used to prepare liposomes were purchased from Avanti Polar Lipids. Size-exclusion chromatography was performed using Sephadex G-25. Liposome fluorimetric assays were recorded using a Hitachi F-4500 spectrophotometer.

5.3.2. **Preparation of liposomes.** A stock solution of egg-yolk phosphatidylcholine (EYPC) in CHCl_3 (60 mg in 3 mL) was evaporated under reduced pressure to produce a thin film that was dried *in vacuo* for 2 h. This lipid film was hydrated with 1 mL of 10 mM sodium phosphate containing different sodium salts and 0.1 mM HPTS. Freeze/thaw cycles were repeated at least 10 times until no solid particles were visible. The frozen solution was warmed to 30-35 °C before every freeze cycle. The mixture was also placed on a vortexer 3 times for 1 min to facilitate hydration. The cloudy solution was extruded through a 100 nm polycarbonate membrane at least 20 times until the solution was transparent. This solution was passed down a Sephadex G-25 column (11 cm x 1 cm) to remove extravesicular HPTS dye. The eluant was identical to the solution used to hydrate the EYPC films except that it was free of HPTS. The 2.5-3.0 mL of solution isolated from gel filtration was 26-32 mM in lipid, assuming all EYPC was incorporated into the liposomes. Each stock solution of liposomes was used that same day for any ion transport assays.

5.3.3. Ion transport assays. This procedure describes the typical ion transport assay as depicted in Fig. 2 of the paper. A 40 μL aliquot of the stock solution of EYPC liposomes was added to a cuvette containing 2 mL of a solution of salt NaX and 10 mM phosphate buffer to give a 0.52 – 0.63 mM solution of phospholipid. The fluorescence of intravesicular HPTS was monitored by excitation at both 403 nm and 460 nm and the emission at 510 nm was recorded. Some time within the first 100 s of the experiment, a 10- μL aliquot of a 12.5 mM solution of amphiphiles was injected to give a solution that was 0.0625 mM in amphiphile. At the end of the experiment, 10% aqueous Triton-X was injected to lyse the liposomes.

-
- ¹ G. Bock, J. Marsh "Proton passage across cell membranes" *Ciba Foundation* **1988**, 1.
- ² (a) K. N. Raymond, E. A. Dertz, S. S. Kim "Bioorganic chemistry special feature: enterobactin: an archetype for microbial iron transport" *Proc. Nat. Acad. Sci.*, **2003**, *100*, 3584 - 3588.
- (b) K. N. Raymond group web-page at <http://www.cchem.berkeley.edu/knrgrp/fe.html>.
- ³ C. Miller "Ion channels: doing hard chemistry with hard ions" *Curr. Opin. Chem. Biol.*, **2000**, *4*, 148 – 151.
- ⁴ (a) T. J. Franklin, G. A. Snow "Biochemistry and molecular biology of antimicrobial drug action" 6th ed., **2005**, 54.
- (b) Yu. A. Ovchinnikov, V. T. Ivanov, A. M. Shkrob "Membrane-active complexones", **1974**, Elsevier Scientific Pub. Co. (Amsterdam, New York).
- ⁵ G. M. Whitesides, R. F. Ismagilov "Complexity in chemistry" *Science*, **1999**, *5411*, 89 – 92.
- ⁶ G. Cevc, "Phospholipids Handbook," Marcel Dekker, Inc., **1993**.
- ⁷ L. Heginbotham, L. Kolmakova-Partensky, C. Miller "Functional reconstitution of a prokaryotic K⁺ channel" *J. Gen. Physiol.*, **1998**, *111*, 741 – 749.
- ⁸ (a) S. Paula, A. Volkov, D. Deamer "Permeation of halide anions through phospholipid bilayers occurs by the solubility-diffusion mechanism" *Biophys. J.*, **1998**, *74*, 319 – 327.
- (b) A. Volkov, S. Paula, D. Deamer "Two mechanisms of permeation of small neutral molecules and hydrated ions across phospholipid bilayers" *Bioelectrochem. Bioenerg.*, **1997**, *42*, 153 – 160.
- (c) S. Paula, A. G. Volkov, A. N. Van Hoek, T. H. Haines, D. W. Deamer "Permeation of protons, potassium ions, and small polar molecules through phospholipid bilayers as a function of membrane thickness" *Biophys J.*, **1996**, *70*, 339 – 348.
- (d) D. W. Deamer, J. W. Nichols "Proton-hydroxide permeability of liposomes" *PNAS*, **1983**, *80*, 165 - 168.
- ⁹ See review and references in it: C. Miller "Ion channels in liposomes" *Ann. Rev. Physiol.*, **1984**, *46*, 549 – 558.
- ¹⁰ A. H. Rose, J. F. Wilkinson "Advances in microbial physiology" **1970**, *4*, Academic press, London and New York, 53 - 80.

¹¹ (a) B. C. Pressman “Biological applications of ionophores” *Ann. Rev. Biochem.*, **1976**, *45*, 501 – 530.

(b) B. C. Pressman, N. T. deGuzman “Biological applications of ionophores: theory and practice” *Ann. N. Y. Acad. Sci.* **1975**, *264*, 373-386.

¹² (a) <http://www.livonlabs.com/cgi-bin/start.cgi/LypoC/liposomal-encapsulation.html>

(b) <http://www.whatman.com/CycloporePolycarbonateandPolyesterMembranes.aspx>

¹³ (a) T. Jin, M. Kinjo, Y. Kobayashi, H. Hirata “Ion transport activity of calix[*n*]arene (*n* = 4, 5, 6, 7, 8) esters toward alkali-metal cations in a phospholipid bilayer membrane” *J. Chem. Soc., Faraday Trans.*, **1998**, *94*, 3135 – 3140.

(b) A. Gliozzi, M. Robello, L. Fittabile, A. Relini, A. Gambacorta “Valinomycin acts as a channel in ultrathin lipid membranes”, *Biochim. Biophys. Acta - Biomembranes*, **1996**, *1283*, 1 - 3.

¹⁴ B. Hille “Ion Channels of Excitable Membranes”, 3rd ed., Sinauer, Sanderland, **2001**.

¹⁵ A. Accardi, C. Miller “Secondary active transport mediated by a prokaryotic homologue of Cl⁻ channels” *Nature*, **2004**, *427*, 803 – 807.

¹⁶ M. Walden, A. Accardi, F. Wu, C. Xu, C. Williams, C. Miller “Uncoupling and turnover in a Cl⁻/H⁺ exchange transporter” *J. Gen. Physiol.*, **2007**, *129*, 317 – 329.

¹⁷ D. A. Doyle, J. M. Cabral, R. A. Pfuetzner, A. Kuo, J. M. Gulbis, S. L. Cohen, B. T. Chait, R. MacKinnon “The structure of the potassium channel: molecular basis of K⁺ conduction and selectivity” *Science*, **1998**, *280*, 69 – 77.

¹⁸ Recent reviews of synthetic ion channels and carriers:

(a) C. Caltagirone, P. A. Gale “Anion receptor chemistry: highlights from 2007” *Chem. Soc. Rev.*, **2009**, *38*, 520 – 563.

(b) G. W. Gokel and N. Barkey “Transport of chloride ion through phospholipid bilayers mediated by synthetic ionophores” *New J. Chem.*, **2009**, *33*, 947 – 963.

(c) P. A. Gale, S. E. García-Garrido, J. Garric “Anion receptors based on organic frameworks: highlights from 2005 and 2006” *Chem. Soc. Rev.*, **2008**, *37*, 151 – 190.

(d) T. M. Fyles “Synthetic ion channels in bilayer membranes” *Chem. Soc. Rev.*, **2007**, *36*, 335.

(e) A. P. Davis, D. N. Sheppard, B. D. Smith “Development of synthetic membrane transporters for anions” *Chem. Soc. Rev.*, **2007**, *36*, 348.

(f) G. W. Gokel, I. A. Carasel “Biologically active, synthetic ion transporters” *Chem. Soc. Rev.*, **2007**, *36*, 378.

(g) A. L. Sisson, M. R. Shah, S. Bhosale, S. Matile “Synthetic ion channels and pores (2004-2005)” *Chem. Soc. Rev.*, **2006**, *35*, 1269 -1286.

(h) S. Matile, A. Som, N. Sorde “Recent synthetic ion channels and pores” *Tetrahedron*, **2004**, *31*, 6405.

¹⁹ V. E. Carmichael, P. J. Dutton, T. M. Fyles, T. D. James, J. A. Swan, M. Zojaji “Biomimetic ion transport: a functional model of a unimolecular ion channel” *J. Am. Chem. Soc.*, **1989**, *111*, 767 – 769.

²⁰ A. Nakano, Q. Xie, J. V. Mallen, L. Echegoyen, G. W. Gokel “Synthesis of a membrane-insertable, sodium cation conducting channel: kinetic analysis by dynamic sodium-23 NMR” *J. Am. Chem. Soc.*, **1990**, *112*, 1287 – 1289.

²¹ (a) T. M. Fyles, D. Loock, W. F. van Straaten-Nijenhuis, X. Zhou “Pores formed by bis-macrocyclic bola-amphiphiles in vesicle and planar bilayer membranes” *J. Org. Chem.*, **1996**, *61*, 8866 – 8874.

(b) T. M. Fyles, D. Loock, X. Zhou “A voltage-gated ion channel based on a bis-macrocyclic bolaamphiphile” *J. Am. Chem. Soc.*, **1998**, *120*, 2997 – 3003.

(c) T. M. Fyles, T. D. James, K. C. Kaye “Activities and modes of action of artificial ion channel mimics” *J. Am. Chem. Soc.*, **1993**, *115*, 12315 – 12321.

²² O. Murillo, I. Suzuki, E. Abel, C. L. Murray, E. S. Meadows, T. Jin, G. W. Gokel “Synthetic transmembrane channels: functional characterization using solubility calculations, transport studies, and substituent effects” *J. Am. Chem. Soc.*, **1997**, *119*, 5540 – 5549.

²³ T. M. Fyles, C. Hu, R. Knoy “Transmembrane ion conductance by an acyclic bolaamphiphile” *Org. Lett.*, **2001**, *3*, 1335 – 1337.

²⁴ W. Wang, R. Li, G. W. Gokel “"Aplosspan:" a bilayer-length, ion-selective ionophore that functions in phospholipid bilayers” *Chem. Commun.*, **2009**, 911 – 913.

²⁵ (a) L. Ma, W. A. Harrell, Jr., J. T. Davis "Stabilizing guanosine-sterol ion channels with a carbamate to urea modification in the linker" *Org. Lett.*, **2009**, *11*, 1599 - 1602.

(b) L. Ma, M. Melegari, M. Colombini, J. T. Davis "Large and stable transmembrane pores from guanosine-bile acid conjugates" *J. Am. Chem. Soc.* **2008**, *130*, 2938 - 2939.

²⁶ S. Matile, A. Som, N. Sorde "Recent synthetic ion channels and pores" *Tetrahedron*, **2004**, *31*, 6405.

²⁷ N. Madhavan, E. C. Robert, M. S. Gin "A highly active anion-selective aminocyclodextrin ion channel" **2005**, *44*, 7584 - 7587.

²⁸ A. Satake, M. Yamamura, M. Oda, Y. Kobuke "Transmembrane nanopores from porphyrin supramolecules" *J. Am. Chem. Soc.*, **2008**, *130*, 6314 – 6315.

²⁹ K. S. Iqbal, M. C. Allen, F. Fucassi, P. J. Cragg "Artificial transmembrane ion channels from commercial surfactants" *Chem. Commun.*, **2007**, 3951 – 3953.

³⁰ D. C. Dawson, S. S. Smith, M. K. Mansoura "CFTR: mechanism of anion conduction", *Physiol. Rev.*, **1999**, *79*, 47-75.

³¹ M. Jung, H. Kim, K. Baek, K. Kim "Synthetic ion channel based on metal-organic polyhedra" *Angew. Chem. Int. Ed.*, **2008**, *47*, 5755 – 5757.

³² P. V. Santacroce, J. T. Davis, M. E. Light, P. A. Gale, J. C. Iglesias-Sánchez, P. Prados, R. Quesada "Conformational control of transmembrane Cl⁻ transport." *J. Am. Chem. Soc.* **2007**, *129*, 1886 – 1887.

³³ (a) G. Deng, T. Dewa, S. L. Regen "A synthetic ionophore that recognizes negatively charged phospholipid membranes" *J. Am. Chem. Soc.*, **1996**, *118*, 8975 – 8976.

(b) A. Sadownik, G. Deng, V. Janout, S. L. Regen, E. M. Bernard, K. Kikuchi, D. Armstrong "Rapid construction of a squalamine mimic" *J. Am. Chem. Soc.*, **1995**, *117*, 6138 – 6139.

³⁴ (a) P. H. Schlesinger, R. Ferdani, J. Liu, J. Pajewska, R. Pajewski, M. Saito, H. Shabany, G. W. Gokel "SCMTR: A chloride-selective, membrane-anchored peptide channel that exhibits voltage gating" *J. Am. Chem. Soc.*, **2002**, *124*, 1848 – 1849.

(b) J. L. Atwood, J. W. Steed "Encyclopedia of supramolecular chemistry", CRC Press, **2004**, 745.

³⁵ R. Ferdani, G. W. Gokel "Planar bilayer studies reveal multiple conductance states for synthetic anion transporters" *Org. Biomol. Chem.*, **2006**, *4*, 3746 – 3750.

³⁶ J. C. Iglesias-Sanchez, W. Wang, R. Ferdani, P. Prados, J. deMendoza, G. W. Gokel "Synthetic cation transporters incorporating crown ethers and calixarenes as headgroups

and central relays: a comparison of sodium and chloride selectivity” *New J. Chem.*, **2008**, *32*, 878 – 890.

³⁷ S. Matile, N. Sakai “The characterization of synthetic ion channels and pores” In *Analytical Methods in Supramolecular Chemistry*, Schalley, C., Ed.; Wiley, Weinheim, **2007**, 391 – 418.

³⁸ (a) N. Sakai, S. Matile “The determination of the ion selectivity of synthetic ion channels and pores in vesicles” *J. Phys. Org. Chem.*, **2006**, *19*, 452 – 460.

(b) Single channel conductance measurements

P. Talukdar, G. Bollot, J. Mareda, N. Sakai, S. Matile “Synthetic ion channels with rigid-rod π -stack architecture that open in response to charge-transfer complex formation” *J. Am. Chem. Soc.*, **2005**, *127*, 6528 – 6529.

P. Talukdar, G. Bollot, J. Mareda, N. Sakai, S. Matile “Ligand-gated synthetic ion channels” *Chem. Eur. J.*, **2005**, *11*, 6525 – 6532.

(c) “Multichannel conductance experiment”

N. Sakai, D. Houdebert, S. Matile “Voltage-dependent formation of anion channels by synthetic rigid-rod push-pull β -barrels” *Chem. Eur. J.*, **2003**, *9*, 223 – 232.

Naomi Sakai and Stefan Matile “Recognition of polarized lipid bilayers by p-oligophenyl ion channels: from push-pull rods to push-pull barrels” *J. Am. Chem. Soc.*, **2002**, *124*, 1184 – 1185.

³⁹ T. M. Fyles, H. Luong “Structure-activity relationships in linear oligoester ion-channels” *Org. Biomol. Chem.*, **2009**, *7*, 733 – 738.

⁴⁰ M. Merritt, M. Lanier, G. Deng, S. L. Regen “Sterol-polyamine conjugates as synthetic ionophores” *J. Am. Chem. Soc.*, **1998**, *120*, 8494 – 8501.

⁴¹ (a) V. Sidorov, F. W. Kotch, G. Abdrakhmanova, R. Mizani, J. C. Fetting, J. T. Davis “Ion channel formation from a calix[4]arene amide that binds HCl” *J. Am. Chem. Soc.*, **2002**, *124*, 2267 – 2278.

(b) J. L. Seganish and J. T. Davis “Prodigiosin is a chloride carrier that can function as an anion exchanger” *Chem. Commun.*, **2005**, 5781 – 5783.

(c) P. V. Santacroce, O. A. Okunola, P. Zavalij, J. T. Davis “A transmembrane anion transporter selective for nitrate over chloride” *Chem. Commun.*, **2006**, 3246 – 3248.

(d) S. K. Berezin, J. T. Davis “Catechols as membrane anion transporters” *J. Am. Chem. Soc.*, **2009**, *131*, 2458 – 2459.

⁴² A. Perez-Velasco, V. Gorteau, S. Matile “Rigid oligoperylenediimide rods: anion- π slides with photosynthetic activity” *Angew. Chem. Int. Ed.*, **2008**, *47*, 921- 923.

⁴³ V. Gorteau, G. Bollot, J. Mareda, S. Matile “Rigid-rod anion- π slides for multiion hopping across lipid bilayers”, *Org. Biomol. Chem.* **2007**, *5*, 3000 – 3012.

⁴⁴ N. Sakai, J. Mareda, S. Matile “Ion channels and pores, made from scratch” *Mol. Biosyst.*, **2007**, *3*, 658 – 666.

⁴⁵ On-line google book preview:

J. L. Lakowicz “Principles of fluorescence spectroscopy”, **2006**, Springer, 3rd ed, 8, 640.

⁴⁶ P. Bühlmann, E. Pretsch, E. Bakker “Carrier-based ion-selective electrodes and bulk optodes. 2. Ionophores for potentiometric and optical sensors” *Chem. Rev.*, **1998**, *98*, 1593 – 1688.

⁴⁷ D. R. Pfeiffer, P. W. Reed, H. A. Lardy “Ultraviolet and fluorescent spectral properties of the divalent cation ionophore A23187 and its metal ion complexes” *Biochem.*, **1974**, *13*, 4007 – 4014.

⁴⁸ U. Schaller, E. Bakker, E. Pretsch “Carrier mechanism of acidic ionophores in solvent polymeric membrane ion-selective electrodes” *Anal. Chem.*, **1995**, *67*, 3123 – 3132.

⁴⁹ R. Custelcean, J. Bosano, P. V. Bonnesen, V. Kertesz, B. P. Hay “Computer-aided design of a sulfate-encapsulating receptor” *Angew. Chem. Int. Ed.*, **2009**, *48*, 4025 – 4029.

⁵⁰ R. Custelcean, P. Remy, P. V. Bonnesen, D. E. Jiang, B. A. Moyer “Sulfate recognition by persistent crystalline capsules with rigidified hydrogen-bonding cavities” *Angew. Chem. Int. Ed.*, **2008**, *47*, 1866 – 1870.

⁵¹ R. Custelcean “Ion separation by selective crystallization of organic frameworks”, *Cur. Opin. Solid. State. Mater. Sci.*, **2009**, ASAP.

⁵² J. L. Sessler, D. An, W.-S. Cho, V. Lynch, M. Marquez “Calix[4]bipyrrrole—a big, flexible, yet effective chloride-selective anion receptor” *Chem. Commun.*, **2005**, 540 – 542.

⁵³ (a) J. R. Hiscock, C. Caltagirone, M. E. Light, M. B. Hursthouse, P. A. Gale “Fluorescent carbazolylurea anion receptors”, *Org. Biomol. Chem.*, **2009**, *7*, 1781 – 1783.

(b) G. W. Bates, Triyanti, M. E. Light, M. Albrech, P. A. Gale “2,7-Functionalized indoles as receptors for anions”, *J. Org. Chem.*, **2007**, *27*, 8921 – 8927.

⁵⁴ K. M. Mullen, J. Mercurio, C. J. Serpell, P. D. Beer “Exploiting the 1,2,3-triazolium motif in anion-templated formation of a bromide-selective rotaxane host assembly” **2009**, *121*, 4875 – 4878.

⁵⁵ (a) W.-H. Chen, X.-B. Shao, R. Moellering, C. Wennersten, S. L. Regen “A bioconjugate approach toward squalamine mimics: insight into the mechanism of biological action” *Bioconjugate Chem.*, **2006**, *17*, 1582 – 1591.

(b) M. Merritt, M. Lanier, D. Gang, S. L. Regen “Sterol–polyamine conjugates as synthetic ionophores” *J. Am. Chem. Soc.*, **1998**, *120*, 8494 – 8501.

(c) W.-H. Chen, V. Janout, M. Kondo, A. Mosoian, G. Mosoyan, R. R. Petrov, M. E. Klotman, S. L. Regen “A fine line between molecular umbrella transport and ionophoric activity” *Bioconjugate Chem.*, Articles ASAP.

⁵⁶ D. Bemporad, J. W. Essex, C. Luttmann “Permeation of small molecules through a lipid bilayer: a computer simulation study” *J. Phys. Chem. B*, **2004**, *108*, 4875 – 4884.

⁵⁷ D. K. Smith, “Rapid NMR screening of chloride receptors: uncovering catechol as a useful anion binding motif” *Org. Biomol. Chem.*, **2003**, *1*, 3874.

⁵⁸ K. S. Winstanley, A. M. Sayer, D. K. Smith, “Anion binding by catechols - an NMR, optical and electrochemical study” *Org. Biomol. Chem.* **2006**, *4*, 1760.

⁵⁹ K. J. Winstanley, D. K. Smith, “Ortho-substituted catechol derivatives: the effect of intramolecular hydrogen-bonding pathways on chloride anion recognition” *J. Org. Chem.*, **2007**, *72*, 2803.

⁶⁰ M. A. Khan, A. W. McCulloch; A. G. McInnes “Novel hydrogen bonding in crystalline tetra-n-butylammonium salts of catechol halides” *Can. J. Chem.*, **1985**, *63*, 2119 – 2122.

⁶¹ N. Schweigert, A. J. B. Zehnder, R. I. L. Eggen, “Chemical properties of catechols and their molecular modes of toxic action in cells, from microorganisms to mammals” *Environ. Microbiol.*, **2001**, *2*, 81 - 91.

⁶² N. Schweigert, R. W. Hunziker, B. I. Escher, R. I. Eggen, “Acute toxicity of (chloro-) catechols and (chloro-)catechol-copper combinations in *Escherichia coli* corresponds to their membrane toxicity in vitro” *Environ-Toxicol-Chem.*, **2001**, *20*, 239.

⁶³ Propyl, Octyl, Dodecyl gallate are currently permitted for use as antioxidant additives in food. Octylgallate and structurally relevant compounds were found to possess broad spectrum of antimicrobial properties:

I. Kubo, K. Fujita, K. Nihei, "Molecular design of multifunctional antibacterial agents against methicillin resistant *Staphylococcus aureus* (MRSA)" *Bioorg. Med. Chem.*, **2003**, *11*, 4255.

⁶⁴ I. Kubo, H. Muroi, A. Kubo, "Structural functions of antimicrobial long-chain alcohols and phenols" *Bioorg. Med. Chem.*, **1995**, *3*, 873.

⁶⁵ C. Z. Chen, N. C. Beck-Tan, P. Dhurjati, T. K. van Dyk, R. A. LaRossa, S. L. Cooper "Quaternary ammonium functionalized poly(propylene imine) dendrimers as effective antimicrobials: structure-activity studies" *Biomacromol.*, **2000**, *1*, 473 – 480.

⁶⁶ E. Kenawy, S. D. Worley, R. Broughton, "The chemistry and application of antimicrobial polymers: a state-of-the-art review" *Biomacromol.*, **2007**, *8*, 1361.

⁶⁷ Urushiols are *n*-alkenyl and alkyl-substituted catechols responsible for poison ivy and poison oak dermatitis.

(a) K. H. Markiewitz, C. R. Dawson, "On the isolation of the allergenically active components of the toxic principles of poison ivy" *J. Org. Chem.*, **1965**, *30*, 1610.

(b) W. M. Draper, D. Wijekoon, M. McKinney, P. Behniwal, S. K. Perera, C. P. Flessel, "Atmospheric pressure ionization LC-MS-MS determination of urushiol congeners" *J. Agric. Food Chem.*, **2002**, *50*, 1852.

(c) M. A. ElSohly, P. D. Adawadkar, C. Ma, C. E. Turner, "Separation and characterization of poison ivy and poison oak urushiol components" *J. Nat. Prod.*, **1982**, *45*, 532.

⁶⁸ A. Kozubek, J. H. Tyman, "Resorcinolic lipids, the natural non-isoprenoid phenolic amphiphiles and their biological activity" *Chem. Rev.*, **1999**, *99*, 1.

⁶⁹ *Surfactants and Interfacial Phenomena, Third Edition*. M. J. Rosen, **2004** John Wiley&Sons, Inc., 6.

⁷⁰ (a) H. Itokawa, N. Totsuka, K. Nakahara, M. Maezuru, K. Takeya, M. Kondo, M. Inamatsu, H. Morita "A quantitative structure-activity relationship for antitumor activity of long-chain phenols from Ginkgo biloba L." *Chem. Pharm. Bull.*, **1998**, *37*, 1619 – 1621.

(b) H. Itokava, N. Totsuka, K. Nakahara, K. Takeya, J.-P. Lepoittevin, Y. Askawa “Antitumor principles from Ginkgo biloba L.” *Chem. Pharm. Bull.*, **1987**, *35*, 3016 – 3020.

⁷¹ (a) A. B. Hendrich, A. Kozubek “Calorimetric study on the interactions of 5-n-heptadec(en)ylresorcinols from cereal grains with zwitterionic phospholipid (DPPC).” *Z. Naturforsch.*, **1991**, *46c*, 423 – 427.

(b) S. Gerdon, S. Hoffmann, A. Blume “Properties of mixed monolayers and bilayers of long-chain 5-n-alkylresorcinols and dipalmitoylphosphatidylcholine” *Chem. Phys. Lipids*, **1994**, *71*, 229-243.

(c) A. Kozubek, A. Jezierski, A. F. Sikorski “The effect of nonadec(en)ylresorcinol on the fluidity of liposome and erythrocyte membranes. *Biochim. Biophys. Acta*, **1988**, *944*, 465 – 472.

⁷² A. S. Kaprelyants, M. K. Suleimenov, A. D. Sorokina, G. A. Deborin, G. I. El-Registan, F. M. Stoyanovich, Y. E. Lille, D. N. Ostrovsky “Structural-functional changes in bacterial and model membranes induced by phenolic lipids” *Biol. Membr.*, **1987**, *4*, 254 – 261.

⁷³ A. Kozubek, R. A. Demel “Permeability changes of erythrocytes and liposomes by 5-(n-alk(en)yl)resorcinols from rye” *Biochim. Biophys. Acta*, **1980**, *603*, 220 – 227.

⁷⁴ A. Kozubek, R. A. Demel “The effect of 5-(n-alk(en)yl)resorcinols from rye on membrane structure” *Biochim. Biophys. Acta*, **1981**, *642*, 242 – 251.

⁷⁵ (a) M. Stasiuk, A. Kozubek, “Modulation of 5-n-alkylresorcinol hemolytic properties by divalent cations. Dependence of the effect of cations on alkylresorcinol structure” *Cell. Mol. Biol. Lett.*, **1997**, *2*, 77 – 87.

(b) M. Stasiuk, A. Kozubek “Modulation of hemolytic properties of resorcinolic lipids by divalent cations” *Cell. Mol. Biol. Lett.*, **1996**, *1*, 189 – 198.

⁷⁶ (a) A. E. V. Gorden, J. Xu, K. N. Raymond “Rational design of sequestering agents for plutonium and other actinides” *Chem. Rev.*, **2003**, *103*, 4207-4282.

(b) G. Winkelmann, C. J. Carrano “Transition metals in microbial metabolism”, **1997**, Harwood Academic Publishers (Amsterdam).

⁷⁷ (a) L. Heinisch, S. Wittmann, T. Stoiber, A. Berg, D. Ankel-Fuchs, U. Mollmann “Highly antibacterial active aminoacyl penicillin conjugates with acylated bis-catecholate siderophores based on secondary diamino acids and related compounds” *J. Med. Chem.*, **2002**, *45*, 3032.

(b) S. Wittmann, L. Heinisch, I. Scherlitz-Hofmann, T. Stoiber, D. Ankel-Fuchs, U. Möllmann "Catecholates and mixed catecholate hydroxamates as artificial siderophores for mycobacteria" *Biometals*, **2004**, *17*, 53-56.

⁷⁸ H. Keberle "The biochemistry of desferrioxamine and its relation to iron methabolism" *Ann. NY Acad. Sci.*, **1964**, *119*, 758-775.

⁷⁹ S. J. Rodgers, C. Lee, C. Y. Ng, K. N. Raymond, "Ferric iron sequestering agents. 15. synthesis, solution chemistry, and electrochemistry of a new cationic analogue of enterobactin" *Inorg. Chem.*, **1987**, *26*, 1622.

⁸⁰ J. S. Martinez, G. P. Zhang, P. D. Holt, H.-T. Jung, C. J. Carrano, M. G. Haygood, A. Butler, "Self-assembling amphiphilic siderophores from marine bacteria" *Science*, **2000**, *287*, 1247.

⁸¹ M. Apostol, P. Baret, G. Serratrice, J. Desbrieres, J.-L. Putaux, M.-J. Stebe, D. Expert, J.-L. Pierre "Self-assembly of an amphiphilic iron(III) chelator: mimicking iron acquisition in marine bacteria" *Angew. Chem. Int. Ed.*, **2005**, *44*, 2580.

⁸² D. Yang, J. Qu, W. Li, Y.-H. Zhang, Y. Ren, D.-P. Wang, Y.-D. Wu "Cyclic Hexapeptide of $\underline{d,l}$ - α -aminoxy acids as a selective receptor for chloride ion" *J. Am. Chem. Soc.*, **2002**, *124*, 12410.

⁸³ F. Huang, J. W. Jones, C. Sleboznick, H. W. Gibson "Ion pairing in fast-exchange host-guest systems: concentration dependence of apparent association constants for complexes of neutral hosts and divalent guest salts with monovalent counterions" *J. Am. Chem. Soc.*, **2003**, *125*, 14458 - 14464.

⁸⁴ F. Werner, H.-J. Schneider "Complexation of anions including nucleotide anions by open-chain host compounds with amide, urea, and aryl functions" *Helv. Chim. Acta*, **2000**, *83*, 465 - 478.

⁸⁵ R. Pajewski, R. Ferdani, P. H. Schlesinger, G. W. Gokel "Chloride complexation by heptapeptides: influence of C- and N-terminal sidechains and counterion" *Chem. Commun.*, **2004**, *2*, 160 - 161.

⁸⁶ R. Shukla, T Kida, B. D. Smith "Effect of competing alkali metal cations on neutral host's anion binding ability" *Org. Lett.*, **2000**, *2*, 3099 - 3102.

⁸⁷ F. Arnaud-Neu, R. Delgado, S. Chaves "Critical evaluation of stability constants and thermodynamic functions of metal complexes of crown ethers" *Pure Appl. Chem.*, **2003**, *75*, 71 - 102.

⁸⁸ R. Vilar, D. M. P. Mingos, A. J. P. White, D. J. Williams "Anion control in the self-assembly of a cage coordination complex" **1998**, *37*, 1258 - 1261.

-
- ⁸⁹ C. M. G. dos Santos, T. McCabe, T. Gunnlaugsson “Selective fluorescent sensing of chloride” *Tetrahedr. Lett.*, **2007**, *48*, 3135 – 3139.
- ⁹⁰ B. P. Hay, T. K. Firman, B. A. Moyer “Structural design criteria for anion hosts: strategies for achieving anion shape recognition through the complementary placement of urea donor groups” *J. Am. Chem. Soc.*, **2005**, *127*, 1810 -1819.
- ⁹¹ *The Organic Chemistry of Electrolyte Solutions*, J. E. Gordon, A Wiley-Interscience Publication, John Wiley & Sons, NewYork·London·Sydney·Toronto, **1975**.
- ⁹² R. L. Buckson, S. G. Smith “Concentration effects on the nuclear magnetic resonance of quaternary ammonium salts” *J. Phys. Chem.*, **1964**, *68*, 1875 – 1878.
- ⁹³ E. A. Moelwyn - Hughes, *The Chemical Statics and Kinetics of Solutions*, **1971**, Academic Press, London and New York, 66.
- ⁹⁴ P. Chen, T. J. Meyer “Medium effects on charge transfer in metal complexes” *Chem. Rev.*, **1998**, *98*, 439 – 1477.
- ⁹⁵ D. Meshcheryakov, V. Böhmer, M. Bolte, V. Hubscher-Bruder, F. Arnaud-Neu, H. Herschbach, A. Van Dorsselaer, I. Thondorf, W. Mögelin “Two chloride ions as a template in the formation of a cyclic hexaurea” *Angew. Chem. Int. Ed.* **2006**, *45*, 1648 - 1652.
- ⁹⁶ S. L. Tobey, E. V. Anslyn “Studies into the thermodynamic origin of negative cooperativity in ion-pairing molecular recognition” *J. Am. Chem. Soc.*, **2003**, *125*, 10963 – 10970.
- ⁹⁷ A. D. Hughes, E. V. Anslyn “A cationic host displaying positive cooperativity in water” *PNAS* **2007**, *104*, 6538 – 6543.
- ⁹⁸ J. W. Jones, H. W. Gibson “Ion pairing and host–guest complexation in low dielectric constant solvents” *J. Am. Chem. Soc.*, **2003**, *125*, 7001 – 7004.
- ⁹⁹ HyperChem Professional software developed by Hypercube, Inc.
- ¹⁰⁰ Calculated using Advanced Chemical Development (ACD/Labs) Software V 8.14 for Solaris (1994-2006 ACD/Labs).
- ¹⁰¹ A. Shivanyuk , K. Rissanen , S. K. Körner, D. M. Rudkevich, J. Jr. Rebek, *Helv. Chim. Acta*, **2000**, *83*, 1778 – 1790.
- ¹⁰² M. Kondo “Spectroscopic studies of solvent effects on intramolecular hydrogen bonding in *N*-substituted salicylamides” *Bull. Chem. Soc. Japan*, **1979**, *52*, 521 – 523.

¹⁰³ K. J. Winstanley, S. J. Allen, D. K. Smith “Encapsulated binding sites — synthetically simple receptors for the binding and transport of HCl” *Chem. Commun.*, **2009**, 4299 – 4301.

¹⁰⁴ S. M. Cohen, K. N. Raymond “Catecholate/Salicylate heteropodands: demonstration of a catecholate to salicylate coordination change” *Inorg. Chem.*, **2000**, *39*, 3624 – 3631.

¹⁰⁵ A. M. Albrecht-Gary, S. Blanc, F. Biaso, F. Thomas, P. Baret, G. Gellon, J. L. Pierre, G. Serratrice “Iron(III) chelation: Tuning of the pH dependence by mixed ligands” *Eur. J. Inorg. Chem.*, **2003**, *14*, 2596 – 2605.

¹⁰⁶ (a) M. Albrecht, S. J. Franklin, K. N. Raymond “Macrobicyclic Tris(catecholate ligand) complexes: spectroscopy, electrochemistry, and the structure of K₂[(H₂-biccappedTRENAM)MoO₂]” *Inorg. Chem.*, **1994**, *33*, 5785 – 5793.

(b) E. A. Dertz, J. Xu, K. N. Raymond “Tren-based analogues of bacillibactin: structure and stability” *Inorg. Chem.*, **2006**, *45*, 5465 – 5478.

¹⁰⁷ M. Llinas, D. M. Wilson, J. B. Neilands “Effect of metal binding on the conformation of enterobactin. Proton and carbon-13 nuclear magnetic resonance study” *Biochem.*, **1973**, *12*, 3836 – 3843.

¹⁰⁸ J. H. van Esch “We can design molecular gelators, but do we understand them?” *Langmuir*, **2009**, *25*, 8392 – 8394.

¹⁰⁹ Origin 7.0 software developed by OriginLab Corporation, Northampton, MA

¹¹⁰ V. Sidorov, F. W. Kotch, Y.-F. Lam, J. L. Kuebler, J. T. Davis “Chloride transport across lipid bilayers and transmembrane potential induction by an oligophenoxyacetamide” *J. Am. Chem. Soc.*, **2003**, *125*, 2840.

¹¹¹ F. Hofmeister “Zur Lehre von der Wirkung der Salze” *Arch. Exp. Pathol. Pharmacol.* **1888**, *24*, 247 - 260.

¹¹² Svetlana Lutsenko web page, Oregon Health & Science University
<http://www.ohsu.edu/biochem/lutsenko/lutsenko.cfm>
<http://www.ohsu.edu/biochem/lutsenko/images/transport1color.pdf>

¹¹³ S. S. Smith, E. D. Steinle, M. E. Meyerhoff, D. C. Dawson “Cystic fibrosis transmembrane conductance regulator: physical basis for lyotropic anion selectivity patterns” *J. Gen. Physiol.*, **1999**, *114*, 799 – 818.

¹¹⁴ N. A. McCarty “Permeation through the CFTR chloride channel” *J. Exp. Biol.*, **2000**, *203*, 1947–1962.

¹¹⁵ Y. Markus *Ion properties* Marcel Dekker, **1997**, New York, NY. pg. 56.

¹¹⁶ P. J. F. Henderson, J. D. McGivan, and J. B. Chappell “The action of certain antibiotics on mitochondrial, erythrocyte and artificial phospholipid membranes. The role of induced proton permeability” *Biochem J.*, **1969**, February; *111*, 521 – 535.

¹¹⁷The potential of the anionophores as tools for biomedical research of membrane transport was mentioned, for instance by A. P. Davis and B. D. Smith in the article:

B. A. McNally, A.V. Koulov, T. N. Lambert, B. D. Smith, J. B. Joos, A. L. Sisson, J. P. Clare, V. Sgarlata, L. W. Judd, G. Magro, A. P. Davis “Structure-activity relationships in cholapod anion carriers: enhanced transmembrane chloride transport through substituent tuning” *Chem. Eur. J.*, **2008**, *14*, 9599 – 9606.

¹¹⁸ A. L. Sisson, J. P. Clare, A. P. Davis “Contra-Hofmeister anion extraction by cyclosteroidal receptors” *Chem. Commun.*, **2005**, *5*, 5263 – 5265.

¹¹⁹ (a) V. Janout, S. L. Regen “Bioconjugate-based molecular umbrellas” *Bioconjugate Chem.*, **2009**, *20*, 183 – 192.

(b) V. Janout, S. L. Regen “A needle-and-thread approach to bilayer transport: permeation of a molecular umbrella–oligonucleotide conjugate across a phospholipid membrane”, *J. Am. Chem. Soc.*, **2005**, *127*, 22 – 23.